Recognition of the CCT5 Di-Glu Degron by CRL4^{DCAF12} is Incompatible with TRiC Assembly

INAUGURALDISSERTATION

zur

Erlangung der Würde eines

DOKTORS DER PHILOSOPHIE

vorgelegt der

PHILOSOPHISCH-NATURWISSENSCHAFTLICHEN FAKULTÄT

der

UNIVERSITÄT BASEL

von

CARLOS PLA PRATS

Basel, 2023

Originaldokument gespeichert auf dem Dokumentenserver der Universität Basel

edoc.unibas.ch

Genehmigt von der Philosophisch-Naturwissenschaftlichen Fakultät

auf Antrag von

First supervisor: Dr. NICOLAS H. THOMÄ

Second supervisor: Prof. Dr. MARC BÜHLER

External expert: Prof. Dr. BRENDA A. SCHULMAN

Basel, den 15. November 2022

Dekan

Prof. Dr. Marcel Mayor

Abstract

The molecular processes within all living organisms rely on the correct functioning of proteins, most of which must assemble into multimeric complexes of defined architecture and composition. In eukaryotes, assembly quality control (AQC) E3 ubiquitin ligases target incomplete or incorrectly assembled protein complexes for degradation to ensure protein complex functionality and proteostasis. The CUL4-RBX1-DDB1-DCAF12 ($CRL4^{DCAF12}$) E3 ubiquitin ligase induces the proteasomal degradation of proteins with a C-terminal double glutamate (di-Glu) motif. Putative $CRL4^{DCAF12}$ substrates include CCT5, a subunit of the eukaryotic TRiC chaperonin. TRiC is responsible for the folding of around 10% of the human proteome. Its functionality relies on the correct arrangement of its eight subunits, but how TRiC assembly is ensured has not yet been investigated. Furthermore, how DCAF12 recognizes its substrates is unknown. Here the cryo-EM structure of the CCT5-bound DDB1-DCAF12 complex at 2.8 Å resolution is presented. DCAF12 serves as a canonical WD40 DCAF substrate receptor and uses a positively charged pocket at the center of its β-propeller to bind the C-terminus of CCT5. DCAF12 specifically reads out the CCT5 di-Glu side chains, and contacts other visible degron amino acids through weaker Van der Waals interactions, explaining the flexibility in substrate recognition. The CCT5 C-terminus is inaccessible in an assembled TRiC complex, and functional assays demonstrate that $CRL4^{DCAF12}$ binds and ubiquitinates monomeric CCT5, but not TRiC. The presented results suggest a previously unanticipated AQC role for the $CRL4^{DCAF12}$ E3 ligase towards TRiC, and likely other complexes.

Contents

Chapter 1

Introduction

1.1 The Ubiquitin-Proteasome System

Pioneering isotopic labelling experiments by Rudolph Schönheimer almost a century ago revealed the unexpected finding that all cellular components are in a constant state of chemical renewal (*The Dynamic State of Body Constituents*, Harvard university Press, 1942). Over a decade later, Melvin Simpson published the again surprising observations that intracellular proteolysis requires energy, despite peptide bond hydrolysis being exergonic [1]. The discovery of lysosomes in 1955 suggested that they, with their high pH and internal concentration of proteases, were the site of protein degradation, and that the requirement of ATP for protein degradation was owed to the transport of proteolytic targets into the lysosome or to maintain the lysosomal pH [2-4]. ATP-dependent proteolysis was however later observed in rabbit reticulocytes, which do not contain lysosomes [5], and the cytosol was established as the main site of selective proteolysis [6]. In the following years, those observations would be exploited in a series of discoveries that lead to the discovery of the pathway we now call the ubiquitin-proteasome system (UPS). Ciechanover A. *et al.* reconstituted protein degradation in cell-free reticulocyte extracts, identifying two

chromatographic fractions that needed to be combined for proteolysis [7]. Fraction I was shown to be a heat-stable protein termed APF-1, while fraction II contained the other components of the pathway [7, 8]. In two seminal 1980 papers, A. Ciechanover, A. Hershko, I. Rose and collaborators then showed that the association between APF-1 and target proteins was processive, covalent and ATP-dependent [9, 10]. Their proposal that this post-translational modification was the signal that stimulated downstream proteases gained support after experiments *in vivo* showed a correlation between ubiquitin conjugation and protein half-life [11-14]. It was simultaneously found that ubiquitin, a highly abundant and extremely conserved small protein discovered in 1975, was APF-1 [15, 16]. Covalent modification between ubiquitin and histone H2A had been recently reported [17], but the biological implications of this modification were unknown [18]. The following decades would progressively unravel the characteristics of the UPS. Ubiquitin was found to form an isopeptide bond between its C-terminal Gly76 residue and a lysine residue in the target protein [19]. The 20S [20] and 26S [21] proteasome were identified as ATP-dependent downstream proteases acting on polyubiquitinated substrates, and the 20S was found to be a subcomplex of the larger 26S complex [22, 23]. The components of the pathway were resolved into ATP-dependent ubiquitin activating (E1) [24, 25], ubiquitin conjugating (E2) [26, 27] and ubiquitin ligase (E3) [27, 28] enzymatic activities. The first deubiquitinating enzymes were characterized [29, 30] and then cloned [31, 32], confirming the reversibility of ubiquitination suggested by the studies on reticulocyte extracts [9, 10]. The first determinants of protein ubiquitination (degrons) were found at the extreme N-termini of proteins, giving rise to the N-end rule of protein stability [13, 33]. Polyubiquitin chains, in contrast to mono-ubiquitination [17, 34],

were found to be the recognition signal for proteolysis [35], and different functions were ascribed in the following years to the different possible polyubiquitin linkages [35-38], all of which were eventually observed *in vivo* [39].

The discovery and characterization of the UPS thus solved the energy requirement conundrum some 50 years after it was posed: energy, in the form of ATP, was required for the conjugation of ubiquitin to the target substrate and for the assembly and activity of the proteasome. The myriad of cellular roles attributed to the UPS have not ceased to expand since its discovery. With over 600 human E3 ligases that target each a variety of substrates, the UPS can potentially regulate every cellular process.

1.1.1 Ubiquitin

Ubiquitin (Ub) is encoded by four human genes. An anomaly in eukaryotic genome organization, two of those genes encode spacerless tandem arrays of sequences (three for the *UBB* gene, nine for the *UBC* gene) encoding monomeric ubiquitin [40-42]. The resulting polypeptide contains an additional C-terminal capping residue to prevent premature and aberrant ubiquitination reactions and is then cleaved into monomeric, mature ubiquitin. The two other genes encode ubiquitin C-terminally fused to two different ribosomal subunits [43, 44]. The 76-amino acid ubiquitin is the highest conserved protein known, with a variation of only three amino acids from yeast to humans. Ubiquitin owes its exceptional stability to its very compact structure, with extensive secondary structure and a very hydrophobic core **(Figure 1.1)** [45].

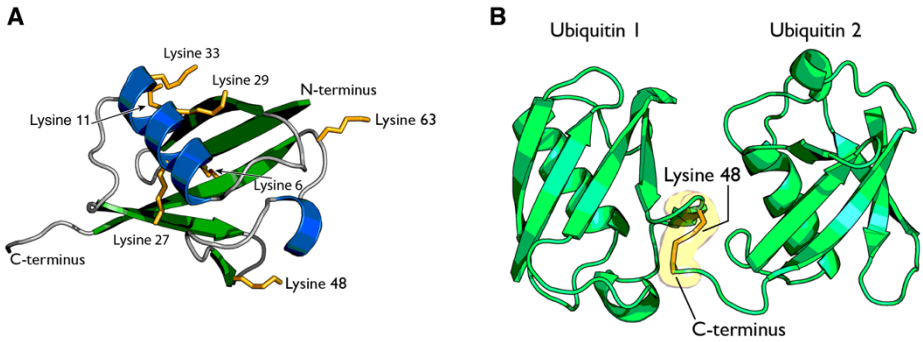

Figure 1.1. Structure of ubiquitin. (A) Schematic structure of ubiquitin (PDB ID 1UBI [46]). Ubiquitin is shown in cartoon representation, with α-helices in blue and β-strands in green. Lysines are shown as orange sticks. **(B)** Schematic structure of lysine 48-linked di-ubiquitin, shown as green cartoons. The isopeptide bond is shown in orange.

In the UPS, ubiquitin is conjugated through its C-terminal (Gly76) carboxylate to an acceptor lysine in a target protein [35], although N-terminal, cysteine, serine, and threonine ubiquitination have also been observed [47]. After an initial ubiquitination event, processive ubiquitination quickly follows [48, 49]. The resulting polyubiquitin chains can be built on either of ubiquitin's seven lysines (Lys6, Lys11, Lys 27, Lys29, Lys33, Lys48, Lys63) as well as the initiator methionine (Met1) [37, 38, 50-52]. A complex signaling code originates from these linkages [47, 53], all of which are abundant in cells [39]. The majority of polyubiquitin linkages found *in vivo* are Lys11- and Lys48-mediated, signaling proteolysis [36, 39]. Polyubiquitin chains with other linkages have been associated with autophagy, as well as non-proteolytic functions like regulating substrate localization, NF-kB signaling, DNA repair, RNA splicing, cell cycle progression and endocytosis [39, 47, 53, 54]. Ubiquitin is the founding member of a family of structurally similar ubiquitin-like proteins (Ubls) including SUMO and NEDD8, which

have their own E1-E2-E3 cascades and impart distinct functions to their targets, usually modulating their localization or activation [55-57].

1.1.2 Ubiquitin activation

To enter the ubiquitin-proteasome pathway, monomeric ubiquitin must be "activated" by one of the two E1 enzymes present in human cells, UBA1 and UBA6 [58, 59]. Ub and Ubl activation by E1s connects them to their downstream pathways, and E1s have evolved mechanisms to ensure selectivity towards their Ub/Ubl substrate [60, 61]. This is important because Ub and Ubls can compete for the same acceptor lysine *in vivo* to trigger different cellular responses [62]. In a two-step nucleophilic substitution reaction, the catalytic cysteine of the E1 carries out a nucleophilic attack on the C-terminal carboxyl group of Ub/Ubl Gly76. The reaction proceeds through an "activated" Gly76-adenylate intermediate that is generated through ATP hydrolysis [25]. Adenylation induces a large conformational change that releases pyrophosphate to prevent reaction reversal and remodels the active site, replacing active site residues required for adenylation with residues required for covalent conjugation to the E1, including the catalytic cysteine [63]. The resulting E1~Ub complex is covalently linked through a thioester bond (denoted "~"). Formation of the E1~Ub and binding and adenylation of a second Ub induces a conformational change in the E1 that exposes a binding site for an E2~Ub (but not E2~Ubl) [64, 65]. Binding of the E2 juxtaposes the E1 and E2 catalytic cysteines [65]. Proximity between the cysteines induces a transthiolation reaction, and an E2~Ub product is formed, releasing AMP to again prevent reaction reversal [66]. Ub transfer to the E2 removes the E2 binding site on the E1 enzyme, displacing the E2~Ub

conjugate and restarting the E1 conformational cycle [67]. E2~Ub conjugates are then free to progress along the UPS enzymatic cascade.

1.1.3 Ubiquitin conjugation

Whereas only a few E2 enzymes act on Ubls, at least 38 E2s have been identified to act on ubiquitin in humans [68]. They influence key characteristics of substrate ubiquitination, like chain length and linkage, as well as triaging between polyubiquitin chain initiation and elongation [68-71]. E2s can thus specialize in chain initiation [62, 72] or elongation [73-75], in the generation of Lys48- [49], Lys63- [74, 76] or Lys11- [75] linked chains, and determine polyubiquitin chain length and the order of substrate degradation [77]. Chain linkage is often determined by contacts between the E2 and the recognized substrate that orient a specific substrate lysine towards the E2 catalytic cysteine [71, 78]. To facilitate the directionality of the cascade, E1s and E3s often compete for the same binding sites on E2 enzymes **(Figure 1.2)** [79-81], and E1s have a significantly lower affinity for E2s in their free state than in their Ub-loaded state [26, 66]. E2s bind E3s in a topologically conserved site shared by all E2s, and sequence variability within this site controls their specificity towards E3s [82]. E2s fully activate upon binding to E3s, allowing them to catalyze the ubiquitination of their targets.

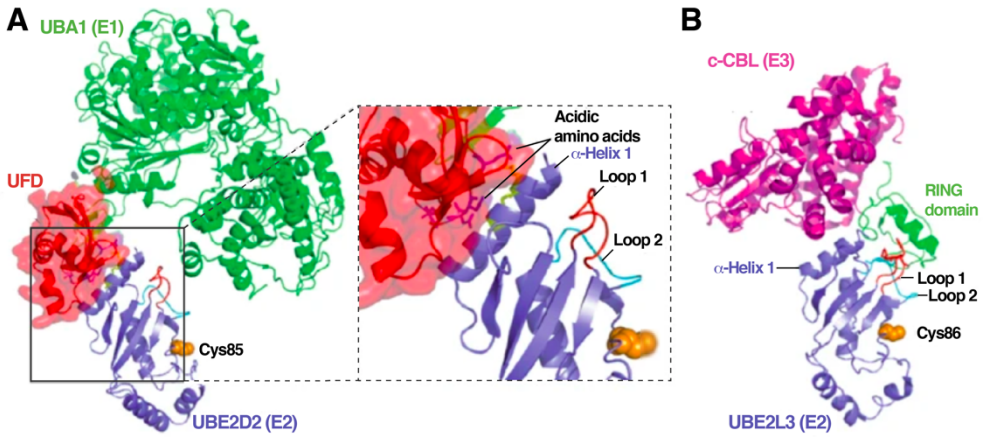

Figure 1.2. Overlapping sites for E1 and E3 enzymes on E2s. (A) Structural representation of a complex between the E2 UBE2D2 (lavender) and the E1 UBA1 (green). The model has been created from structures of *Saccharomyces cerevisiae* E1~Ub (PDB ID 3CMM [64]) and *Homo Sapiens* E1-E2 (PDB ID 1Y8X [80]). E2s use their basic α-helix 1 to bind an acidic patch in the ubiquitin fold domain (UFD, red) of the E1. Basic and acidic residues mediating the interaction are shown as yellow and blue sticks, respectively. The catalytic cysteine is shown in surface representation. **(B)** Structural representation of a complex between the E2 UBE2L3 (lavender) and the E3 c-CBL (magenta, RING motif in green)(PDB ID 1FBV [83]). E2s use two hypervariable loops (Loop 1, Loop 2) to bind their E3s. The catalytic cysteine is shown in surface representation. Note that the E2 has overlapping binding sites on α-helix 1 for the E1 and the E3. Adapted from Ye Y. *et al.* 2009 [68].

To increase processivity, several E2 monomers can self-assemble around an E3 to promote Ub discharge [82], and an E3 can associate with several different E2s [84-87]. A similar result can be achieved by the pre-assembly of polyubiquitin chains in the E2 active site that are then transferred simultaneously to the substrate [88, 89], by directly recognizing substrate motifs to orient an acceptor lysine [71, 90], and by increasing their affinity for their E3. Mechanisms to achieve this include binding additional regions of the E3 [91] and non-covalent interactions with ubiquitin or Ubls that increase the E2-E3 interface [92, 93]. The processivity of ubiquitin transfer is biologically important, because substrates must have a polyubiquitin chain

of at least four ubiquitins to be recognized by the proteasome [36, 94]. Despite continuing research, the identities of most E2-E3 pairings *in vivo* are unknown [68, 87].

1.1.4 Ubiquitin ligation

Ubiquitin ligases (E3s) associate with E2s to mediate the final ubiquitination of the substrate. E3s act as scaffolds that bind their substrates to bring them in close proximity to the conjugated E2~Ub, thus catalyzing ubiquitin transfer [83, 95]. By directly binding their substrates, E3 ligases control the specificity of ubiquitination, and are therefore the most abundant enzymes of the UPS. Their specificity is modulated by coupling a limited number of catalytic cores with a wide range of substrate-recruiting modules [96]. The cellular importance of E3 is highlighted by their expansion from yeast (less than 100 genes identified) to over 600 genes in humans [97], although not all identified E3 genes have intrinsic E3 activity [98-100]. Eukaryotic E3s are currently classified into three main families, although research is ongoing [101, 102]. E6AP, the first E3 ubiquitin ligase to be identified, became the founding member of the HECT (homology to E6AP carboxyl-terminus) E3 family, comprising approximately 30 members in humans [103, 104]. A RING motif first identified in RING1 (really interesting new gene 1) [105, 106] and later shown to possess ubiquitin ligase activity [107, 108] became the label for the RING E3 family [96]. With approximately 300 members in humans by recent estimates [96], RING E3s comprise 95% of all predicted E3 ligases [97]. Approximately 12 human proteins comprise a third family of ring-between-ring (RBR) E3 ligases, characterized by the presence of two RING motifs labeled RING1 and RING2 separated by an in-between RING (IBR) domain **(Figure 1.3)** [109].

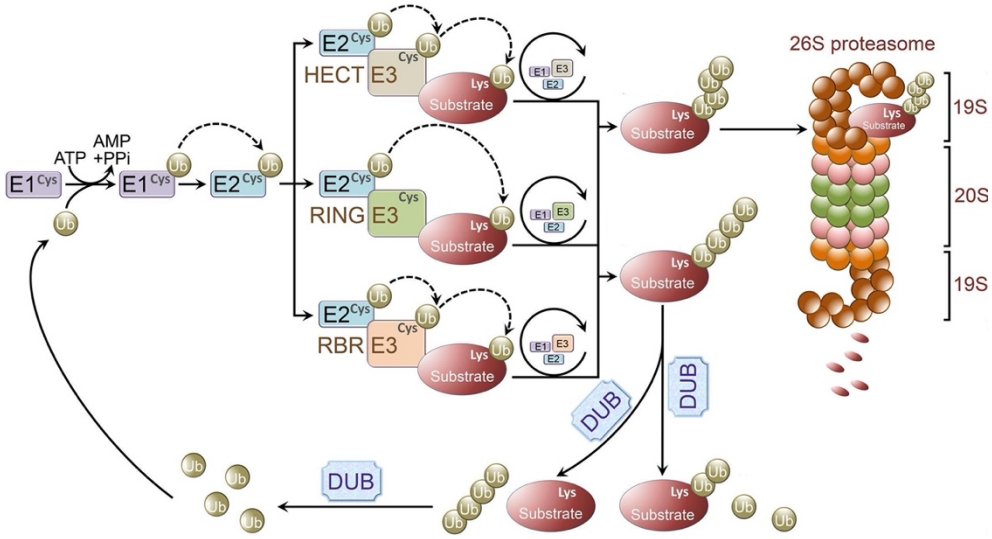

Figure 1.3. Catalytic mechanisms of the ubiquitin-proteasome system. After ATP-mediated activation, ubiquitin (Ub) gets transferred to the catalytic cysteine of an E2 enzyme. E2s then act in concert with E3 ligases to ubiquitinate a substrate lysine either directly (RING and RBR E3s) or through an E3~Ub intermediate (HECT E3s). Polyubiquitin chains can then be removed by deubiquitinating enzymes (DUBs), or the polyubiquitinated substrates recognized by proteins to be escorted to the proteasome for degradation, among other possible fates. Adapted from Zheng Q. *et al.*, 2016 [110].

RING E3s contain a RING (or a related U-box) motif that serves to recruit Ub-loaded E2s [107, 108]. The motif is defined by spaced cysteine and histidine residues that chelate two structural zinc ions within the motif core [83, 105, 107]. Through a mechanism that is shared by Ubl E3s [111, 112], RING E3s activate their bound E2~Ub by inducing conformational changes that optimally present the thioester bond for attack by a substrate lysine [113, 114]. This activation is sometimes stimulated by a Ub or Ubl non-covalently bound to the E2 [93, 115]. The resulting E3-E2~Ub complex then directly transfers ubiquitin to a substrate lysine in a thioester aminolysis reaction. By contrast, HECT E3s form an E3~Ub intermediate before transferring the Ub to a substrate lysine, in a manner analogous to E1-E2 ubiquitin transfer [116].

HECT E3s have a C-terminal catalytic domain formed by two (N-, C-) flexibly connected lobes that cooperate to bind E2~Ub [117, 118]. Transthiolation induces a conformational change that orients the C-lobe~Ub thioester intermediate towards the substrate, stimulating ubiquitin transfer [119, 120]. RBR E3s incorporate mechanistic aspects of both RING and HECT E3s. They use one of their RING motifs to bind and activate an E2~Ub, which then transfers the ubiquitin to a catalytic cysteine in the other RING motif. The RBR E3~Ub intermediate then ubiquitinates the substrate [121, 122].

E3s recognize sequences in their substrates named degrons [123]. Degrons are transferable, inducing E3:substrate interactions when synthetically fused to an unrelated protein [124]. Proteins can be detected through unmodified degrons, such as those in the N-terminus [125], C-terminus [126] or internal sequences [127, 128] of proteins, or those exposed when a protein misfolds [129, 130] or mislocalizes [131, 132]. To regulate and integrate substrate recognition with other signaling events, however, degrons are often post-translationally modified by regulatory enzymes. Examples include proline hydroxylation on HIF-1α [133-136], serine phosphorylation on IκB [137, 138], threonine phosphorylation on p27 [139, 140], multi-site phosphorylation on Cyclin E [141-143], cysteine reduction in FNIP1 [144], and N-terminal acetylation and myristoylation [145, 146]. To additionally couple degradation with cellular signals, some E3s only recognize their substrates in the presence of natural [147-153] or synthetic [154-161] organic compounds, an effect that can be exploited for biomedical purposes [162-170]. Current knowledge of the E3:substrate interactome is sparse [171-173]. Only a small fraction of E3s have known

substrate pairings, and most proteins known to undergo ubiquitination, in turn, have not been mapped to a corresponding E3 ligase [124].

A further layer of regulation is achieved by modulating the catalytic activity of E3 ligases. E3 ligases can associate with other E3s [102, 174, 175] as well as oligomerize. E3 oligomerization can bring additional E2~Ub conjugates near the bound substrate to increase Ub discharge [141] or keep E3s in an autoinhibited state [176], and can be disrupted following conformational changes induced by a binding partner or post-translational modification [153, 176-178]. Other mechanisms to regulate E3 activity include redox states [179], modulating the accessibility of E2 binding sites [180] and post-translational modifications such as phosphorylation [181-186] and ubiquitination, which can have activating [187-189] or inhibitory [190, 191] effects and be carried out by themselves [190, 192, 193] or other E3 ligases [126, 194, 195]. The archetypal regulatory E3 modification is the covalent conjugation to the ubiquitin-like protein NEDD8 (neddylation), which is fundamental for the activity of Cullin-RING ligases [196].

Cullin-RING ligases and their regulation

Cullin-RING ligases (CRLs) are the largest subfamily of RING E3s. They are involved in virtually every cellular process and are responsible for ~20% of all proteasomal degradation [197]. CRLs are multiprotein complexes that separate their catalytic and substrate-recruitment functions into different subunits [198]. CRLs share a conserved architecture and mechanism of action that was first described for Cullin 1-based CRLs (termed CRL1s or SCFs) [95, 199, 200] and then expanded to other CRLs [201, 202]. Human genomes encode six canonical Cullin (CUL1, 2, 3, 4A, 4B, 5) subunits [198, 203, 204], as well as three proteins with Cullin homology regions: CUL7, CUL9 and the

APC2 subunit of the APC/C complex [205-208]. CRLs are nucleated by one of the six canonical Cullins (CUL1, 2, 3, 4A, 4B, 5) [198]. Their globular C-terminal domains form a docking site for RBX1 [209-213] or RBX2 [214, 215], the catalytic RING subunit that binds E2~Ub. The Cullin N-terminal domain binds adaptor proteins, which in turn bind specific substrate receptors [198, 216-218]. Approximately 287 proteins in humans have motifs found in CRL substrate receptors [96]. Substrate receptors are interchangeable and target a select range of substrates each, greatly expanding the substrate recognition potential of each CRL [198]. Substrates bound by substrate receptors are juxtaposed to an RBX1/RBX2-bound E2~Ub, catalyzing the ubiquitin transfer reaction. Substrate recognition by CRLs is quickly followed by processive polyubiquitination [71], helped by assembly-disassembly cycles between CRLs and their E2s [219].

CRL activity is stimulated by neddylation of the Cullin C-terminus **(Figure 1.4)** [196, 220]. Neddylation remodels the complex, increasing the reactivity of the E2~Ubiquitin, its affinity for RBX1, and the proximity of the E2~Ub to the receptor-bound substrate [93, 221, 222]. Neddylation additionally blocks inhibitory interactions between Cullins and CAND1, an exchange factor that ejects substrate receptors from unneddylated, inactive CRLs [223-226]. Cullin neddylation is countered by the COP9 signalosome (CSN) complex, a key regulator of CRL activity [202, 227, 228]. Binding to neddylated Cullins releases an autoinhibitory interaction in CSN, which then cleaves the Culllin-NEDD8 isopeptide bond to prevent E2~Ub recruitment [229, 230]. CSN and substrate binding to CRLs is mutually exclusive [229], thus ensuring that only substrate-bound, active CRLs stay neddylated [231-233], and inactive CRLs can undergo CAND1-mediated receptor exchange to probe available substrates.

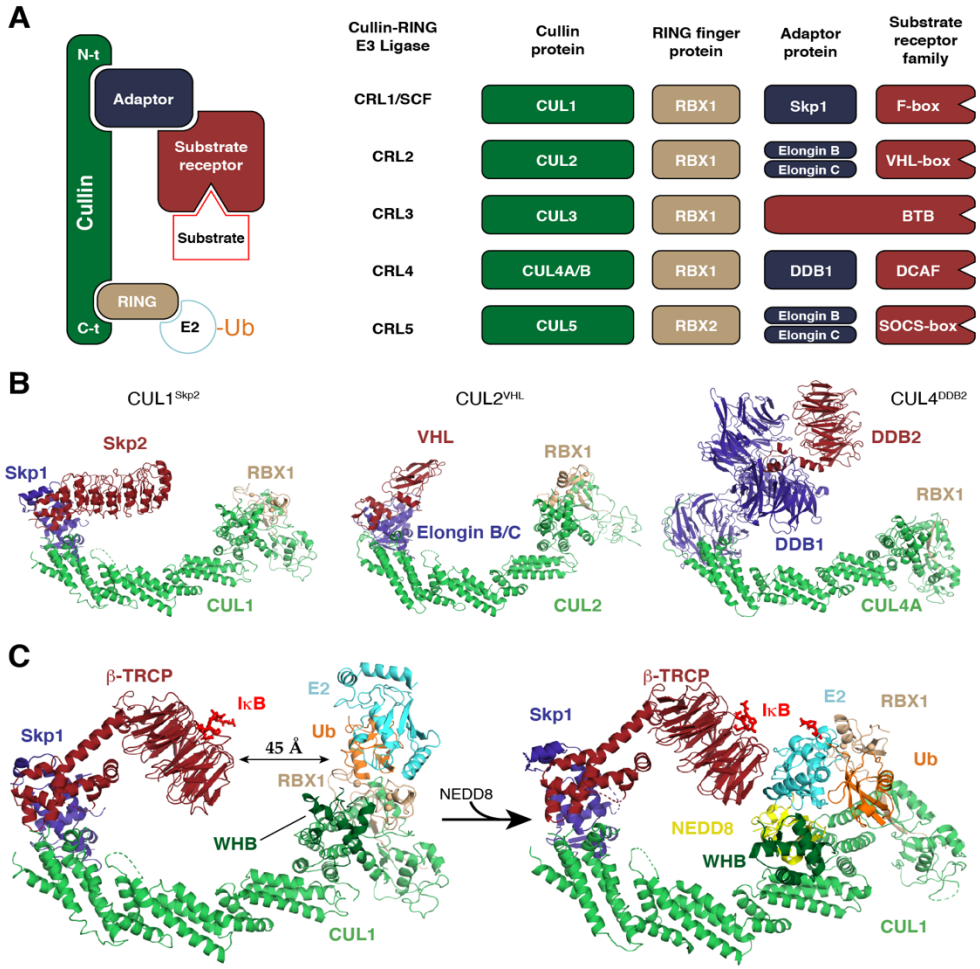

Figure 1.4. Structure and regulation of CRLs. (A) Schematic representation of the structures of canonical CRLs. Proteins with a common motif (such as F-boxes or VHL-boxes) act as substrate receptors for each Cullin. **(B)** Structural models for $CRL1^{Skp2}$ (left), $CRL2^{VHL}$ (middle) and $CRL4^{DDB2}$ (right), colored as in (A). $CRL1^{Skp2}$ was modeled from PDB IDs 1LDK [95] and 1FQV [234], $CRL2^{VHL}$ from PDB IDs 5N4W [235] and 1VBC [236], and $CRL4^{DDB2}$ from PDB ID 4A0K [202]. E2~Ub and bound substrates are not depicted. **(C)** Activation of CRLs. An unneddylated $CUL1^{β\text{-}TrCP}$ (left) becomes competent for substrate ubiquitination upon neddylation (right). Neddylation rearranges the WHB domain of Cullin 1, bringing the RBX1-bound E2~Ub conjugate in close proximity to the substrate receptor, thus allowing $CUL1^{β\text{-}TrCP}$ to ubiquitinate its bound substrate IκB. $CUL1^{β\text{-}TrCP}$ and bound E2~Ub are shown as cartoons. IκB is shown as red sticks. The unneddylated $CUL1^{β\text{-}TrCP}$ is modeled from PDB IDs 1LDK [95], 1P22 [138] and 6TTU [93]. The neddylated $CUL1^{β\text{-}TrCP}$ is modeled from PDB ID 6TTU [93].

1.1.5 Substrate degradation

Although ubiquitination can mark substrates for lysosomal degradation, the majority of eukaryotic proteins are degraded by the proteasome [47, 237]. Substrates with polyubiquitin chains signaling proteolysis are recognized by proteins that escort them to the proteasome for degradation [238-240]. With a size of ~2.5 MDa and comprising 47 subunits in humans, the proteasome is a highly complex molecular machine and the largest known eukaryotic protease [241]. Proteasomal function is indispensable for cellular proteostasis, and drugs targeting the proteasome have been used as therapeutic agents against several diseases, particularly in oncology [242, 243].

The functions of the proteasome are compartmentalized into distinct 20S and 19S subcomplexes. The 19S regulatory particle (RP) directs the processing and entry of ubiquitinated cargo into a 20S core particle (CP), in which substrates are proteolytically cleaved into short peptides [241]. To prevent premature catalytic activation, several assembly factors protect individual proteasomal subunits during their assembly, and many subunits are synthesized as precursors [244-247]. The 20S CP is formed by four heteroheptameric rings of *alpha* and *beta* subunits stacked back-to-back. The 19S RP sits on either end of the 20S CP and is formed by *lid* and *base* subcomplexes of ten and nine subunits, respectively [241]. *In vivo*, the proteasome is found as a mixture of barrel-like 20S, 26S (19S-20S) and 30S (19S-20S-19S) species, although the two latter complexes are usually referred to as “26S” in the literature [248]. Ubiquitinated substrates are recognized by the 19S base [249-251] and deubiquitinated by the 19S lid [252, 253]. Entry into the proteasome catalytic core is regulated by the concerted actions of the

19S RP and the α ring of the 20S CP, which forms an antechamber to the catalytic β core [241]. ATP hydrolysis drives the opening of the α antechamber, and substrates enter the β core to encounter catalytic threonine residues contributed by subunits of the 20S β rings [241]. These β subunits contain active sites with different proteolytic specificities, giving the 20S CP the ability to degrade a broad range of peptide bonds, including those in ubiquitin itself [254]. The peptides generated by the proteasome are then further hydrolyzed into amino acids [255], and polyubiquitin chains removed *en bloc* from the substrates [253] used to regenerate monomeric ubiquitin by polyubiquitin-specific deubiquitinases [256, 257].

1.2 *In Vivo* Aspects of Protein Complex Biogenesis

Proteins are the effectors of life. To carry out their biological role, most proteins assemble into multimeric complexes of defined architecture and composition [258]. Three fundamental processes are required to generate functional protein complexes: transcription, translation, and the folding and assembly of newly synthesized polypeptides into functional three-dimensional structures.

1.3.1 Protein synthesis

The RNA Polymerases tasked with DNA transcription are highly processive enzymes subject to fidelity errors, and have evolutionarily developed proofreading strategies to ensure transcriptional accuracy [259].

Nevertheless, transcription stochastically creates aberrant mRNA transcripts that must be efficiently detected. The high energetic cost of protein synthesis demands that translation preferentially be carried out on functional transcripts, and organisms have evolved a series of surveillance mechanisms to resolve aberrant transcription. Nonsense-mediated decay [260] and nonstop decay [261, 262] target transcripts with premature or absent stop codons, respectively. No-go decay additionally targets mRNAs stalled during elongation [263]. mRNA transcripts without functional poly(A) tails are quickly decapped and degraded by exonucleases [264].

mRNA transcripts passing these quality control checks must then be engaged by ribosomes, the large ribonucleoproteins tasked with coupling the codon-based information contained in nucleic acids to the amino acid code of proteins. Such fundamental task is ensured by built-in systems within ribosomes and further overseen by a network of quality control mechanisms [265-267]. Nonstop mRNAs induce ribosome stalling and encode aberrant proteins that are ubiquitinated co-translationally by the E3 ligase Ltn1 [266, 268, 269]. Proteins resulting from stop codon read-through contain aberrant C-terminal extensions and are similarly unstable and proteasomally degraded [270, 271]. If translation further continues into the 3' poly(A) region, it generates proteins with poly-lysine tails, which triggers ubiquitination of the nascent protein by the E3 enzyme Not4p [272, 273] and ubiquitination of the ribosome by ZNF598 [274-276]. The E3 ligases Upf1 and Ubr1 have been implicated in the ubiquitination of nascent proteins with premature stop codons [277-279]. In the case of selenoproteins, prematurely terminated chains arising from faulty decoding of a selenomethionine/stop codon are directly recognized by CRL2 E3 ligases [173]. In total, up to 15% of

ribosome-bound nascent protein chains have been proposed to be ubiquitinated *in vivo* [130, 280].

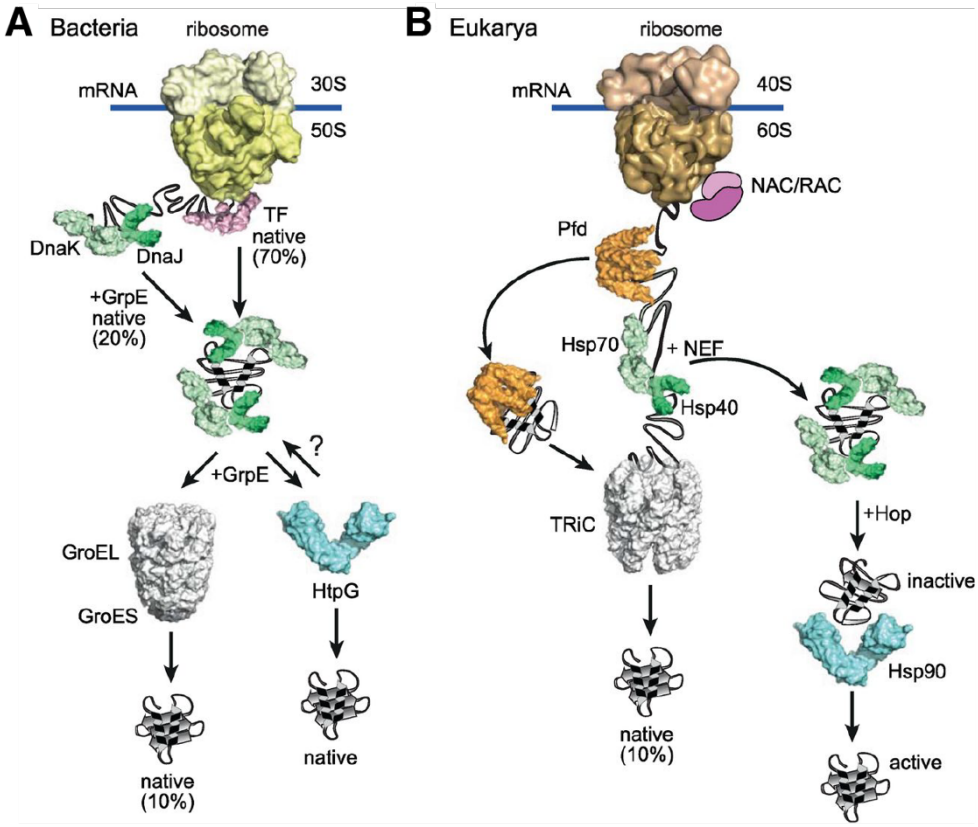

Figure 1.5. The pathways of protein folding are conserved from bacteria to humans. For ~70% of bacterial **(A)** and eukaryotic **(B)** proteins, the ribosome and associated factors [trigger factor (TF) in bacteria; nascent chain-associated complex (NAC) and ribosome-associated complex (RAC) in eukaryotes] provide folding assistance. Downstream of the ribosome, Hsp70 (DnaK in bacteria) cooperates with Hsp40s (DnaJ in bacteria) and nucleotide exchange factors (NEFs; GrpE in bacteria) to fold ~20% of the proteome. The remaining ~10% of the proteome requires chaperonins for folding [GroEL/ES in bacteria, TRiC in eukaryotes]. In eukaryotes, some nascent proteins are transferred directly to TRiC by prefoldin (Pfd). Eukaryotes also employ the Hsp90 chaperone system to catalyze the activation of metastable proteins such as kinases and transcription factors. Clients are transferred to Hsp90 via the Hsp70 system and the cochaperone Hop. The bacterial Hsp90, HtpG, is thought to act more generally in folding and functions without known cochaperones. Adapted from Balchin D. *et al.*, 2016 [281].

The folding of most proteins is driven by differences in hydrophobicity between its residues, which induce burial of hydrophobic amino acids into the protein core to form soluble domains. To facilitate this process, ribosomes associate with a network of chaperones -like the NAC/RAC complexes- that help to fold polypeptides emerging from the ribosome exit tunnel [281]. Around 70% of proteins can attain their biologically active conformation in this manner, while ~30% of proteins require further assistance from specialized chaperones like the HSP70 and HSP90 systems **(Figure 1.5)** [281]. Misfolded or misassembled proteins are prone to cytotoxic aggregation, and defects in protein folding (proteinopathies) and assembly underlie conditions like aging, cancer, and neurodegeneration [282, 283]. E3 ligases exist that detect determinants of aberrant folding, like exposed hydrophobic patches [129, 279, 284]. Proteins that pass these quality control checks are competent for assembly into complexes.

1.3.2 Protein complex assembly

While the molecular determinants of transcription and translation are relatively well characterized, current knowledge of protein complex formation is comparatively sparse. The biogenesis of protein complexes is a complex process. Human ribosomes, as an example, are composed of 80 protein subunits and four rRNA molecules, but require over 200 assembly factors for their assembly [285].

For protein complexes to form, newly synthesized subunits must come together spatially and temporally, developing inter-subunit interfaces while simultaneously avoiding aberrant interactions with unrelated cellular components. Assembly must additionally happen stoichiometrically and not generate potentially cytotoxic intermediates. To facilitate this process,

organisms -most notably prokaryotes- organize functionally related genes into operons, and differentially express the ORFs within the resulting mRNAs to match the stoichiometry in the final complex [286-288]. A similar effect is achieved by genetic fusions between separate functional domains into single proteins, predominantly in yeast [289]. Several post-transcriptional mechanisms further promote complex assembly. The mRNAs of functionally related proteins often co-localize *in vivo* [290, 291], and nascent subunits frequently interact with their partners co-translationally [292, 293]. Interactions between folded proteins can be further aided by assembly-guiding chaperones [241, 294-296].

Despite these regulatory mechanisms, complex assembly remains an intrinsically error-prone process and non-stoichiometric subunit synthesis, as well as stochastic errors in assembly, continuously generate protein orphans and defective protein complexes [297-299]. Around half of all mammalian protein complexes are produced with at least one subunit synthesized in non-stoichiometric amounts [300], and up to 10% of the nascent proteome is estimated to arise from non-stoichiometric or failed assembly [297]. Furthermore, the subunit stoichiometry of many eukaryotic complexes varies across cell types and throughout differentiation [300]. Subunit imbalances, particularly in the context of altered gene expression like stress or cancers, can generate cytotoxic species through aggregation or gain as well as loss of function [241, 299].

1.3.3 Assembly Quality Control

Biochemical observations over the last half a century have shed light on the *in vivo* mechanisms regulating complex assembly. Over 40 years ago it was seen that loss of one subunit can induce the degradation of its partners within

the complex [301], and that non-stoichiometric subunit synthesis can generate stoichiometric complexes [302]. An explanation offered to explain such behavior was that the stability of proteins is linked to assembly into complexes [303-308]. This hypothesis gained weight after proteomic experiments showed that subunits of protein complexes follow different degradation kinetics in cells than monomeric proteins [297]. The stability of most proteins *in vivo* cannot be accurately predicted from factors such as mRNA half-life and protein abundance alone, and instead appears to depend on post-translational events like ubiquitination [297, 309]. With its vast array of degron-recognizing E3 ligases, the UPS is a prime candidate for the regulation of complex assembly. Supporting a role for the UPS as a major assembly regulator, up to 30% of the nascent proteome has been seen to be degraded shortly after synthesis [310], although the actual number might be lower [297, 311], and most ubiquitinated proteins are relatively young [312]. The necessity for robust ubiquitination and degradation of unassembled proteins is highlighted by observations that up to 10% of the proteome arises from non-stoichiometric subunit synthesis and failed assembly [297].

Analogous to transcription and translation, it has become evident in recent years that the UPS ensures the correct assembly of several protein complexes [313, 314]. AQC E3 ligases detect degrons that become hidden or nonexistent when the proteins harboring them correctly assemble into functional complexes **(Figure 1.6)**. AQC E3 ligases employ several strategies to detect incorrect or incomplete assembly. These include the recognition of exposed inter-subunit surfaces [132, 315-318], reading out chaperone-subunit interactions to verify complete assembly [319], probing the stability of protein complexes to dissolve unstable assemblies [298, 320], and detecting

unassembled subunits that mislocalize to the wrong cellular compartment [321].

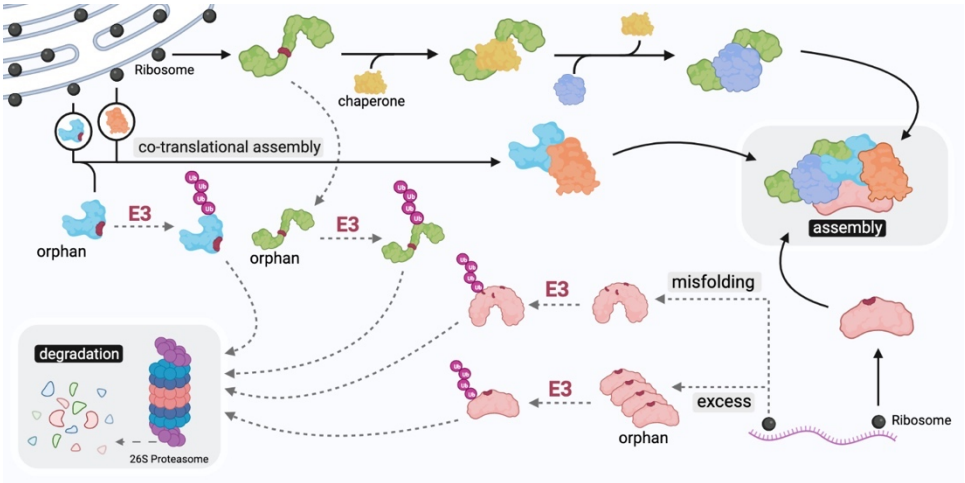

Figure 1.6. The UPS oversees complex assembly. The subunits of a protein complex might be synthesized in different cellular locations and must come together for functional assembly. Unassembled subunits of protein complexes are often recognized via degrons (shown in red) hidden in the assembled complex. Proteins can hide these surfaces with the help of chaperones or by assembling with their partners post- or co-translationally. Proteins that misfold or fail to bind their partners are polyubiquitinated (Ub) by E3 ligases for proteasomal degradation. Adapted from Pla-Prats C. & Thomä NH, 2022 [313].

1.3 The CRL4^{DCAF12} E3 Ubiquitin Ligase

DCAF12, also known as WDR40A and TCC52 [322], was first identified in proteomic experiments as the substrate receptor subunit of a CUL4-RBX1-DDB1-DCAF12 (CRL4^{DCAF12}) E3 ubiquitin ligase [201]. As such, DCAF12 directs the catalytic activity of the CRL4^{DCAF12} ligase towards the substrates that it directly binds. CRL4s are comprised of a

CUL4A/CUL4B E3 ligase arm that simultaneously binds an activated E2~Ub enzyme on its C-terminal region through protein RBX1 and a DDB1 adaptor protein on its N-terminus [201]. Like other CRLs, CRL4s are modular, and DDB1 recruits interchangeable substrate receptors that in turn bind their substrates to induce their ubiquitination [201, 323-326]. DCAF12 is conserved across metazoans and ubiquitously expressed in human tissues [327]. DCAF12 has been broadly linked to the transduction of pro-apoptotic signals required for programmed cell death in tissue growth and morphogenesis, and in supporting synaptic plasticity and function [328-330]. DCAF12 further regulates the Hippo pathway, a conserved regulator of tissue growth across metazoans and a common driver of tumorigenesis in human cancers [331]. DCAF12 has also been proposed to regulate T cell homeostasis and spermatogenesis in mice and humans by downregulating MOV10, and to induce autophagy in human cells by downregulating MAGEA-3 and MAGEA-6 [332, 333].

Reporter screens have identified proteins that are degraded in a DCAF12-dependent manner in human cells [126]. Common to over 40 of these proteins is a di-Glu motif at their extreme C-terminus. The motif is necessary and sufficient for ubiquitination of their hosts and has been described as the canonical degron recognized by DCAF12 [126]. Additional DCAF12 substrates were however later identified that do not harbor di-Glu degrons [331, 332]. DCAF12 downregulates MOV10, an RNA helicase involved in post-transcriptional gene silencing, during T cell development and spermatogenesis [332]. Recognition is mediated by the Glu-Leu end of MOV10, and a range of proteins with noncanonical Glu-Leu degrons appear to be substrates of DCAF12 [332]. Yet of the potential di-Glu degron-containing substrates identified to date, only MAGEA-3, MAGEA-6,

MOV10 and GART have been shown to bind DCAF12 *in vitro* [332, 333]. Hippo pathway effectors Yki/Yap/Taz and synaptic glutamate receptor subunits GluRIIA/GluRIIB/GluRIIC do not bear C-terminal degrons, and likely carry alternative degrons or are indirect targets of DCAF12 [331]. To date, the molecular mechanism of substrate binding by DCAF12 is unknown. Other E3 ubiquitin ligases exist that recognize degrons located at the extreme C-terminus of their substrates [334], but only a subset of these "C-end" ligases has been structurally and functionally characterized [335-338].

In contrast to degrons requiring post-translational modifications for recognition, C-end degrons are seemingly unmodified, and their presence and availability appears sufficient to trigger degradation of their hosts [339]. C-end degrons were initially discovered in aberrant protein products and postulated to signal defective protein synthesis [173], but they were later identified in full-length, functional human proteins [126, 339], raising the question of whether their recognition mechanism results in constitutive substrate ubiquitination or if additional regulatory mechanisms are in place. One of the di-Glu degron-containing proteins identified as a potential substrate of DCAF12 *in vivo* is CCT5, a subunit of the TRiC chaperonin [126].

1.4 The Eukaryotic Chaperonin TRiC

Chaperonins are multi-subunit chaperones specialized in the folding of aggregation-prone substrates. Their barrel-like structures have large internal

cavities within which substrates can fold unimpeded by aggregation. Chaperonins are divided into two groups, both of which share a common architecture composed of two rings of seven to nine subunits stacked back-to-back. Group I chaperonins occur in bacteria (GroEL) and cellular compartments of endosymbiotic origin (Hsp60 in mitochondria [340] and Cpn60 in chloroplasts [341]) and require a “lid" cofactor for substrate encapsulation (GroES in bacteria, Hsp10 in Eukarya [342]) [343, 344]. Group II chaperonins occur in archaea (thermosome [345]) and the eukaryotic cytosol (TRiC) and encapsulate their substrates via helical extensions in each subunit [346, 347]. Chaperone subunits are highly allosteric, and sequential ATP-induced conformational changes modulate the energetic landscape inside the cavity to guide the substrate along a productive conformational pathway **(Figure 1.7)** [348, 349]. Chaperonins are fundamental for cellular proteostasis and essential in all domains of life [281].

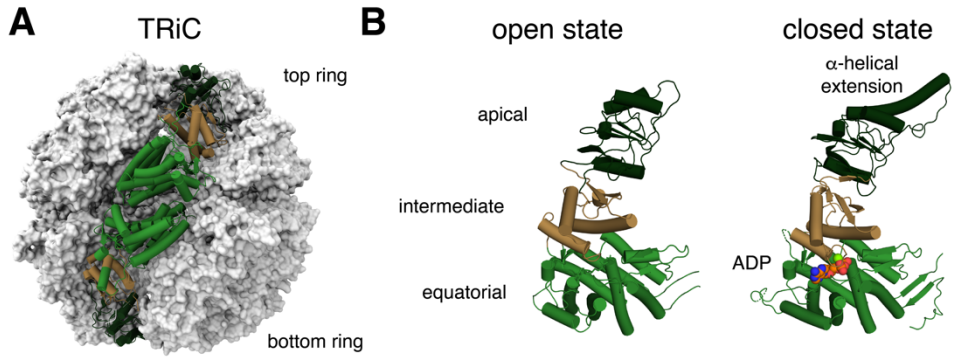

Figure 1.7. The eukaryotic chaperonin TRiC. (A) Structure of TRiC (PDB ID 4V94 [350]) in the closed conformation, shown as surface. Two subunits occupying opposite positions in either ring are shown as cartoons. **(B)** Structures of chaperonin subunits in the open (PDB ID 3KFK [351]) and closed (PDB ID 4V94 [350]) states. Substrates are encapsulated inside the cavity with the help of α-helical extensions in individual chaperonin subunits. ADP (shown as spheres) is bound in the equatorial domain in the closed state with the help of a magnesium cation (shown as a green sphere).

TRiC, also called CCT (Chaperone Containing TCP1) is the only chaperonin present in the cytosol of eukaryotes [352]. TRiC directly interacts and cooperates with chaperones like the Hsp70, Hsp90 and prefoldin systems, from which it receives difficult to fold substrates for encapsulation [353-358]. In contrast to group I and thermosome chaperonins, which are formed by less than three subunits and are often homo-oligomeric [342], TRiC is formed by eight paralogue subunits (and a testes-specific CCT6 isoform, CCT6B) named CCT1-8, which differ in substrate preference and affinity for ATP. This variability allows TRiC to specialize in the folding of a unique range of client proteins [356, 359, 360]. All CCT subunits adopt a curved shape formed by equatorial, intermediate and apical domains connected by hinge regions. The equatorial domains bind ATP, while the intermediate domains transmit nucleotide-induced conformational changes to the apical domains, which bind substrates [346]. CCT subunits arrange into double octameric rings stacked back-to-back through their equatorial domains [352, 361]. The resulting barrel-like structure contains a large cavity with surfaces contributed by each CCT subunit. Inside the cavity, TRiC substrates rely on a correct arrangement of electrostatic patches to fold [362]. Uncertainty around the precise subunit arrangement within TRiC rings [363-368] was resolved after proteomic and combinatorial homology studies [350, 362, 369] determined and later structural studies [361, 370] confirmed an intra-ring subunit order of CCT 1-3-6-8-7-5-2-4. All CCT genes are essential, and reductions in TRiC activity have detrimental effects in cells [371, 372]. TRiC is absolutely necessary for the folding of ~10% of the human proteome, including key cytoskeletal components actin and tubulin, Alzheimer's Tau protein and mTOR [356, 370, 373-375], and has been linked to human pathologies such

as cancers and neurodegenerative diseases [376, 377], making it a key cellular complex to alleviate proteotoxic stress.

1.5 Scope and Thesis Outline

The scope of this Thesis is to examine whether the C-terminal degrons recognized by DCAF12 serve as signals for complex assembly. To dissect the molecular determinants of di-Glu degron recognition and gain insight into the role of DCAF12 in AQC, this work focused on the interaction between $CRL4^{DCAF12}$ and CCT5, a subunit of the TRiC chaperonin. CCT5 harbors a C-terminal di-Glu degron, and has been proposed to be an *in vivo* substrate of DCAF12 [126]. It was hypothesized that $CRL4^{DCAF12}$, through its interaction with CCT5, serves as an AQC ligase assisting TRiC assembly and homeostasis. To address this question, structural studies of a CCT5-bound DCAF12 were combined with a biochemical characterization of its interaction with CCT5 and TRiC. The goal of this work is thus to understand the molecular mechanisms of CCT5 binding by DCAF12 and the behavior of $CRL4^{DCAF12}$ towards TRiC. The main research question is thus:

> **Main research question:** Can C-terminal degrons recognized by DCAF12 serve as signals for complex assembly?

This main research question is addressed through a series of subquestions:

1. Does DCAF12 assemble into a functional E3 ubiquitin ligase?
2. Does $CRL4^{DCAF12}$ target CCT5 for degradation? If so, what are the binding determinants of the interaction between CCT5 and DCAF12?
3. What is the structure of DCAF12?
4. How does DCAF12 recognize the CCT5 di-Glu degron?
5. What is the architecture of the CCT5-bound $CRL4^{DCAF12}$ E3 ligase?
6. Does $CRL4^{DCAF12}$ differentially recognize CCT5 and TRiC? If so, what is the reason behind the differential recognition?

This Thesis contains nine distinct chapters. **Chapter 2** presents the efforts carried out to reconstitute and purify the DDB1-DCAF12 complex and its substrate CCT5. CCT5 is shown to bind DDB1-DCAF12, and the molecular determinants of the interaction between CCT5 and DDB1-DCAF12 are examined. **Chapter 3** present high-resolution structures that elucidate the structure of DDB1-DCAF12 and the molecular mechanism of di-Glu degron binding by DCAF12. The proposed mode of binding is consistent with the observations of Chapter 2 and suggests a mechanism by which $CRL4^{DCAF12}$ can recognize TRiC assembly. **Chapter 4** tests out that possibility and lays out functional findings that show that $CRL4^{DCAF12}$ differentially recognizes CCT5 and TRiC, along with a structural rationale for the differential targeting. **Chapter 5** presents a discussion of the experimental results presented in chapters 2, 3 and 4. It returns to the research questions outlined in this section to answer them with insights from the previous chapters, further analyzing the implications of the presented experimental results and addressing biological questions unanswered by this Thesis. **Chapter 6** and

Chapter 7 contain a published review article and a submitted research article originating from the candidate's doctoral work, respectively. **Chapter 8** contains the detailed experimental procedures carried out to obtain the findings presented in this Thesis. **Chapter 9** concludes the Thesis by providing references to the scientific literature used to introduce this work and to support the arguments used throughout.

Chapter 2

Biochemical Characterization of DDB1-DCAF12-CCT5 Complexes

The experiments presented in this chapter were carried out to gain an insight into the binding determinants of CCT5 to DCAF12 and to produce specimens for structure determination. Figures are labeled numerically by the order in which they are referenced in the text with a prefix for the chapter number (2). Mass-spectrometric identification of MC30 was carried out by Vytautas Iesmantavicius [378] and Daniel Hess [379]. Negative-stain EM analysis of DDB1-DCAF12-CCT5 was performed under the guidance and support of Simone Cavadini [380].

2.1 Purification of DDB1-DCAF12-CCT5 Complexes

2.1.1 DDB1-DCAF12

Very little information was published on DCAF12 at the time of the start of this project [126, 201, 322, 329, 381, 382]. Domain predictions on the UniProt [383] or HHPred database [384, 385] showed a 6-bladed β-propeller with a C-terminal domain of unknown function (which will be shown in Chapter 3 to be incorrect) and an N-terminal helical region. In 2006, DCAF12 was identified in a landmark study by Angers S. *et al.* [201] as a putative CRL4 substrate receptor, but none of its substrates were identified. In 2019, Koren I. *et al.* [126] confirmed the functional association of DCAF12 into a $CRL4^{DCAF12}$ E3 ubiquitin ligase and reported that DCAF12 ubiquitinated a

series of GFP-polypeptide reporters that ended in a double glutamate (di-Glu) motif. Their study identified TRiC subunit CCT5 as a potential *in vivo* substrate of DCAF12. DDB1-DCAF12 is the minimal soluble substrate receptor module of the $CRL4^{DCAF12}$ E3 ligase with a known mode of binding to CUL4-RBX1 [201], and so studies on the subcomplex can inform on the larger $CRL4^{DCAF12}$ E3 ubiquitin ligase. A first aim was therefore to biochemically reconstitute the DDB1-DCAF12 complex and study its interaction with CCT5. The studies on di-Glu degron degradation were carried out in human cells, and sequences encoding *H. sapiens* DCAF12 were codon-optimized for recombinant expression in *Trichoplusia ni*. Anticipating crystallization trials of DDB1-DCAF12 complexes, additional expression vectors were created for the expression of *Rattus Norvegicus* (rat), *Gallus gallus* (chicken) and *Danio rerio* (zebrafish) DCAF12, which are 98-71 % homologous to *H. sapiens* DCAF12. CRL4 substrate receptors CSA and DDB2 -the closest human homologue to DCAF12- bind DDB1 through an N-terminal helix-loop-helix motif, and bind their substrates through globular C-terminal domains [202, 386]. To test whether DCAF12 similarly assembles into a CRL4 ligase through its N-terminus, additional expression vectors were created for the expression of Δ(1-63) human DCAF12 and the equivalent truncations for rat, chicken, and zebrafish DCAF12, which do not contain the predicted N-terminal helical regions.

Full-length and N-terminally truncated human DCAF12 and its rat, chicken and zebrafish homologues were first tested for their expression level and association with DDB1 in small-scale affinity pull-downs. In short, a small quantity of insect cells was co-infected with baculovirus expressing his6-tagged human DDB1 and strep(II)-tagged DCAF12 constructs. 2 days after infection, the cells were lysed and the lysate incubated with anti-strep(II)

affinity resin. The beads were then washed and incubated with SDS protein dye to elute bound proteins. Complex expression and stoichiometry were analyzed by SDS-PAGE. Full-length (FL) human (hs) and zebrafish (dr) DCAF12 associated with DDB1, and expressed well in their full-length or truncated forms **(Figure 2.1A)**. Chicken (gg) DCAF12 did not appear to stably associate with DDB1. Rat (rn) DCAF12 did not express, and these constructs were not pursued further. All truncated DCAF12 constructs did not pull down DDB1 *in vitro*, confirming that DCAF12 uses its N-terminal helical region to bind DDB1 **(Figure 2.1A)**. A ~30 kDa contaminant was seen in these pull-downs and in subsequent purifications of the human DDB1-DCAF12 complex **(Figure 2.1B)**. Size exclusion chromatography showed that this contaminant stably associated with DDB1-DCAF12, generating a DDB1-DCAF12-MC30 species of slightly larger molecular weight **(Figure 2.1B)**. Although its elution slightly overlapped with that of the pure DDB1-DCAF12 complex, the purification protocol developed allowed for the minimization of the co-purification of the two complexes **(Figure 2.1B)**. Purification was not attempted for hsDDB1-rnDCAF12 or hsDDB1-ggDCAF12 after the insight gained from the expression tests **(Figure 2.1A)**. hsDDB1-drDCAF12 complexes showed a tendency to aggregate and/or bind the HSP70 and HSP90 chaperones, and were not pursued further. hsDDB1-hsDCAF12 complexes could however be purified in satisfactory quantities and purity **(Figure 2.1B)**. Purifications of N-terminally truncated zebrafish DCAF12 were avoided due to the excessive amino acid divergence and unstable behavior of the hsDDB1-drDCAF12 complex, and efforts were focused on the N-terminally truncated human and chicken DCAF12, which were purified to homogeneity **(Figure 2.1C)**.

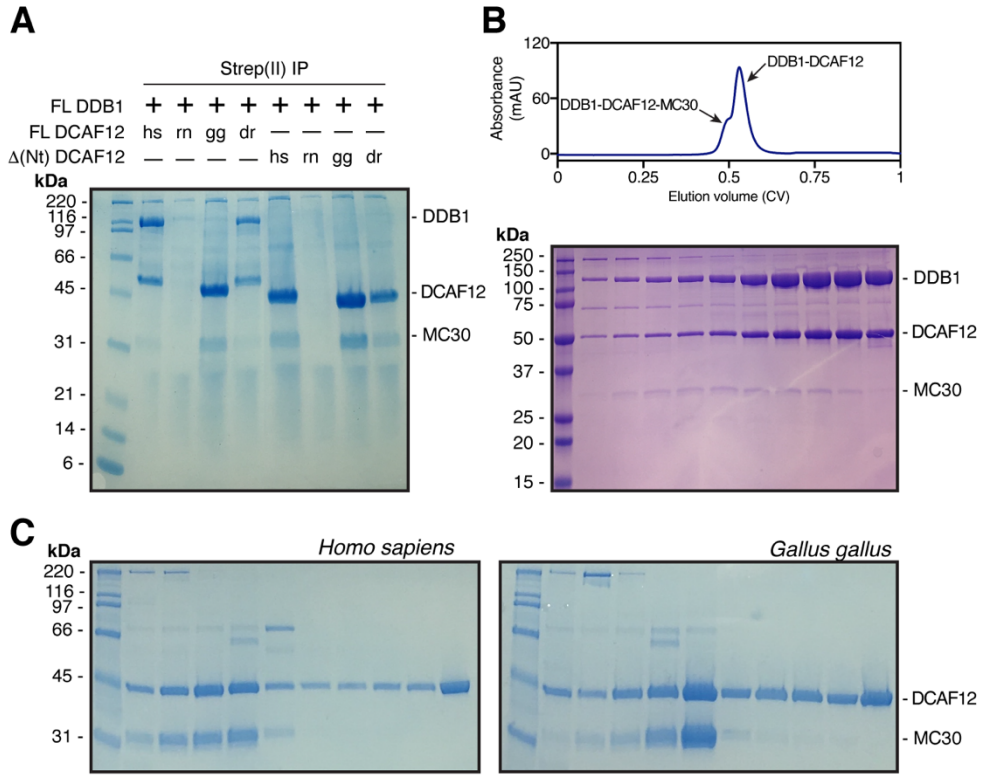

Figure 2.1. Purification of DDB1-DCAF12 complexes. (A) Expression tests for DDB1-DCAF12 and DCAF12 Δ(Nt) constructs. **(B)** Top: a size exclusion chromatograph for a low-yield purification of hsDDB1-hsDCAF12. The contribution of the DDB1-DCAF12-MC30 species to the chromatograph absorbance (measured in arbitrary absorbance units, mAu) is evident in low-yield purifications as a smaller peak that elutes before the DDB1-DCAF12 peak. Bottom: SDS-PAGE of contiguous chromatography fractions of a high-yield elution peak corresponding to the hsDDB1-hsDCAF12 complex. The DDB1-DCAF12-MC30 species elutes earlier and co-purified with chaperone HSP70, a sign of an unstable complex. **(C)** SDS-PAGE of non-contiguous fractions of size exclusion chromatographs of the human and chicken Δ(Nt) DCAF12. The pronounced size different between the Δ(Nt) DCAF12 (~46 kDa) and Δ(Nt) DCAF12-MC30 (~76 kDa) complexes facilitates their chromatographic separation.

Although initially believed to be a degradation product of DDB1, the ~30 kDa contaminant was however observed in purifications of Δ(Nt) DCAF12 constructs -which do not co-purify with DDB1-, identifying the contaminant

as a separate protein entity that directly binds DCAF12. Furthermore, its binding to DCAF12 in the presence or absence of DDB1 signaled that they do not compete for the same surface. It was therefore likely that MC30 bound the DCAF12 substrate-binding domain and could thus be a substrate of DCAF12. The contaminant was identified mass-spectrometrically as originating from the baculoviral expression system (UniProt ID P41473). The protein, which was given the name MC30, is a 265-amino acid uncharacterized polypeptide from the IAP2-VLF1 intergenic region of the Autographa californica nuclear polyhedrosis virus (AcMNPV) and ends in a Glu-Leu motif. This suggested that the DCAF12 pocket can accommodate substrates with the C-terminal residue substituted with a different amino acid. Two years later it was reported that DCAF12 recognizes noncanonical Glu-Leu degrons [332].

2.1.2 DDB1-DCAF12-CCT5

Purifications were then attempted for the 59.7 kDa human CCT5 protein. CCT5 expressed well in insect cells and could be purified with minimal contaminants **(Figure 2.2A)**. Purified CCT5 was monomeric, as judged by multi-angle light scattering in combination with size exclusion chromatography (SEC-MALS) **(Figure 2.2B)**. Unexpectedly, CCT5 bound DCAF12 efficiently *in vitro*. In anti-strep(II) pull-downs, purified CCT5 displaced MC30 from a his6-DDB1-strep(II)-DCAF12-MC30 complex, indicating that the two compete for the same binding site and confirming that MC30 is a substrate of DCAF12 **(Figure 2.2C)**. The interaction between CCT5 and DCAF12 persisted through different chromatographic steps, allowing for the purification of a hsDDB1-hsDCAF12-hsCCT5 complex **(Figure 2.2D)**. Studies on the DDB1-DCAF12-CCT5 complex were

thereafter carried out with all human proteins. MC30 impurities were not observed in DDB1-DCAF12-CCT5 purifications.

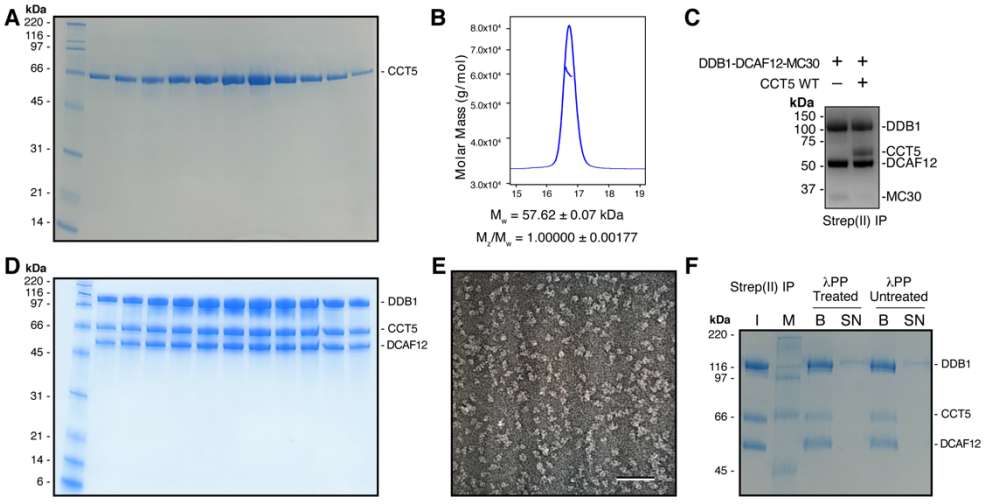

Figure 2.2. Purification of CCT5 and DDB1-DCAF12-CCT5 complexes. (A) SDS-PAGE of contiguous size exclusion chromatography fractions of an elution peak corresponding to human CCT5. **(B)** SEC-MALS analysis of purified wild type CCT5. The chromatogram displays Rayleigh ratio curves for CCT5 together with the molar mass (in Da) of the main peak. The calculated molecular weight (M_w) corresponds to a CCT5 monomer. The polydispersity of the peak (M_z/M_w) indicates a uniform species in the peak. **(C)** Untagged CCT5 displaces MC30 from his_6-DDB1-strep(II)-DCAF12 *in vitro*. A his_6-DDB1-strep(II)-DCAF12-MC30 complex was immobilized on anti-strep(II) beads and incubated with untagged CCT5. The beads were then washed and incubated with SDS protein buffer to elute bound proteins. **(D)** SDS-PAGE of contiguous chromatography fractions of an elution peak corresponding to the human DDB1-DCAF12-CCT5 complex. **(E)** Negative-stain EM micrograph image of a human DDB1-DCAF12-CCT5 complex. Scale bar: 50 nm. **(F)** Input (I) his6-DDB1-strep(II)-DCAF12-his6-CCT5 was bound to anti-strep(II) beads 30 min at 30 °C in the presence or absence of lambda protein phosphatase (λPP). The supernatant (SN) was removed and the beads washed. The fraction bound to the beads (B) contained stoichiometric amounts of CCT5 in both cases, and no CCT5 was observed in the supernatant. M: molecular weight marker.

The human DDB1-DCAF12-CCT5 complex showed heterogeneous albeit discrete and well-behaved particles in negative-stain transmission electron microscopy (EM) **(Figure 2.2E)**. Subsequent EM studies were therefore

carried out with all human proteins. The traditional view of E3 ligases is that they are not constitutively active but instead target substrates in response to specific cues such as post-translational modifications. Treatment of a DDB1-DCAF12-CCT5 complex with lambda protein phosphatase, an enzyme that efficiently dephosphorylates serine, threonine and tyrosine residues, did not abolish the interaction between CCT5 and DCAF12 **(Figure 2.2F)**. These observations showed a unique mode of substrate biding by DCAF12 and suggested that its substrate binding site is plastic [332], while simultaneously establishing protocols for the recombinant expression and purification of DDB1-DCAF12, CCT5 and DDB1-DCAF12-CCT5 complexes for biochemical and structural studies.

2.2 Characterization of CCT5 Binding by DCAF12

To quantify the affinity and identify the binding determinants of the interaction between CCT5 and DCAF12, untagged wild type CCT5 or a CCT5 (1-529) mutant without the 12 C-terminal amino acids were recombinantly expressed and purified. Wild type CCT5 efficiently bound DDB1-DCAF12 in vitro **(Figure 2.3A)**. The interaction was dependent on the di-Glu degron: a CCT5 (1-529) mutant without the 12 C-terminal residues (Δ(Ct)) did not bind DDB1-DCAF12 **(Figure 2.3A)**. A time-resolved fluorescence energy transfer (TR-FRET) assay was then set up to monitor binding of a CCT5 C-terminal peptide to DDB1-DCAF12. In the assay, biotinylated DDB1-DCAF12 was complexed to terbium-streptavidin

(Tb-SA), a high yield fluorescence donor. The resulting $_{Tb}$DDB1-DCAF12 complex was mixed with a peptide corresponding to the 20 C-terminal amino acids of CCT5 (^{488}CCT5$_{20}$; CCT5 amino acids 522-541) conjugated to the fluorescent label ATTO488, which contains the di-Glu motif and acts as a fluorescence acceptor. Spatial proximity between the donor and acceptor groups results in fluorescence energy transfer, establishing a readout for binding. Increasing concentrations of ^{488}CCT5$_{20}$ were titrated to a $_{Tb}$DDB1-DCAF12 complex. The observed binding isotherm was biphasic and exhibited an initial hyperbolic phase followed by a linear increase. The observed K_d for the ^{488}CCT5$_{20}$ peptide was 245 ± 52 nM after subtraction of the unspecific linear component **(Figure 2.3B)**, which becomes predominant at ^{488}CCT5$_{20}$ concentrations above ~1 µM **(Figure 2.3C)**. The specific nature of the hyperbolic part of the isotherms was verified by counter-titrating with an unlabeled CCT5$_{20}$ peptide **(Figure 2.3D)**, and the corresponding concentration range was used for subsequent experiments. Back-titration with an unlabeled CCT5$_{20}$ peptide resulted in a similar affinity (IC_{50} = 404 ± 103 nM; Ki = 212 ± 53 nM) demonstrating that the presence of the N-terminal ATTO488 fluorescence label does not significantly contribute to binding **(Figure 2.3E)**. Competitive titrations were carried out to determine the contribution of the di-Glu degron to DCAF12 binding. Unlabeled full-length CCT5 or an unlabeled CCT5$_{20}$ peptide were titrated against a $_{Tb}$DDB1-DCAF12 complex pre-assembled with a ^{488}CCT5$_{20}$ peptide ($_{Tb}$DDB1-DCAF12^{488}), and the resulting decrease in fluorescence was used as a readout for binding. Full-length CCT5 bound DDB1-DCAF12 (IC_{50} = 219 ± 43 nM) with an apparent affinity that was similar to that of the CCT5$_{20}$ degron peptide (IC_{50} = 404 ± 103 nM) **(Figure 2.3E)**. Thus, DDB1-DCAF12

directly binds CCT5 with an affinity in the low nanomolar range, and binding is driven by the C-terminus of CCT5.

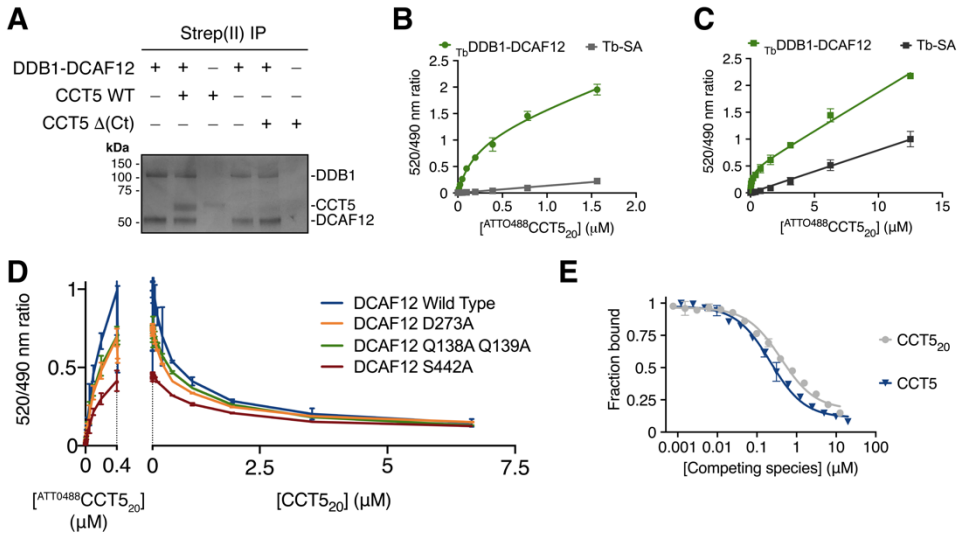

Figure 2.3. CCT5 is a substrate of DCAF12. (A) In vitro pull-downs between strep(II)-tagged DDB1-DCAF12 and untagged wild type (WT) CCT5 or CCT5 (1-529) (Δ(Ct)) seen on a Coomassie-stained SDS-PAGE gel. **(B)** Titration curves between a fluorescent $^{ATTO488}CCT5_{20}$ degron peptide and $_{Tb}$DDB1-DCAF12 or terbium-coupled streptavidin (Tb-SA) (n=3). Signal originating in the absence of $_{Tb}$DDB1-DCAF12 is unspecific and was subtracted in subsequent experiments. **(C)** Titration curves between a fluorescent $^{ATTO488}CCT5_{20}$ degron peptide and $_{Tb}$DDB1-DCAF12 or Tb-SA (n=3). Signal originating in the absence of $_{Tb}$DDB1-DCAF12 is unspecific and becomes dominant at high $^{ATTO488}CCT5_{20}$ concentrations. **(D)** Left: titrations between 0-0.4 μM $^{ATTO488}CCT5_{20}$ and mutant DDB1-DCAF12 complexes. The maximum fluorescent signal originating from the titrations was then outcompeted with a label-free $CCT5_{20}$ peptide (right). **(E)** TR-FRET counter-titration of unlabeled wild type CCT5 or an unlabeled $CCT5_{20}$ peptide into pre-assembled $_{Tb}$DDB1-DCAF12^{488} (n=3).**Data information:** In **(B,C,D,E)**, data is presented as means ± 95% confidence interval (CI).

The TR-FRET assay was then used to carry out competition experiments with label-free CCT5 degron peptides ranging in lengths between 20 to 2 amino acids, all of which retain the C-terminal di-Glu motif. These peptides were titrated against $_{Tb}$DDB1-DCAF12^{488} complex, and the resulting decrease in

fluorescence was used as a readout for binding. Maximal binding was observed when the C-terminal CCT5 peptide were eight residues or longer **(Figure 2.4A)**. Truncating the degron peptide to six residues or less impaired binding, such that the $^{488}CCT5_{20}$ probe was not fully outcompeted at a concentration of 12.5 μM. Only traces of binding were observed for a di-Glu di-peptide at 12.5 μM, the highest tested experimental concentration **(Figure 2.4A)**. The sequence features of di-Glu degrons were initially identified in peptides of at least ten residues in length [126]. In accordance, the measurements presented here show that a sequence context of eight residues is sufficient for di-Glu degron binding.

The sequence dependence of the CCT5 di-Glu degron for binding to DCAF12 was then studied. In vivo screening of DCAF12 substrates previously identified the two C-terminal glutamates (designated -1 and -2 from the C-terminus) as the core DCAF12 recognition element [126]. A greater relative importance of the -2 degron position was later suggested by the discovery of noncanonical Glu-Leu degrons [332] and observations presented here that DCAF12 binds Glu-Thr ends **(Figure 2.2C)**. To study the importance of sequence-specific contacts between DCAF12 and CCT5, the TR-FRET competition assay was used on a peptide comprising the CCT5 C-terminal degron ($CCT5_{10}$; CCT5 amino acids 532-541) with individual alanine mutations introduced at each degron position. The mutant peptides were titrated assay against a $_{Tb}$DDB1-$DCAF12^{488}$ complex **(Figure 2.4B)**. The $CCT5_{10}$ peptide showed a 15-fold decrease in affinity when mutated to alanine in the -1 position (E541A; IC_{50} ~ 6.2 μM) compared to wild type $CCT5_{10}$ (IC_{50} = 390 ± 115 nM) **(Figure 2.4B)**. The effect was more pronounced when the -2 position was mutated (E540A; IC_{50} > 50 μM). DCAF12 tolerated mutations to hydrophobic amino acids in the -1 and -2

degron positions better than mutations to polar or charged amino acids, including lysine and aspartate **(Fig 2.4C)**. Mutations in the amino acids preceding the C-terminal glutamates did not exhibit equally pronounced effects when mutated to alanine, and displayed different behaviors **(Fig 2.4B)**. Peptides mutated in degron positions -4 (E538A; IC_{50} = 571 ± 103 nM), -6 (P536A; IC_{50} = 417 ± 53 nM) and -8 (R534A; IC_{50} = 395 ± 68 nM) displayed similar affinities than the wild type sequence (WT; IC_{50} = 363 ± 78 nM), while mutations in positions -3 (S539A; IC_{50} = 125 ± 15 nM), -5 (G537A; IC_{50} = 100 ± 11 nM), -7 (L535A; IC_{50} = 208 ± 26 nM), -9 (I539A; IC_{50} = 209 ± 25 nM) and -10 (E532A; IC_{50} = 222 ± 25 nM) gave rise to slightly better binding when mutated to alanine (**Fig 2.4B**). These measurements confirm that degron binding is driven by the C-terminal glutamates and highlight the importance of the -2 degron position for binding. DCAF12 shows only moderate preference for individual degron residues preceding the -2 position, in line with degradation reporters in cells that show little effect for mutations N-terminal of the di-Glu motif [126]. However, the increased binding of alanine mutants of degron positions -3, -5, -7, -9 and -10 suggest that the CCT5 C-terminus is not the optimal di-Glu degron sequence bound by $CRL4^{DCAF12}$.

To study the substrate specificity of $CRL4^{DCAF12}$ in more detail, the TR-FRET competition assay was used to compare unlabeled $CCT5_{20}$ to equivalent C-terminal peptides of DCAF12 substrates MAGEA-3 ($MAGEA\text{-}3_{20}$; amino acids 295-314) and SAT1 ($SAT1_{20}$; amino acids 152-171) [126]. Competitive titrations against a $_{Tb}$DDB1-$DCAF12^{488}$ complex showed that the affinity of a $CCT5_{20}$ peptide for DCAF12 was lower (IC_{50} = 404 ± 103 nM) than that of $SAT1_{20}$ (IC_{50} = 291 ± 38 nM), but exceeded that of $MAGEA\text{-}3_{20}$ (IC_{50} ≈ 2700 nM) **(Figure 2.4D)**. Thus, despite the relatively

minor contribution of individual amino acids when mutated to alanine **(Figure 2.4B)**, the collective variability of residues preceding the di-Glu motif is sufficient to account for differences in binding affinities of up to 10-fold **(Figure 2.3C)**. DCAF12 tolerates significant variability in the residues preceding the di-Glu motif, explaining how the different C-termini of many di-Glu-containing proteins can be recognized by DCAF12 [126].

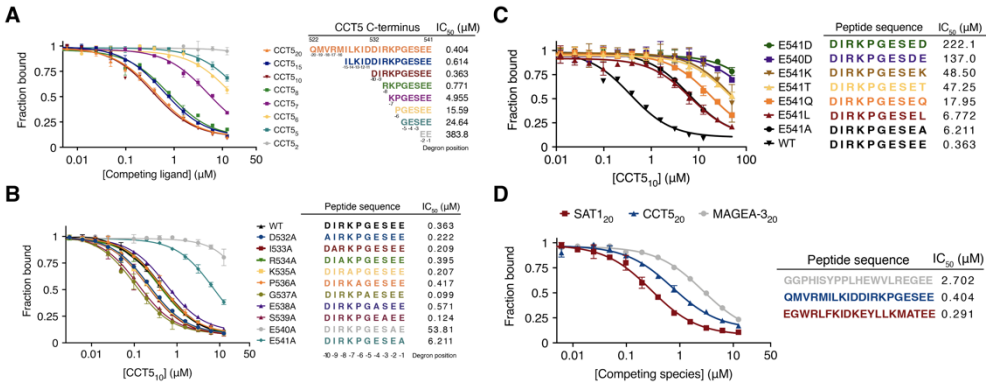

Figure 2.4. Determinants of di-Glu degron binding to DCAF12. (A) TR-FRET counter-titrations of label-free CCT5 C-terminal peptides into $_{Tb}$DDB1-DCAF12^{488} (n=3). Sequences of the peptides and IC_{50} values for the titrations are listed on the table. Peptides are labeled for their degron position and corresponding CCT5 amino acid number. **(B)** Counter-titration of unlabeled $CCT5_{10}$ C-terminal peptides into $_{Tb}$DDB1-DCAF12^{488} (n=3). Sequences of the peptides and IC_{50} values for the titrations are listed on the table. Peptides are labeled for their degron position and corresponding CCT5 amino acid number. **(C)** TR-FRET counter-titrations of label-free $CCT5_{10}$ degron peptides with mutant C-terminal amino acids. Sequences of the peptides and IC_{50} values for the titrations are listed on the table. **(D)** TR-FRET counter-titrations of label-free degron peptides of different DCAF12 substrates [126] into $_{Tb}$DDB1-DCAF12^{488} (n=3). **Data information:** In **(A,B,C,D)**, data is presented as means ± 95% confidence interval (CI).

Table 2.1. IC50 values of degron peptides.

Peptide name	Sequence	Kd (μM)	95% CI (symmetric)	95% CI (asymmetric)
$^{ATTO488}CCT5_{20}$	ATTO488-QMVRMILKIDDIRKPGESEE	0.215	0.080 – 0.350	0.108 – 0.473

Peptide name	Sequence	IC50 (μM)	95% CI (symmetrical)	95% CI (asymmetrical)
$CCT5_2$	EE	383.8	13.74 – 753.90	193.30 – 6448.00
$CCT5_5$	GESEE	24.64	20.51 – 28.76	20.98 – 29.36
$CCT5_6$	PGESEE	15.59	11.95 – 19.23	12.50 – 19.86
$CCT5_7$	KPGESEE	4.955	4.137 – 5.965	4.060 – 5.850
$CCT5_8$	RKPGESEE	0.771	0.621 – 0.920	0.631 – 0.942
$CCT5_{10}$	DIRKPGESEE	0.363	0.285 – 0.441	0.291 – 0.453
$CCT5_{15}$	ILKIDDIRKPGESEE	0.614	0.564 – 0.664	0.567 – 0.666
$CCT5_{20}$	QMVRMILKIDDIRKPGESEE	0.404	0.361 – 0.457	0.363 - 0.461
$CCT5_{10}$ D532A	AIRKPGESEE	0.222	0.198 – 0.247	0.198 – 0.250
$CCT5_{10}$ I533A	DARKPGESEE	0.209	0.184 – 0.234	0.185 – 0.236
$CCT5_{10}$ R534A	DIAKPGESEE	0.395	0.327 – 0.464	0.330 – 0.474
$CCT5_{10}$ K535A	DIRAPGESEE	0.208	0.182 – 0.234	0.182 – 0.236
$CCT5_{10}$ P536A	DIRKAGESEE	0.417	0.364 – 0.470	0.366 – 0.475
$CCT5_{10}$ G537A	DIRKPAESEE	0.100	0.089 – 0.111	0.089 – 0.112
$CCT5_{10}$ E538A	DIRKPGASEE	0.571	0.468 – 0.674	0.473 – 0.688
$CCT5_{10}$ S539A	DIRKPGEAEE	0.125	0.110 – 0.139	0.110 – 0.141
$CCT5_{10}$ E540A	DIRKPGESAE	53.810	35.83 – 72.60	40.08 – 79.85
$CCT5_{10}$ E541A	DIRKPGESEA	6.211	3.182 – 9.228	3.923 – 10.490
$CCT5_{10}$ E541L	DIRKPGESEL	6.772	5.305 – 8.684	5.112 – 8.432
$CCT5_{10}$ E541Q	DIRKPGESEQ	17.95	15.06 – 21.50	14.76 – 21.15
$CCT5_{10}$ E541T	DIRKPGESET	47.25	35.44 – 64.86	33.25 – 61.25
$CCT5_{10}$ E541K	DIRKPGESEK	48.50	40.16 – 59.28	38.61 – 58.39
$CCT5_{10}$ E540D	DIRKPGESDE	137.0	88.36 – 250.3	67.49 – 206.4
$CCT5_{10}$ E541D	DIRKPGESED	222.1	102.1 – 1981	0.000 – 448.5
$MAGEA3_{20}$	GGPHISYPPLHEWVLREGEE	2.702	2.109 – 3.295	2.170 – 3.385
$SAT1_{20}$	EGWRLFKIDKEYLLKMATEE	0.291	0.253 – 0.330	0.257 – 0.332

2.3 Conclusion

The results presented in this chapter establish protocols for the recombinant expression and purification of DDB1-DCAF12-CCT5 complexes for biochemical and structural studies. Co-purification of an unrelated and previously uncharacterized protein of baculoviral origin highlights the high affinity of DCAF12 for its substrates and hints at the plasticity of its binding site [332]. DCAF12 was shown to readily bind its substrates *in vitro*, including CCT5. The measurements shown confirm that CCT5 binding to DCAF12 is driven by its C-terminal glutamates, and in particular by the -2 glutamate. Taken together, the findings presented in this chapter establish CCT5 as a substrate of the $CRL4^{DCAF12}$ E3 ubiquitin ligase. Similar to other C-end ligases [126, 173, 335-339], submicromolar binding of a flexible C-terminal tail is achieved by a plastic binding site on the substrate receptor. While recognition is strictly dependent on only a few critical degron residues, interactions with other degron residues significantly contribute to binding.

Chapter 3

Structural Characterization of DDB1-DCAF12-CCT5 Complexes

The specimens purified in Chapter 2 were subjected to diverse biochemical and structural techniques, yielding high-resolution maps of the DDB1-DCAF12-CCT5 complex. This chapter presents the main findings from these experiments as well as efforts to improve the structures. Figures are labeled numerically by the order in which they are referenced in the text with a prefix for the chapter number (3). Cryo-EM data was collected by Simone Cavadini [380], who also prepared graphene oxide and pentylamine grids and under whose guidance and support the cryo-EM data was analyzed. Model building was carried out principally by Georg Kempf [387].

3.1 Structure of the CCT5-bound DDB1-DCAF12 Complex

To understand the molecular mechanisms of CCT5 recognition by the $CRL4^{DCAF12}$ E3 ligase, DCAF12-containing complexes were pursued for structural characterization. The structure of the ~180 kDa DDB1-DCAF12 complex was determined by single-particle cryogenic electron microscopy (cryo-EM) in the presence and absence of CCT5 to a resolution of 2.8 Å **(Figure 3.1)** and 3.0 Å **(Figure 3.2)**, respectively. Signal for the majority of the CCT5 protein was absent from the DDB1-DCAF12-CCT5 cryo-EM map. The two maps resembled each other, but presented key differences in electron

density around the substrate-binding pocket of DCAF12. These differences will be analyzed in detail in Section 3.2.

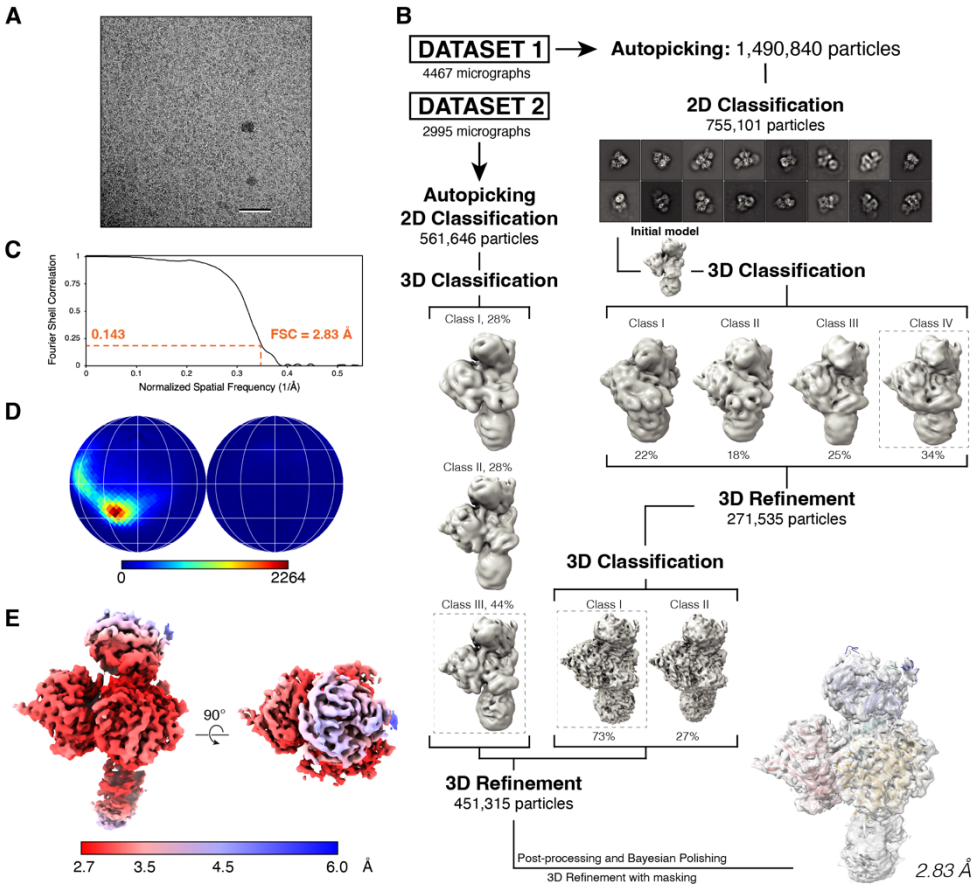

Figure 3.1. DDB1-DCAF12-CCT5 cryo-EM structure determination. (A) Representative micrograph from the DDB1-DCAF12-CCT5 collection. Scale bar: 50 nm. **(B)** Workflow of cryo-EM data analysis for the DDB1-DCAF12-CCT5 cryo-EM map. **(C)** Gold standard Fourier shell correlation (FSC) curve for the DDB1-DCAF12-CCT5 reconstruction. (**D**) Angular distribution for DDB1-DCAF12-CCT5 **(E)** Final cryo-EM map colored according to its local resolution, in angstroms.

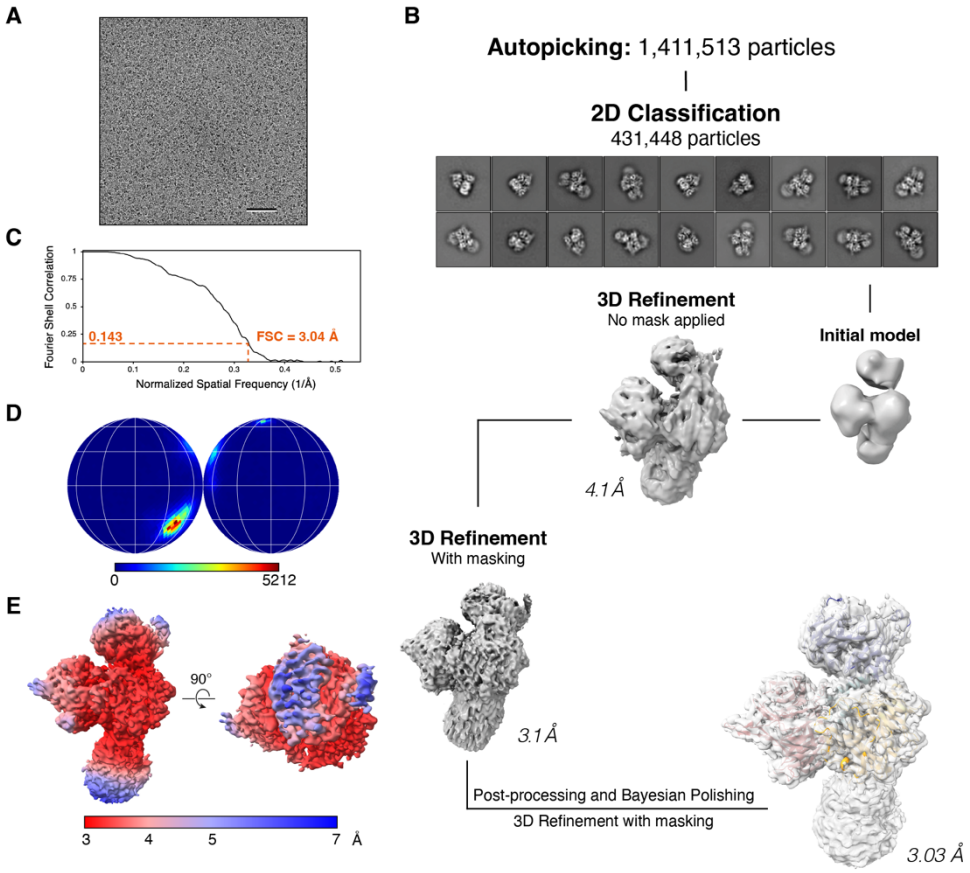

Figure 3.2. DDB1-DCAF12 cryo-EM structure determination. (A) Representative micrograph from the DDB1-DCAF12 collection. Scale bar: 50 nm. **(B)** Workflow of cryo-EM data analysis for the DDB1-DCAF12 cryo-EM map. 4568 micrographs were collected **(C)** Gold standard Fourier shell correlation (FSC) curve for the DDB1-DCAF12 reconstruction. (**D**) Angular distribution for DDB1-DCAF12 **(E)** Final cryo-EM map colored according to its local resolution, in angstroms.

The resolution of the cryo-EM maps allowed the modeling of the CCT5-bound DDB1-DCAF12 complex. Structural models were created for the DDB1-DCAF12 complex in the presence **(Figure 3.1)** and absence **(Figure 3.2)** of CCT5. The cryo-EM data collection, refinement and validation statistics are shown in **Table 3.1**.

Table 3.1. Cryo-EM data collection, refinement and validation statistics.

	DDB1-DCAF12-CCT5 (PDB-8AJM) (EMDB-15484)	DDB1-DCAF12 (PDB-8AJN) (EMDB-15485)
Data collection and processing		
Microscope	Titan Krios TEM	Titan Krios TEM
Camera	K2	Falcon 4
Voltage (kV)	300	300
Total dose ($e^-/Å^2$)	51.8	50
Magnification	130,000	75,000
Defocus (μm)	-0.5 to -2.5	-0.5 to -2.5
Number of frames	50	50
No. of micrographs	7462	4568
Pixel size (Å)	0.86	0.845
Initial particle images (no.)	1,490,840	1,411,513
Final particle images (no.)	451,315	431,448
Symmetry imposed	C1	C1
Map resolution (Å), FSC threshold 0.143	2.83	3.03
Refinement		
Non-hydrogen atoms	12,106	12,009
Protein residues	1,540	1,530
RMSD		
Bond lengths (Å)	0.008	0.006
Bond angles (°)	1.056	0.940
B factor ($Å^2$)	169.50	199.44

Validation		
MolProbity Score	0.89	1.17
Clashscore	1.25	1.67
Poor rotamers (%)	0.52	0.60
Ramachandran plot		
Favored (%)	97.78	96.19
Allowed (%)	2.22	3.81
Outliers (%)	0.00	0.00
C-beta deviations	0.00	0.00
Model-to-data fit*		
CC_{mask}	0.82	0.58
CC_{box}	0.85	0.74
CC_{peaks}	0.81	0.58
CC_{volume}	0.85	0.65

* The map was locally sharpened (LocScale).

DDB1 folds into a tri-lobed structure formed by three WD40 β-propeller domains (BPA, BPB, BPC) and a small C-terminal domain (CTD; amino acids 1043-1140) [201] **(Figure 3.3A)**. The BPB β-propeller connects DDB1 to CUL4, while the BPA and BPC β-propellers engage substrate receptors. The CTD bridges the BPA, BPB and BPC domains **(Figure 3.3B)** [201].

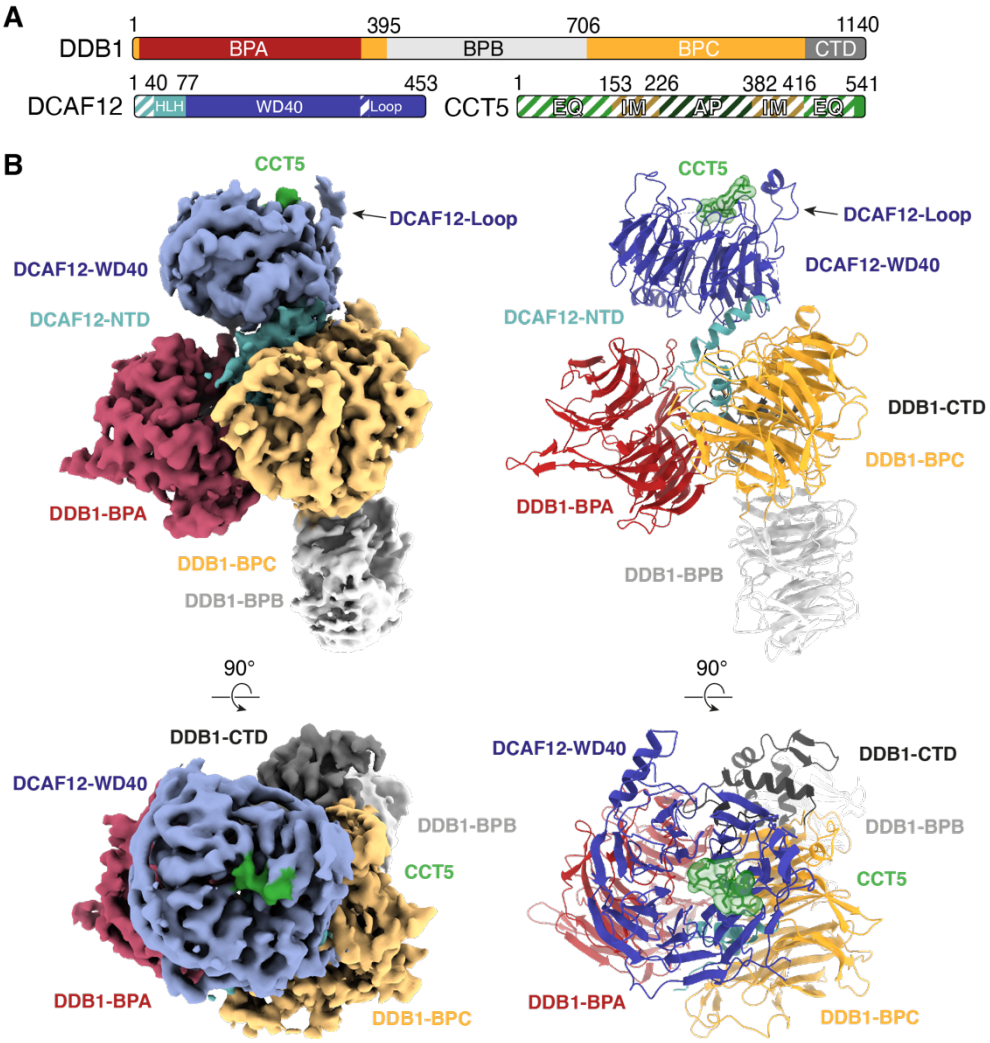

Figure 3.3. Cryo-EM structure of DDB1-DCAF12-CCT5. (A) Domain organization of the proteins present in the cryo-EM sample. Unmodeled regions are shown as stripes. **(B)** Different views of the DDB1-DCAF12-CCT5 cryo-EM map (left) with fit structures (right). The map and models are colored as in (A). DDB1 and DCAF12 are shown as cartoons. The CCT5 peptide is shown as sticks with surface representation.

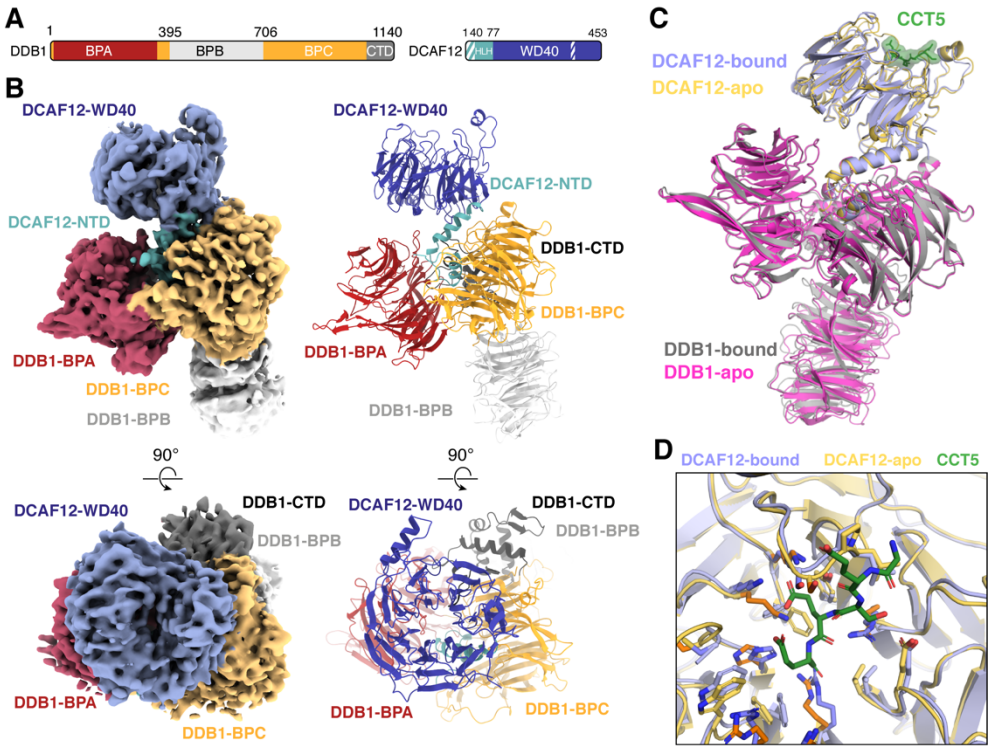

Figure 3.4. Cryo-EM structure of DDB1-DCAF12 in the absence of CCT5. (A) Domain organization of the proteins present in the sample. Unmodeled regions are shown as stripes. **(B)** Different views of the DDB1-DCAF12 cryo-EM map (left) with fit structures (right). The map and models are colored as in (A). **(C)** Superposition of the DDB1-DCAF12 (apo) and DDB1-DCAF12-CCT5 (bound) structures. Density corresponding to the CCT5 peptide (shown as green sticks with surface representation) was only observed in the DDB1-DCAF12-CCT5 structure (Figure 3.3). The root-mean-square deviation (side) between the two structures is 1.241 Å between all atoms and 1.029 Å when excluding the flexible BPB domain of DDB1. **(D)** Superposition of the residues forming the DCAF12 pocket between the DDB1-DCAF12 (apo) and DDB1-DCAF12-CCT5 (bound) cryo-EM structures.

The DCAF12 body is comprised of a WD40 β-propeller domain (WD40; amino acids 78-453) formed by seven "blades" of antiparallel β-sheets **(Figure 3.3B, Figure 3.5A)**. The DCAF12 WD40 β-propeller is preceded by a helix-loop-helix motif (HLH; amino acids 40-77) and an N-terminal domain

(NTD; amino acids 1-39) **(Figure 3.3A)**, which is found disordered in the structure. The HLH is lodged between the DDB1 BPA and BPC domains and anchors DCAF12 to DDB1 in a manner similar to other DDB1 substrate receptors **(Figure 3.5B and C)** [202, 386, 388, 389]. The WD40 β-propeller domain adopts the shape of a truncated cone tightly contacting DDB1 **(Figure 3.3B, Figure 3.5A)**. The crest of the WD40 cone points away from DDB1. The base of the DCAF12 β-propeller cone engages the BPC and CTD domains of DDB1 through the loops connecting the β strands of the WD40 blades one and seven, creating a 578 $Å^2$ interface between the two proteins **(Figure 3.3B, Figure 3.5D)**. An additional 1478 $Å^2$ interface between DDB1 and DCAF12 is contributed by the DCAF12 HLH motif **(Figure 3.3B, Figure 3.5C)**. DCAF12 contacts DDB1 residues that have previously been shown to bind substrate receptors **(Figure 3.5C and D)**. Overall, DCAF12 assumes an architecture common to other WD40 DDB1 substrate receptors.

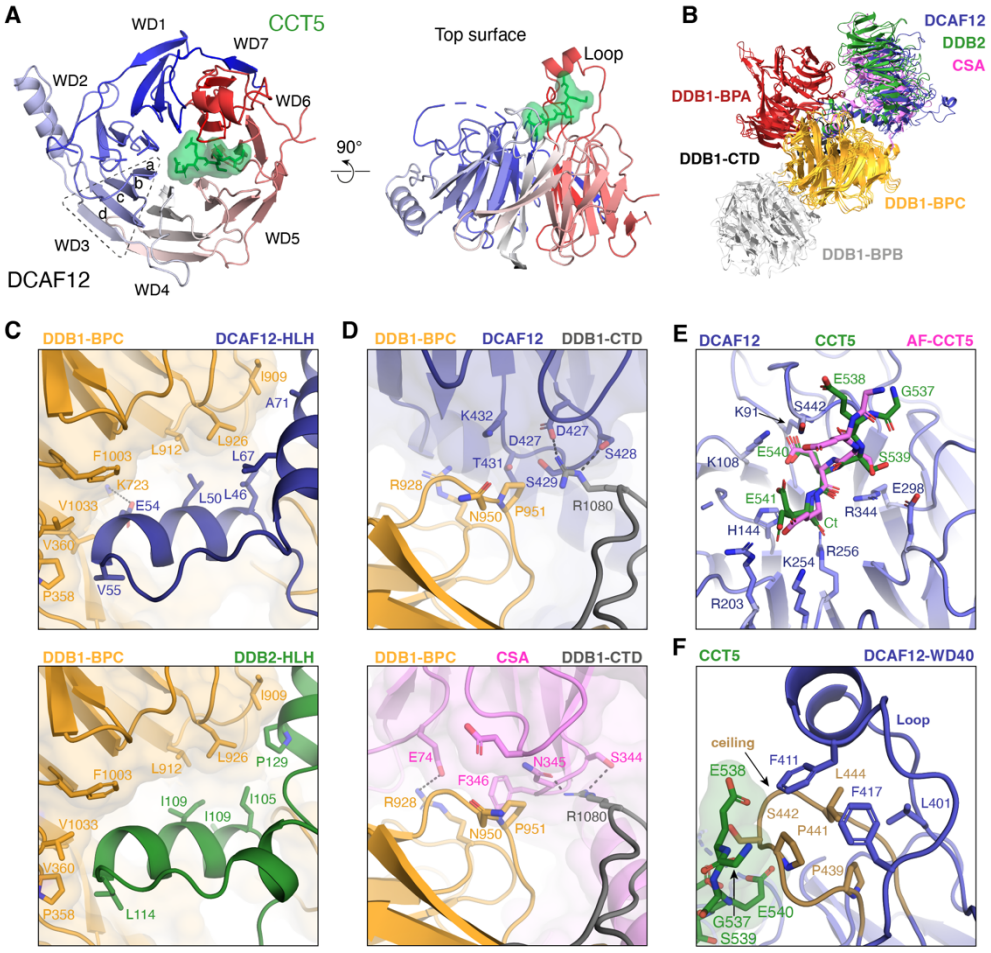

Figure 3.5. DCAF12 assembles into a CRL4 ligase. (A) Structural organization of the DCAF12 WD40 domain. The blades of the DCAF12 ß-propeller are labeled WD1-WD7 and colored according to their proximity to the N- or C-terminus. Each blade is composed of four ß strands labeled a-d in the outward direction. The CCT5 degron peptide is shown as green sticks and surface representation. **(B)** Superposition between the coordinates of DDB1-DCAF12 (this work), DDB1-DDB2 (PDB ID 4A0K) [202] and DDB1-CSA (PDB ID 4A11) [202]. **(C,D)** Close-up of DDB1 residues contacted by the HLH motif (C) or ß-propeller (D) of DCAF12 (top) that are involved in binding other substrate receptors (bottom). **(E)** Superposition of the AlphaFold prediction for the CCT5 peptide (AF-CCT5, violet) onto the cryo-EM coordinates of DDB1-DCAF12-CCT5 (CCT5 shown in green). The two modeled conformations of the CCT5 Glu541 side chain are depicted. **(F)** Close-up of the hydrophobic residues mediating the interaction between the DCAF12 Loop (amino acids 370-416) and ceiling (amino acids 438-447).

3.2 Structural Basis of di-Glu Degron Binding by DCAF12

DDB1 and DCAF12 adopt a similar overall conformation in the presence or absence of CCT5 (RMSD = 1.029 Å excluding the flexible DDB1 BPB domain) **(Figure 3.4C)**. In the presence of CCT5, however, an additional density is observed at the crest of the DCAF12 WD40 cone **(Figure 3.3B)**. The density is linear and occupies a surface pocket formed by all seven blades of the WD40 propeller **(Figure 3.6A and B)**. This central site at the narrow end of the WD40 cone is a common site used by WD40 propellers to engage substrate peptides [390, 391]. Alphafold2, in an un-supervised modeling run, placed a CCT5 peptide in a similar position and orientation **(Figure 3.5E)** [392, 393]. The density was therefore initially assigned to the five C-terminal amino acids of CCT5**(Figure 3.6C)**. No additional density attributable to CCT5 was evident in the cryo-EM maps or along the cryo-EM processing steps **(Figure 3.1)**.

The DCAF12 substrate-binding pocket is ~15 Å long and ~10 Å wide and composed of a base, a wall, and a ceiling **(Figure 3.6B)**. The base is contributed by basic and hydrophobic amino acids (Phe93, His144, Phe188, Arg256, Leu272, Val300, Arg344, Tyr422). The wall is formed by loops connecting blades one and two (amino acids 138-144) and blades two and three (amino acids 186-188). A loop connecting strands b and c in blade seven (amino acids 438-447) is kinked by two proline residues (Pro439, Pro441) and protrudes above the pocket, creating the ceiling **(Figure 3.6B)**. A large loop between blades six and seven (Loop; amino acids 370-416) forms a short α-helical protrusion above the ceiling, pinning it in place against the WD40 β-sheets **(Figure 3.6B)**. Interactions between the Loop and the pocket ceiling are driven by hydrophobic and conserved amino acids **(Figure 3.5F)**, and are

necessary for the structural integrity of the substrate-binding pocket **(Figure 3.6D)**. The amino acids forming the pocket, especially those of the base, are highly conserved **(Figure 3.6B)**, and adopt a similar side chain conformation in the presence or absence of CCT5 **(Figure 3.4D)**.

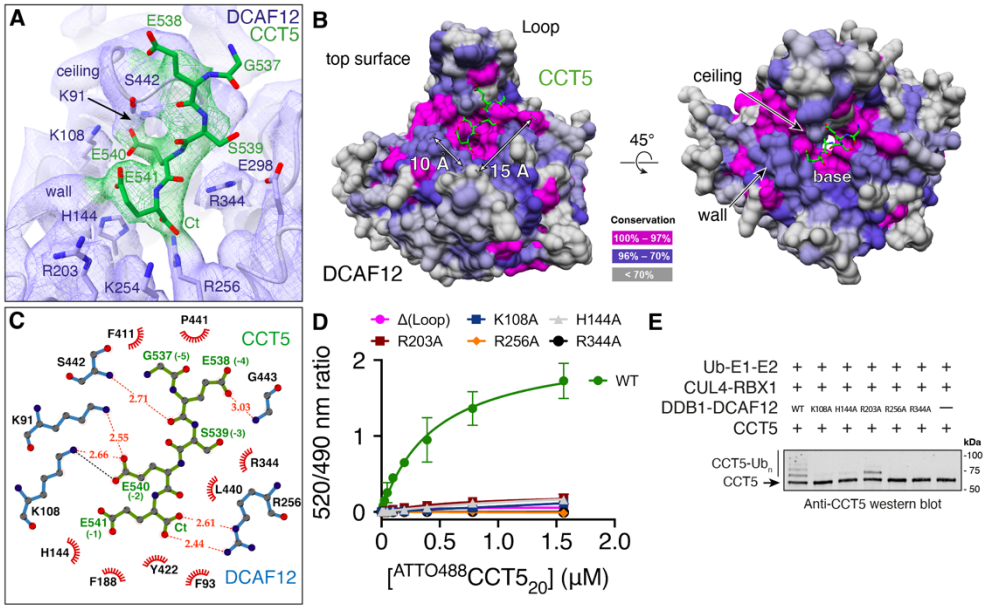

Figure 3.6. DCAF12 uses a surface pocket to bind the CCT5 di-Glu degron. (A) A close-up view of the cryo-EM map around the DCAF12 pocket. DCAF12 is shown in light blue as cartoons, with key pocket residues shown as sticks. CCT5 residues are shown as green sticks. **(B)** Conservation surface mapping of the DCAF12 WD40 domain. The DCAF12 pocket is annotated for its dimensions and structural components. CCT5 degron residues are shown as green sticks. **(C)** LigPlot+ diagram of the interactions between DCAF12 and the CCT5 di-Glu degron [394]. The DCAF12 residues forming hydrogen bonds with CCT5 are shown in blue. DCAF12 residues involved in Van der Waals packing are shown with eyelashes in red. CCT5 residues are shown in green with degron positions in parentheses. Hydrogen bonds and salt bridges are shown as orange and black dashed lines, respectively. **(D)** Titration curves between $^{ATTO488}CCT5_{20}$ and wild type (WT) or mutant $_{Tb}$DDB1-DCAF12 complexes (n=3). DCAF12 amino acids 370-416 have been replaced in the Δ(Loop) mutant by a flexible glycine-serine linker. Unspecific signal arising from the Tb-SA label was subtracted. **(E)** In vitro ubiquitination of CCT5 by wild type (WT) or mutant $CRL4^{DCAF12}$ complexes in the presence of ubiquitin, ATP, E1 and E2 enzymes. **Data information:** In **(D)**, data is presented as means ± 95% CI.

The DCAF12 pocket wall is flanked by two patches of positively charged amino acids (Lys91, Lys108, Arg203, Lys254) **(Figure 3.6A and B)**. On the side bridging the wall to the ceiling, a patch formed by Lys91 and Lys108 contacts the gamma carboxyl group of the -2 glutamate (CCT5 Glu540), locking down its side chain under the pocket ceiling **(Figure 3.6B and C)**. TR-FRET assays using the $^{488}CCT5_{20}$ reporter peptide and a DCAF12 Lys108Ala mutant demonstrate that Lys108 is essential for binding **(Figure 3.6D)**. The C-terminal carboxyl group of CCT5 faces the WD40 core, where it is engaged by DCAF12 Arg256 **(Figure 3.6A)**. Introducing an Arg256Ala mutation into DCAF12 abolished $^{ATTO488}CCT5_{20}$ binding in vitro **(Figure 3.6D)**. By recognizing the C-terminal carboxyl group of its substrates through Arg256, DCAF12 reads out the C-terminal nature of the degron. Accordingly, internal di-Glu motifs have not been reported as substrates of DCAF12, despite their prevalence in human proteins. While the CCT5 C-terminal carboxyl group is engaged by Arg256 deep within the core of the DCAF12 propeller, its Glu541 side chain points towards the solvent, where the gamma carboxyl group can engage positively charged groups contributed by DCAF12 His144, Arg203 and Lys254, as well as the DCAF12 protein backbone between residues 140-141 **(Figure 3.6A and C)**. The interaction between the CCT5 Glu541 side chain and the imidazole moiety of DCAF12 His144, as well as the DCAF12 Arg256 side chain interaction with the CCT5 C-terminal carboxyl group, is the predominant feature in the cryo-EM map **(Figure 3.6A)**. Additional density was however observed consistent with an alternative conformation of the Glu541 side chain wherein its gamma carboxyl group engages the positively charged patch formed by DCAF12 Arg203 and Lys254 **(Figure 3.7)**.

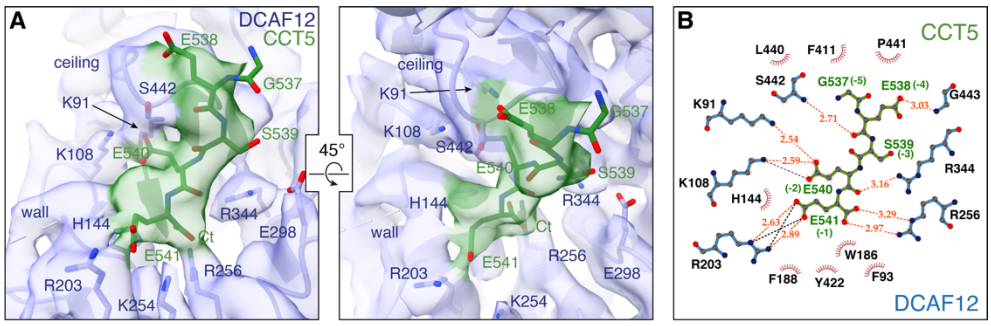

Figure 3.7. Alternative conformation of the CCT5 Glu541 side chain. (A) A close-up view of the electron density around the DCAF12 pocket with an alternative conformation for the CCT5 Glu541 side chain modeled. DCAF12 is shown in light blue as cartoons, with key pocket residues shown as sticks. CCT5 residues are shown as green sticks. The electron density map is shown at a higher contour level than Figure 3.6A **(B)** LigPlot+ diagram of the interactions between DCAF12 and the alternative conformation of the CCT5 di-Glu degron [394]. The DCAF12 residues forming hydrogen bonds with CCT5 are shown in blue. DCAF12 residues involved in Van der Waals packing are shown with eyelashes in red. CCT5 residues are shown in green with degron positions in parentheses. Hydrogen bonds and salt bridges are shown as orange and black dashed lines, respectively.

Mutating DCAF12 His144 or Arg203 to alanine abrogated substrate binding in vitro, suggesting that both types of interactions contribute to binding **(Figure 3.6D)**. At the degron position -3, the Ser539 side chain points toward DCAF12 Glu298 and Arg344 **(Figure 3.6A and C)**. At the base of the pocket, Arg344 further contributes to substrate binding through interactions with the CCT5 peptide backbone **(Figure 3.6A and C)**. Mutating DCAF12 Arg344 to alanine abrogated substrate binding in vitro **(Figure 3.6D)**. At degron position -4, CCT5 Glu538 engages in backbone carbonyl interactions with DCAF12 Ser442, while simultaneously binding the DCAF12 backbone around Ser442 through its side chain **(Figure 3.6A and C)**. At degron position -5, CCT5 Gly537 exits the pocket towards the solvent and is found largely disordered **(Figure 3.6A)**.

Experiments were then carried out to study the catalytic activity of the $CRL4^{DCAF12}$ E3 ligase. $CRL4^{DCAF12}$ was reconstituted *in vitro* and mixed with CCT5 in the presence of E1 and E2 enzymes, ubiquitin and ATP. In these conditions, substrate binding by E3 ligases leads to ubiquitination, which was followed fluorometrically after immunoblots with labeled antibodies. CCT5 was robustly ubiquitinated by $CRL4^{DCAF12}$ in vitro **(Figure 3.6E)**. Ubiquitination by $CRL4^{DCAF12}$ was dependent on di-Glu binding: DCAF12 Lys108Ala, His144Ala, Arg256Ala and Arg344Ala mutants that failed to bind $^{ATTO488}CCT5_{20}$ in the TR-FRET assay **(Figure 3.6D)** showed no ubiquitination activity towards CCT5 **(Figure 3.6E)**, although some ubiquitination activity was retained by an Arg203Ala mutant. Thus, DCAF12 assembles into a functional $CRL4^{DCAF12}$ E3 ubiquitin ligase, and its catalytic activity reflects the mechanism of degron binding by DCAF12.

3.3 Structure Optimization Trials

The structural work hitherto presented produced two high-resolution structures that identified how key CCT5 degron residues bind DCAF12. Signal for the remainder of the CCT5 protein was absent in the cryo-EM maps that was believed would be informative to understanding substrate recognition by DCAF12 and the biological function of the $CRL4^{DCAF12}$ ligase. Samples could be produced in sufficient quantities for structural studies, and extensive efforts were directed at obtaining a complete high-resolution structure of a substrate-bound DDB1-DCAF12 complex.

Optimization of Cryo-EM experimental conditions

Despite yielding a sub-3Å map of the CCT5-bound DDB1-DCAF12 complex, the particles suffered from preferential orientation and lower resolution near the DCAF12-CCT5 interface **(Figure 3.1, Figure 3.2)**. Crucially, signal for the remainder of the CCT5 protein was absent from cryo-EM maps. Substantial efforts were directed at improving the cryo-EM reconstructions of substrate-bound DDB1-DCAF12 complexes.

Preferential particle orientation can arise from non-uniform interactions between the vitrified particles and the components of the grids used for data collection or the air-water interface. The Quantifoil grids used for cryo-EM data collection tend to be hydrophobic before plasma treatment [395], and a series of different supports were used to minimize the adsorption of protein particles onto the grids. Cryo-EM data was collected on graphene oxide grids [396] and grids treated with pentylamine [397]. Graphene oxide grids contain a layer of graphene that is oxidized before sample application to increase the hydrophilicity of the grid [398]. Grids glow discharged in the presence of air become negatively charged [399]. By contrast, grids glow discharged in a chamber with pentylamine incorporate positively charged chemical groups that can change the interaction with vitrified particles [397]. These supports did not however improve the preferential orientation of the particles, and did not show additional signal for CCT5 **(Figure 3.8)**. Data was then collected on grids made less hydrophilic by avoiding the plasma treatment (glow discharging) step before sample application. Collection of these grids showed particles that were homogeneous and well dispersed, but with no improvements on the preferential orientation or signal for CCT5 **(Figure 3.8)**. Additional grids were used with a gold support. Gold is a chemically inert and biocompatible material, and is additionally highly

conductive, non-oxidizing and radiation resistant, which reduces particle motion and image blurring during irradiation and differential thermal contraction during vitrification [400]. Collection in UltrAuFoil R 1.2/1.3 gold grids (#Q350AR13A, Ted Pella) did not, however, yield a map with significantly improved signal for CCT5, preferential orientation or resolution.

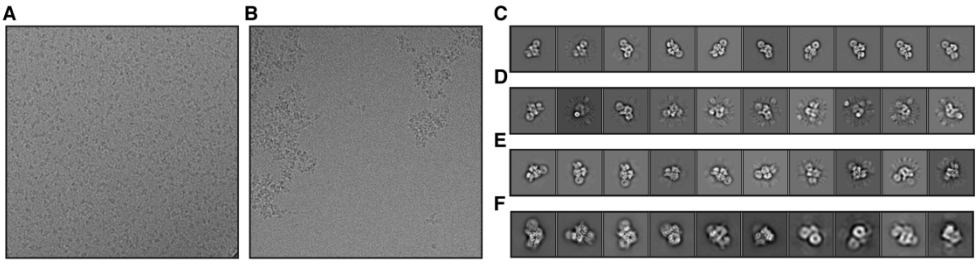

Figure 3.8. Optimization of cryo-EM conditions. Left: representative micrograph images from the collection of DDB1-DCAF12-CCT5 complexes in the presence of 5% glycerol **(A)** or NP-40 **(B)**. Right: 2D class averages for DDB1-DCAF12-CCT5 complexes collected in grids with graphene oxide support **(C)**, reconstituted in a 1:3 DDB1-DCAF12:CCT5 molar ratio **(D)**, collected on non-glow-discharged grids **(E)** and in complex with MC30 **(F)**.

Concerns existed about the integrity of the complex, which can be often compromised during cryo-EM specimen preparation [401]. It was deemed likely that the DDB1-DCAF12-CCT5 complex was falling apart during vitrification, driven by preferential adsorption of DDB1-DCAF12 or CCT5 to the grids or the air-water interface [402]. Grids were therefore prepared in the presence of non-ionic NP-40, n-octyl-β-D-glucoside (OG) and n-dodecyl-β-D-maltoside (DDM) detergents that are commonly used to solubilize protein samples [403]. These detergents caused moderate to heavy aggregation of the protein samples, even when applied at 50% of their critical micellar concentration [403], and images were not collected. The binding mechanism of CCT5 to DCAF12 is governed by the CCT5 di-Glu degron **(Figure 2.3E)**, suggesting that the remainder of CCT5 makes weaker contacts

with DCAF12 easily disrupted by unfavorable experimental conditions. Data was therefore collected in a variety of different buffers aiming at improving the stability of the complex in solution. Glycerol favors compact protein conformations, prevents protein unfolding and stabilizes aggregation-prone intermediates [404], but it can reduce the contrast in cryo-EM micrographs and is traditionally avoided during specimen preparation [405]. Data was collected in the presence of 5% glycerol, which had no drastic effect on the quality of the micrograph images but did not improve the stability of the DDB1-DCAF12-CCT5 complex in solution **(Figure 3.8)**. A screening of buffer conditions was also used for samples varying in pH (5.5-8.9) and salt concentrations (150-300 mM NaCl), but micrograph images were not collected due to visible defects in particle distribution and abundance.

Further efforts were directed at improving the sample used for collection. CRL4s often associate with DDA1, a flexible protein that binds the BPA domain of DDB1 and has been hypothesized to bind substrate receptors and even their bound substrates [406, 407]. DDA1 stably associated with a DDB1-DCAF12-CCT5 complex, and a cryo-EM map of a DDB1-DCAF12-CCT5-DDA1 complex was obtained that did not offer additional signal for CCT5. CCT subunits undergo ATP-induced conformational changes, and 5mM ATP was added to the specimens before collection to no significant avail. DDB1-DCAF12-CCT5 complexes were then treated with cross-linking agents glutaraldehyde (at 0.1% w/v and 1% w/v concentrations), DSSO (0.1% w/v) and BS3 (0.1% w/v) using the GraFix method [408]. Processing of cryo-EM data collected for cross-linked DDB1-DCAF12-CCT5 complexes did not reveal additional signal for CCT5, despite an electrophoretic mobility of ~240 kDa consistent with a fully assembled complex. Recombinant fusions, a proven strategy to promote

macromolecular assembly [229], was attempted via the addition of a flexible 12-residue glycine-serine linker between the C-terminus of DCAF12 and the N-terminus of CCT5, but yielded a highly insoluble proteins that could not be purified. Data was additionally collected for a DDB1-DCAF12-MC30 complex, but yielded no density attributable to MC30 **(Figure 3.8)**. Data processed for a DDB1-DCAF12 complex incubated with a 2-fold molar excess of purified CCT5 or a 9-fold molar excess of a $CCT5_{20}$ peptide also did not improve the signal for CCT5, but created background signal in the micrograph images that made particle alignment difficult **(Figure 3.8)**. Therefore, extensive experimental work did not improve the signal observed for CCT5 in the cryo-EM map.

Crystallization trials for DDB1-DCAF12-CCT5 complexes

X-ray crystallography (XR) relies on the generation of protein crystals and their subsequent irradiation with high-energy synchrotron radiation. The resulting diffraction patterns can be interpreted to determine the three-dimensional position of the atoms in the crystal [409]. XR generally requires larger sample amounts and a larger screening of buffer conditions than cryo-EM, but it can provide the atomic structure of macromolecules at high resolution. DDB1-DCAF12-CCT5 complexes were purified to homogeneity and concentrated to achieve a final concentration of DCAF12 in the crystallization drop of ~80 µM [158]. Crystallization trials were set up on 96-well plates using the sitting drop vapor diffusion method by mixing 200 nl sample and 200 nl of commercially available screenings of crystallization buffers such as Index HT, Morpheus, JCSG Core I-IV, JCSG+, PEGs Suite I, PEGs Suite II, Classics Suite, and ProComplex Suite. These screens were also used in all cases after a 1:2 and 7:10 dilution in water.

Crystallization trials for wild type DDB1-DCAF12 complexes in the absence or presence of CCT5 at 1:1 and 1:3 molar ratio yielded no crystals. Crystallization trials on a DDB1-DCAF12-MC30 complex were similarly unsuccessful **(Figure 3.9)**.

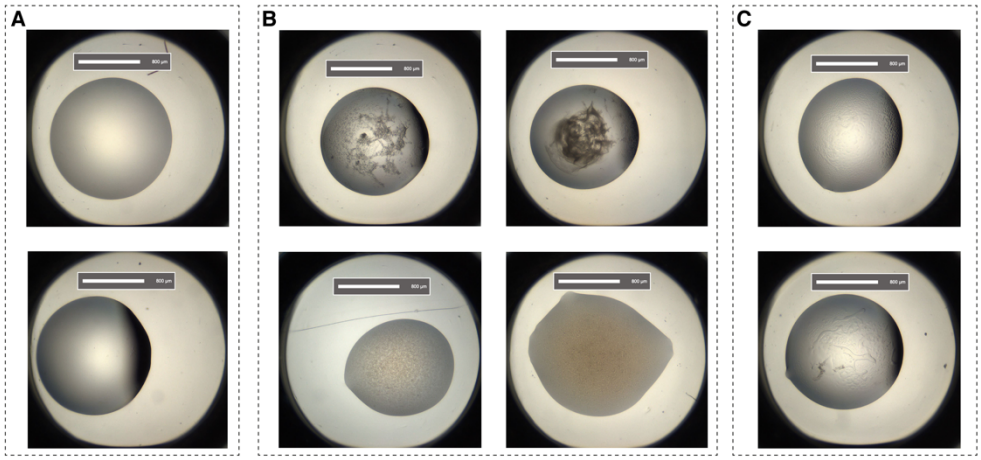

Figure 3.9. Crystallization trials for DDB1-DCAF12 complexes. Representative crystallization drops for substrate-bound DDB1-DCAF12 complexes. Crystallization trays presented drops that were mostly clear **(A)**, contained protein precipitates **(B)**, or had undergone phase separation **(C)**.

The crystallization of protein samples, as well as the crystallographic resolution after diffraction, is limited by the structural homogeneity within the crystal, which is improved when proteins are devoid of unstructured or flexible regions. The flexibility of the DDB1 BPB domain allows CRL4s to better ubiquitinate their substrates [202], and CCT5 undergoes large rearrangements of its apical domain during the opening and closing of the TRiC cavity [373]. To reduce structural heterogeneity, a DDB1 construct with the BPB domain (amino acids 396-705) replaced by a GNGNSG linker ($DDB1^{\Delta BPB}$) was used for subsequent crystallization trials **(Figure 3.10)** [158]. CCT5 was truncated to isolate its rigid equatorial domain ($CCT5^{eq}$, amino acids 1-154, 418-541), which is discontinuous but can be conjoined

with minimum distortions to the peptide chain **(Figure 3.10)** [410]. Truncations were similarly designed to reduce the flexibility of DCAF12. A DCAF12$^{\Delta Nt}$ (37-453) construct was made that conserved the DDB1-binding HLH motif (amino acids 40-77) but lacked the unstructured N-terminal domain that was not visible in the cryo-EM maps **(Figure 3.1)**. Crystallization trials were carried out for DDB1$^{\Delta BPB}$-DCAF12$^{\Delta Nt}$-CCT5 and DDB1$^{\Delta BPB}$-DCAF12$^{\Delta Nt}$-CCT5^{eq} complexes with CCT5 at 1:1 and 1:3 molar ratio, but no crystals were observed in the drops.

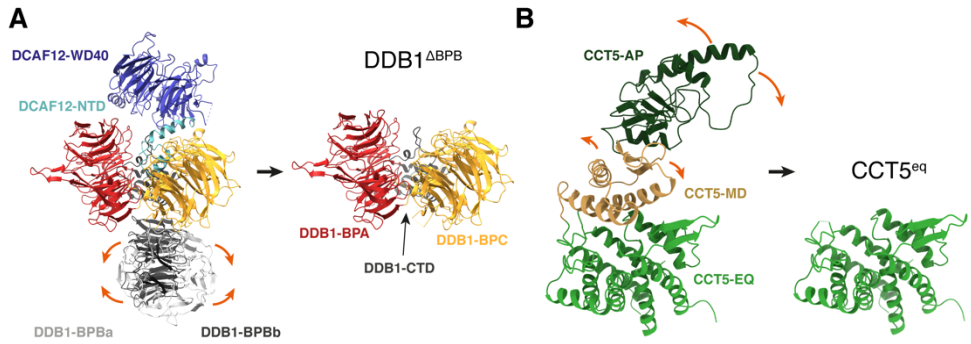

Figure 3.10. Truncation constructs for the highly flexible proteins DDB1 and CCT5. (A) DDB1$^{\Delta BPB}$ construct designed to eliminate structural flexibility arising from rotations of the flexible BPB domain. Two known conformations of the BPB domain are shown labeled a (PDB ID 2HYE [201]) and b (PDB ID 8AJM, this work). Motion within a DDB1-DCAF12 complex is shown with orange arrows. **(B)** CCT5^{eq} construct designed to eliminate structural flexibility arising from the CCT5 middle (MD) and apical (AP) domains. Only the rigid equatorial (EQ) domain remains. Allosteric motion is shown with orange arrows.

N-terminal truncations of *H. sapiens* (amino acids 64-453) and *G. gallus* (49-427) DCAF12 that do not bind DDB1 **(Figure 2.1A and C)** were similarly tested for crystallization. A further minimal construct was designed for the DCAF12 β-propeller (DCAF12^{min}, amino acids 70-453), which additionally contained a Y70A mutation and a substitution of flexible amino acids 226-

253 and 374-416 (Loop) for glycine-serine linkers of 6 and 12 residues in length, respectively. Crystallization screens were set up for these standalone DCAF12 constructs, but they did not yield crystals. DCAF12-containing complexes proved refractory to crystallization, and structural efforts were directed to their characterization by cryo-EM.

3.4 Conclusion

The structural work presented in this chapter elucidates the structure of the CCT5-bound DDB1-DCAF12 complex. Despite lacking signal for the globular CCT5 protein, the structures identify five C-terminal CCT5 residues that interact with DCAF12. The corresponding substrate peptide assignment is supported by mutagenesis and functional data. Key carboxyl groups of the CCT5 di-Glu motif are extensively read out through strong interactions with conserved and positively charged amino acids in the DCAF12 pocket. The C-terminal degron glutamate is engaged by DCAF12 in a solvent-exposed location that can accommodate multiple conformations and types of side chains, explaining the laxer identity requirements for the -1 degron residue. The remainder of contacts observed between DCAF12 and CCT5 are mediated by the CCT5 backbone or involve weak side chain interactions, reflecting the small differences in binding affinity of the alanine-mutant peptides, and the cumulative differences seen for the MAGEA-3 and SAT-1 C-terminal peptides. Taken together, the results presented in this chapter

confirm that the $CRL4^{DCAF12}$ E3 ligase binds and ubiquitinates CCT5 in vitro, and that its specificity and affinity is governed by the di-Glu degron.

Chapter 4

Characterization of the Interaction Between CRL4^{DCAF12} and TRiC

The work presented in Chapter 2 and Chapter 3 establish a clear ligase-substrate relationship between CRL4^{DCAF12} and CCT5. CCT5 functions in cells as part of a large multiprotein assembly, the TRiC chaperonin. This chapter presents structural and biochemical experiments carried out to determine the relationship between CRL4^{DCAF12} and TRiC. Figures and tables are labeled numerically by the order in which they are referenced in the text with a prefix for the chapter number (4). Negative-stain EM data was collected and processed under the guidance and support of Simone Cavadini [380]. Mass-spectrometric analysis of TRiC subunit stoichiometry was carried out by Vytautas Iesmantavicius [378] and Daniel Hess [379].

4.1 Architecture of the CCT5-bound CRL4^{DCAF12} E3 Ubiquitin Ligase

Negative-stain transmission electron microscopy (EM) involves the treatment of a sample with a heavy metal salt to create an electron-dense medium with comparatively translucent particles [411]. Negative-stain EM resolution is practically limited to 10-20 Å, but it is a quick technique and helps to recognize problems such as aggregation, disintegration and heterogeneity of a sample, and requires a relatively inexpensive and simple to operate microscope [412].

DDB1-DCAF12-CCT5 complexes were subjected to analysis by negative-stain EM, yielding a structure of a DDB1-DCAF12-CCT5 complex at a resolution of 30 Å **(Figure 4.1)**. The negative-stain EM map matched the previously obtained coordinates for DDB1-DCAF12-CCT5, and additionally showed clear density consistent with published structures of CCT5 [361, 410]. Due to the low resolution of the negative-stain map, domains were docked as rigid bodies with no side chains included. The negative-stain EM data collection, refinement and validation statistics are shown in **Table 4.1**.

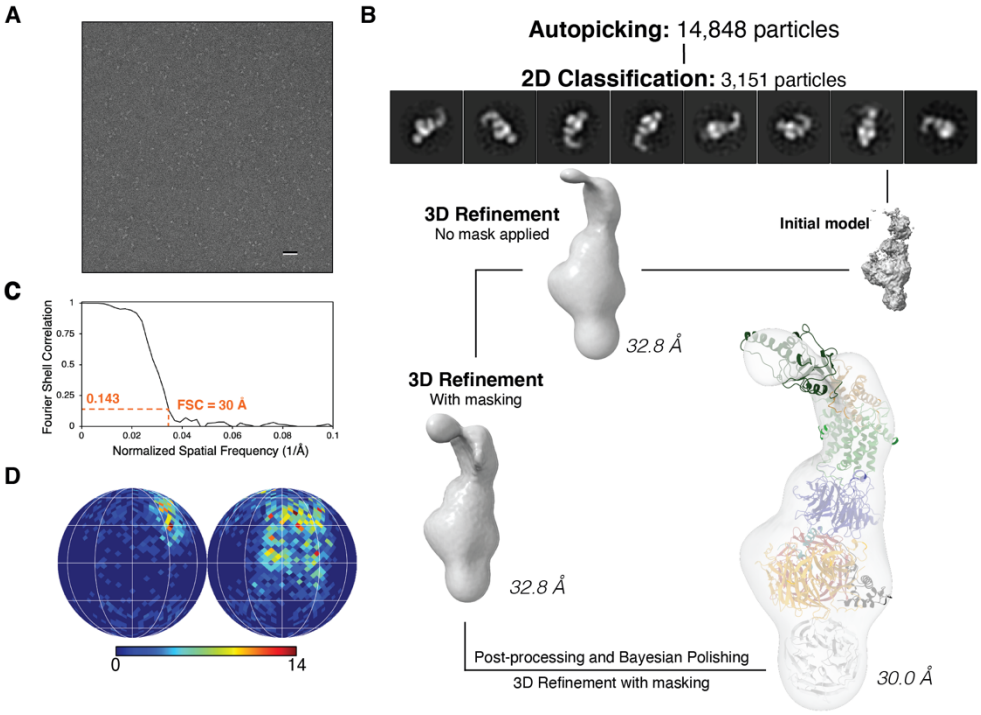

Figure 4.1. DDB1-DCAF12-CCT5 negative-stain EM structure determination. **(A)** Representative micrograph from the DDB1-DCAF12-CCT5 negative-stain collection. Scale bar: 50 nm. **(B)** Workflow of cryo-EM data analysis for the DDB1-DCAF12-CCT5 negative-stain map. **(C)** Gold standard Fourier shell correlation (FSC) curve for the DDB1-DCAF12-CCT5 negative-stain reconstruction. **(D)** Angular distribution for DDB1-DCAF12-CCT5 **(E)** Final cryo-EM map colored according to its local resolution, in angstroms.

Table 4.1. Negative-stain EM data collection, refinement and validation statistics.

	DDB1-DCAF12-CCT5 (PDB-8AJO) (EMDB-15486)
Data collection and processing	
Microscope	FEI Tecnai Spirit
Camera	FEI Eagle
Voltage (kV)	120
Magnification	49,000
Defocus (μm)	-1 to -3
No. of micrographs	167
Pixel size (Å)	2.125
Initial particle images (no.)	14,848
Final particle images (no.)	2,923
Symmetry imposed	C1
Map resolution (Å),	30
Refinement	
Non-hydrogen atoms	10,269
Protein residues	2,052
Map sharpening *B* factor (Å^2)	N.A.[1)]
RMSD	
Bond lengths (Å)	0.005
Bond angles (°)	1.106
B factor (Å^2)	600.00
Validation	
Clashscore	0.26
Poor rotamers (%)	N.A.[2)]
Ramachandran plot	98.48
C-beta deviations	0.00
Model-to-data fit*	
CC_{mask}	0.5736
CC_{box}	0.8041
CC_{peaks}	0.3107
CC_{volume}	0.4072

1) No sharpening was performed.
2) Side chains were removed from final model.

CCT5 adopts a curved shape formed by equatorial (EQ), intermediate (IM) and apical (AP) domains connected by hinge regions **(Figure 3.3A, Figure 4.2A)** [361, 410]. In published structures, the N- and C-termini of all TRiC subunits protrude from the equatorial domain as flexible tails with no regular secondary structure [361, 410]. The negative-stain EM map shows that CCT5 uses its equatorial domain to dock to the crest of the DCAF12 β-propeller **(Figure 4.2A)**. Binding of the equatorial domain largely covers the pocket, yet allows a passage over DCAF12 blade six for the CCT5 C-terminus to enter the pocket **(Figure 4.3)**. The CCT5 C-terminal tail is approximately 15 residues in length and offers sufficient flexibility to engage the pocket as observed in the high-resolution cryo-EM map **(Figure 3.3B)**. Additional contacts likely exist between the CCT5 equatorial domain and the DCAF12 β-propeller, although their precise identity could not be determined from the negative-stain map. In TR-FRET competition assays, full-length CCT5 bound DDB1-DCAF12 (IC_{50} = 219 ± 43 nM) with a similar affinity than that of a $CCT5_{20}$ degron peptide (IC_{50} = 404 ± 103 nM) **(Figure 2.3E)**. Contacts mediated by the DCAF12 β-propeller could fine-tune the specificity of the CRL4^{DCAF12} ligase towards its substrates. In the case of CCT5, however, these appear to have only a minor contribution to binding.

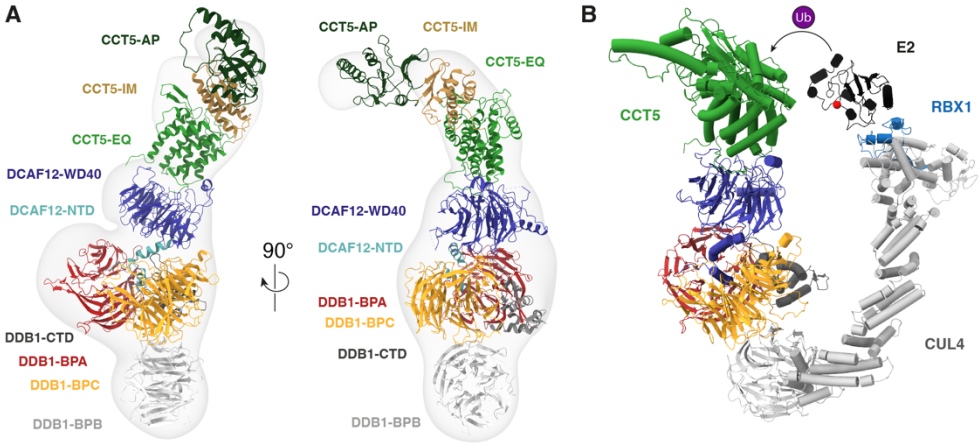

Figure 4.2. Structure of the CCT5-bound CRL4^{DCAF12} ubiquitin ligase. (A) Different views of the negative-stain EM map of the DDB1-DCAF12-CCT5 complex with fit coordinates for DDB1-DCAF12 (this work) and CCT5 (PDB ID 6NR8, chain E [361]). **(B)** Model of the CCT5-bound CRL4^{DCAF12} E3 ubiquitin ligase. CUL4 and RBX1 (PDB ID 4A0K [202]) bridge DDB1-DCAF12 to an E2 ubiquitin ligase (UBCH7 depicted, PDB ID 1FBV [83]). Spatial proximity between the E2 and the substrate catalyzes the ubiquitin (Ub) transfer reaction, facilitated by allosterism within the Cullin-RING ligase complex [413]. The catalytic cysteine of UBCH7 is depicted as a red sphere.

The presented cryo-EM and negative-stain EM structures of the DDB1-DCAF12-CCT5 complex allow constructing a model for the CCT5-bound CRL4^{DCAF12} ligase **(Figure 4.2B)** [201, 202, 361]. The ~280 kDa CRL4^{DCAF12} complex uses the DCAF12 β-propeller to engage the CCT5 equatorial domain and di-Glu motif. CCT5 binding to CRL4^{DCAF12} juxtaposes it to an E2-Ub enzyme in a manner similar to other CRL4 substrates **(Figure 4.2B)** [154, 158, 202, 386, 388]. The surface of CCT5 near the E2 is decorated by lysines that can be covalently modified with polyubiquitin chains. Spatial proximity to the E2-Ub enzyme allows CCT5 to be ubiquitinated [414], in agreement with the in vitro ubiquitination assays **(Figure 3.6E)**.

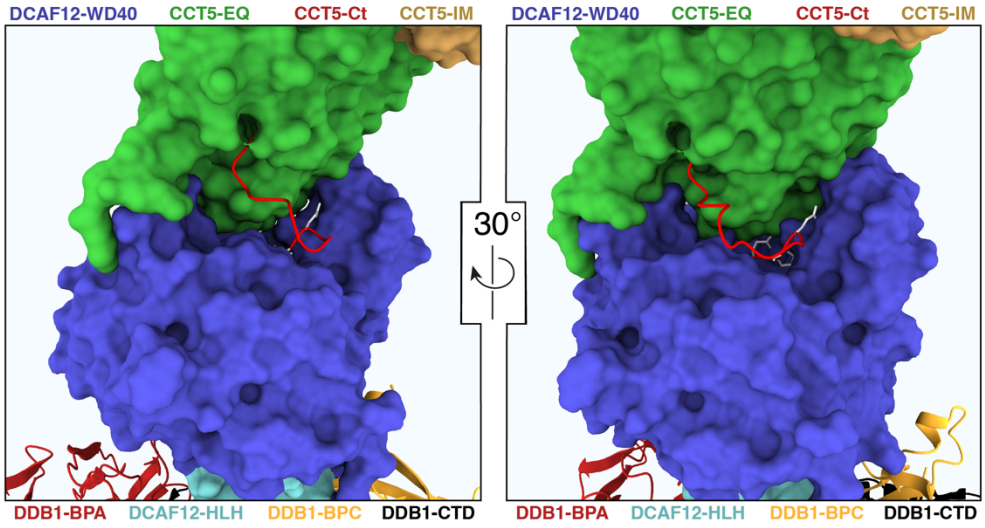

Figure 4.3. Binding of CCT5 to DCAF12 covers the pocket. Different views of the interface between DCAF12 and CCT5 from the negative-stain EM map, shown in surface representation. DDB1 and the CCT5 C-terminal tail (Ct) are shown as cartoons. Side chains are shown in white for CCT5 residues seen interacting with DCAF12 in the cryo-EM structure (Figure 3.6A).

4.2 Purification of the TRiC Chaperonin Complex

At the start of this project, no high-resolution structure of human TRiC had been solved, and no protocol was available for the large-scale recombinant expression and purification of human TRiC. Most structures of mammalian TRiC had been obtained for bovine or murine TRiC extracted from animal tissue through rather cumbersome methods [415]. These studies had produced TRiC reconstructions up to ~4 Å (PDB ID 3IYG) in resolution that did not allow for the unequivocal identification of TRiC subunits [363, 367, 368, 374, 416]. Higher resolution structures existed for yeast TRiC [365, 417]. These

studies relied on the generation of *Saccharomyces cerevisiae* strains with affinity tags inserted at the genomic locus of TRiC subunits CCT3 [365, 417, 418] or CCT5 [365]. Of note, several of these structures predate the proteomic studies that resolved the arrangement of TRiC subunits [350, 362, 369], and display incorrect subunit arrangements [363, 365, 367, 368]. TRiC subunits are only partially conserved from yeast to humans (~60% amino acid identity for individual subunits), and *S. cerevisiae* CCT5 does not end in a di-Glu motif. Overall, non-human TRiC had been recombinantly purified using a variety of methods including the use of internal [365, 417, 418] and N-terminal [365] tags on its subunits. Described protocols for the purification of TRiC from human cells did not allow for the recombinant modification of proteins, and gave insufficient yields for the envisioned biochemical experiments [419, 420]. Furthermore, structural and biochemical work on TRiC has been historically hindered by the similarity between its subunits, which are paralogues (~40% amino acid identity between human subunits) and can exhibit cross-reactivity in immunoblotting assays [366]. The eight CCT subunits are very similar in size, with a molecular weight within 5 kDa of each other (57.5 kDa to 60.5 kDa), making identification through their electrophoretic mobility challenging. SDS-PAGE analysis of TRiC complexes has described a “characteristic band pattern” that does not show more than five discrete bands [361, 370, 419, 420]. To study the relationship between $CRL4^{DCAF12}$ and TRiC, a protocol for the recombinant expression and purification of human TRiC was established.

The baculovirus expression vector system is widely used due to its ability to correctly co-express human proteins, especially those reliant on eukaryotic chaperones for folding or post-translational modifications [421]. DNA sequences encoding all human TRiC subunits were codon-optimized

for expression in *T. ni* as wild type or N-terminal fusions of strep(II) affinity tags. These sequences were commercially obtained as double-stranded DNA fragments with compatible overhangs for cloning into expression plasmids [422]. Cloning was complicated by faulty DNA synthesis by the manufacturer and required the sequencing of up to 35 bacterial colonies for some plasmids. After cloning, the plasmids were used to generate baculoviruses for expression. Small-scale expression tests were then carried out on all strep(II)-tagged subunits. All subunits except CCT4 expressed well and were soluble **(Figure 4.4A)**. Proteins that function within complexes are often only stable in the presence of their partner subunits. CCT4 is flanked by CCT1 and CCT2 in its TRiC ring, and shares its equatorial interface with a CCT5 subunit in the opposite ring **(Figure 4.4B)**. Expression tests for CCT4 were carried out in the presence of ring partners CCT1 and CCT2. Co-expression with any of these subunits allowed for the robust recovery of CCT4 in the *in vitro* pull-downs **(Figure 4.4C)**. This improvement did not translate to the hexadecameric complex: in expression tests, TRiC complexes could not be recovered from cells expressing an individual strep(II)-tagged subunit. Instead, subunit monomers or dimers were obtained, and these species formed regardless of the presence of other TRiC subunits **(Figure 4.4D)**. Large scale purification trials for TRiC with one strep(II)-tagged CCT subunit were then carried out. Insect cells were co-infected with baculoviruses for the expression of all untagged CCT subunits and one N-terminally his6-tagged subunit. Although the trials differed, the protocol generally involved lysing the cells by sonication in a buffer containing 50 mM Tris pH 7.5, 200 mM NaCl, 5 mM $MgCl_2$, 25 mM imidazole, 0.5 mM TCEP, 10% v/v glycerol and 1x protease inhibitor cocktail (Sigma-Aldrich). The lysate was cleared by centrifugation and the resulting supernatant applied to a gravity column

loaded with cOmplete His-tag purification resin (Roche). The resin was washed with the same buffer used for the cell lysis, and bound proteins were eluted in the same buffer supplemented with 400 mM imidazole. The eluate was further purified by ion exchange chromatography on Poros 50 HE or HQ columns (ThermoFisher scientific) using 100 mM – 1M NaCl gradients and then on a Superose 6 size exclusion column (Cytiva). The purification trials for TRiC with N-terminal his6 tags recapitulated the behaviors seen in the expression tests **(Figure 4.4E)**. Purification attempts after co-infection with baculoviruses expressing all TRiC subunits strep(II)-tagged showed that these individual proteins did not assemble into a protein complex. These results suggested that TRiC would be better produced by co-expressing its subunits from a single polycistronic expression vector, which often improves the yield, homogeneity, reproducibility, and biological activity of recombinantly produced protein complexes [422-424]. All TRiC subunits were cloned into a single expression vector using the biGBac method [425]. Expression from a single plasmid did not, however, allow for the purification of TRiC with N-terminal tags **(Figure 4.4E)**. Although mass-spectrometric analysis of chromatographic samples revealed the presence of all TRiC subunits, the estimated concentrations of some TRiC subunits were orders of magnitude higher than that of the less abundant subunits.

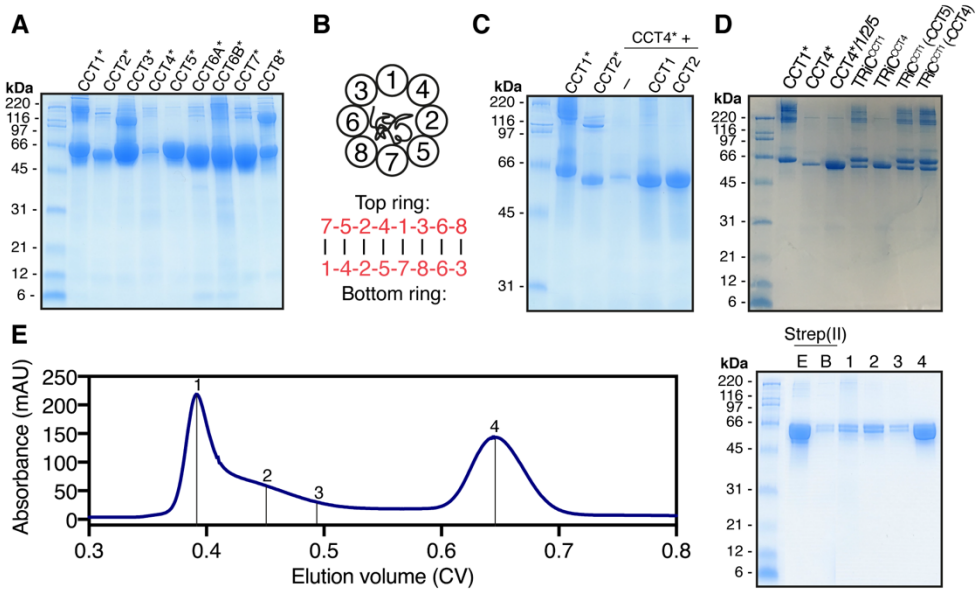

Figure 4.4. Expression tests for TRiC. (A) Expression tests for single N-terminally strep(II)-tagged CCT subunits. **(B)** Schematic top view of one ring of the TRiC chaperonin (top) and the inter-subunit connectivity between TRiC rings (bottom). **(C)** Expression test for CCT4 in the presence of CCT1 and CCT2. **(D)** Expression tests for TRiC complexes with a single N-terminally strep(II)-tagged CCT subunit. CCT4 did not pull-down other CCT subunits. Pull-downs through CCT1 show a dimeric species that does not contain all TRiC subunits, as shown for CCT1 (lane 7) and CCT5 (lane 8). **(E)** Left: size exclusion chromatograph on a Superdex 200 (Cytiva) 120 ml column from an attempted purification of an N-terminally strep(II)-tagged TRiC complex. The elution peak at ~0.38 CV corresponds to large molecular weight assemblies (like TRiC) and/or aggregated species. Right: SDS-PAGE analysis along the chromatograph reveals that the predominant soluble species is the monomeric tagged CCT1 subunit (4), whereas high molecular weight fractions (1, 2, 3) contain the dimer seen in expression tests (panel D, lanes 7 and 8). The relative absorbances and protein content of the 1 and 4 gel lanes further suggest that the high molecular weight fractions are complexed to DNA. **Data information:** In **(A,C,D,E)**, an asterisk denotes an N-terminal strep(II) tag, and TRiC is superscripted for the N-terminally strep(II)-tagged subunit. All expression tests were done with anti-strep(II) affinity resin.

The purification was then attempted with internal tags on CCT subunits. A study had previously described a favorable location for an internal his6 tag on human CCT1 [420]. Two studies were published around this time that

presented structures of human TRiC [361, 370]. Cuéllar J. *et al* purified endogenous TRiC from genetically modified human cells through tandem-affinity protocols [370]. Gestaut D. *et al* purified TRiC recombinantly from insect cells using an internal his6 tag on TRiC subunit CCT7 [361]. Baculoviruses were made for the expression of human CCT1 and CCT7 with internal his6 tags as per the two studies [361, 420]. The resulting proteins expressed poorly in comparison to N-terminally his6-tagged CCT1 and CCT7, but pulled down other TRiC subunits in co-expression tests **(Figure 4.5A)**.

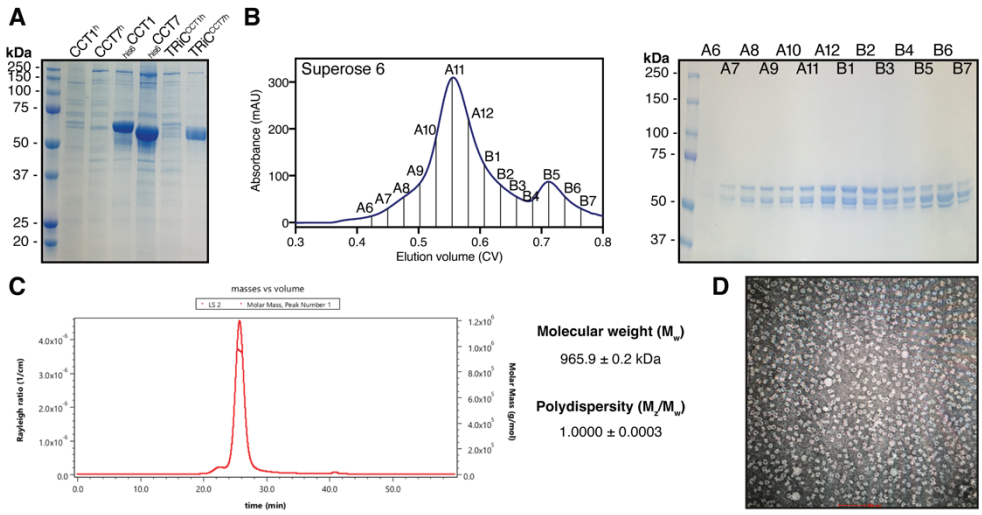

Figure 4.5. Purification of human TRiC. (A) Expression tests show that internally his6-tagged CCT1 (CCT1^{h}) and CCT7 (CCT7^{h}) express worse than their N-terminally his6-tagged counterparts ($_{his6}$CCT1, $_{his6}$CCT7), but co-expression with all other TRiC subunits yields more complete band patterns than N-terminal his6 tags (Figure 4.4D). **(B)** Left: Elution profile of human TRiC on a Superose 6 column (Cytiva), with SDS-PAGE analysis of the peak fractions (right), revealing a characteristic TRiC band pattern for the peak centered around fraction A11. **(C)** SEC-MALS analysis of purified TRiC^{CCT7h}. The chromatogram displays Rayleigh ratio curves for CCT5 together with the molar mass (in Da) of the main peak. The calculated molecular weight (M_w) corresponds to a hexadecameric TRiC complex. The polydispersity of the peak (M_z/M_w) indicates a uniform species in the peak. **(D)** Negative-stain micrograph image of a TRiC^{CCT7h} complex.

Purification for TRiC with internal his6 tags on subunit CCT1 or CCT7 was then carried out. High Five insect cells were infected using the manufacturer's recommendations with eight different baculoviruses for the expression of single CCT subunits. After cell lysis and supernatant clearance, the resulting sample was purified following the published protocol from Gestaut D. *et al* [361]. After several unsuccessful trials the authors were contacted, who generously shared an improved protocol. The application of that protocol was successful for the purification of human TRiC with internal his6 tags on CCT1 (TRiC^{CCT1h}) or CCT7 (TRiC^{CCT7h}) **(Figure 4.5B)**. SEC-MALS analysis performed on the purified TRiC^{CCT1h} or TRiC^{CCT7h} revealed that the purified TRiC complex was monodisperse and had a molecular weight consistent with that of an assembled TRiC complex (~950 kDa) **(Figure 4.5C)**. Mass-spectrometric analysis of the purified sample revealed that all subunits were present in comparable concentrations. When subjected to negative-stain EM, the purified TRiC complex had the barrel-like morphology reported in all structures of TRiC **(Figure 4.5D)** [361, 367, 368, 370, 416]. Of note, *in vivo* studies have reported that after depletion of one CCT subunit all other TRiC subunits are found monomeric in the cytosol [426-428]. Recombinant expression and purification using this protocol yielded human TRiC in sufficient quantities and purity for the envisioned assays and allowed the investigation of the biological role of CRL4^{DCAF12} towards TRiC.

4.3 CRL4^{DCAF12} Differentially Recognizes CCT5 and TRiC

The two octameric rings of TRiC contact each other through the equatorial domains of each CCT subunit **(Figure 4.6C)** [352]. This arrangement places the C-termini of all CCT subunits inside the cavity [361]. TRiC contains one copy of CCT5 in each of the two rings, both of which make extensive contacts with neighboring subunits in their respective ring. In available structures of TRiC, the CCT5 C-terminal tail observed inside the barrel, where it folds back onto itself to mediate contacts with the sensor loop of neighboring subunit CCT7 [361, 370]. In the structure by Gestaut D. *et al.*, the CCT5 C-terminal carboxyl group that is read out by DCAF12 Arg256 hydrogen bonds with the peptide backbone around CCT7 Asp51 [361]. The gamma carboxyl group of CCT5 Glu541 folds back to interact with CCT5 Lys535 (degron position -7) [361]. The side chain of CCT5 Glu540, which is docked under the pocket ceiling in the cryo-EM structure **(Figure 3.6A)**, establishes strong polar interactions with CCT7 Lys47 [361]. CCT7 Lys47 further engages CCT5 Ser539, which contacts DCAF12 Glu298 and Arg344 in the cryo-EM structure **(Figure 3.4A)**. A structure by Cuéllar J. *et al.* shows instead a C-terminus with the gamma carboxyl groups of CCT5 Glu540 and Glu541 engaged in interactions with CCT5 Arg27 and Lys25, respectively, but similarly involved in interactions with the sensor loop of CCT7 [370]. The sensor loops of CCT subunits interact with peptides folding inside the TRiC chamber and are supported by contacts with neighboring subunits [410]. The C-termini of chaperonin subunits take part in substrate folding, and the CCT5 C-terminus has been shown to contact proteins folding inside the TRiC chamber [370, 429]. As such, the CCT5 degron is engaged in a

network of interactions that supports TRiC function and is not available for binding to DCAF12 in an assembled TRiC complex.

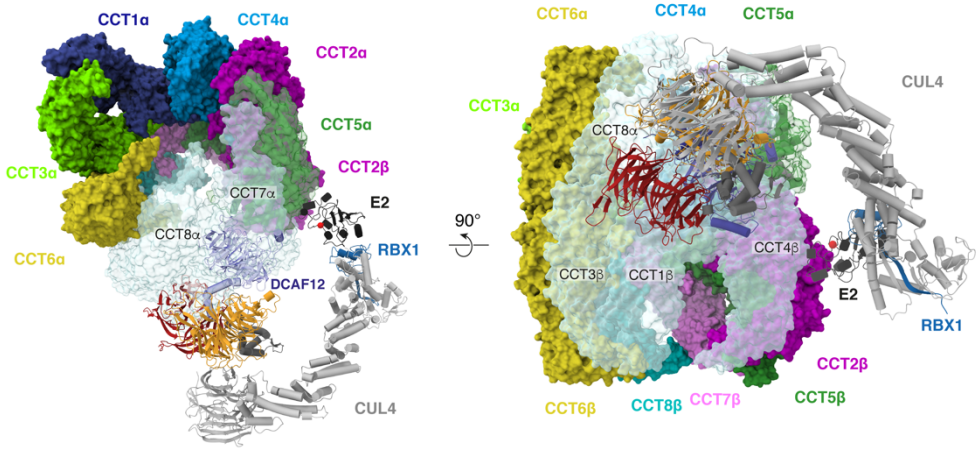

Figure 4.6. Recognition of the CCT5 Di-Glu Degron is Incompatible with TRiC Assembly. Superposition of the coordinates of CRL4^{DCAF12} onto TRiC (PDB ID 6NR8 [361]) reveals clashes and access restrictions between DCAF12 and DDB1 and several TRiC subunits (colored pale blue). TRiC subunits are labeled α or β according to the ring they occupy.

The CCT5 surfaces of the equatorial domain bound by DCAF12 **(Figure 4.2A)** are occupied in an assembled TRiC complex by ring neighbor CCT7, as well as CCT1 and CCT4 on the opposite ring **(Figure 4.6)**. As such, CCT5 within a TRiC complex does not expose the surfaces needed for recognition by DCAF12. Structural modeling of a TRiC-embedded CCT5 bound by CRL4^{DCAF12} reveals further clashes and access restrictions with the CCT8 subunit located in the same ring as the CRL4^{DCAF12}-bound CCT5, as well as with CCT3 on the opposite ring **(Figure 4.6)**. A structurally intact TRiC complex is therefore expected to protect CCT5 from recognition by the CRL4^{DCAF12} E3 ligase.

Experiments were then carried out to test whether the CRL4^{DCAF12} E3 ligase can biochemically and functionally differentiate between CCT5 in its

assembled (TRiC) and unassembled forms. The TR-FRET competition assay was used to compare the binding affinity between DDB1-DCAF12 and monomeric or TRiC-embedded CCT5. Purified CCT5 or TRiC were separately titrated against a $_{Tb}$DDB1-DCAF12^{488} complex. While DDB1-DCAF12 readily bound full-length unassembled CCT5 (IC_{50} = 219 ± 43 nM), TRiC caused a decrease in fluorescence consistent with an affinity more than two orders of magnitude lower than that of CCT5 (IC_{50} > 10 µM) despite containing within itself two binding sites for the C-terminus of its two CCT5 subunits **(Figure 4.7A)**. *In vitro* ubiquitination assays were then set up to study the catalytic activity of CRL4^{DCAF12} towards TRiC. Although CRL4^{DCAF12} robustly ubiquitinated monomeric CCT5, it showed no ubiquitination activity towards TRiC **(Figure 4.7B)**, demonstrating that the differential substrate binding by DCAF12 translated into the CRL4^{DCAF12} catalytic activity.

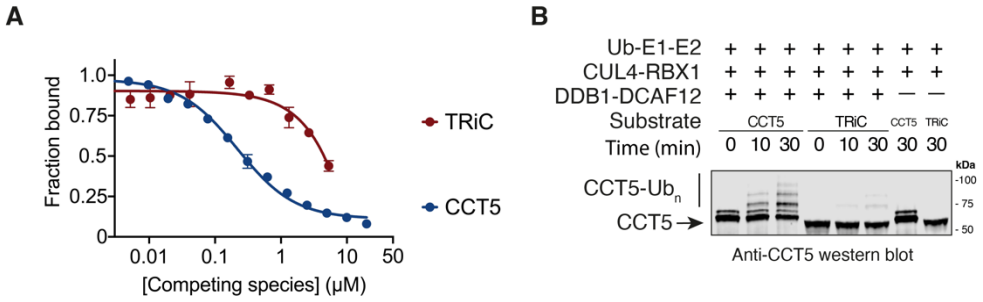

Figure 4.7. CRL4^{DCAF12} Differentially Recognizes CCT5 and TRiC. (A) Counter-titration of unlabeled CCT5 or unlabeled TRiC into pre-assembled $_{Tb}$DDB1-DCAF12^{488} (n=3). **(B)** In vitro ubiquitination of monomeric wild type CCT5 or TRiC by CRL4^{DCAF12} in the presence of ubiquitin, ATP, E1 and E2 enzymes. CCT5, but not TRiC, is modified with polyubiquitin (Ub_n) chains by CRL4^{DCAF12}. Free CCT5 protein carries an N-terminal strep(II) tag and differs in electrophoretic mobility from untagged CCT5 purified in complex with TRiC. **Data information:** In **(A)**, data is presented as means ± 95% CI.

4.4 Conclusion

The results presented in this chapter elucidate the architecture of the CCT5-bound CRL4^{DCAF12} E3 ubiquitin ligase. The architecture is consistent with the cryo-EM structures of the DDB1-DCAF12-CCT5 complex presented in Chapter 3, and suggest that CRL4^{DCAF12} carries out AQC in cells. To test that hypothesis, a recombinant expression system for human TRiC was established, and purified TRiC was tested in functional assays for its biochemical interaction with DCAF12. These assays show that CRL4^{DCAF12} binds and ubiquitinates CCT5, but not TRiC.

Taken together, the results presented in Chapter 2, Chapter 3 and Chapter 4 demonstrate that CCT5 is a substrate of the CRL4^{DCAF12} E3 ubiquitin ligase, and that its binding is driven by the di-Glu motif. DCAF12 readily binds its substrates without apparent prior post-translational modifications. In the case of CCT5, this recognition mechanism enables CRL4^{DCAF12} to read out the assembly state of the TRiC chaperonin. Detecting degrons present in monomeric proteins that become hidden in a protein complex is a hallmark of AQC E3 ubiquitin ligases [313, 314]. By targeting monomeric, but not TRiC-embedded CCT5 for degradation, CRL4^{DCAF12} displays the key characteristic of an AQC ligase.

Chapter 5

Discussion

5.1 Research Questions

The main research question introduced in **Chapter 1** is addressed by subdividing it into a series of minor questions:

1. *Does DCAF12 assemble into a functional E3 ubiquitin ligase?*

The biochemical findings presented in **Chapter 2** and **Chapter 3** unequivocally show that DCAF12 acts together with DDB1 to bind substrates. DCAF12 tightly assembles with DDB1 *in vitro*, and the resulting complex exhibits high affinity for CCT5. Analysis of the binding determinants recapitulates the findings from *in vivo* studies [126]. DCAF12 assembles with DDB1 using its HLH motif, which had been predicted to mediate interactions with DDB1 [201, 202]. The resulting complex further assembles with purified CUL4 and RBX1 to form a functional E3 ubiquitin ligase that efficiently ubiquitinates CCT5, in accordance with the functional association between CUL4, DDB1, RBX1 and DCAF12 *in vivo* [126].

2. *Does CRL4^{DCAF12} target CCT5 for degradation? If so, what are the binding determinants of the interaction between CCT5 and DCAF12?*

As shown in **Chapter 3**, a reconstituted CRL4^{DCAF12} E3 ubiquitin ligase efficiently ubiquitinates CCT5, which leads to its proteasomal degradation [126]. **Chapter 2** and **Chapter 3** show that binding of CCT5 is driven by its C-terminal degron: a CCT5$_{20}$ peptide binds DCAF12 *in vitro* with an affinity comparable to that of full-length CCT5, and C-terminal CCT5 peptides show that a length around 10 amino acids is sufficient for optimal di-Glu degron binding. Within the degron, recognition is strictly dependent only on the C-terminal glutamates, and in particular on the -2 glutamate. Despite the minimal length of the di-Glu degron, mutations in the C-terminal glutamate are tolerated by DCAF12. Although individual residues preceding the C-terminal glutamates are not strictly required for binding, collective variability in these residues significantly impacts binding to DCAF12.

3. *What is the structure of DCAF12?*

Chapter 3 presents two high-resolution cryo-EM structures that provide the atomic coordinates of the DDB1-DCAF12 complex. Reproducing structures from previous studies, DDB1 is formed by three β-propeller domains (BPA, BPB, BPC) bridged by a small C-terminal domain [201]. The structure of DCAF12 is obtained, showing an N-terminal helix-loop-helix motif and a WD40 β-propeller domain. The DCAF12 β-propeller is formed by seven blades of antiparallel β-sheets and adopts the shape of a truncated cone resting on DDB1. Further contacts are mediated by the DCAF12 helix-loop-helix, which protrudes from the base of the cone to dock between the DDB1 BPA

and BPC β-propellers in a manner similar to other DDB1 substrate receptors [154, 201, 202, 386]. At the crest of the DCAF12 β-propeller, several loops converge to form a surface pocket that is kept in place by a large loop between DCAF12 blades six and seven.

4. *How does DCAF12 recognize the CCT5 di-Glu degron?*

The amino acids of the DCAF12 pocket are basic and hydrophobic, and have been very highly conserved throughout evolution. Between the pocket wall and the ceiling, DCAF12 Lys91 and Lys108 form a patch that locks down the gamma carboxyl group of the -2 degron glutamate (CCT5 Glu540) under the pocket ceiling. In contrast, the C-terminal degron glutamate is engaged by DCAF12 in a solvent-exposed location that can accommodate multiple conformations and types of side chain. The C-terminal carboxyl group of the degron faces the core of the β-propeller, where it forms a tight interaction with DCAF12 Arg256. Importantly, this interaction signals the C-terminal nature of the degron. The remainder of contacts observed between DCAF12 and CCT5 are mediated by the CCT5 backbone or involve weak side chain interactions. This mode of binding, exposed in **Chapter 3**, is supported by the mutagenesis and functional data presented in **Chapter 2**, is consistent with published reports on the binding determinants to DCAF12 [126] and explains the laxer identity requirements for the -1 degron residue [332]. Accordingly, the interactions mediated by the DCAF12 amino acids contacting the CCT5 di-Glu degron are necessary for substrate binding and ubiquitination *in vitro*.

5. *What is the architecture of the CCT5-bound CRL4^{DCAF12} E3 ligase?*

The high-resolution cryo-EM structures of the DDB1-DCAF12 complex shown in **Chapter 3** can be used to model the architecture of the CCT5-bound $CRL4^{DCAF12}$ E3 ubiquitin ligase, fitting the negative-stain map presented in **Chapter 4**. CRLs adopt a U-shaped architecture that brings together the bound ubiquitination substrate and activated E2-Ub enzyme to catalyze the ubiquitin transfer reaction. To achieve this architecture, DDB1 uses its BPB domain to bind the N-terminus of CUL4, which connects it to an RBX1 protein bound to the CUL4 C-terminus. RBX1 then acts as a docking platform for an activated E2~Ub enzyme. Substrate binding juxtaposes the substrate to the active site of the E2 enzyme, catalyzing the ubiquitin transfer reaction [413].

6. *Does $CRL4^{DCAF12}$ differentially recognize CCT5 and TRiC? If so, what is the reason behind the differential recognition?*

As shown in **Chapter 4**, DDB1-DCAF12 binds CCT5 *in vitro*, but not TRiC. Accordingly, this differential binding translates into the catalytic activity of the E3 ligase: CCT5, but not TRiC, is modified with polyubiquitin chains by $CRL4^{DCAF12}$ *in vitro*. This differential binding can be explained using published structures of TRiC [361, 370] and the architecture of $CRL4^{DCAF12}$ modeled from the negative-stain structure presented in **Chapter 4**. In a TRiC complex the CCT5 C-terminus, which drives recognition by DCAF12, is engaged in a network of interactions with the sensor loops of CCT7 and with folding substrates that supports TRiC function. Further surfaces of the CCT5 equatorial domain contacted by DCAF12 are sequestered in the TRiC complex by CCT1, CCT4 and CCT7, preventing recognition by DCAF12. The presence of DDB1, as is necessary for recognition by a functional $CRL4^{DCAF12}$ E3 ubiquitin ligase, is further impeded by CCT3 and CCT8. A

structurally intact TRiC complex therefore protects CCT5 from $CRL4^{DCAF12}$-mediated degradation.

Therefore, the main research question guiding the work carried out for this Thesis

> **Main research question:** *Can C-terminal degrons recognized by DCAF12 serve as signals for complex assembly?*

can be positively answered. In the case of CCT5/TRiC, the nature of C-terminal di-Glu degrons clearly allows $CRL4^{DCAF12}$ to sense the assembly state of the TRiC chaperonin. The following section contains a justification for the necessity of such an activity in vivo, along with a discussion on questions unanswered by this Thesis.

5.2 Outlook

Regulation of most cellular processes necessitates coordinated and specific protein degradation. In humans, substrate recognition by E3 ubiquitin ligases is followed by rapid, processive polyubiquitination and subsequent proteasomal degradation of the substrate. Understanding the molecular determinants of degron recognition is therefore crucial to understand ubiquitin-mediated signaling. The $CRL4^{DCAF12}$ E3 ubiquitin ligase triggers the downregulation of substrates with a C-terminal di-Glu motif [126]. This

work has confirmed the association of DCAF12 into an E3 ligase that targets CCT5. It demonstrated that di-Glu degron binding drives substrate recruitment to DCAF12 and that alternative DCAF12 degrons exist, in agreement with published studies [126, 332]. Two high-resolution cryo-EM maps of the substrate recognition module of the $CRL4^{DCAF12}$ E3 ligase are presented, alone and in complex with CCT5. The maps elucidate the previously unknown structure of DCAF12 and identify the molecular determinants of di-Glu degron recognition. Key carboxyl groups of the CCT5 di-Glu motif are extensively read out through strong interactions with conserved and positively charged amino acids in the DCAF12 pocket. Residues preceding the C-terminal glutamates (degron residues -3 to -5) predominantly engage in Van der Waals interactions with DCAF12 and display little sequence preference. DCAF12 reads however a larger degron sequence, and displays different affinity for different substrates. Extensive trials were carried out to improve the completeness and quality of the structures to no avail. Of note, no structure of a C-end ligase has been determined that shows a degron peptide longer than 11 residues (PDB ID 7EL6 [338]), and significant variability in binding affinity exists between substrates bound through the same degron [334-338]. It now appears likely that C-end degron-containing substrates are recognized almost exclusively through their C-termini, and retain limited but significant flexibility when bound to their substrate receptor [334-338], hindering high-resolution structural studies.

The ultimate goal of this line of research is to understand the biological function of the proteins studied. To that end, the architecture of the CCT5-bound $CRL4^{DCAF12}$ E3 ubiquitin ligase was elucidated. The modeled structure was used to predict that recognition of CCT5 by DCAF12 is

mutually exclusive with its assembly into a TRiC complex. Subsequent experiments confirm that $CRL4^{DCAF12}$ differentiates between CCT5 in its monomeric and TRiC-embedded forms, and structural data provides a fitting rationale: unassembled, monomeric CCT5 has a flexible and solvent-exposed C-terminus that in a TRiC complex is engaged in a network of interactions necessary for chaperonin activity. The CCT5 di-Glu degron, as well as the other CCT5 surfaces bound by DCAF12, is unavailable for binding in a TRiC complex. The ability to differentiate between the assembled and unassembled forms of their substrates is a hallmark of AQC E3 ligases. The biochemical and structural data presented in this work supports a role for the $CRL4^{DCAF12}$ E3 ubiquitin ligase in the AQC of the TRiC chaperonin *in vivo*.

It is currently unknown how TRiC assembles in cells. The eight CCT genes are transcribed from eight different chromosomes and must occupy defined positions in the rings. Most TRiC subunits have been shown to assemble co-translationally to minimize the abundance of orphaned CCT subunits [293], yet how cells survey their assembly is unknown. CCT5 forms TRiC-like double homo-octameric rings *in vitro*, and it has been proposed that these homo-octamers nucleate the assembly of other TRiC subunits *in vivo* [410, 430]. Cells might therefore promote TRiC assembly by comparatively overexpressing CCT5 to nucleate the assembly of other TRiC subunits, and TRiC subcomplexes originating from incomplete assembly would the cleared out by $CRL4^{DCAF12}$. In that context, a tight control of incompletely assembled CCT5 would be necessary to ensure productive TRiC assembly. Competition between DCAF12 and other TRiC subunits for CCT5 binding could be an efficient mechanism to promote TRiC assembly and minimize premature degradation of TRiC subcomplexes. That strategy is plausible, because the cellular abundance of TRiC subunits is ~180x larger

than that of DCAF12 [431]. Crude mammalian cell extracts contain very low amounts of low-molecular-weight oligomers of CCT subunits [366]. Crucially, the connectivity between these oligomers differs from that in the functional TRiC complex [366]. It is possible that these oligomers are the product of defective TRiC biogenesis and their low abundance is due to, among others, $CRL4^{DCAF12}$-mediated degradation.

These findings similarly implicate $CRL4^{DCAF12}$ in the clearance of supernumerary CCT5 subunits. Human proteomes are characteristically non-stoichiometric, and are greatly burdened by non-stoichiometric subunit assembly [297, 300, 310, 432]. Subunit imbalances can generate cytotoxic species, particularly in the context of altered gene expression [241, 299]. TRiC activity is required for optimal viability and fitness of human cells [371, 372]. Based on the biochemical and structural findings presented in this work, $CRL4^{DCAF12}$ is ideally suited to prevent the accumulation of potentially toxic TRiC assembly intermediates and orphaned CCT5 subunits that expose the C-terminus of CCT5, and in this manner support proteostasis. The half-lives of individual TRiC subunits are very tightly correlated *in vivo*, supporting a mechanism by which an exposed CCT5 C-terminus induces the degradation of several TRiC subcomplexes [433].

It is likely that DCAF12 has cellular functions other than AQC. In drosophila, it has recently been shown that DCAF12 binds inhibitor of apoptosis proteins (IAPs) via recognition of their BIR motifs [330]. BIR binding activity has not been unequivocally mapped to a specific surface in DCAF12: DCAF12 constructs lacking individual β-propeller blades, which are not expected to correctly fold and be functional, retain affinity to IAP proteins [330]. BIR recognition does not lead to IAP downregulation. Instead, binding to DCAF12 displaces inhibitory IAPs from pro-apoptotic caspases

[330]. These interactions are CUL4 and DDB1-independent, and partially underlie the pro-apoptotic functions of DCAF12 [330]. Two DCAF12 paralogues (protein sequence similarity ~70%) exist in placental mammals, likely arising from retrotransposition and tandem duplication [434, 435]. Despite having a conserved pocket, these DCAF12-like proteins greatly differ in sequence around the HLH motif and Loop. Their expression patterns differ from that of DCAF12, and the two paralogues appear to be functionally redundant and unrelated in biological function to DCAF12 [330, 332].

$CRL4^{DCAF12}$ is however ideally suited to oversee the assembly of other protein complexes. The N- and C-termini of proteins are structurally more flexible than internal protein sequences, and many might only fold upon binding their partners in a complex [436]. Diamine acetyltransferase 1 (SAT1) is a small globular protein that is active as a homodimer [437]. SAT1 contains a di-Glu degron and is a reported substrate of DCAF12 [126]. In the dimer, the C-terminal tail of SAT1 forms an antiparallel β-sheet between monomers continued by a short alpha helix containing the di-Glu degron, which contributes to interactions between monomers. The C-terminal tail of SAT1 mediates dimerization and is not accessible in the dimeric form. In its monomeric state, however, the SAT1 di-Glu degron is expected to become solvent-exposed and competent for binding to DCAF12. The precise orders of subunit incorporation into a complex are conserved in evolution, likely reflecting a way to minimize mis-assembly [438]. It stands to reason that conservation of assembly steps allows for their regulation by dedicated E3 ligases. It is thus reasonable to speculate that most protein complexes have dedicated E3 ligases that oversee their assembly.

It is similarly likely that other degrons signal defective complex assembly. A number of E3 ligases (including $CRL4^{DCAF12}$, $CRL2^{FEM1A/B/C}$

and $CRL2^{KLHDC2}$) have been identified that recognize specific sequences in the C-terminus of proteins [126]. FEM1 proteins recognize different degrons with a common C-terminal arginine (R-end). KLHDC2 recognizes a C-terminal di-glycine (di-Gly) motif that similarly tolerates mutations better at the -1 than the -2 position [337]. Despite having a different protein fold and recognition mechanism, these ligases are mechanistically related to $CRL4^{DCAF12}$. Like di-Glu degrons, the di-Gly and R-end degrons have been found in prematurely terminated or otherwise aberrant proteins, but also in a number of biologically active polypeptides and full-length proteins [126, 339]. The traditional view of E3 ligases is that they are not constitutively active but rather target substrates in response to specific cues. It is therefore likely that other C-end ligases that bind unmodified C-termini participate in AQC in cells.

Chapter 6

Review Article: Quality Control of Protein Complex Assembly by the Ubiquitin-Proteasome System

Bibliographical work during the candidate's doctoral period has led to the publication of a review article in the journal *Trends in Cell Biology* [313]. The article, titled *"Quality Control of Protein Complex Assembly by the Ubiquitin-Proteasome System"* focuses on recent discoveries on the mechanisms by which the ubiquitin-proteasome system regulates the assembly of cellular complexes. Parts of this Thesis have been adapted from the contents of this article. This chapter contains the review article in its final edited form by the publishers.

CellPress
OPEN ACCESS

Trends in
Cell Biology

Review

Quality control of protein complex assembly by the ubiquitin–proteasome system

Carlos Pla-Prats[1,2] and Nicolas H. Thomä[1,*]

The majority of human proteins operate as multimeric complexes with defined compositions and distinct architectures. How the assembly of these complexes is surveyed and how defective complexes are recognized is just beginning to emerge. In eukaryotes, over 600 E3 ubiquitin ligases form part of the ubiquitin–proteasome system (UPS) which detects structural characteristics in its target proteins and selectively induces their degradation. The UPS has recently been shown to oversee key quality control steps during the assembly of protein complexes. We review recent findings on how E3 ubiquitin ligases regulate protein complex assembly and highlight unanswered questions relating to their mechanism of action.

Highlights

The majority of human proteins function as part of multimeric protein complexes.

Subunit stoichiometry *in vivo* is highly variable, and a significant fraction of the proteome arises from non-stoichiometric synthesis.

The ubiquitin–proteasome system (UPS) can detect failures in complex assembly and target unassembled or incorrectly assembled complexes for degradation.

Key cellular complexes such as hemoglobin, BTB (broad complex, Tramtrack, and Bric-à-brac) dimers, the proteasome, and the ribosome have recently been shown to undergo assembly quality control (AQC).

AQC safeguards cellular function and health.

Principles of protein complex synthesis and assembly

Proteins are key effectors of all cellular processes. To carry out their biological roles, most proteins assemble into multimeric complexes of defined architecture and composition [1]. Three fundamental steps are required to generate functional protein complexes: transcription, translation, and the folding and assembly of newly synthesized polypeptides into functional three dimensional structures. Protein folding starts in the ribosome exit tunnel, facilitated by a network of ribosome-associated chaperones [2], and 30% of proteins require further assistance from specialized chaperones to attain their biologically active conformation [2]. Misfolded or misassembled proteins are prone to cytotoxic aggregation, and defects in protein folding and assembly underlie conditions including aging, cancer, and neurodegeneration [3,4]. For protein complexes to form, newly-synthesized subunits must come together spatially and temporally, and develop inter-subunit interfaces while simultaneously avoiding interactions with unrelated cellular components. Assembly must additionally take place stoichiometrically and not generate potentially cytotoxic intermediates. To facilitate this process, organisms – most notably prokaryotes – organize functionally related genes into operons, and differentially express the open reading frames (ORFs) within the resulting mRNAs to match the stoichiometry in the final complex [5–7]. A similar effect is achieved by genetic fusions between separate functional domains into single proteins, predominantly in yeast [8]. Several post-transcriptional mechanisms further promote complex assembly. The mRNAs of functionally related proteins often colocalize *in vivo* [9,10], and nascent subunits frequently interact with their partners cotranslationally [11,12]. Interactions between nascent proteins can be further aided by assembly-guiding chaperones [13,14]. Despite these regulatory mechanisms, the assembly of protein complexes remains an intrinsically error-prone process, and nonstoichiometric subunit synthesis, as well as stochastic errors in assembly, continually generate protein orphans and defective protein complexes [15–17]. Around half of all mammalian protein complexes are produced with at least one subunit synthesized in nonstoichiometric amounts [18], and ~10% of the nascent proteome is estimated to arise from nonstoichiometric synthesis or failed assembly [15]. Furthermore, the subunit stoichiometry of many eukaryotic complexes varies across cell types and throughout differentiation [18]. Subunit imbalances, particularly

[1]Friedrich Miescher Institute for Biomedical Research, Maulbeerstrasse 66, 4058 Basel, Switzerland
[2]Faculty of Science, University of Basel, Petersplatz 1, 4001 Basel, Switzerland

*Correspondence:
Nicolas.Thoma@fmi.ch (N.H. Thomä).

© 2022 The Authors. Published by Elsevier Ltd. This is an open access article under the CC BY-NC-ND license (http://creativecommons.org/licenses/by-nc-nd/4.0/).

in the context of altered gene expression such as in stress and cancer, can generate cytotoxic species through subunit aggregation as well as by gain, or loss, of function [14,17].

The stability of most proteins *in vivo* cannot be accurately predicted from factors such as mRNA half-life and protein abundance, and instead depends on post-translational events such as ubiquitination [15,19]. It has long been known that loss of one subunit can induce the degradation of its partners within the complex [20], and that non-stoichiometric subunit synthesis can generate stoichiometric complexes [21]. An attractive explanation for such behavior is that the stability of proteins is linked to their assembly into complexes. This long-standing hypothesis gained weight after proteomic experiments showed that subunits of protein complexes follow different degradation kinetics *in vivo* than monomeric proteins [15]. Supporting this hypothesis, most ubiquitinated proteins are relatively young [24], and up to 30% of the nascent proteome is degraded shortly after synthesis [22], although the extent of this degradation remains controversial [15,23]. The UPS is the major route for selective protein degradation in eukaryotic cells. Following a three-enzyme (E1–E2–E3) cascade, the 76 amino acid protein ubiquitin is covalently linked to a target protein. A complex code of ubiquitination signals determines the fate of the target protein [25]. Ubiquitination events with lysine 48-containing linkages serve as the main signals for degradation by the 26S proteasome. Lysine 63 linkages, for example, have been associated with NF-κB signaling, DNA repair, and autophagy, a process that degrades misfolded, large, or aggregation-prone cellular components that cannot be removed by the 26S proteasome [25,26]. The specificity of the UPS is conferred by E3 ubiquitin ligases, which directly engage their substrates through epitopes in the target protein termed degrons [27]. Although >600 E3 ligases have been identified in human cells [28], only a small fraction have known substrate pairings, and most proteins known to undergo ubiquitination, in turn, have not been mapped to a corresponding E3 ligase [29]. The role of the UPS in the quality control of monomeric proteins is well established [30,31], and defects in this pathway are associated with cytotoxicity [4]. The UPS has recently been shown to distinguish between and differentially target the monomeric and assembled forms of some substrates, and it has been proposed that such differential targeting plays an important role in correct protein complex assembly. We term this functionality 'assembly quality control' (AQC). AQC E3 ubiquitin ligases target unassembled or incorrectly assembled subunits of protein complexes for degradation to safeguard proteostasis (Figure 1), as exemplified by the following examples.

COG complex regulation by Not4

The conserved oligomeric Golgi (COG) complex is a ~500 kDa tethering complex that coordinates retrograde vesicle trafficking within the Golgi [32,33]. Defects in the COG complex affect the cellular glycosylation balance, and mutations in COG subunits result in congenital glycosylation disorders [34–37]. COG is composed of eight subunits, COG1–8, which are arranged into a bilobed structure in which the two lobes are composed of subunits COG2/3/4 and COG5/6/7, respectively [32,33]. The two lobes are bridged together by subunits COG1 and COG8 which interact through their N termini [38]. The N terminus of COG1 is acetylated, and the modification directly mediates the interaction with COG8 in the fully assembled complex. This in turn sequesters the COG1 N terminus from the solvent.

Around 60% of yeast proteins and 90% of human proteins are N-terminally acetylated [39]. N-terminal acetylation (Ac) serves as a recognition signal for a family of E3 ligases named N-recognins which mediate the degradation of N-acetylated substrates through the Ac/N-end pathway [40]. Yeast Cog1 is N-terminally acetylated *in vivo*, and the resulting Ac/N-end degron is recognized by the N-recognin Not4 [41]. This occurs in the monomeric, orphaned form of Cog1, where its exposed acetylated N terminus serves as the degradation signal for the Ac/N-end pathway. In the COG complex, however, the N-terminal acetylation mark in Cog1 is not accessible. Through

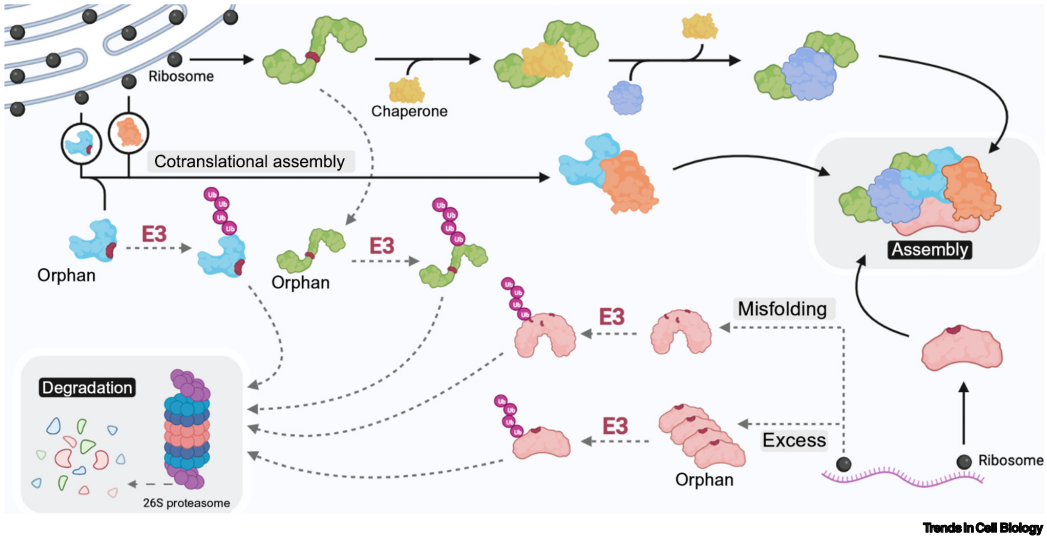

Figure 1. The ubiquitin–proteasome system (UPS) oversees protein complex assembly. The subunits of a protein complex may be synthesized in different cellular locations and must come together for functional assembly. Unassembled subunits of protein complexes are often recognized via degrons (shown in red) that are hidden or nonexistent in the assembled complex. Proteins can hide these surfaces with the help of chaperones or by post- and co-translationally assembling with their partners, among others. Proteins that misfold or fail to bind their partners are polyubiquitinated by AQC E3 ligases which target them for proteasomal degradation. Abbreviation: Ub, ubiquitin.

cycloheximide-chase experiments, it was shown that the half-life of Cog1 depends on the assembly state of the COG complex [41]. In the absence of stoichiometric amounts of Cog8, as mimicked by Cog1 overexpression, Cog1 is quickly polyubiquitinated by Not4 and subsequently degraded [41]. In this manner, an E3 ligase is able to read out the assembly state of a protein complex by targeting the free, accessible form of a protein over its complexed, inaccessible counterpart.

The same study found analogous regulatory principles for the APC/C complex and its Hcn1 subunit [41]. Hcn1 is similarly N-terminally acetylated, and its Ac/N-end degron is nested inside a deep chamber formed by the APC/C subunit Cut9 [42]. The monomeric, unassembled Hcn1 is quickly ubiquitinated by the Not4 E3 ligase, whereas Hnc1 in the assembled APC/C is spared [41]. These examples suggest a mechanism whereby stoichiometric complex assembly is controlled by ubiquitin ligases that preferentially target orphan subunits, and this degron-hiding mechanism has been termed 'subunit decoy' [41].

BTB (broad complex, Tramtrack, and Bric-à-brac) dimerization regulation by FBXL17

BTB domains are found in >200 human proteins, most of which assemble into CUL3 E3 ubiquitin ligases, transcription factors, and membrane channels to regulate crucial cellular processes such as cell division and differentiation [43–45]. To ensure correct signaling output of CUL3 E3 ubiquitin ligases, most BTB proteins must homodimerize. BTB homodimerization is mediated through contacts between each BTB core, and is followed by a strand swap between monomers that connects the dimers through antiparallel β-sheets. Two consecutive studies demonstrated that productive BTB homodimerization is ensured via FBXL17-dependent degradation of

misassembled BTB pairs, thereby providing the first molecular mechanism of dimerization quality control [16,46].

FBXL17 is the substrate-binding module of a CUL1 E3 ubiquitin ligase [27]. Its F-box domain mediates the interaction with Skp1 that is necessary for its assembly into an E3 ligase, while two motifs in its C-terminal region mediate substrate binding: a solenoid formed by 12 leucine-rich repeats (LRRs) and a C-terminal helix (CTH), which together bind a single BTB domain. In its substrate-bound form, the FBXL17 LRR solenoid closely wraps around the bound BTB domain in a manner that is incompatible with CUL3 binding, while the CTH extends beyond the solenoid to encircle the BTB substrate and block its homodimerization interface [46]. BTB engagement with FBXL17 is thus mutually exclusive with dimeric BTB assembly into aberrant CUL3 E3 ubiquitin ligase complexes (Figure 2).

Dimerization quality control by FBXL17 significantly differs from the substrate decoy mechanism. Instead of detecting a degron that is hidden in a correctly assembled homodimer, FBXL17 detects an aberrant, metastable dimer interface [16]. BTB binding to FBXL17 only occurs if the intermolecular β-sheet between monomers is disrupted, and it is the intrinsic instability of the

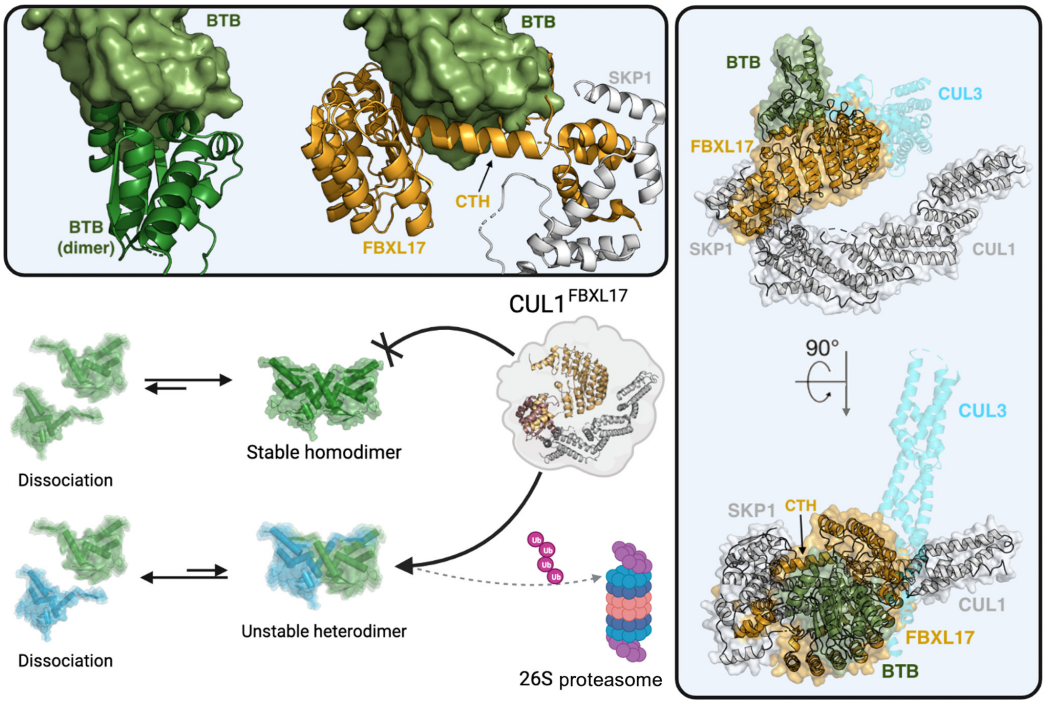

Figure 2. The CUL1^{FBXL17} E3 ubiquitin ligase ensures correct BTB domain dimerization. Misassembled BTB dimers are quickly detected by the CUL1^{FBXL17} E3 ligase, which polyubiquitinates them for proteasomal degradation [16]. FBXL17 assembles with the N terminus of CUL1 through adaptor SKP1. At the CUL1 C terminus, RBX1 recruits E2 enzymes to allow substrate ubiquitination. In its substrate-bound form, FBXL17 blocks the interfaces used by BTB proteins for homodimerization and assembly with CUL3 (shown clashing with the FBXL17 LRRs) [46]. Abbreviations: BTB, broad complex, Tramtrack, and Bric-à-brac; LRR, leucine-rich repeat; Ub, ubiquitin.

BTB dimer that gates substrate recognition [46]. In this manner, FBXL17 recognizes the shape of the BTB domain through its LRRs while simultaneously probing the stability of the BTB dimer interface with its CTH. Two physiologically relevant species present such metastable interfaces: inactive heterodimers and mutated homodimers. BTB domains dimerize cotranslationally [12], and aberrant BTB heterodimers arising from stochastic errors in translation are readily detected by FBXL17 [46]. A small subset of BTB proteins functionally heterodimerize, and these heterodimers appear to evade ubiquitination by FBXL17 [16].

A model was suggested whereby aberrant BTB dimers are detected and ubiquitinated by FBXL17 in a manner reminiscent of an exchange factor [47]. As such, FBXL17 facilitates the formation of more thermodynamically stable BTB complexes by dissolving and ultimately inducing the degradation of incorrect BTB dimers. A single ligase is thereby capable of proofreading the assembly of a myriad of protein complexes. This elegant dimer quality control mechanism is likely the founding example of AQC systems for modular domains.

Hemoglobin quality control by UBE2O

Erythrocytes transport oxygen transport across human tissues. In healthy adults, 2 million erythrocytes are produced every second in a process termed erythropoiesis [48]. During erythropoiesis, erythrocyte precursors lose most organelles, including mitochondria, ribosomes, and even their nucleus, to become highly specialized in oxygen transport [48]. This crucial function is carried out by the tetrameric protein complex hemoglobin, which is present at ~100 million copies per erythrocyte and constitutes ~98% of the soluble proteome of erythrocytes [49,50]. Hemoglobin is composed of two α and two β globin subunits, each of which uses a heme cofactor to bind and transport oxygen. Assembly of hemoglobin occurs in a sequential manner. After synthesis, α-globin is sequestered by the chaperone alpha-hemoglobin-stabilizing protein (AHSP), which binds to and protects a basic and hydrophobic (BH) patch occupied by β-globin in the assembled complex [51]. AHSP is eventually displaced by β-globin to form an α–β dimer, which then binds to another α–β dimer to form a mature hemoglobin complex. Single α and β subunits have suboptimal oxygen-binding dynamics, and positive cooperativity between the correctly assembled hemoglobin complex is necessary for efficient oxygen transport. Whereas assembled hemoglobin has an exceptionally long half-life, orphaned α-globin precipitates, distorting erythrocyte morphology and triggering their removal by the spleen. In human thalassemia, exaggerated globin precipitation causes anemia [52]. The integrity of the hemoglobin complex is therefore fundamental for human life.

To mitigate these challenges, erythrocytes upregulate quality control factors during their differentiation. One such factor is UBE2O, a 143 kDa ubiquitin-conjugating (E2) enzyme that also displays ubiquitin ligase (E3) activity [53]. Two studies recently showed that UBE2O detects and binds to the exposed BH patch in monomeric α-globin to mediate its ubiquitination, whereas an assembled hemoglobin complex that hides this patch is spared [54,55]. Accordingly, pathological mutations in α-globin that impede binding to AHSP trigger α-globin ubiquitination [55], and α-globin is preferentially ubiquitinated in β-thalassemia, a disease characterized by substoichiometric β-globin synthesis [56]. UBE2O thus contributes to functional oxygen transport across tissues by regulating the stoichiometric assembly of the hemoglobin complex (Figure 3).

However, such BH degrons are not exclusive to α-globin, and UBE2O appears to have a wider range of substrates. UBE2O is known to bind to orphaned or mislocalized ribosomal subunits in the cytosol through a subunit decoy mechanism similar to that of hemoglobin (Figure 3) [54,55]. UBE2O contains multiple substrate recognition domains with different binding specificities, and, when overexpressed in HEK cells, drives the downregulation of >600 proteins [54].

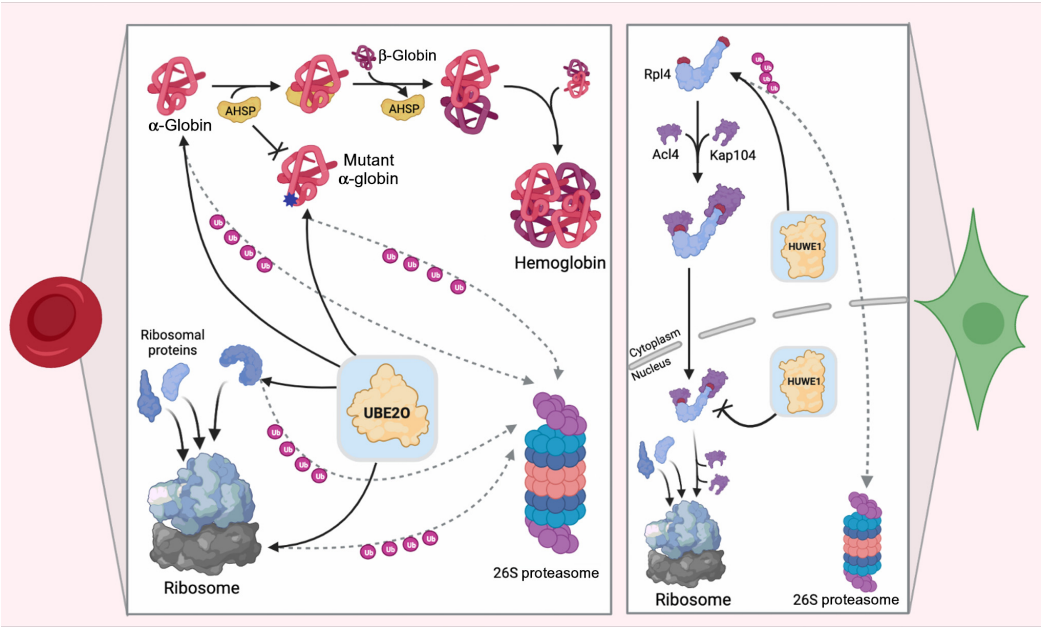

Figure 3. UBE2O and HUWE1 carry out assembly quality control (AQC) in human cells. UBE2O safeguards oxygen transport in humans by targeting unassembled α-globin in reticulocytes [54,55]. In addition, UBE2O targets unassembled ribosomal proteins [54,55], and may also ubiquitinate fully assembled ribosomes [54]. Additional AQC pathways for ribosomes have been described in human cells, where HUWE1 polyubiquitinates unassembled ribosomal subunits such as Rpl4 [59]. Other substrates have been described for HUWE1, most of which are likely orphans of multiprotein complexes [62].

Ribosome assembly regulation by HUWE1/UBE2O

Ribosomes are central to all cellular life. Human ribosomes are composed of 80 protein subunits and four rRNA molecules which must come together stoichiometrically for functional ribosome assembly [57]. Ribosome biogenesis requires the concerted action of >200 protein and RNA factors which engage newly synthesized ribosomal subunits in the cytosol and traffic them into the nucleus for assembly [58]. Ribosomal proteins are known to be exceptionally unstable in their monomeric form, but are stable when assembled into ribosomes [19,59].

Evidence for selective degradation of individual ribosome subunits is long-standing. Proteomic studies over 40 years ago showed that newly synthesized ribosomal subunits are undetectable in the absence of rRNA [20], and, accordingly, superstoichiometric subunits resulting from overexpression or synthetic aneuploidy are quickly degraded [60,61]. Many ribosomal subunits appear in fact to be endogenously synthesized in superstoichiometric amounts that are then degraded in their free form through dedicated E3 ligases as part of their natural assembly process [60]. A recent study identified human HUWE1 as one such ligase [59]. Recognition of unassembled ribosomal subunits by HUWE1 involves basic patches that mediate contacts with the rRNA core and are inaccessible in an assembled ribosome, allowing HUWE1 to ubiquitinate excess subunits while sparing an assembled ribosome [59]. Tom1, the yeast homolog of HUWE1, ubiquitinates at least 20 different ribosomal subunits, including Rpl4. Rpl4 binds chaperone Acl4 and karyopherin Kap104 after synthesis before being translocated into the nucleus. Tom1 preferentially

ubiquitinates three lysines in RPL4 that are hidden in both the Rpl4–Acl4–Kap104 complex and the assembled ribosome (Figure 3) [59]. Degradation of unassembled ribosomal subunits through a subunit decoy mechanism appears to be a conserved strategy for the quality control of ribosome assembly across eukaryotes.

Key questions remain, however. HUWE1 is an extremely large (450 kDa) E3 ligase with multiple substrate-binding domains, and it has been shown to additionally recognize orphan subunits from many different complexes, most likely through degrons different from those in ribosomal subunits [62]. Simultaneously, other ligases are known to target the ribosome and its components. Similar to α-globin, many ribosomal subunits contain BH patches that are putative targets of UBE2O. Several of these have been shown to bind to and be ubiquitinated by UBE2O when unassembled, highlighting an AQC function of UBE2O for the ribosome [54,55]. In one study, however, UBE2O expression was associated with degradation of both orphaned ribosomal subunits and intact ribosomes, pointing to a broader role of UBE2O in reticulocyte maturation (Figure 3) [54]. The emerging picture is arguably an initial snapshot of a complex regulatory process, given the hundreds of factors involved in ribosome maturation.

Proteasome assembly control by HERC1

The 26S proteasome degrades ubiquitinated cargo to restart the life cycle of the majority of eukaryotic proteins. Its 19S regulatory particle (RP) directs the processing and entry of ubiquitinated cargo into a 20S core particle (CP), in which substrates are proteolytically cleaved into short peptides with no structural information [14]. Proteasome function is indispensable for cellular proteostasis, and drugs targeting the proteasome have been used as therapeutic agents against several diseases, particularly in oncology [63,64]. With a size of ~2.5 MDa and comprising 47 subunits in humans, the proteasome is a highly complex molecular machine and the largest known eukaryotic protease. The proteasomal 20S CP is formed by two heteroheptameric rings of α and β subunits stacked back-to-back. Its assembly is initiated by the formation of an α ring, which then serves as a nucleation template for the β ring. The 19S RP sits on either end of the 20S CP and is formed by lid and base subcomplexes that assemble independently before joining to form a 19S RP [14]. To prevent premature catalytic activation, several assembly factors protect individual subunits during their assembly. One such factor, PAAF1, binds to subunit PSMC5 throughout its assembly into the 19S base, and dissociates only when the 20S and 19S subcomplexes assemble together [65–68].

A recent study identified HERC1 as an E3 ligase that targets unassembled PSMC5 [69]. In direct contrast to other AQC pathways, HERC1 does not recognize orphaned PSMC5 but instead recognizes PAAF1:PSMC5-containing complexes. Binding of PSMC5 to PAAF1 or to neighboring 19S base subunits alone does not protect PSMC5 from ubiquitination. Protection is conferred only when PAAF1 is displaced following complete and accurate assembly with the 20S CP [69]. The abundance of PAAF1 in human cells greatly surpasses that of HERC1 [70,71], likely favoring assembly over degradation and allowing intermediates to be degraded only after a significant delay in assembly. Owing to PAAF1 persistence during the assembly of the 19S base, several PSMC5:PAAF1-containing intermediates are likely recognized and ubiquitinated by HERC1 [69]. HERC1 therefore does not probe the assembly state of only the PSMC5 subunit but also that of the larger 19S:20S complex. By recognizing a chaperone–subunit interaction, HERC1 safeguards the integrity of the proteasome in a manner that does not depend on potentially cytotoxic intermediates.

OST/GPI-T regulation by the Asi complex

The endoplasmic reticulum (ER) coordinates the synthesis and distribution of protein cargo within the cell. Several post-translational modifications are carried out in the ER by essential protein biosynthesis factors such as the oligosaccharyltransferase (OST) and glycosylphosphatidylinositol

transamidase (GPI-T) complexes [72–74]. Misfolded or otherwise aberrant proteins in the ER are eliminated by ER-associated degradation (ERAD), of which there are several branches [75]. One such branch comprises the Asi complex, a three-subunit transmembrane E3 ubiquitin ligase that functions in the inner nuclear membrane (INM), a compartment of the ER [76–78].

A recent study identified the Asi complex as an AQC ligase that targets OST and GPI-T [79]. Composed of eight and five transmembrane subunits, respectively, OST and GPI-T rely on complete assembly for functional substrate processing. If unassembled into functional complexes, OST subunit Wbp1 and GPI-T subunit Gpi8 are quickly recognized and ubiquitinated by the Asi complex. Recognition is mediated by the Asi2 subunit, which directly binds the transmembrane domains of Wbp1 and Gpi8 and directs them to Asi1 and Asi3 for ubiquitination [79]. In this manner, the Asi ubiquitin ligase complex recognizes unassembled complexes through surfaces embedded in the lipid membrane that are hidden from other quality control factors.

Nuclear pores connect the membranes of the bulk ER and the INM and allow a limited exchange of factors between the two. Unassembled subunits of the OST and GPI-T complexes, which reside in the bulk ER, can therefore be recognized by the Asi complex as they diffuse into the INM. Spatial segregation of protein complex assembly and degradation is advantageous for the cell because it provides opportunities for unassembled proteins to find their partners before being committed for degradation. There is likely to be a multitude of similar protein quality control pathways that operate across compartments.

Concluding remarks

Organisms facilitate the assembly of protein complexes through careful control of transcription and translation. A further layer of regulation is carried out by the UPS which selectively degrades potentially cytotoxic unassembled species to oversee complex integrity and quality. Notwithstanding variability, there is a common theme whereby AQC E3 ligases ensure correct complex assembly by detecting epitopes that are hidden or nonexistent in functionally assembled complexes. The three major strategies employed by known AQC E3 ligases are: (i) recognizing degrons in unassembled, orphaned proteins that are hidden in an assembled complex (NOT4/Cog1; UBE2O/α-globin, UBE2O/ribosomal proteins, Tom1/Rpl4, Asi/Wbp1 and Gpi8), (ii) detecting protein–chaperone interactions (HERC1/PAAF1:PSMC5) to verify complete complex assembly, and (iii) probing the stability of protein complexes to dissolve unstable assemblies (FBXL17/BTB). These mechanisms serve as initial examples and are not necessarily mutually exclusive.

It is remarkable that simple molecular recognition events coupled to E3 ligase-mediated degradation give rise to sophisticated oversight functions even for the most complex cellular machines (such as the ribosome and the 26S proteasome). The precise order of subunit incorporation into a complex is conserved in evolution, likely reflecting a way to minimize misassembly [80]. It stands to reason that conservation of assembly steps allows for their regulation by dedicated E3 ligases. It is thus tempting to speculate that most protein complexes, and particularly large assemblies, have dedicated E3 ligases that oversee their assembly.

Several unresolved issues remain (see Outstanding questions). Protein complexes *in vivo* are often dynamic and are subject to varying stoichiometries [18,81]. Degradation of a single subunit could be a mechanism to switch between functional states or to trigger the disassembly of the entire complex in response to biological cues. Analogously, degron availability in a protein complex could vary with allosteric states, providing mechanisms to regulate its activity. Several protein complexes have been described in which E3 ligases could drive such regulatory switches, most notably in transcription and replication [82–84].

Outstanding questions

Are all cellular protein complexes subject to AQC?

What features within a protein complex signal assembly defects?

Do known AQC E3 ligases have the same roles in different cellular contexts?

Most known E3 ligase degrons require post-translational modifications for recognition. Do unmodified degrons signal the lack of a binding partner and are they therefore involved in AQC?

Given the relevance of protein complex assembly in human disease, can AQC ligases be exploited for therapeutic purposes?

A frequent paradigm for E3 ligase action, particularly for Cullin-RING ligases, is protein degradation following a signal cue involving a post-translational modification. Several studies have recently identified a family of E3 ligases that recognize unstructured and seemingly unmodified degrons at the extreme N and C termini of proteins [31,85–89]. Because continuous degradation of these proteins seems unlikely, it is tempting to speculate that the biological signal governing their stability is degron availability, and that their associated ligases perform AQC. Future studies to examine the role of these ligases *in vivo* are required. Clarification is similarly needed about the link between AQC E3 ligases and chaperone function. It is known that chaperones can associate with E3 ligases to earmark substrates for degradation [90,91], but key cellular chaperone systems such as HSP70, HSP90, and TRiC have so far only been superficially linked to E3 ligases.

The majority of cellular complexes are likely subject to AQC. The near future will undoubtedly bring the discovery of many more such quality control systems, establishing the UPS as a key regulator of protein complex assembly.

Acknowledgments

We thank Micha Rape, Eric Fischer, Colby Sandate, Zuzanna Kozicka, and Pius Galli for critical feedback on the manuscript. Work in our laboratory is supported by the European Research Council (ERC) under the European Union's Horizon 2020 research program (NucEM, No. 884331), the Novartis Research Foundation, and the Swiss National Science Foundation (N.H.T. Sinergia-CRSII3_160734/1, SNF 31003A_179541 and SNF 310030_201206).

Declaration of interests

The authors declare no competing interests.

References

1. Huttlin, E.L. *et al.* (2017) Architecture of the human interactome defines protein communities and disease networks. *Nature* 545, 505–509
2. Balchin, D. *et al.* (2016) In vivo aspects of protein folding and quality control. *Science* 353, aac4354
3. Ellis, R.J. (2007) Protein misassembly: macromolecular crowding and molecular chaperones. *Adv. Exp. Med. Biol.* 594, 1–13
4. Hipp, M.S. *et al.* (2014) Proteostasis impairment in protein-misfolding and -aggregation diseases. *Trends Cell Biol.* 24, 506–514
5. Li, G.W. *et al.* (2014) Quantifying absolute protein synthesis rates reveals principles underlying allocation of cellular resources. *Cell* 157, 624–635
6. Burkhardt, D.H. *et al.* (2017) Operon mRNAs are organized into ORF-centric structures that predict translation efficiency. *eLife* 6, e22037
7. Chen, J. *et al.* (2020) Pervasive functional translation of noncanonical human open reading frames. *Science* 367, 1140–1146
8. Zhang, X. and Smith, T.F. (1998) Yeast 'operons'. *Microb. Comp. Genomics* 3, 133–140
9. Pizzinga, M. *et al.* (2019) Translation factor mRNA granules direct protein synthetic capacity to regions of polarized growth. *J. Cell Biol.* 218, 1564–1581
10. Nair, R.R. *et al.* (2021) Multiplexed mRNA assembly into ribonucleoprotein particles plays an operon-like role in the control of yeast cell physiology. *eLife* 10, e660050
11. Shiber, A. *et al.* (2018) Cotranslational assembly of protein complexes in eukaryotes revealed by ribosome profiling. *Nature* 561, 268–272
12. Bertolini, M. *et al.* (2021) Interactions between nascent proteins translated by adjacent ribosomes drive homomer assembly. *Science* 371, 57–64
13. Shieh, Y.W. *et al.* (2015) Operon structure and cotranslational subunit association direct protein assembly in bacteria. *Science* 350, 678–680
14. Livneh, I. *et al.* (2016) The life cycle of the 26S proteasome: from birth, through regulation and function, and onto its death. *Cell Res.* 26, 869–885
15. McShane, E. *et al.* (2016) Kinetic analysis of protein stability reveals age-dependent degradation. *Cell* 167, 803–815
16. Mena, E.L. *et al.* (2018) Dimerization quality control ensures neuronal development and survival. *Science* 362, eaap8236
17. Harper, J.W. and Bennett, E.J. (2016) Proteome complexity and the forces that drive proteome imbalance. *Nature* 537, 328–338
18. Ori, A. *et al.* (2016) Spatiotemporal variation of mammalian protein complex stoichiometries. *Genome Biol.* 17, 47
19. Schwanhausser, B. *et al.* (2011) Global quantification of mammalian gene expression control. *Nature* 473, 337–342
20. Warner, J.R. (1977) In the absence of ribosomal RNA synthesis, the ribosomal proteins of HeLa cells are synthesized normally and degraded rapidly. *J. Mol. Biol.* 115, 315–333
21. Blikstad, I. *et al.* (1983) Synthesis and assembly of spectrin during avian erythropoiesis: stoichiometric assembly but unequal synthesis of alpha and beta spectrin. *Cell* 32, 1081–1091
22. Schubert, U. *et al.* (2000) Rapid degradation of a large fraction of newly synthesized proteins by proteasomes. *Nature* 404, 770–774
23. Vabulas, R.M. and Hartl, F.U. (2005) Protein synthesis upon acute nutrient restriction relies on proteasome function. *Science* 310, 1960–1963
24. Kim, W. *et al.* (2011) Systematic and quantitative assessment of the ubiquitin-modified proteome. *Mol. Cell* 44, 325–340
25. Komander, D. and Rape, M. (2012) The ubiquitin code. *Annu. Rev. Biochem.* 81, 203–229
26. Zaffagnini, G. and Martens, S. (2016) Mechanisms of selective autophagy. *J. Mol. Biol.* 428, 1714–1724
27. Zheng, N. and Shabek, N. (2017) Ubiquitin ligases: structure, function, and regulation. *Annu. Rev. Biochem.* 86, 129–157
28. Li, W. *et al.* (2008) Genome-wide and functional annotation of human E3 ubiquitin ligases identifies MULAN, a mitochondrial E3 that regulates the organelle's dynamics and signaling. *PLoS One* 3, e1487
29. Meszaros, B. *et al.* (2017) Degrons in cancer. *Sci. Signal.* 10, eaak9982
30. Bross, P. *et al.* (1999) Protein misfolding and degradation in genetic diseases. *Hum. Mutat.* 14, 186–198

31. Lin, H.C. *et al.* (2015) CRL2 aids elimination of truncated selenoproteins produced by failed UGA/Sec decoding. *Science* 349, 91–95
32. Ungar, D. *et al.* (2005) Subunit architecture of the conserved oligomeric Golgi complex. *J. Biol. Chem.* 280, 32729–32735
33. Oka, T. *et al.* (2005) Genetic analysis of the subunit organization and function of the conserved oligomeric golgi (COG) complex: studies of COG5- and COG7-deficient mammalian cells. *J. Biol. Chem.* 280, 32736–32745
34. Li, G. *et al.* (2019) Compound heterozygous variants of the COG6 gene in a Chinese patient with deficiency of subunit 6 of the conserved oligomeric Golgi complex (COG6-CDG). *Eur. J. Med. Genet.* 62, 44–46
35. Yin, S. *et al.* (2019) Novel compound heterozygous COG5 mutations in a Chinese male patient with severe clinical symptoms and type IIi congenital disorder of glycosylation: A case report. *Exp. Ther. Med.* 18, 2695–2700
36. Zeevaert, R. *et al.* (2009) Cerebrocostomandibular-like syndrome and a mutation in the conserved oligomeric Golgi complex, subunit 1. *Hum. Mol. Genet.* 18, 517–524
37. Wu, X. *et al.* (2004) Mutation of the COG complex subunit gene COG7 causes a lethal congenital disorder. *Nat. Med.* 10, 518–523
38. Foulquier, F. *et al.* (2007) A new inborn error of glycosylation due to a Cog8 deficiency reveals a critical role for the Cog1–Cog8 interaction in COG complex formation. *Hum. Mol. Genet.* 16, 717–730
39. Arnesen, T. *et al.* (2009) Proteomics analyses reveal the evolutionary conservation and divergence of N-terminal acetyltransferases from yeast and humans. *Proc. Natl. Acad. Sci. U. S. A.* 106, 8157–8162
40. Hwang, C.S. *et al.* (2010) N-terminal acetylation of cellular proteins creates specific degradation signals. *Science* 327, 973–977
41. Shemorry, A. *et al.* (2013) Control of protein quality and stoichiometries by N-terminal acetylation and the N-end rule pathway. *Mol. Cell* 50, 540–551
42. Zhang, Z. *et al.* (2010) The APC/C subunit Cdc16/Cut9 is a contiguous tetratricopeptide repeat superhelix with a homo-dimer interface similar to Cdc27. *EMBO J.* 29, 3733–3744
43. Geyer, R. *et al.* (2003) BTB/POZ domain proteins are putative substrate adaptors for cullin 3 ubiquitin ligases. *Mol. Cell* 12, 783–790
44. Chevrier, S. and Corcoran, L.M. (2014) BTB-ZF transcription factors, a growing family of regulators of early and late B-cell development. *Immunol. Cell Biol.* 92, 481–488
45. Stogios, P.J. *et al.* (2005) Sequence and structural analysis of BTB domain proteins. *Genome Biol.* 6, R82
46. Mena, E.L. *et al.* (2020) Structural basis for dimerization quality control. *Nature* 586, 452–456
47. Pierce, N.W. *et al.* (2013) Cand1 promotes assembly of new SCF complexes through dynamic exchange of F box proteins. *Cell* 153, 206–215
48. Moras, M. *et al.* (2017) From erythroblasts to mature red blood cells: organelle clearance in mammals. *Front. Physiol.* 8, 1076
49. Bryk, A.H. and Wisniewski, J.R. (2017) Quantitative analysis of human red blood cell proteome. *J. Proteome Res.* 16, 2752–2761
50. Roux-Dalvai, F. *et al.* (2008) Extensive analysis of the cytoplasmic proteome of human erythrocytes using the peptide ligand library technology and advanced mass spectrometry. *Mol. Cell. Proteomics* 7, 2254–2269
51. Kihm, A.J. *et al.* (2002) An abundant erythroid protein that stabilizes free alpha-haemoglobin. *Nature* 417, 758–763
52. Goldberg, A.L. (2003) Protein degradation and protection against misfolded or damaged proteins. *Nature* 426, 895–899
53. Zhang, X. *et al.* (2013) Fine-tuning BMP7 signalling in adipogenesis by UBE2O/E2-230K-mediated monoubiquitination of SMAD6. *EMBO J.* 32, 996–1007
54. Nguyen, A.T. *et al.* (2017) UBE2O remodels the proteome during terminal erythroid differentiation. *Science* 357, eaan0218
55. Yanagitani, K. *et al.* (2017) UBE2O is a quality control factor for orphans of multiprotein complexes. *Science* 357, 472–475
56. Shaeffer, J.R. (1988) ATP-dependent proteolysis of hemoglobin alpha chains in beta-thalassemic hemolysates is ubiquitin-dependent. *J. Biol. Chem.* 263, 13663–13669
57. Khatter, H. *et al.* (2015) Structure of the human 80S ribosome. *Nature* 520, 640–645
58. Klinge, S. and Woolford Jr., J.L. (2019) Ribosome assembly coming into focus. *Nat. Rev. Mol. Cell Biol.* 20, 116–131
59. Sung, M.K. *et al.* (2016) A conserved quality-control pathway that mediates degradation of unassembled ribosomal proteins. *eLife* 5, e19105
60. Sung, M.K. *et al.* (2016) Ribosomal proteins produced in excess are degraded by the ubiquitin-proteasome system. *Mol. Biol. Cell* 27, 2642–2652
61. Torres, E.M. *et al.* (2007) Effects of aneuploidy on cellular physiology and cell division in haploid yeast. *Science* 317, 916–924
62. Xu, Y. *et al.* (2016) The HECT domain ubiquitin ligase HUWE1 targets unassembled soluble proteins for degradation. *Cell Discov.* 2, 16040
63. Cromm, P.M. and Crews, C.M. (2017) The proteasome in modern drug discovery: second life of a highly valuable drug target. *ACS Cent. Sci.* 3, 830–838
64. Dou, Q.P. and Goldfarb, R.H. (2002) Bortezomib (millennium pharmaceuticals). *IDrugs* 5, 828–834
65. Roelofs, J. *et al.* (2009) Chaperone-mediated pathway of proteasome regulatory particle assembly. *Nature* 459, 861–865
66. Funakoshi, M. *et al.* (2009) Multiple assembly chaperones govern biogenesis of the proteasome regulatory particle base. *Cell* 137, 887–899
67. Kaneko, T. *et al.* (2009) Assembly pathway of the Mammalian proteasome base subcomplex is mediated by multiple specific chaperones. *Cell* 137, 914–925
68. Saeki, Y. *et al.* (2009) Multiple proteasome-interacting proteins assist the assembly of the yeast 19S regulatory particle. *Cell* 137, 900–913
69. Zavodszky, E. *et al.* (2021) Identification of a quality-control factor that monitors failures during proteasome assembly. *Science* 373, 998–1004
70. Kulak, N.A. *et al.* (2014) Minimal, encapsulated proteomic-sample processing applied to copy-number estimation in eukaryotic cells. *Nat. Methods* 11, 319–324
71. Itzhak, D.N. *et al.* (2016) Global, quantitative and dynamic mapping of protein subcellular localization. *eLife* 5, e16950
72. Wild, R. *et al.* (2018) Structure of the yeast oligosaccharyltransferase complex gives insight into eukaryotic N-glycosylation. *Science* 359, 545–550
73. Bai, L. *et al.* (2018) The atomic structure of a eukaryotic oligosaccharyltransferase complex. *Nature* 555, 328–333
74. Fraering, P. *et al.* (2001) The GPI transamidase complex of *Saccharomyces cerevisiae* contains Gaa1p, Gpi8p, and Gpi16p. *Mol. Biol. Cell* 12, 3295–3306
75. Brodsky, J.L. (2012) Cleaning up: ER-associated degradation to the rescue. *Cell* 151, 1163–1167
76. Smoyer, C.J. *et al.* (2019) Distribution of proteins at the inner nuclear membrane is regulated by the Asi1 E3 ligase in *Saccharomyces cerevisiae*. *Genetics* 211, 1269–1282
77. Khmelinskii, A. *et al.* (2014) Protein quality control at the inner nuclear membrane. *Nature* 516, 410–413
78. Foresti, O. *et al.* (2014) Quality control of inner nuclear membrane proteins by the Asi complex. *Science* 346, 751–755
79. Natarajan, N. *et al.* (2020) Quality control of protein complex assembly by a transmembrane recognition factor. *Mol. Cell* 77, 108–119
80. Marsh, J.A. *et al.* (2013) Protein complexes are under evolutionary selection to assemble via ordered pathways. *Cell* 153, 461–470
81. Leake, M.C. *et al.* (2006) Stoichiometry and turnover in single, functioning membrane protein complexes. *Nature* 443, 355–358
82. Sonneville, R. *et al.* (2017) CUL-2(LRR-1) and UBXN-3 drive replisome disassembly during DNA replication termination and mitosis. *Nat. Cell Biol.* 19, 468–479
83. Sonneville, R. *et al.* (2019) TRAIP drives replisome disassembly and mitotic DNA repair synthesis at sites of incomplete DNA replication. *eLife* 8, e48686
84. Kokic, G. *et al.* (2021) Structural basis of human transcription-DNA repair coupling. *Nature* 598, 368–372
85. Lin, H.C. *et al.* (2018) C-terminal end-directed protein elimination by CRL2 ubiquitin ligases. *Mol. Cell* 70, 602–613

86. Koren, I. *et al.* (2018) The eukaryotic proteome is shaped by E3 ubiquitin ligases targeting C-terminal degrons. *Cell* 173, 1622–1635
87. Rusnac, D.V. *et al.* (2018) Recognition of the diglycine C-end degron by CRL2(KLHDC2) ubiquitin ligase. *Mol. Cell* 72, 813–822
88. Timms, R.T. *et al.* (2019) A glycine-specific N-degron pathway mediates the quality control of protein N-myristoylation. *Science* 365, eaaw4912
89. Chen, X. *et al.* (2021) Molecular basis for arginine C-terminal degron recognition by Cul2(FEM1) E3 ligase. *Nat. Chem. Biol.* 17, 254–262
90. Jiang, J. *et al.* (2001) CHIP is a U-box-dependent E3 ubiquitin ligase: identification of Hsc70 as a target for ubiquitylation. *J. Biol. Chem.* 276, 42938–42944
91. Murata, S. *et al.* (2001) CHIP is a chaperone-dependent E3 ligase that ubiquitylates unfolded protein. *EMBO Rep.* 2, 1133–1138

Chapter 7

Research Article: Recognition of the CCT5 Di-Glu Degron is Dependent on TRiC Assembly

Experimental work during the candidate's doctoral period has led to the publication of a research article in *The EMBO Journal* [439]. The article, titled *"Recognition of the CCT5 Di-Glu degron is dependent on TRiC assembly"* presents findings on the mechanism of CCT5 recognition by DCAF12 and its biological implications. Parts of this Thesis have been adapted from the contents of this manuscript. This chapter contains the research article in its final edited form by the publishers, together with a summary of the editorial decision process.

Article

TRANSPARENT PROCESS OPEN ACCESS

THE EMBO JOURNAL

Recognition of the CCT5 di-Glu degron by CRL4^{DCAF12} is dependent on TRiC assembly

Carlos Pla-Prats[1,2], Simone Cavadini[1], Georg Kempf[1] & Nicolas H Thomä[1,*]

Abstract

Assembly Quality Control (AQC) E3 ubiquitin ligases target incomplete or incorrectly assembled protein complexes for degradation. The CUL4-RBX1-DDB1-DCAF12 (CRL4^{DCAF12}) E3 ligase preferentially ubiquitinates proteins that carry a C-terminal double glutamate (di-Glu) motif. Reported CRL4^{DCAF12} di-Glu-containing substrates include CCT5, a subunit of the TRiC chaperonin. How DCAF12 engages its substrates and the functional relationship between CRL4^{DCAF12} and CCT5/TRiC is currently unknown. Here, we present the cryo-EM structure of the DDB1-DCAF12-CCT5 complex at 2.8 Å resolution. DCAF12 serves as a canonical WD40 DCAF substrate receptor and uses a positively charged pocket at the center of the β-propeller to bind the C-terminus of CCT5. DCAF12 specifically reads out the CCT5 di-Glu side chains, and contacts other visible degron amino acids through Van der Waals interactions. The CCT5 C-terminus is inaccessible in an assembled TRiC complex, and functional assays demonstrate that DCAF12 binds and ubiquitinates monomeric CCT5, but not CCT5 assembled into TRiC. Our biochemical and structural results suggest a previously unknown role for the CRL4^{DCAF12} E3 ligase in overseeing the assembly of a key cellular complex.

Keywords Assembly Quality Control; CCT5; DCAF12; TRiC; Ubiquitin
Subject Categories Post-translational Modifications & Proteolysis; Structural Biology; Translation & Protein Quality
DOI 10.15252/embj.2022112253 | Received 30 July 2022 | Revised 21 October 2022 | Accepted 14 December 2022
The EMBO Journal (2023) e112253

Introduction

Cullin-RING E3 ubiquitin (Ub) ligases of the CUL4-RBX1-DDB1 (CRL4) family are comprised of a CUL4A/CUL4B E3 ligase arm that simultaneously binds an activated E2-Ubiquitin enzyme on its C-terminal region through protein RBX1 and a DDB1 adaptor protein on its N-terminus (Angers *et al*, 2006). CRL4s are modular, and DDB1 recruits interchangeable substrate receptors that in turn bind their substrates to induce their ubiquitination. Over 20 DDB1 substrate receptors have been described (Angers *et al*, 2006; He *et al*, 2006; Higa *et al*, 2006; Jin *et al*, 2006; Fukumoto *et al*, 2008). DCAF12, also known as WDR40A (Angers *et al*, 2006) and TCC52 (Li *et al*, 2008), is conserved across metazoans and ubiquitously expressed in human tissues (Uhlen *et al*, 2015). DCAF12 has been broadly linked to the transduction of pro-apoptotic signals required for programmed cell death in tissue growth and morphogenesis, and in supporting synaptic plasticity and function (Hwangbo *et al*, 2016; Patron *et al*, 2019; Jiao *et al*, 2022). DCAF12 further regulates the Hippo pathway, a conserved regulator of tissue growth across metazoans and a common driver of tumorigenesis in human cancers (Cho *et al*, 2020). DCAF12 has also been proposed to regulate T cell homeostasis and spermatogenesis in mice and humans by downregulating MOV10, and to induce autophagy in human cells by downregulating MAGEA-3 and MAGEA-6 (Ravichandran *et al*, 2019; Lidak *et al*, 2021).

Reporter screens have identified proteins that are degraded in a DCAF12-dependent manner in human cells (Koren *et al*, 2018). Common to over 40 of these proteins is a di-Glu motif at their extreme C-terminus. The motif is necessary and sufficient for ubiquitination of their hosts and was described as the canonical degron recognized by DCAF12 (Koren *et al*, 2018). Additional DCAF12 substrates were however later identified that do not harbor di-Glu degrons (Cho *et al*, 2020; Lidak *et al*, 2021). DCAF12 downregulates MOV10, an RNA helicase involved in post-transcriptional gene silencing, during T cell development and spermatogenesis (Lidak *et al*, 2021). Recognition is mediated by the Glu-Leu end of MOV10, and a range of proteins with noncanonical Glu-Leu degrons appear to be substrates of DCAF12 (Koren *et al*, 2018; Lidak *et al*, 2021). Yet of the potential di-Glu-containing substrates identified to date, only MAGEA-3, MAGEA-6, MOV10 and GART have been shown to bind DCAF12 *in vitro* (Ravichandran *et al*, 2019; Lidak *et al*, 2021). Hippo pathway effectors Yki/Yap/Taz and synaptic glutamate receptor subunits GluRIIA/GluRIIB/GluRIIC do not bear C-terminal degrons, and likely carry alternative degrons or are indirect targets of DCAF12 (Cho *et al*, 2020). To date, the molecular mechanism of substrate binding by DCAF12 is unknown.

Other E3 ubiquitin ligases exist that recognize degrons located at the extreme C-terminus of their substrates (Sherpa *et al*, 2022), but only a small subset of these C-end ligases has been structurally and functionally characterized (Rusnac *et al*, 2018; Chen *et al*, 2021; Yan *et al*, 2021; Zhao *et al*, 2021). In contrast to degrons requiring post-

1 Friedrich Miescher Institute for Biomedical Research, Basel, Switzerland
2 University of Basel, Basel, Switzerland
*Corresponding author. Tel: +41 61 697 66 51; E-mail: nicolas.thoma@fmi.ch

© 2023 Friedrich Miescher Institute for Biomedical Research. Published under the terms of the CC BY NC ND 4.0 license

14602075, 0, Downloaded from https://www.embopress.org/doi/10.15252/embj.2022112253 by Schweizerische Akademie Der, Wiley Online Library on [08/02/2023]. See the Terms and Conditions (https://onlinelibrary.wiley.com/terms-and-conditions) on Wiley Online Library for rules of use; OA articles are governed by the applicable Creative Commons License

translational modifications for recognition, C-end degrons are seemingly unmodified, and their presence appears sufficient to trigger degradation of their hosts (Lin *et al*, 2018). While initially discovered in aberrant protein products and postulated to signal defective protein synthesis (Lin *et al*, 2015), they were later identified in full-length, functional human proteins (Koren *et al*, 2018; Lin *et al*, 2018), raising the question of whether this recognition mechanism results in constitutive substrate ubiquitination or additional regulatory mechanisms are in place.

The biogenesis of protein complexes is a complex process subject to several layers of regulation. In metazoans, a network of Assembly Quality Control (AQC) E3 ubiquitin ligases induces the degradation of incompletely or incorrectly assembled complexes while sparing their correct counterparts (Padovani *et al*, 2022; Pla-Prats & Thoma, 2022). The majority of CRL4 E3 ligases recognize their substrate following post-translational or other modifications of the substrate (Scrima *et al*, 2008; Fischer *et al*, 2011, 2014). The AQC degrons characterized to date, on the other hand, become hidden or are nonexistent when the proteins harboring them correctly assemble into complexes (Padovani *et al*, 2022; Pla-Prats & Thoma, 2022). In addition to their apparent unmodified nature, di-Glu degrons were initially identified as GFP-peptide fusions, and are thus assumed to be flexible and solvent-exposed (Koren *et al*, 2018).

We examined whether C-terminal degrons recognized by DCAF12 could serve as signals for complex assembly. To dissect the molecular determinants of di-Glu degron recognition and gain insight into the role of DCAF12 in AQC, we focused on the interaction between $CRL4^{DCAF12}$ and CCT5, a subunit of the TRiC chaperonin. TRiC, also called CCT (Chaperone Containing TCP1) is the only chaperonin present in the cytosol of eukaryotes, where it specializes in the folding of aggregation-prone substrates (Jin *et al*, 2019). TRiC has been implicated in the folding of ~ 10% of the human proteome (Yam *et al*, 2008) and has been linked to human pathologies such as cancers and neurodegenerative diseases (Roh *et al*, 2015; Grantham, 2020). TRiC is a ~ 1 MDa complex formed by eight paralogue subunits named CCT1-8, which are transcribed from eight different chromosomes and arrange into double octameric rings stacked back-to-back (Gestaut *et al*, 2019; Jin *et al*, 2019). The resulting structure contains a large cavity with surfaces contributed by each CCT subunit. Inside the cavity, TRiC substrates rely on a correct arrangement of electrostatic patches to fold. All CCT genes are essential, and reductions in TRiC activity have detrimental effects in cells (Blomen *et al*, 2015; Wang *et al*, 2015). CCT5 harbors a C-terminal di-Glu degron, and has been proposed to be an *in vivo* substrate of DCAF12 (Koren *et al*, 2018). We hypothesized that $CRL4^{DCAF12}$, through its interaction with CCT5, serves as an AQC ligase assisting TRiC assembly and homeostasis. To address this question, we combined structural studies of a CCT5-bound DCAF12 with a biochemical characterization of its interaction with CCT5 and TRiC.

Results

The CCT5 C-terminus binds the $CRL4^{DCAF12}$ E3 ubiquitin ligase

The reported degron recognized by DCAF12 comprises a short C-terminal double glutamate (di-Glu) motif (Koren *et al*, 2018). We first set out to determine the binding affinity between the CCT5 degron and DDB1-DCAF12, the minimal soluble substrate receptor module of the $CRL4^{DCAF12}$ E3 ligase. The human DDB1-DCAF12 complex was recombinantly expressed in insect cells and purified to homogeneity. Purified CCT5 efficiently bound DDB1-DCAF12 *in vitro* (Fig 1A). The interaction was dependent on the di-Glu degron: a CCT5 (1–529) mutant without the 12 C-terminal residues (Δ(Ct)) did not bind DDB1-DCAF12 (Fig 1A). A time-resolved fluorescence energy transfer (TR-FRET) assay was set up to quantify the binding affinity of a CCT5 C-terminal peptide to DDB1-DCAF12. In the assay, biotinylated DDB1-DCAF12 was complexed to terbium-streptavidin (Tb-SA), a high-yield fluorescence donor. The resulting $_{Tb}$DDB1-DCAF12 complex was mixed with a peptide corresponding to the 20 C-terminal amino acids of CCT5 ($^{488}CCT5_{20}$; CCT5 amino acids 522–541) conjugated to the fluorescent label ATTO488, which contains the di-Glu motif and acts as a fluorescence acceptor. Spatial proximity between the donor and acceptor species results in fluorescence energy transfer, establishing a readout for binding. We titrated increasing concentrations of $^{488}CCT5_{20}$ to a $_{Tb}$DDB1-DCAF12 complex. In agreement with the pull-downs (Fig 1A), DDB1-DCAF12 bound CCT5 in the TR-FRET assay with high affinity (Fig 1B). The observed binding isotherm was biphasic and exhibited an initial hyperbolic phase followed by a linear increase. The observed K_D for the $^{488}CCT5_{20}$ peptide was 245 ± 52 nM after subtraction of the unspecific linear component, which becomes predominant at $^{488}CCT5_{20}$ concentrations above ~ 1 μM (Fig EV1A). We verified the specific nature of the hyperbolic part of the isotherms by counter-titrating with an unlabeled $CCT5_{20}$ peptide (Fig EV1B), and the corresponding concentration range was used for subsequent experiments. Back-titration with an unlabeled $CCT5_{20}$ peptide resulted in a similar affinity (IC_{50} = 404 ± 103 nM; Ki = 249 ± 63 nM) demonstrating that the presence of the N-terminal ATTO488 fluorescence label does not significantly contribute to binding. Thus, DDB1-DCAF12 directly binds the C-terminus of CCT5 with an affinity in the mid-nanomolar range.

We then carried out competition experiments with label-free wild-type CCT5 or CCT5 degron peptides ranging in lengths between 20 and 2 amino acids, all of which retained the C-terminal di-Glu motif. These peptides were titrated against a $_{Tb}$DDB1-DCAF12 complex pre-assembled with $^{488}CCT5_{20}$ ($_{Tb}$DDB1-$DCAF12^{488}$), and the resulting decrease in fluorescence was used as a readout for binding. Full-length CCT5 bound DDB1-DCAF12 (IC_{50} = 219 ± 43 nM) with an apparent affinity that was similar to that of the $CCT5_{20}$ degron peptide (IC_{50} = 404 ± 103 nM; K_i = 249 ± 63 nM) (Fig 1C). We observed maximal binding when the C-terminal CCT5 peptides were eight residues or longer (Fig 1D). Truncating the degron peptide to seven residues or less impaired binding, such that the $^{488}CCT5_{20}$ probe was not fully outcompeted at a concentration of 12.5 μM. Only traces of binding were observed for a CCT5 di-peptide at 12.5 μM, our highest tested experimental concentration (Fig 1D). The sequence features of di-Glu degrons were initially identified in peptides of at least 10 residues in length (Koren *et al*, 2018). Our measurements show that a sequence context of eight residues is sufficient for di-Glu degron binding.

Next, we examined the sequence dependence of the CCT5 di-Glu degron for binding to DCAF12. *In vivo* screening of DCAF12 substrates previously identified the two C-terminal glutamates

© 2023 Friedrich Miescher Institute for Biomedical Research

14602075, 0, Downloaded from https://www.embopress.org/doi/10.15252/embj.2022112253 by Schweizerische Akademie Der, Wiley Online Library on [08/02/2023]. See the Terms and Conditions (https://onlinelibrary.wiley.com/terms-and-conditions) on Wiley Online Library for rules of use; OA articles are governed by the applicable Creative Commons License

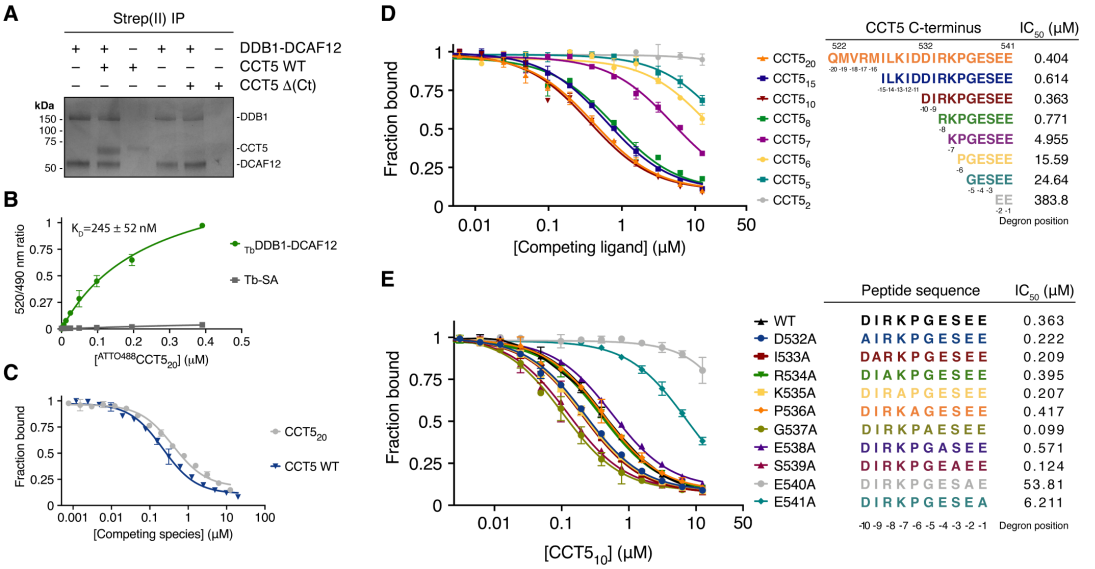

Figure 1. CCT5 is a substrate of DCAF12.

A *In vitro* pull-downs between strep(II)-tagged DDB1-DCAF12 and untagged wild-type (WT) CCT5 or CCT5 (1–529) (Δ(Ct)) seen on a Coomassie-stained SDS–PAGE gel.

B Titration curves between a fluorescent ^{488}CCT5$_{20}$ degron peptide and $_{Tb}$DDB1-DCAF12 or terbium-coupled streptavidin (Tb-SA) ($n = 3$). Signal originating in the absence of $_{Tb}$DDB1-DCAF12 is unspecific and was subtracted in subsequent experiments.

C TR-FRET counter-titration of unlabeled wild-type (WT) CCT5 or an unlabeled CCT5$_{20}$ peptide into pre-assembled $_{Tb}$DDB1-DCAF12^{488} ($n = 3$).

D TR-FRET counter-titrations of label-free CCT5 C-terminal peptides into $_{Tb}$DDB1-DCAF12^{488} ($n = 3$). Sequences of the peptides and IC$_{50}$ values for the titrations are listed as a table. Peptides are labeled for their degron position and corresponding CCT5 amino acid number.

E Counter-titration of unlabeled CCT5$_{10}$ mutant peptides into $_{Tb}$DDB1-DCAF12^{488} ($n = 3$). Sequences of the peptides and IC$_{50}$ values for the titrations are listed as a table. Peptides are labeled to indicate their degron position.

Data information: In (B–E), data are presented as mean ± 95% confidence interval (CI). Where indicated, "*n*" represents biological replicates.

(designated −1 and −2 from the C-terminus) as the core recognition element (Koren *et al*, 2018). A greater relative importance of the −2 degron position was later suggested by the discovery of noncanonical Glu-Leu degrons (Lidak *et al*, 2021). Accordingly, we observe that DCAF12 binds Glu-Thr ends (Fig EV1E). To study the importance of sequence-specific contacts between DCAF12 and CCT5, we focused on individual alanine mutations introduced at all positions of a peptide comprising the CCT5 C-terminal degron (CCT5$_{10}$; CCT5 amino acids 532–541). The mutant peptides were titrated in our TR-FRET competition assay against a $_{Tb}$DDB1-DCAF12^{488} complex. The CCT5$_{10}$ peptide showed a 15-fold decrease in affinity when mutated to alanine in the −1 position (Glu541Ala; IC$_{50}$ ~ 6.2 μM) compared with wild-type CCT5$_{10}$ (IC$_{50}$ = 390 ± 115 nM) (Fig 1E; Appendix Table S1). The effect was more pronounced when the −2 position was mutated to alanine (Glu540Ala; IC$_{50}$ > 50 μM). DCAF12 tolerated mutations to hydrophobic amino acids in the −1 and −2 degron positions better than mutations to polar or charged amino acids, including lysine and aspartate (Fig EV1F). Mutations in the amino acids preceding the C-terminal glutamates did not exhibit equally pronounced effects when mutated to alanine, and displayed different behaviors (Fig 1E). Peptides mutated in degron positions −4 (Glu538Ala; IC$_{50}$ = 571 ± 103 nM), −6 (Pro536Ala; IC$_{50}$ = 417 ± 53 nM) and − 8 (Arg534Ala; IC$_{50}$ = 395 ± 68 nM) displayed similar affinities than the wild-type sequence (WT; IC$_{50}$ = 363 ± 78 nM), while mutations in positions −3 (Ser539Ala; IC$_{50}$ = 125 ± 15 nM), −5 (Gly537Ala; IC$_{50}$ = 100 ± 11 nM), −7 (Lys535Ala; IC$_{50}$ = 208 ± 26 nM), −9 (Ile539Ala; IC$_{50}$ = 209 ± 25 nM) and − 10 (Glu532Ala; IC$_{50}$ = 222 ± 25 nM) gave rise to slightly better binding when mutated to alanine (Fig 1E). Taken together, our measurements confirm that degron binding is driven by the C-terminal glutamates and highlight the importance of the −2 degron position for binding. We find that DCAF12 shows only moderate preference for individual degron residues preceding the C-terminal glutamates, in line with degradation reporters in cells that show little effect for mutations N-terminal of the di-Glu motif (Koren *et al*, 2018). However, the increased binding of alanine mutants of degron positions −3, −5, −7, −9 and −10 suggest that the CCT5 C-terminus is not the optimal di-Glu degron sequence bound by CRL4^{DCAF12}.

To study the substrate specificity of CRL4^{DCAF12} in more detail, we used the TR-FRET competition assay to compare an unlabeled CCT5$_{20}$ peptide to equivalent C-terminal peptides of DCAF12 substrates MAGEA-3 (MAGEA-3$_{20}$; amino acids 295–314) and SAT1 (SAT1$_{20}$; amino acids 152–171) (Koren *et al*, 2018). Competitive titrations against a $_{Tb}$DDB1-DCAF12^{488} complex showed that the affinity of a CCT5$_{20}$ peptide for DCAF12 was lower

© 2023 Friedrich Miescher Institute for Biomedical Research

14602075, 0, Downloaded from https://www.embopress.org/doi/10.15252/embj.2022112253 by Schweizerische Akademie Der Wiley Online Library on [08/02/2023]. See the Terms and Conditions (https://onlinelibrary.wiley.com/terms-and-conditions) on Wiley Online Library for rules of use; OA articles are governed by the applicable Creative Commons License

14602075, 0, Downloaded from https://www.embopress.org/doi/10.15252/embj.2021112253 by Schweizerische Akademie Der, Wiley Online Library on [08/02/2023]. See the Terms and Conditions (https://onlinelibrary.wiley.com/terms-and-conditions) on Wiley Online Library for rules of use; OA articles are governed by the applicable Creative Commons License

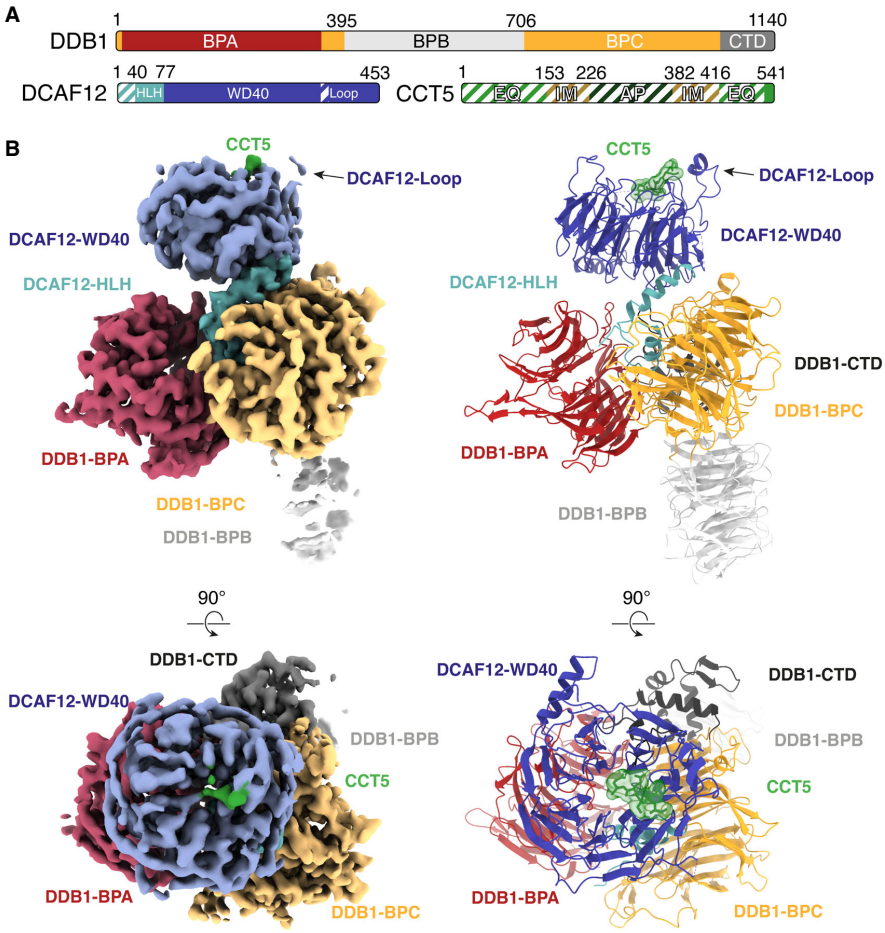

Figure 2. Cryo-EM structure of DDB1-DCAF12-CCT5.

A Domain organization of the proteins present in the cryo-EM sample. Unmodeled regions are shown as stripes.

B Different views of the DDB1-DCAF12-CCT5 cryo-EM map (left) with fit structures (right). The map and models are colored as in (A). DDB1 and DCAF12 are shown as cartoons. The CCT5 peptide is shown as sticks with surface representation.

(IC_{50} = 404 ± 103 nM) than that of $SAT1_{20}$ (IC_{50} = 291 ± 38 nM), but exceeded that of $MAGEA\text{-}3_{20}$ (IC_{50} ≈ 2,700 nM) (Fig EV1G). Thus, despite the relatively minor contribution of individual amino acids when mutated to alanine (Fig 1E), the collective variability of residues preceding the di-Glu motif is sufficient to account for differences in binding affinities of up to 10-fold (Fig EV1G). DCAF12 tolerates significant variability in the residues preceding the di-Glu motif, explaining how the different C-termini of many di-Glu-containing proteins can be recognized by DCAF12 (Koren *et al*, 2018).

Our biochemical findings establish CCT5 as a substrate of DCAF12. Analogous to other C-end ligases (Lin *et al*, 2015, 2018; Koren *et al*, 2018; Rusnac *et al*, 2018; Chen *et al*, 2021; Yan *et al*, 2021; Zhao *et al*, 2021), submicromolar binding of a flexible C-terminal tail is achieved by a plastic binding site on the substrate receptor. While recognition is strictly dependent on only a few critical degron residues, interactions with other degron residues collectively contribute to binding.

Structure of the DDB1-DCAF12 complex

To understand the molecular mechanisms of CCT5 recognition by the $CRL4^{DCAF12}$ E3 ligase, we pursued DCAF12-containing complexes for structural characterization. The structures of the ~ 240 kDa DDB1-DCAF12-CCT5 complex and the ~ 180 kDa DDB1-DCAF12 complex were determined by single-particle cryogenic electron microscopy (cryo-EM) to a resolution of 2.8 Å (Fig 2A and B) and 3.0 Å (Fig EV2A and B), respectively. DDB1 folds into a tri-

© 2023 Friedrich Miescher Institute for Biomedical Research

14602075, 0, Downloaded from https://www.embopress.org/doi/10.15252/embj.2022112253 by Schweizerische Akademie Der, Wiley Online Library on [08/02/2023]. See the Terms and Conditions (https://onlinelibrary.wiley.com/terms-and-conditions) on Wiley Online Library for rules of use; OA articles are governed by the applicable Creative Commons License

lobed structure formed by three WD40 β-propeller domains (BPA, BPB, BPC) and a small C-terminal domain (CTD; amino acids 1,043–1,140) (Angers *et al*, 2006) (Fig 2A). The BPB β-propeller connects DDB1 to CUL4, while the BPA and BPC β-propellers engage substrate receptors. The CTD bridges the BPA, BPB and BPC domains (Fig 2B) (Angers *et al*, 2006). The DCAF12 body is comprised of a WD40 β-propeller domain (WD40; amino acids 78–453) formed by seven "blades" of antiparallel β-sheets (Figs 2B and EV3A). The DCAF12 WD40 β-propeller is preceded by a helix–loop–helix motif (HLH; amino acids 40–77) and an N-terminal domain (NTD; amino acids 1–39) (Fig 2A), which is found disordered in our structure. The HLH is lodged between the DDB1 BPA and BPC domains and anchors DCAF12 to DDB1 in a manner similar to other DDB1 substrate receptors (Fig EV3B and C) (Scrima *et al*, 2008; Fischer *et al*, 2011; Bussiere *et al*, 2020; Slabicki *et al*, 2020). The WD40 β-propeller domain adopts the shape of a truncated cone tightly contacting DDB1 (Figs 2B and EV2A). The crest of the WD40 cone points away from DDB1. The base of the DCAF12 β-propeller cone engages the BPC and CTD domains of DDB1 through the loops connecting the β strands of the WD40 blades one and seven, creating a 578 Å^2 interface between the two proteins (Figs 2B and EV3D). An additional 1,478 Å^2 interface between DDB1 and DCAF12 is contributed by the DCAF12 HLH motif (Figs 2B and EV2C). DCAF12 contacts DDB1 residues that have previously been shown to bind substrate receptors (Fig EV3C and D). Overall, DCAF12 assumes an architecture common to other WD40 DDB1 substrate receptors (Fig EV3B).

The DCAF12 WD40 β-propeller binds CCT5

DDB1 and DCAF12 adopt a similar overall conformation in the presence or absence of CCT5 (root-mean-square deviation [RMSD] = 1.0 Å excluding the flexible DDB1 BPB domain) (Fig EV2C and D). In the presence of CCT5, however, an additional density is observed at the crest of the DCAF12 WD40 cone (Figs 2B and 3A). The density is linear and occupies a surface pocket formed by all seven blades of the WD40 propeller (Figs 3B and EV3A). This central site at the narrow end of the WD40 cone is a common site used by WD40 propellers to engage substrate peptides (Xu & Min, 2011; Schapira *et al*, 2017). Alphafold2, in an un-supervised modeling run, placed a CCT5 peptide in a similar position and orientation (Fig EV3E; Appendix Fig S1) (Jumper *et al*, 2021; Varadi *et al*, 2022). The density was therefore initially assigned to five amino acids at the C-terminus of CCT5. No additional density attributable to CCT5 was evident in the cryo-EM maps or along the cryo-EM processing steps.

The DCAF12 substrate binding pocket is ~ 15 Å long and ~ 10 Å wide and composed of a base, a wall, and a ceiling (Fig 3B). The surfaces of the base are contributed by basic and hydrophobic amino acids (Phe93, His144, Phe188, Arg256, Leu272, Val300, Arg344, Tyr422). The wall is formed by loops connecting blades one and two (amino acids 138–144) and blades two and three (amino acids 186–188). A loop connecting strands b and c in blade seven (amino acids 438–447) is kinked by two proline residues (Pro439, Pro441) and protrudes above the pocket, creating the ceiling (Fig 3B). A large loop between blades six and seven (Loop; amino acids 370–416) forms a short α-helical protrusion above the ceiling, pinning it in place against the WD40 β-sheets (Fig 3B). Interactions between the Loop and the pocket ceiling are driven by hydrophobic and conserved amino acids (Fig EV3F), and are necessary for the structural integrity of the substrate binding pocket (Fig EV1C). The amino acids forming the pocket, especially those of the base, are highly conserved (Fig 3B), and adopt a similar side chain conformation in the presence or absence of CCT5 (Fig EV2D).

Structural basis for di-Glu degron recognition

The DCAF12 pocket wall is flanked by two patches of positively charged amino acids (Lys91, Lys108; Arg203, Lys254) (Fig 3A and B). On the side bridging the wall to the ceiling, a patch formed by Lys91 and Lys108 contacts the gamma carboxyl group of the −2 glutamate (CCT5 Glu540), locking down its side chain under the pocket ceiling (Fig 3B and C). TR-FRET assays using the ^{488}CCT5$_{20}$ reporter peptide and a DCAF12 Lys108Ala mutant demonstrate that Lys108 is essential for binding (Fig 3D). The C-terminal carboxyl group of CCT5 faces the WD40 core, where it is engaged by DCAF12 Arg256 (Fig 3A). Introducing an Arg256Ala mutation into DCAF12 abolished ^{488}CCT5$_{20}$ binding *in vitro* (Fig 3D). By recognizing the C-terminal carboxyl group of its substrates through Arg256, DCAF12 reads out the C-terminal nature of the degron. Accordingly, internal di-Glu motifs have not been reported as substrates of DCAF12, despite their prevalence in human proteins. While the CCT5 C-terminal carboxyl group is engaged by Arg256 deep within the core of the DCAF12 propeller, its Glu541 side chain points toward the solvent, where the gamma carboxyl group can engage positively charged groups contributed by DCAF12 His144, Arg203 and Lys254, as well as the DCAF12 protein backbone between residues 140–141 (Fig 3A and C). The interactions between the CCT5 Glu541 side chain and the imidazole moiety of DCAF12 His144 and between the DCAF12 Arg256 side chain and the CCT5 C-terminal carboxyl group are the predominant features in the cryo-EM map (Fig 3A). Additional density was however observed consistent with an alternative conformation of the Glu541 side chain wherein its gamma carboxyl group engages the positively charged patch formed by DCAF12 Arg203 and Lys254 (Fig EV3E; Appendix Fig S2). Mutating DCAF12 His144 or Arg203 to alanine abrogated substrate binding *in vitro*, suggesting that both types of interactions contribute to binding (Fig 3D). At the degron position −3, the Ser539 side chain points toward DCAF12 Glu298 and Arg344 (Fig 3A and C). At the base of the pocket, Arg344 further contributes to substrate binding through interactions with the CCT5 peptide backbone (Fig 3A and C). Mutating DCAF12 Arg344 to alanine abrogated substrate binding *in vitro* (Fig 3D). At degron position −4, CCT5 Glu538 engages in backbone carbonyl interactions with DCAF12 Ser442, while simultaneously binding the DCAF12 backbone around Ser442 through its side chain (Fig 3A and C). At degron position −5, CCT5 Gly537 exits the pocket toward the solvent and is found largely disordered (Fig 3A).

The structure identifies five C-terminal CCT5 residues that interact with DCAF12, and this substrate peptide assignment (Fig 3A) is supported by mutagenesis data (Fig 1E). Key carboxyl groups of the CCT5 di-Glu motif are extensively read out through strong interactions with conserved and positively charged amino acids in the DCAF12 pocket. The C-terminal degron glutamate is engaged by DCAF12 in a solvent-exposed location that can accommodate multiple conformations and types of side chains, explaining the laxer

© 2023 Friedrich Miescher Institute for Biomedical Research

14602075, 0, Downloaded from https://www.embopress.org/doi/10.15252/embj.2021112253 by Schweizerische Akademie Der, Wiley Online Library on [08/02/2023]. See the Terms and Conditions (https://onlinelibrary.wiley.com/terms-and-conditions) on Wiley Online Library for rules of use; OA articles are governed by the applicable Creative Commons License

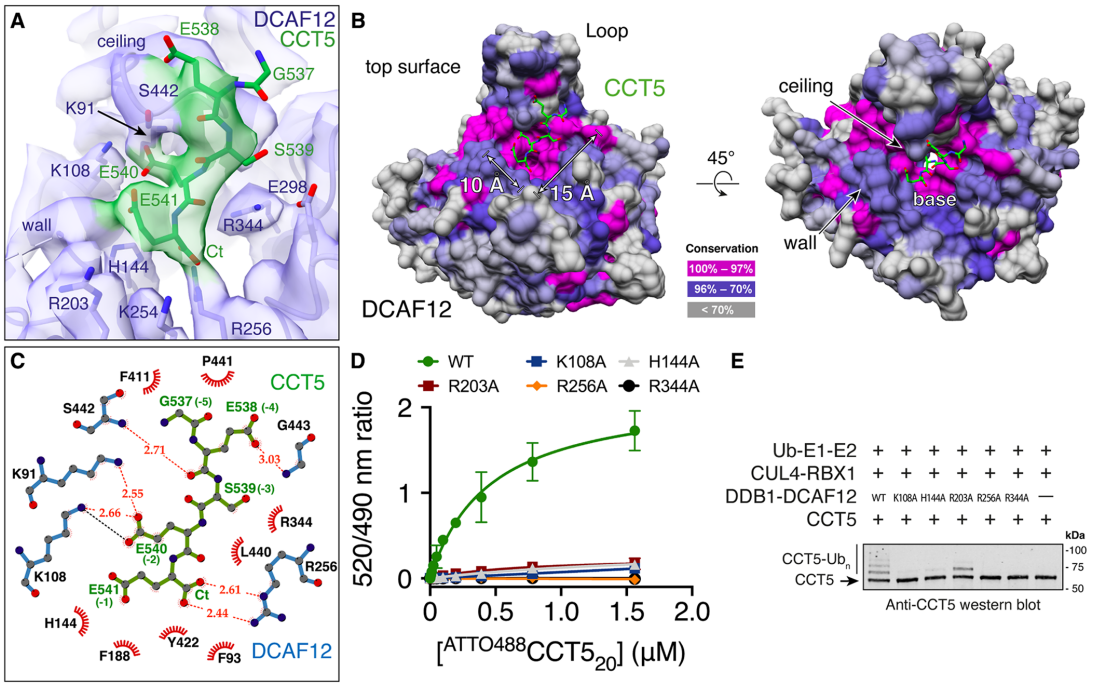

Figure 3. DCAF12 uses a surface pocket to bind the CCT5 di-Glu degron.

A A close-up view of the cryo-EM map around the DCAF12 pocket. DCAF12 is shown in light blue as cartoons, with key pocket residues shown as sticks. CCT5 residues are shown as green sticks.

B Conservation surface mapping of the DCAF12 WD40 domain. The DCAF12 pocket is annotated for its dimensions and structural components. CCT5 degron residues are shown as green sticks.

C LigPlot+ diagram of the interactions between DCAF12 and the CCT5 di-Glu degron (Laskowski & Swindells, 2011). The DCAF12 residues forming hydrogen bonds with CCT5 are shown in blue. DCAF12 residues involved in Van der Waals packing are shown with eyelashes in red. CCT5 residues are shown in green with degron positions in parentheses. Hydrogen bonds and salt bridges are shown as orange and black dashed lines, respectively.

D Titration curves between a fluorescent $^{488}CCT5_{20}$ degron peptide and wild-type (WT) or mutant $_{Tb}$DDB1-DCAF12 complexes ($n = 3$). Unspecific signal arising from the Tb-SA label was subtracted.

E *In vitro* ubiquitination of CCT5 by wild-type (WT) or mutant $CRL4^{DCAF12}$ complexes in the presence of ubiquitin, ATP, E1 and E2 enzymes.

Data information: In (D), data are presented as mean ± 95% CI. Where indicated, "*n*" represents biological replicates.

identity requirements for the −1 degron residue. The remainder of contacts observed between DCAF12 and CCT5 are mediated by the CCT5 backbone or involve weak side chain interactions, reflecting the small differences in binding affinity of our alanine mutant peptides (Fig 1E), and the cumulative differences seen for the MAGEA-3 and SAT-1 C-terminal peptides (Fig EV1G).

$CRL4^{DCAF12}$ ubiquitinates CCT5

We then focused on the catalytic activity of the $CRL4^{DCAF12}$ E3 ligase. $CRL4^{DCAF12}$ was reconstituted *in vitro* and mixed with CCT5 in the presence of E1 and E2 enzymes, ubiquitin and ATP. Substrate binding by DCAF12 leads to ubiquitination, which was followed through immunoblots with labeled antibodies. CCT5 was robustly ubiquitinated by $CRL4^{DCAF12}$ *in vitro* (Fig 3E). Ubiquitination by $CRL4^{DCAF12}$ was dependent on di-Glu binding: DCAF12 Lys108Ala, His144Ala, Arg256Ala and Arg344Ala mutants that failed to bind $^{488}CCT5_{20}$ in our TR-FRET assay (Fig 3D) showed no ubiquitination activity toward CCT5 (Fig 3E), although some ubiquitination activity was retained by an Arg203Ala mutant. Taken together, these results confirm that the $CRL4^{DCAF12}$ E3 ligase binds and ubiquitinates CCT5 *in vitro*, and that its specificity and affinity are governed by the di-Glu degron.

Architecture of the CCT5-bound $CRL4^{DCAF12}$ E3 ubiquitin ligase

In the process of optimizing conditions for cryo-EM structure determination, we were also able to solve the structure of a DDB1-DCAF12-CCT5 complex by negative-stain electron microscopy (EM) to a resolution of 30 Å (Fig 4A, Appendix Fig S3). The negative-stain EM map matched our previously obtained coordinates for DDB1-DCAF12-CCT5, and additionally showed clear density

© 2023 Friedrich Miescher Institute for Biomedical Research

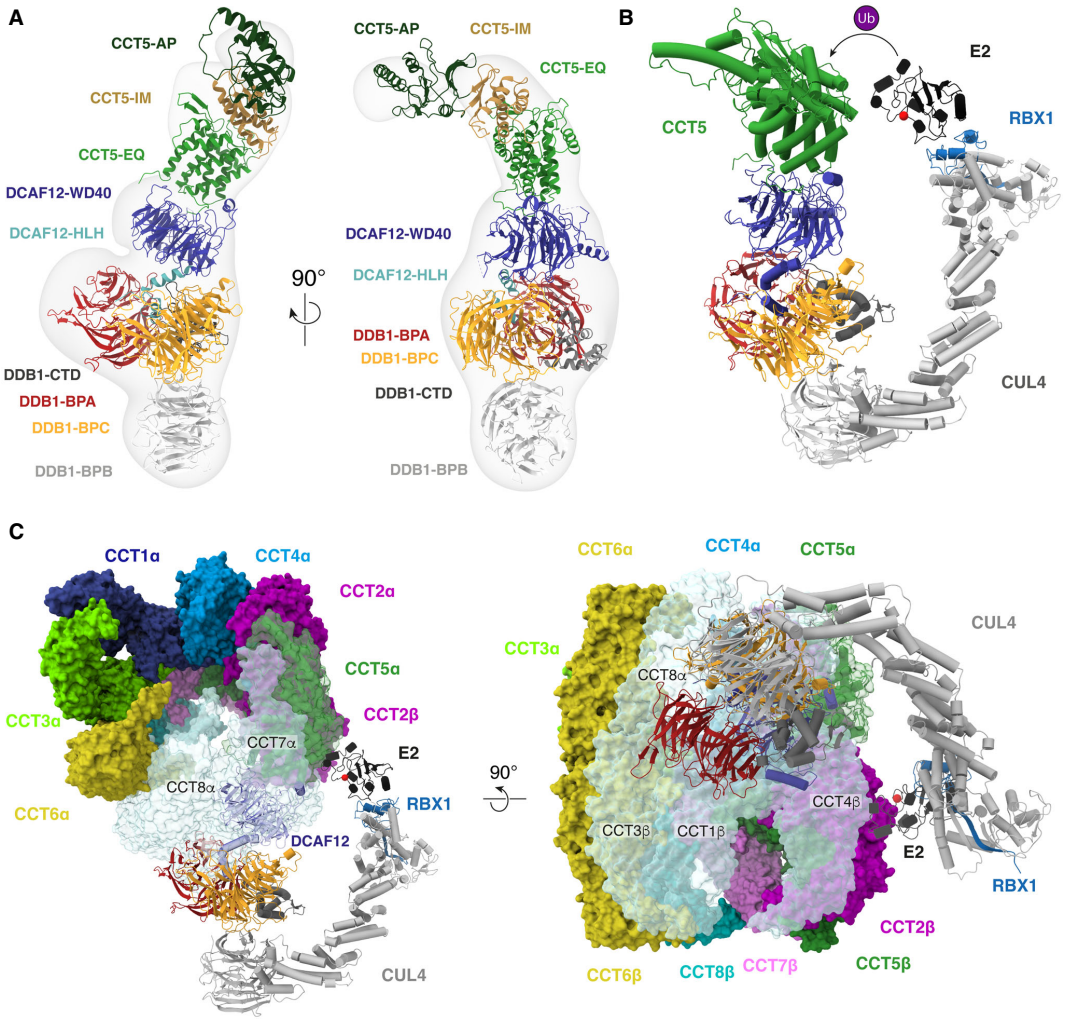

Figure 4. CRL4^{DCAF12} binding to CCT5 is mutually exclusive with TRiC assembly.

A Different views of the negative-stain EM map of the DDB1-DCAF12-CCT5 complex with fit coordinates for DDB1-DCAF12 (this study) and CCT5 (PDB ID 6NR8, chain E; Gestaut *et al*, 2019).

B Model of the CCT5-bound CRL4^{DCAF12} E3 ubiquitin ligase. CUL4 and RBX1 (PDB ID 4A0K; Fischer *et al*, 2011) bridge DDB1-DCAF12 to an E2 ubiquitin ligase (UBCH7 depicted, PDB ID 1FBV; Zheng *et al*, 2000). Spatial proximity between the E2 and the substrate catalyzes the ubiquitin (Ub) transfer reaction, aided by allosterism within the complex (Baek *et al*, 2020). The catalytic cysteine of UBCH7 is depicted as a red sphere.

C Superposition of the coordinates of CRL4^{DCAF12} onto TRiC (PDB ID 6NR8; Gestaut *et al*, 2019) reveals clashes and access restrictions between DCAF12 and DDB1 and several TRiC subunits (colored pale blue). TRiC subunits are labeled α or β according to the ring they occupy.

consistent with published structures of CCT5 (Pereira *et al*, 2017; Gestaut *et al*, 2019). CCT5 adopts a curved shape formed by equatorial (EQ), intermediate (IM) and apical (AP) domains connected by hinge regions (Figs 2A and 4A; Pereira *et al*, 2017; Gestaut *et al*, 2019). In published structures, the CCT5 N- and C-termini protrude from the equatorial domain as flexible tails with no regular secondary structure (Pereira *et al*, 2017; Gestaut *et al*, 2019). The negative-stain EM map shows that CCT5 uses its equatorial domain to dock to the crest of the DCAF12 β-propeller, tightly contacting the Loop and the pocket wall (Fig 4A). Binding of the equatorial domain largely covers the pocket, yet allows a passage opposite the wall (DCAF12 amino acids 338–343) for the CCT5 C-terminus to enter

© 2023 Friedrich Miescher Institute for Biomedical Research

14602075, 0, Downloaded from https://www.embopress.org/doi/10.15252/embj.2022112253 by Schweizerische Akademie Der Wiley Online Library on [08/02/2023]. See the Terms and Conditions (https://onlinelibrary.wiley.com/terms-and-conditions) on Wiley Online Library for rules of use; OA articles are governed by the applicable Creative Commons License

14602075, 0, Downloaded from https://www.embopress.org/doi/10.15252/embj.2021112253 by Schweizerische Akademie Der, Wiley Online Library on [08/02/2023]. See the Terms and Conditions (https://onlinelibrary.wiley.com/terms-and-conditions) on Wiley Online Library for rules of use; OA articles are governed by the applicable Creative Commons License

the pocket (Appendix Fig S4). The CCT5 C-terminal tail is approximately 15 residues in length and offers sufficient flexibility to engage the pocket as observed in the high-resolution cryo-EM map (Fig 2B). Additional contacts likely exist between the CCT5 equatorial domain and the DCAF12 β-propeller (Fig 4A), although their precise identity could not be determined from the map. Contacts mediated by the DCAF12 β-propeller could fine-tune the specificity of the CRL4^{DCAF12} ligase toward its substrates. In the case of CCT5, however, these appear to have only a minor contribution to binding (Fig 1C).

Our cryo-EM and negative-stain EM structures of the DDB1-DCAF12-CCT5 complex allow constructing a model of the CCT5-bound CRL4^{DCAF12} ligase (Fig 4B) (Angers *et al*, 2006; Fischer *et al*, 2011). The ~ 280 kDa CRL4^{DCAF12} complex uses the DCAF12 β-propeller to engage the CCT5 equatorial domain and C-terminus. CCT5 binding to CRL4^{DCAF12} juxtaposes it to the E2-Ub enzyme in a manner similar to other CRL4 substrates (Fig 4B; Scrima *et al*, 2008; Fischer *et al*, 2011, 2014; Petzold *et al*, 2016; Slabicki *et al*, 2020). Spatial proximity to the E2-Ub enzyme allows CCT5 to be ubiquitinated, in agreement with our *in vitro* assays (Fig 3E) (Baek *et al*, 2020).

CCT5 recognition by CRL4^{DCAF12} is mutually exclusive with assembly

The two octameric rings of TRiC contact each other through the equatorial domains of each CCT subunit (Fig 4C; Jin *et al*, 2019). This arrangement places the C-termini of all CCT subunits inside the cavity (Gestaut *et al*, 2019). TRiC contains one copy of CCT5 in each of the two rings, both of which make extensive contacts with neighboring subunits. In available structures of TRiC, the CCT5 C-terminal tail is observed inside the barrel, where it folds back onto itself to mediate contacts with the sensor loop of neighboring subunit CCT7 (Gestaut *et al*, 2019). The CCT5 C-terminal carboxyl group that is read out by DCAF12 Arg256 hydrogen bonds in an assembled TRiC complex with the peptide backbone around CCT7 Asp51 (Gestaut *et al*, 2019). The gamma carboxyl group of CCT5 Glu541 folds back to interact with CCT5 Lys535 (degron position −7) (Gestaut *et al*, 2019). The side chain of CCT5 Glu540, which is docked under the pocket ceiling in our cryo-EM structure (Fig 3A and B), establishes strong polar interactions with CCT7 Lys47 (Gestaut *et al*, 2019). CCT7 Lys47 further engages CCT5 Ser539, which contacts DCAF12 Glu298 and Arg344 in our cryo-EM structure (Fig 3A). The C-termini of chaperonin subunits take part in substrate folding, and the CCT5 C-terminus has been shown to contact proteins folding inside the TRiC chamber (Chen *et al*, 2013; Cuellar *et al*, 2019). Sensor loops within CCT subunits interact with peptides folding inside the TRiC chamber and are supported by contacts with neighboring subunits (Pereira *et al*, 2017). As such, the CCT5 C-terminus is engaged in a network of interactions that supports TRiC function and is not available for binding to DCAF12 in an assembled TRiC complex.

The CCT5 surfaces of the equatorial domain bound by DCAF12 are occupied in an assembled TRiC complex by ring neighbor CCT7, as well as CCT1 and CCT4 on the opposite ring (Fig 4C). As such, CCT5 within a TRiC complex is not competent for binding to DCAF12. Structural modeling of a TRiC-embedded CCT5 bound by CRL4^{DCAF12} reveals further clashes and access restrictions with the CCT7 and CCT8 TRiC subunits located in the same ring as the bound CCT5, as well as with CCT1, CCT3 and CCT4 on the opposite ring (Fig 4C). A structurally intact TRiC complex therefore protects CCT5 from recognition by the CRL4^{DCAF12} E3 ubiquitin ligase.

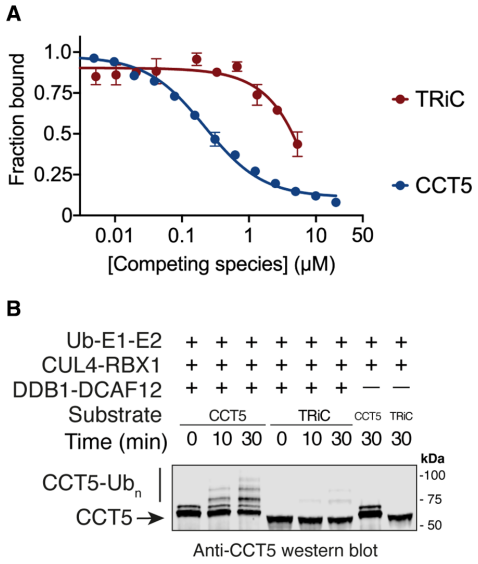

Figure 5. CRL4^{DCAF12} senses the assembly status of TRiC.

A TR-FRET counter-titration of unlabeled CCT5 or unlabeled TRiC into pre-assembled $_{Tb}$DDB1-DCAF12^{488} ($n = 3$).

B *In vitro* ubiquitination of monomeric wild-type CCT5 or TRiC by CRL4^{DCAF12} in the presence of ubiquitin, ATP, E1 and E2 enzymes. CCT5, but not TRiC, is modified with poly-ubiquitin (Ub$_n$) chains by CRL4^{DCAF12}. Free CCT5 protein carries an N-terminal strep(II) tag and differs in electrophoretic mobility from untagged CCT5 purified as a TRiC complex.

Data information: In (A), data are presented as mean ± 95% CI. Where indicated, "*n*" represents biological replicates.

Targeting unassembled proteins for degradation while sparing functional complexes is the key feature of AQC E3 ubiquitin ligases (Padovani *et al*, 2022; Pla-Prats & Thoma, 2022). We therefore tested whether the CRL4^{DCAF12} E3 ligase can biochemically and functionally differentiate between CCT5 in its assembled and unassembled forms. We recombinantly co-expressed the eight human TRiC subunits in insect cells and purified the resulting ~ 1 MDa TRiC complex. We then compared the binding affinity between DDB1-DCAF12 and unassembled or TRiC-embedded CCT5 using our competition TR-FRET assay. Purified CCT5 or TRiC were separately titrated against a $_{Tb}$DDB1-DCAF12^{488} complex. While DDB1-DCAF12 readily bound full-length unassembled CCT5 (IC_{50} = 219 ± 43 nM), TRiC caused a decrease in fluorescence consistent with an affinity more than two orders of magnitude lower than that of CCT5 (IC_{50} > 10 μM) (Fig 5A). The differential binding translated into the CRL4^{DCAF12} catalytic activity: although CRL4^{DCAF12} robustly ubiquitinated monomeric CCT5, it showed no ubiquitination activity toward TRiC (Fig 5B). DCAF12 readily binds

© 2023 Friedrich Miescher Institute for Biomedical Research

14602075, 0, Downloaded from https://www.embopress.org/doi/10.15252/embj.2022112253 by Schweizerische Akademie Der, Wiley Online Library on [08/02/2023]. See the Terms and Conditions (https://onlinelibrary.wiley.com/terms-and-conditions) on Wiley Online Library for rules of use; OA articles are governed by the applicable Creative Commons License

its substrates without apparent prior post-translational modifications. In the case of CCT5, this recognition mechanism enables CRL4^{DCAF12} to read out the assembly state of the TRiC chaperonin. Detecting degrons present in monomeric proteins that become hidden in a protein complex is a hallmark of AQC E3 ubiquitin ligases (Padovani *et al*, 2022; Pla-Prats & Thoma, 2022). By targeting monomeric, but not TRiC-embedded CCT5 for degradation, CRL4^{DCAF12} displays the key characteristic of an AQC ligase.

Discussion

Identifying the molecular determinants of substrate recognition by E3 ligases is crucial for understanding the diverse roles of these enzymes in cellular homeostasis. The CRL4^{DCAF12} E3 ubiquitin ligase triggers the downregulation of substrates with a C-terminal di-Glu motif (Koren *et al*, 2018). Alternative CRL4^{DCAF12} substrate degrons have been reported (Patron *et al*, 2019; Cho *et al*, 2020; Lidak *et al*, 2021), and we observed that proteins with a Glu-Thr end can exhibit tight binding to DCAF12 by identifying viral proteins that co-purify with DDB1-DCAF12 (Fig EV1E). We determined the structure of the substrate recognition module of the CRL4^{DCAF12} E3 ligase alone (Fig EV2) and in complex with CCT5 (Fig 2, Appendix Fig S5) and identified the molecular determinants of di-Glu degron recognition (Fig 3C). DCAF12 engages the C-terminal carboxyl group of the degron and the gamma carboxyl group of the −2 glutamate through strong interactions with positively charged amino acids in a surface pocket. The C-terminal side chain (degron position −1) is solvent-exposed and is offered a variety of polar, positively charged (His144, Arg203, Lys254) and hydrophobic (Phe93, Trp186, Phe188) interactions (Fig 3A). Accordingly, Glu-Leu and Glu-Thr ends are expected to be accommodated by the DCAF12 pocket. Residues preceding the C-terminal glutamates (positions −3 to −5) predominantly engage in Van der Waals interactions with DCAF12 and display little sequence preference (Fig 1E). Their contribution to binding is nonetheless significant, as a C-terminal tail of eight residues is required for optimal binding to DCAF12 (Fig 1D). Mutations in several degron positions, in particular −3 and −5, increase the affinity of the degron for DCAF12. This might be due to favorable contacts with nearby hydrophobic residues of the ceiling including Leu440, Pro441 and Phe411.

We further elucidated the architecture of a CCT5-bound CRL4^{DCAF12} E3 ligase (Fig 4A and B) and showed that recognition of CCT5 by DCAF12 is mutually exclusive with its assembly into a TRiC complex (Fig 4C). Unassembled, monomeric, CCT5 has a flexible and solvent-exposed C-terminus and is readily recognized and ubiquitinated by CRL4^{DCAF12} (Fig 3E). The TRiC chaperonin, on the contrary, protects the CCT5 equatorial domain and C-terminus from recognition. We recombinantly reconstituted the ~ 1 MDa *homo sapiens* TRiC chaperonin and confirmed that it is not bound or ubiquitinated by CRL4^{DCAF12} *in vitro* (Fig 5A and B). The ability to differentiate between the assembled and unassembled forms of their substrates is the hallmark of AQC E3 ligases. Our biochemical and structural dissection therefore supports a role for the CRL4^{DCAF12} E3 ligase in the assembly quality control of the TRiC chaperonin.

It is presently unknown how TRiC assembles in cells. Most TRiC subunits assemble co-translationally to minimize the abundance of orphaned CCT subunits (Bertolini *et al*, 2021), yet how cells survey their assembly is unknown. CCT5 forms TRiC-like double homo-octameric rings *in vitro*, and it has been proposed that these homo-octamers nucleate the assembly of other CCT subunits *in vivo* (Pereira *et al*, 2017; Sergeeva *et al*, 2019). In that context, a tight control of incompletely assembled CCT5 would be necessary to ensure productive TRiC assembly. The cellular abundance of TRiC subunits is ~ 180-fold larger than that of DCAF12 (Kulak *et al*, 2014), suggesting a mechanism by which competition between DCAF12 and other CCT subunits for binding to CCT5 promotes TRiC assembly and minimizes premature degradation of productive TRiC subcomplexes. Human proteomes are characteristically non-stoichiometric and are greatly burdened by non-stoichiometric subunit assembly (Schubert *et al*, 2000; Matalon *et al*, 2014; McShane *et al*, 2016; Ori *et al*, 2016), which can generate cytotoxic species that drive disease progression (Harper & Bennett, 2016; Livneh *et al*, 2016). TRiC activity is required for optimal viability and fitness of human cells (Blomen *et al*, 2015; Wang *et al*, 2015). Based on our biochemical and structural findings, CRL4^{DCAF12} is ideally suited to prevent the accumulation of potentially toxic TRiC assembly intermediates and orphaned CCT5 subunits that expose the C-terminus of CCT5 and in this manner support proteostasis.

It is likely that DCAF12 oversees the assembly of other proteins. The N- and C-termini of proteins are structurally more flexible than internal sequences, and many might only fold upon binding their partners in a complex (Lobanov *et al*, 2010). Diamine acetyltransferase 1 (SAT1) is a small globular protein that is active as a homodimer (Pegg, 2008) and contains a di-Glu degron that is recognized by DCAF12 (Koren *et al*, 2018). In the dimer, the C-terminal tail of SAT1 contributes to interactions between monomers and its residues are not accessible to DCAF12. In its monomeric state, however, the SAT1 di-Glu degron is expected to become solvent-exposed and competent for recognition by CRL4^{DCAF12}.

It is conceivable, however, that the evolution of DCAF12 might have been driven by a substrate whose degradation is independent of assembly into a complex. Recognition might follow the allosteric release of a C-terminal tail in response to a post-translational modification. DCAF12 might also act on specific splicing isoforms or products of caspase cleavage, and have ubiquitin-independent functions. In drosophila, it has recently been shown that the pro-apoptotic functions of DCAF12 involve non-degradative inhibition of inhibitor of apoptosis proteins (IAPs), which do not contain di-Glu degrons (Jiao *et al*, 2022).

A number of E3 ligases (including CRL4^{DCAF12}, CRL2$^{FEM1A/B/C}$ and CRL2^{KLHDC2}) have been identified that recognize specific sequences in the C-terminus of proteins (Koren *et al*, 2018). FEM1 proteins recognize different degrons with a common terminal arginine (R-end). KLHDC2 recognizes a C-terminal di-glycine (di-Gly) motif that similarly tolerates mutations better at the −1 than the −2 position (Rusnac *et al*, 2018). Despite having a different protein fold and recognition mechanism, these ligases are mechanistically related to CRL4^{DCAF12}. Like di-Glu degrons, the di-Gly and R-end degrons have been found in prematurely terminated or otherwise aberrant proteins, but also in a number of biologically active polypeptides and full-length proteins (Koren *et al*, 2018; Lin *et al*, 2018). The traditional view of E3 ligases is that they are not constitutively active but rather target substrates in response to specific cues. It is therefore likely that other C-end

© 2023 Friedrich Miescher Institute for Biomedical Research

14602075, 0, Downloaded from https://www.embopress.org/doi/10.15252/embj.2021112253 by Schweizerische Akademie Der, Wiley Online Library on [08/02/2023]. See the Terms and Conditions (https://onlinelibrary.wiley.com/terms-and-conditions) on Wiley Online Library for rules of use; OA articles are governed by the applicable Creative Commons License

ligases that bind unmodified C-termini also participate in AQC in cells.

Materials and Methods

Cloning, protein expression and purification

DDB1-DCAF12-CCT5 complexes

DNA sequences encoding *homo sapiens* DDB1 (UniProt ID: Q16531), DCAF12 (Q5T6F0) and CCT5 (P48643) were codon-optimized for expression in insect cells. Unless stated otherwise, recombinant proteins were cloned into pAC-derived expression vectors and expressed as N-terminal fusions of his_6, strep(II) or strep (II)-avi affinity tags in *Trichoplusia ni* High Five insect cells using the baculovirus expression system (Invitrogen) (Abdulrahman *et al*, 2009). For structure determination, cells expressing strep(II)-DCAF12 and his_6-DDB1 were harvested 36 h after infection and lysed by sonication in lysis buffer (50 mM tris(hydroxymethyl) aminomethane hydrochloride [Tris] pH 8, 200 mM NaCl, 0.5 mM tris(2-carboxyethyl) phosphine [TCEP] and 1X protease inhibitor cocktail [Sigma-Aldrich]). The lysate was centrifuged at 40,000 rcf for 40 min and the resulting supernatant applied to a gravity column with Strep-Tactin (IBA life sciences) affinity resin. The resin was washed extensively in lysis buffer and eluted in a buffer containing 50 mM Tris pH 8, 100 mM NaCl, 0.5 mM TCEP and 5 mM D-Desthiobiotin (IBA life sciences). The eluate was loaded onto a Poros 50 HQ column (Life Technologies) and eluted with a 100 mM—1 M NaCl gradient. Early peak fractions were subjected to size exclusion chromatography (Superdex200, Cytiva) in a buffer containing 50 mM 4-(2-hydroxyethyl)-1-piperazineethanesulfonic acid (HEPES) pH 7.4, 200 mM NaCl and 0.5 mM TCEP. Fractions were selected with care to not include impurities. Pure fractions were individually flash-frozen in liquid nitrogen without concentrating and stored at −80°C. A persistent contaminant in our CCT5-free DDB1-DCAF12 purifications, which we named MC30, was identified mass-spectrometrically as originating from our baculoviral expression system and ends in a Glu-Leu motif (UniProt ID: P41473) (Fig EV1E). The purification scheme devised allowed separating DDB1-DCAF12 from the DDB1-DCAF12-MC30 complex. For the structural characterization of DDB1-DCAF12-CCT5, the same purification protocol was applied to cells infected with an additional virus encoding his_6-CCT5. MC30 impurities were not observed in DDB1-DCAF12-CCT5 purifications. For TR-FRET and *in vitro* ubiquitination analysis, wild-type or mutant DDB1-DCAF12 complexes were expressed as strep(II)-avi-DDB1-strep(II)-DCAF12 and purified as above.

Monomeric CCT5

Cells expressing wild-type or (1–529) strep(II)-CCT5 were lysed by sonication in a buffer containing 50 mM Tris pH 8, 200 mM NaCl, 0.5 mM TCEP and 1X protease inhibitor cocktail (Sigma-Aldrich). The lysate was cleared by centrifugation at 40,000 rcf for 40 min and the resulting supernatant applied to a gravity column loaded with Strep-Tactin Sepharose affinity resin (IBA life sciences). The sample was washed in lysis buffer and eluted in a buffer containing 50 mM Tris pH 8, 50 mM NaCl, 0.5 mM TCEP and 5 mM D-Desthiobiotin (IBA Life Sciences). The eluate was further purified via ion exchange chromatography on a Poros 50 HQ column (Life Technologies) and subjected to size exclusion chromatography (Superdex200, Cytiva) in a buffer containing 50 mM HEPES pH 7.4, 200 mM NaCl and 0.5 mM TCEP. Pure fractions were pooled, flash-frozen in liquid nitrogen without concentrating and stored at −80°C. The purified CCT5 was monomeric and monodisperse (Fig EV1D).

TRiC

An internal his_6 tag was recombinantly inserted into a surface-exposed loop of TRiC subunit CCT7, resulting in a GGSHHHHHHGS insertion after Gln470 (Gestaut *et al*, 2019). The resulting his_6-CCT7-expressing baculovirus was used to co-infect High Five insect cells with baculoviruses expressing untagged wild-type CCT1-6A and CCT8. Cells were harvested 36 h after infection and lysed by sonication in a buffer containing 150 mM HEPES pH 7.4, 50 mM NaCl, 5 mM $MgCl_2$, 15 mM imidazole, 0.5 mM TCEP, 10% v/v glycerol, 1x protease inhibitor cocktail (Sigma-Aldrich) and 5 U/ml Benzonase (Sigma-Aldrich). The lysate was cleared by centrifugation at 40,000 rcf for 40 min, and the resulting supernatant applied to a gravity column loaded with cOmplete His-tag purification resin (Roche). The resin was washed with buffer A (50 mM HEPES pH 7.4, 5 mM $MgCl_2$, 0.5 mM TCEP, 10% v/v glycerol) + 50 mM NaCl + 20 mM imidazole. Two more washing steps with buffer A + 500 mM NaCl + 20 mM imidazole and then with buffer A + 20 mM imidazole + 1 mM ATP were performed before eluting with buffer A + 400 mM imidazole. The eluate was further purified by ion exchange chromatography on a Poros 50 HE column (ThermoFisher scientific) and then on a MonoQ column (Cytiva) using 100 mM—1 M NaCl gradients. Fractions containing TRiC were concentrated using 100,000 Mw cut-off Amicon concentrators (Merck), supplemented with 1 mM ATP and run on a Superose6 size exclusion chromatography column (Cytiva) in buffer A + 50 mM NaCl. Samples containing TRiC were individually flash-frozen in liquid nitrogen without concentration and stored at −80°C.

Biotinylation of DDB1-DCAF12 complexes

Biotinylation reactions were set *in vitro* by mixing purified wild-type or mutant strep(II)-avi-DDB1-strep(II)-DCAF12 complexes at variable concentrations of 25–50 μM with 2.5 μM BirA enzyme and 0.2 mM D-Biotin in a reaction buffer containing 50 mM HEPES pH 7.4, 200 mM NaCl, 10 mM $MgCl_2$, 0.25 mM TCEP and 20 mM ATP. The reaction was incubated for 30 min at room temperature and then 14–16 h at 4°C. Biotinylated DDB1-DCAF12 complexes were purified by size exclusion chromatography (Superdex200, Cytiva), flash-frozen in liquid nitrogen and stored at −80°C.

Time-resolved fluorescence energy transfer (TR-FRET)

Increasing concentrations of an ATTO488-labeled peptide corresponding to the 20 C-terminal amino acids of CCT5 ($^{488}CCT5_{20}$, Biosyntan GmbH) were added to biotinylated DDB1-DCAF12 complexes at 50 nM pre-mixed with 2 nM terbium-coupled streptavidin (Tb-SA, Invitrogen) or 2 nM Tb-SA as control (final concentrations) in 384-well microplates (Greiner Bio-One, 784075) in a buffer containing 50 mM HEPES pH 7.4, 200 mM NaCl, 0.5 mM TCEP, 0.1% Pluronic acid and 2.5% dimethyl sulfoxide (DMSO). The reactions were incubated for 15 min at room temperature and then measured

© 2023 Friedrich Miescher Institute for Biomedical Research

14602075, 0, Downloaded from https://www.embopress.org/doi/10.15252/embj.2022112253 by Schweizerische Akademie Der, Wiley Online Library on [08/02/2023]. See the Terms and Conditions (https://onlinelibrary.wiley.com/terms-and-conditions) on Wiley Online Library for rules of use; OA articles are governed by the applicable Creative Commons License

using a PHERAstar FS microplate reader (BMG Labtech). Three biological replicates were carried out per experiment, and 60 technical replicates of each data point were measured at intervals of 1 min. After excitation of terbium fluorescence with a 337 nm wavelength, emission at 490 nm (Tb) and at 520 nm (Alexa 488) was recorded with a 70 µs delay to reduce background fluorescence. The TR-FRET signal of each data point was obtained by calculating the 520/490 nm fluorescence ratio. The signal contribution of unspecific interactions between terbium and $^{488}CCT5_{20}$, as measured by the signal in the absence of DDB1-DCAF12, was measured and subtracted for every experiment. Data were analyzed with GraphPad Prism 6 assuming equimolar binding of the probe ($^{488}CCT5_{20}$) to the receptor ($_{Tb}$DDB1-DCAF12).

Competition assays were carried out by mixing increasing concentrations of unlabeled competing ligands with a pre-mixed complex of biotinylated DDB1-DCAF12 at 50 nM, Tb-SA at 2 nM and $^{488}CCT5_{20}$ at 400 nM ($_{Tb}$DDB1-DCAF12^{488}, final concentrations) in 384-well microplates (Greiner Bio-One, 784075) in a buffer containing 50 mM HEPES pH 7.4, 200 mM NaCl, 0.5 mM TCEP, 0.1% Pluronic acid, 2.5% DMSO and 10% glycerol. The reactions were incubated for 15 min at room temperature and then measured using a PHERAstar FS microplate reader (BMG Labtech). Three biological replicates were carried out per experiment. The TR-FRET signal was plotted to calculate the half maximal inhibitory concentrations (IC_{50}) assuming a single binding site using GraphPad Prism 6.

In vitro ubiquitination

In vitro ubiquitination reactions were set by mixing 70 nM wild-type or mutant biotinylated DDB1-DCAF12 with 70 nM CUL4B-RBX1 purified as previously described (Slabicki *et al*, 2020) in the presence or absence of 500 nM CCT5 or 250 nM TRiC (which contains two copies of CCT5) in a reaction mixture containing a 50 nM E1 enzyme (UBA1, Boston Biochem), a 1 µM E2 enzyme (UBCH5α, Boston Biochem) and 20 mM ubiquitin. Reactions were carried out in 50 mM Tris pH 7.5, 200 mM NaCl, 5 mM $MgCl_2$, 0.2 mM $CaCl_2$, 0.5 mM TCEP, 1 mM ATP, 0.1% Triton X-100, 0.1 mg/ml BSA and 10% v/v glycerol and incubated for 0–30 min at 30°C. Reactions were then analyzed by Western blot on 0.2 µm nitrocellulose membranes using a mouse anti-CCT5 primary antibody (Santa Cruz Biotechnology, sc-376188, 1:5,000) and an Alexa Fluor 790-labeled anti-mouse secondary antibody (Invitrogen, #A11375, 1:10,000) using an Odyssey DLx (LiCor Biosciences).

Negative-stain specimen preparation and data collection

3.5 µl of a DDB1-DCAF12-CCT5 sample at ~ 0.01 mg/ml were applied to a PureCarbon grid (#01840, Ted Pella) glow discharged with a Pelco EasyGlow (15 mA current, 45 s) (Ted Pella) and stained three times with 5 µl of a 2% (w/v) uranyl acetate solution. Data for the DDB1-DCAF12-CCT5 complex were acquired with a Tecnai Spirit (FEI) transmission electron microscope operated at 120 keV. 167 images were recorded with an Eagle camera (FEI) at a nominal magnification of 49,000× resulting in a pixel size of 2.125 Å. Images were recorded by varying the defocus between −1 and −3 µm.

Negative-stain EM data processing

14,848 particles were selected from 167 micrograph images using cisTEM (Grant *et al*, 2018) and imported into SPHIRE (Moriya *et al*, 2017) for further processing. CTF parameters for each micrograph were estimated using CTER (Penczek *et al*, 2014). Unbinned particle images were extracted from the micrographs using a box size of 128 × 128 pixels. The dataset was subjected to reference-free 2D classification using ISAC (Yang *et al*, 2012). 2,923 selected particles were then imported into RELION (Zivanov *et al*, 2018) and 3D refined. Particles were then refined, yielding a map at 30 Å resolution.

Cryo-EM specimen preparation and data collection

DDB1-DCAF12: 3.5 µl of a His_6-DDB1-Strep(II)-DCAF12 sample at 3.0 µM were applied to a Quantifoil R 1.2/1.3 Cu 200 mesh carbon grid (Quantifoil Micro Tools GmbH) glow discharged with a Pelco EasyGlow (15 mA current, 45 s). After a 4 s incubation time inside a chamber at 85% humidity, the grid was blotted for 3 s with a blot force of 20 and immediately vitrified by plunging into liquid nitrogen-cooled liquid ethane with a Vitrobot (ThermoFisher Scientific). Cryo-EM data were collected on a Cs-corrected FEI Titan Krios TEM (ThermoFisher Scientific) operated at 300 kV acceleration voltage using a Falcon 4 direct electron detector. 4,568 EER movies were recorded with the microscope set at 75,000× nominal magnification, resulting in a calibrated pixel size of 0.845 Å, using a total dose of 50 electrons per $Å^2$. The EER files were converted to standard MRC file and fractionated into 50 frames for further processing. The defocus range was −0.5 to −2.5 µm.

DDB1-DCAF12-CCT5: 3.5 µl of a His_6-DDB1-Strep(II)-DCAF12-His_6-CCT5 sample at 2.7 µM were applied to a Quantifoil R 1.2/1.3 Cu 200 mesh carbon grid glow discharged with a Pelco EasyGlow (15 mA current, 45 s) (Ted Pella). After a 5 s incubation time inside a chamber at 85% humidity, the grid was blotted for 3 s with a blot force of 25 and immediately vitrified by plunging into liquid nitrogen-cooled liquid ethane with a Vitrobot (ThermoFisher Scientific). Cryo-EM data were collected on a Cs-corrected FEI Titan Krios TEM (ThermoFisher Scientific) operated at 300 kV acceleration voltage using a K2 direct electron detector. 4,467 micrographs were recorded with the microscope set at 130,000× nominal magnification, resulting in a calibrated pixel size of 0.86 Å, using a total dose of 51.8 electrons per $Å^2$ fractionated into 50 frames and a defocus range of −0.5 to −2.5 µm.

Cryo-EM data processing

Unless specified otherwise, all processing steps were done within the RELION3 (v.3.1.3) package (Zivanov *et al*, 2018). For DDB1-DCAF12-CCT5 (Fig EV4), electron micrograph movies were drift-corrected and dose-weighed using MOTIONCOR2 (Zheng *et al*, 2017) and CTF parameters estimated using Gctf (Zhang, 2016). 1.5 m particles were selected using the Laplacian-of-Gaussian algorithm implemented in RELION3, extracted and rescaled to 1.72 Å per pixel. The dataset was refined through sequential 2D and 3D classification, and 272 k selected particles were re-extracted with a pixel size of 0.86 Å and 3D refined. After a round of 3D classification 199 k particles were selected and polished, and a final round of

© 2023 Friedrich Miescher Institute for Biomedical Research

14602075, 0, Downloaded from https://www.embopress.org/doi/10.15252/embj.2021112253 by Schweizerische Akademie Der, Wiley Online Library on [08/02/2023]. See the Terms and Conditions (https://onlinelibrary.wiley.com/terms-and-conditions) on Wiley Online Library for rules of use; OA articles are governed by the applicable Creative Commons License

3D refinement masking out the DDB1 BPB domain was carried out in RELION, yielding a map at 2.83 Å resolution. 3D classification along the processing flowchart did not reveal CCT5 peptide-free 3D classes.

For DDB1-DCAF12 (Fig EV5), electron micrograph movies were drift-corrected and dose-weighed using MOTIONCOR2 (Zheng *et al*, 2017) and CTF parameters estimated using GCTF (Zhang, 2016). 1.4 mio particles were selected using the Laplacian-of-Gaussian algorithm implemented in RELION3, extracted and rescaled to 2.535 Å per pixel. The dataset was refined through several rounds of 2D classification, and 431 k selected particles were re-extracted with a pixel size of 0.845 Å. Particles were 3D refined and the resulting map used to make a mask for a further refinement. Particles were polished and used for a final round of 3D refinement, yielding a map at 3.03 Å resolution (Fig EV2). 3D classification along the processing flowchart did not reveal significant variability in the model.

Model building and refinement

To interpret the DDB1-DCAF12-CCT5 cryo-EM map, the atomic structure of DDB1 (PDB ID 3EI3) (Scrima *et al*, 2008) and a prediction model for DCAF12 from trRosetta (Du *et al*, 2021) were docked into the 2.8 Å cryo-EM map with Coot (Emsley *et al*, 2010). DCAF12 features were evident from the map, but the predicted ß-propeller did not readily fit as a rigid body. Thus, the individual ß-propeller blades were fit into the density with Coot, and the model was manually rebuilt with Coot and ChimeraX/Isolde (Croll, 2018). During the course of this study, AlphaFold2 was released (Jumper *et al*, 2021; Varadi *et al*, 2022), allowing us to cross-validate the model and build the DCAF12 Loop (amino acids 370–416). The structure was then refined using the Rosetta density-guided FastRelax protocol in combination with density scoring (Wang *et al*, 2016). No overfitting was observed when refining against half-maps and the full map was used in final refinement steps. B factors were fit at a final stage using Rosetta. An in-house pipeline was used to run the Rosetta protocols (https://github.com/fmi-basel/RosEM). Phenix real-space refinement in combination with tight reference coordinate restraints was used to further reduce geometry outliers (Afonine *et al*, 2018). For modeling of the CCT5 degron peptide, we sampled different conformations using the Rosetta local rebuilding protocol (described in Wang *et al*, 2016) and predicted the DCAF12-degron complex with AlphaFold-multimer (Bryant *et al*, 2022). Guided by these results, we manually modeled the peptide, assigning an alternative conformation for the CCT5 Glu541 side chain due to more favorable density. Our structural data suggest a conformational equilibrium for the gamma carboxyl group of Glu541, shifting between the Arg203/Lys254 patch and a histidine residue (His144) on the base of the pocket. Occupancies for the two envisioned Glu541 side chain conformations were assigned 70/30 occupancies on the basis of observed density, amino acid conservation and functional effect of the DCAF12 alanine mutations (Fig 3E).

To interpret the DDB1-DCAF12 cryo-EM map, we docked the DDB1-DCAF12 coordinates from our DDB1-DCAF12-CCT5 structure into the map and found that they easily matched the cryo-EM map. Further refinement with Coot/Isolde/Rosetta/Phenix (as described above) showed only minor differences (RMSD = 1.029 Å). Validation for both models was performed using Phenix (Liebschner *et al*, 2019), EMRinger (Barad *et al*, 2015) and MolProbity (Chen *et al*, 2010; Table 1). Side chains without sufficient density were marked by zero occupancy values.

For the DDB1-DCAF12-CCT5 negative-stain map, the coordinates for DDB1-DCAF12-CCT5 and full-length CCT5 (PDB ID 6NR8, chain E) (Gestaut *et al*, 2019) could be confidently fit into the map despite

Table 1. Cryo-EM data collection, refinement and validation statistics.

	DDB1-DCAF12-CCT5 (PDB-8AJM) (EMDB-15484)	DDB1-DCAF12 (PDB-8AJN) (EMDB-15485)
Data collection and processing		
Microscope	Titan Krios TEM	Titan Krios TEM
Camera	K2	Falcon 4
Voltage (kV)	300	300
Total dose ($e^-/Å^2$)	51.8	50
Magnification	130,000	75,000
Defocus (μm)	−0.5 to −2.5	−0.5 to −2.5
Number of frames	50	50
Number of micrographs	7,462	4,568
Pixel size (Å)	0.86	0.845
Initial particle images (no.)	1,490,840	1,411,513
Final particle images (no.)	451,315	431,448
Symmetry imposed	C1	C1
Map resolution (Å), FSC threshold 0.143	2.83	3.03
Refinement		
Non-hydrogen atoms	12,106	12,009
Protein residues	1,540	1,530
RMSD		
Bond lengths (Å)	0.008	0.006
Bond angles (°)	1.056	0.940
B factor ($Å^2$)	169.50	199.44
Validation		
MolProbity score	0.89	1.17
Clashscore	1.25	1.67
Poor rotamers (%)	0.52	0.60
Ramachandran plot		
Favored (%)	97.78	96.19
Allowed (%)	2.22	3.81
Outliers (%)	0.00	0.00
C-beta deviations	0.00	0.00
Model-to-data fit[a]		
CC_{mask}	0.82	0.58
CC_{box}	0.85	0.74
CC_{peaks}	0.81	0.58
CC_{volume}	0.85	0.65

[a]The map was locally sharpened (LocScale).

© 2023 Friedrich Miescher Institute for Biomedical Research

14602075, 0, Downloaded from https://www.embopress.org/doi/10.15252/embj.2022112253 by Schweizerische Akademie Der, Wiley Online Library on [08/02/2023]. See the Terms and Conditions (https://onlinelibrary.wiley.com/terms-and-conditions) on Wiley Online Library for rules of use; OA articles are governed by the applicable Creative Commons License

Table 2. Negative-stain EM data collection, refinement and validation statistics.

	DDB1-DCAF12-CCT5 (PDB-8AJO) (EMDB−15486)
Data collection and processing	
Microscope	FEI Tecnai Spirit
Camera	FEI Eagle
Voltage (kV)	120
Magnification	49,000
Defocus (μm)	−1 to −3
Number of micrographs	167
Pixel size (Å)	2.125
Initial particle images (no.)	14,848
Final particle images (no.)	2,923
Symmetry imposed	C1
Map resolution (Å), FSC threshold 0.143	30
Refinement	
Non-hydrogen atoms	10,269
Protein residues	2,052
Map sharpening B factor ($Å^2$)	N.A.[a]
RMSD	
Bond lengths (Å)	0.005
Bond angles (°)	1.106
B factor ($Å^2$)	600.00
Validation	
Clashscore	0.26
Poor rotamers (%)	N.A.[b]
Ramachandran plot	
Favored (%)	98.48
Allowed (%)	1.52
Outliers (%)	0.00
C-beta deviations	0.00
Model-to-data fit	
CC_{mask}	0.5736
CC_{box}	0.8041
CC_{peaks}	0.3107
CC_{volume}	0.4072

[a]No sharpening performed.
[b]Side chains were removed from final model.

the low resolution according to the distinct shape of the complex. We found that the different structures could be rigid-body fit almost without clashes. CCT5 amino acids 530–536 that connect to the degron (amino acids 537–541) in the DDB1-DCAF12-CCT5 cryo-EM structure are likely flexible in solution and were removed. The structure was minimized using Rosetta FastRelax in torsional space in combination with a low-density weight of 20. This was followed by coordinate restrained minimization with Phenix real-space refinement (Table 2). Side chains were removed from the final model.

Structural figures were generated using PyMol (Schrödinger, Inc.) and ChimeraX (Pettersen *et al*, 2021). Interface areas were calculated using the PDBe PISA server (Krissinel & Henrick, 2007).

Data availability

The model coordinates for the DDB1-DCAF12-CCT5 and DDB1-DCAF12 cryo-EM structures have been deposited in the Protein Data Bank under the accession codes 8AJM (https://www.rcsb.org/structure/8AJM) and 8AJN (https://www.rcsb.org/structure/8AJN), respectively. The model coordinates for the DDB1-DCAF12-CCT5 negative-stain EM structure have been deposited in the Protein Data Bank under the accession codes 8AJO (https://www.rcsb.org/structure/8AJO). The cryo-EM maps of the DDB1-DCAF12-CCT5 and DDB1-DCAF12 complexes have been deposited in the Electron Microscopy Data Bank under the accession codes EMD-15484 (https://www.ebi.ac.uk/emdb/entry/EMD-15484) and EMD-15485 (https://www.ebi.ac.uk/emdb/entry/EMD-15485), respectively. The negative-stain EM map of DDB1-DCAF12-CCT5 has been deposited in the Electron Microscopy Data Bank under the accession code EMD-15486 (https://www.ebi.ac.uk/emdb/entry/EMD-15486).

Expanded View for this article is available online.

Acknowledgements
We thank G. Petzold for initial mentoring, A. Potenza, A. Andres-Pons and M. Schütz-Stoffregen for technical support, D. Hess, V. Iesmantavicius and J. Seebacher for mass spectrometry analysis, L. Kater and A. Schenk for EM support, and members of the Thomä lab for insightful discussions and critical feedback on the manuscript. Work in the laboratory was supported by the European Research Council (ERC) under the European Union's H2020 research program (NucEM, No 884331), the Novartis Research Foundation, the Swiss National Science Foundation (N.H.T. Sinergia CRSII5-186230, SNF 31003A_179541 and SNF 310030_201206) and Krebsforschung Schweiz (KFS 4980-02-2020).

Author contributions
Carlos Pla-Prats: Conceptualization; data curation; formal analysis; validation; investigation; visualization; methodology; writing – review and editing. **Simone Cavadini:** Formal analysis; supervision. **Georg Kempf:** Formal analysis; supervision. **Nicolas H Thomä:** Conceptualization; supervision; funding acquisition; project administration; writing – review and editing.

Disclosure and competing interests statement
NHT is a scientific advisor to Monte Rosa Therapeutics and a shareholder of Novartis.

References

Abdulrahman W, Uhring M, Kolb-Cheynel I, Garnier JM, Moras D, Rochel N, Busso D, Poterszman A (2009) A set of baculovirus transfer vectors for screening of affinity tags and parallel expression strategies. *Anal Biochem* 385: 383 – 385

Afonine PV, Poon BK, Read RJ, Sobolev OV, Terwilliger TC, Urzhumtsev A, Adams PD (2018) Real-space refinement in PHENIX for cryo-EM and crystallography. *Acta Crystallogr D Struct Biol* 74: 531 – 544

© 2023 Friedrich Miescher Institute for Biomedical Research

14602075, 0, Downloaded from https://www.embopress.org/doi/10.15252/embj.2022112253 by Schweizerische Akademie Der, Wiley Online Library on [08/02/2023]. See the Terms and Conditions (https://onlinelibrary.wiley.com/terms-and-conditions) on Wiley Online Library for rules of use; OA articles are governed by the applicable Creative Commons License

Angers S, Li T, Yi X, MacCoss MJ, Moon RT, Zheng N (2006) Molecular architecture and assembly of the DDB1-CUL4A ubiquitin ligase machinery. *Nature* 443: 590 – 593

Baek K, Krist DT, Prabu JR, Hill S, Klügel M, Neumaier LM, von Gronau S, Kleiger G, Schulman BA (2020) NEDD8 nucleates a multivalent cullin-RING-UBE2D ubiquitin ligation assembly. *Nature* 578: 461 – 466

Barad BA, Echols N, Wang RY, Cheng Y, DiMaio F, Adams PD, Fraser JS (2015) EMRinger: side chain-directed model and map validation for 3D cryo-electron microscopy. *Nat Methods* 12: 943 – 946

Bertolini M, Fenzl K, Kats I, Wruck F, Tippmann F, Schmitt J, Auburger JJ, Tans S, Bukau B, Kramer G (2021) Interactions between nascent proteins translated by adjacent ribosomes drive homomer assembly. *Science* 371: 57 – 64

Blomen VA, Majek P, Jae LT, Bigenzahn JW, Nieuwenhuis J, Staring J, Sacco R, van Diemen FR, Olk N, Stukalov A *et al* (2015) Gene essentiality and synthetic lethality in haploid human cells. *Science* 350: 1092 – 1096

Bryant P, Pozzati G, Elofsson A (2022) Improved prediction of protein-protein interactions using AlphaFold2. *Nat Commun* 13: 1265

Bussiere DE, Xie L, Srinivas H, Shu W, Burke A, Be C, Zhao J, Godbole A, King D, Karki RG *et al* (2020) Structural basis of indisulam-mediated RBM39 recruitment to DCAF15 E3 ligase complex. *Nat Chem Biol* 16: 15 – 23

Chen VB, Arendall WB 3rd, Headd JJ, Keedy DA, Immormino RM, Kapral GJ, Murray LW, Richardson JS, Richardson DC (2010) MolProbity: all-atom structure validation for macromolecular crystallography. *Acta Crystallogr D Biol Crystallogr* 66: 12 – 21

Chen DH, Madan D, Weaver J, Lin Z, Schroder GF, Chiu W, Rye HS (2013) Visualizing GroEL/ES in the act of encapsulating a folding protein. *Cell* 153: 1354 – 1365

Chen X, Liao S, Makaros Y, Guo Q, Zhu Z, Krizelman R, Dahan K, Tu X, Yao X, Koren I *et al* (2021) Molecular basis for arginine C-terminal degron recognition by Cul2(FEM1) E3 ligase. *Nat Chem Biol* 17: 254 – 262

Cho YS, Li S, Wang X, Zhu J, Zhuo S, Han Y, Yue T, Yang Y, Jiang J (2020) CDK7 regulates organ size and tumor growth by safeguarding the hippo pathway effector Yki/yap/Taz in the nucleus. *Genes Dev* 34: 53 – 71

Croll TI (2018) ISOLDE: a physically realistic environment for model building into low-resolution electron-density maps. *Acta Crystallogr D Struct Biol* 74: 519 – 530

Cuellar J, Ludlam WG, Tensmeyer NC, Aoba T, Dhavale M, Santiago C, Bueno-Carrasco MT, Mann MJ, Plimpton RL, Makaju A *et al* (2019) Structural and functional analysis of the role of the chaperonin CCT in mTOR complex assembly. *Nat Commun* 10: 2865

Du Z, Su H, Wang W, Ye L, Wei H, Peng Z, Anishchenko I, Baker D, Yang J (2021) The trRosetta server for fast and accurate protein structure prediction. *Nat Protoc* 16: 5634 – 5651

Emsley P, Lohkamp B, Scott WG, Cowtan K (2010) Features and development of coot. *Acta Crystallogr D Biol Crystallogr* 66: 486 – 501

Fischer ES, Scrima A, Bohm K, Matsumoto S, Lingaraju GM, Faty M, Yasuda T, Cavadini S, Wakasugi M, Hanaoka F *et al* (2011) The molecular basis of CRL4DDB2/CSA ubiquitin ligase architecture, targeting, and activation. *Cell* 147: 1024 – 1039

Fischer ES, Bohm K, Lydeard JR, Yang H, Stadler MB, Cavadini S, Nagel J, Serluca F, Acker V, Lingaraju GM *et al* (2014) Structure of the DDB1-CRBN E3 ubiquitin ligase in complex with thalidomide. *Nature* 512: 49 – 53

Fukumoto Y, Dohmae N, Hanaoka F (2008) *Schizosaccharomyces pombe* Ddb1 recruits substrate-specific adaptor proteins through a novel protein motif, the DDB-box. *Mol Cell Biol* 28: 6746 – 6756

Gestaut D, Roh SH, Ma B, Pintilie G, Joachimiak LA, Leitner A, Walzthoeni T, Aebersold R, Chiu W, Frydman J (2019) The chaperonin TRiC/CCT associates with prefoldin through a conserved electrostatic Interface essential for cellular Proteostasis. *Cell* 177: 751 – 765.e15

Grant T, Rohou A, Grigorieff N (2018) cisTEM, user-friendly software for single-particle image processing. *Elife* 7: e35383

Grantham J (2020) The molecular chaperone CCT/TRiC: an essential component of Proteostasis and a potential modulator of protein aggregation. *Front Genet* 11: 172

Harper JW, Bennett EJ (2016) Proteome complexity and the forces that drive proteome imbalance. *Nature* 537: 328 – 338

He YJ, McCall CM, Hu J, Zeng Y, Xiong Y (2006) DDB1 functions as a linker to recruit receptor WD40 proteins to CUL4-ROC1 ubiquitin ligases. *Genes Dev* 20: 2949 – 2954

Higa LA, Wu M, Ye T, Kobayashi R, Sun H, Zhang H (2006) CUL4-DDB1 ubiquitin ligase interacts with multiple WD40-repeat proteins and regulates histone methylation. *Nat Cell Biol* 8: 1277 – 1283

Hwangbo DS, Biteau B, Rath S, Kim J, Jasper H (2016) Control of apoptosis by *Drosophila* DCAF12. *Dev Biol* 413: 50 – 59

Jiao D, Chen Y, Wang Y, Sun H, Shi Q, Zhang L, Zhao X, Liu Y, He H, Lv Z *et al* (2022) DCAF12 promotes apoptosis and inhibits NF-kappaB activation by acting as an endogenous antagonist of IAPs. *Oncogene* 41: 3000 – 3010

Jin J, Arias EE, Chen J, Harper JW, Walter JC (2006) A family of diverse Cul4-Ddb1-interacting proteins includes Cdt2, which is required for S phase destruction of the replication factor Cdt1. *Mol Cell* 23: 709 – 721

Jin M, Liu C, Han W, Cong Y (2019) TRiC/CCT chaperonin: structure and function. *Subcell Biochem* 93: 625 – 654

Jumper J, Evans R, Pritzel A, Green T, Figurnov M, Ronneberger O, Tunyasuvunakool K, Bates R, Zidek A, Potapenko A *et al* (2021) Highly accurate protein structure prediction with AlphaFold. *Nature* 596: 583 – 589

Koren I, Timms RT, Kula T, Xu Q, Li MZ, Elledge SJ (2018) The eukaryotic proteome is shaped by E3 ubiquitin ligases targeting C-terminal degrons. *Cell* 173: 1622 – 1635.e14

Krissinel E, Henrick K (2007) Inference of macromolecular assemblies from crystalline state. *J Mol Biol* 372: 774 – 797

Kulak NA, Pichler G, Paron I, Nagaraj N, Mann M (2014) Minimal, encapsulated proteomic-sample processing applied to copy-number estimation in eukaryotic cells. *Nat Methods* 11: 319 – 324

Laskowski RA, Swindells MB (2011) LigPlot+: multiple ligand-protein interaction diagrams for drug discovery. *J Chem Inf Model* 51: 2778 – 2786

Li S, Hu X, Cui S, He D (2008) Novel centrosome protein, TCC52, is a cancer-testis antigen. *Cancer Sci* 99: 2274 – 2279

Lidak T, Baloghova N, Korinek V, Sedlacek R, Balounova J, Kasparek P, Cermak L (2021) CRL4-DCAF12 ubiquitin ligase controls MOV10 RNA helicase during spermatogenesis and T cell activation. *Int J Mol Sci* 22: 5394

Liebschner D, Afonine PV, Baker ML, Bunkoczi G, Chen VB, Croll TI, Hintze B, Hung LW, Jain S, McCoy AJ *et al* (2019) Macromolecular structure determination using X-rays, neutrons and electrons: recent developments in Phenix. *Acta Crystallogr D Struct Biol* 75: 861 – 877

Lin HC, Ho SC, Chen YY, Khoo KH, Hsu PH, Yen HC (2015) SELENOPROTEINS. CRL2 aids elimination of truncated selenoproteins produced by failed UGA/sec decoding. *Science* 349: 91 – 95

Lin HC, Yeh CW, Chen YF, Lee TT, Hsieh PY, Rusnac DV, Lin SY, Elledge SJ, Zheng N, Yen HS (2018) C-terminal end-directed protein elimination by CRL2 ubiquitin ligases. *Mol Cell* 70: 602 – 613.e3

Livneh I, Cohen-Kaplan V, Cohen-Rosenzweig C, Avni N, Ciechanover A (2016) The life cycle of the 26 S proteasome: from birth, through regulation and function, and onto its death. *Cell Res* 26: 869 – 885

© 2023 Friedrich Miescher Institute for Biomedical Research

Lobanov MY, Furletova EI, Bogatyreva NS, Roytberg MA, Galzitskaya OV (2010) Library of disordered patterns in 3D protein structures. *PLoS Comput Biol* 6: e1000958

Matalon O, Horovitz A, Levy ED (2014) Different subunits belonging to the same protein complex often exhibit discordant expression levels and evolutionary properties. *Curr Opin Struct Biol* 26: 113 – 120

McShane E, Sin C, Zauber H, Wells JN, Donnelly N, Wang X, Hou J, Chen W, Storchova Z, Marsh JA *et al* (2016) Kinetic analysis of protein stability reveals age-dependent degradation. *Cell* 167: 803 – 815.e21

Moriya T, Saur M, Stabrin M, Merino F, Voicu H, Huang Z, Penczek PA, Raunser S, Gatsogiannis C (2017) High-resolution single particle analysis from electron Cryo-microscopy images using SPHIRE. *J Vis Exp* 55448 https://doi.org/10.3791/55448

Ori A, Iskar M, Buczak K, Kastritis P, Parca L, Andres-Pons A, Singer S, Bork P, Beck M (2016) Spatiotemporal variation of mammalian protein complex stoichiometries. *Genome Biol* 17: 47

Padovani C, Jevtic P, Rape M (2022) Quality control of protein complex composition. *Mol Cell* 82: 1439 – 1450

Patron LA, Nagatomo K, Eves DT, Imad M, Young K, Torvund M, Guo X, Rogers GC, Zinsmaier KE (2019) Cul4 ubiquitin ligase cofactor DCAF12 promotes neurotransmitter release and homeostatic plasticity. *J Cell Biol* 218: 993 – 1010

Pegg AE (2008) Spermidine/spermine-N(1)-acetyltransferase: a key metabolic regulator. *Am J Physiol Endocrinol Metab* 294: E995 – E1010

Penczek PA, Fang J, Li X, Cheng Y, Loerke J, Spahn CM (2014) CTER-rapid estimation of CTF parameters with error assessment. *Ultramicroscopy* 140: 9 – 19

Pereira JH, McAndrew RP, Sergeeva OA, Ralston CY, King JA, Adams PD (2017) Structure of the human TRiC/CCT subunit 5 associated with hereditary sensory neuropathy. *Sci Rep* 7: 3673

Pettersen EF, Goddard TD, Huang CC, Meng EC, Couch GS, Croll TI, Morris JH, Ferrin TE (2021) UCSF ChimeraX: structure visualization for researchers, educators, and developers. *Protein Sci* 30: 70 – 82

Petzold G, Fischer ES, Thoma NH (2016) Structural basis of lenalidomide-induced CK1alpha degradation by the CRL4(CRBN) ubiquitin ligase. *Nature* 532: 127 – 130

Pla-Prats C, Thoma NH (2022) Quality control of protein complex assembly by the ubiquitin-proteasome system. *Trends Cell Biol* 32: 696 – 706

Ravichandran R, Kodali K, Peng J, Potts PR (2019) Regulation of MAGE-A3/6 by the CRL4-DCAF12 ubiquitin ligase and nutrient availability. *EMBO Rep* 20: e47352

Roh SH, Kasembeli M, Bakthavatsalam D, Chiu W, Tweardy DJ (2015) Contribution of the type II chaperonin, TRiC/CCT, to oncogenesis. *Int J Mol Sci* 16: 26706 – 26720

Rusnac DV, Lin HC, Canzani D, Tien KX, Hinds TR, Tsue AF, Bush MF, Yen HS, Zheng N (2018) Recognition of the diglycine C-end degron by CRL2 (KLHDC2) ubiquitin ligase. *Mol Cell* 72: 813 – 822.e4

Schapira M, Tyers M, Torrent M, Arrowsmith CH (2017) WD40 repeat domain proteins: a novel target class? *Nat Rev Drug Discov* 16: 773 – 786

Schubert U, Anton LC, Gibbs J, Norbury CC, Yewdell JW, Bennink JR (2000) Rapid degradation of a large fraction of newly synthesized proteins by proteasomes. *Nature* 404: 770 – 774

Scrima A, Konickova R, Czyzewski BK, Kawasaki Y, Jeffrey PD, Groisman R, Nakatani Y, Iwai S, Pavletich NP, Thoma NH (2008) Structural basis of UV DNA-damage recognition by the DDB1-DDB2 complex. *Cell* 135: 1213 – 1223

Sergeeva OA, Haase-Pettingell C, King JA (2019) Co-expression of CCT subunits hints at TRiC assembly. *Cell Stress Chaperones* 24: 1055 – 1065

Sherpa D, Chrustowicz J, Schulman BA (2022) How the ends signal the end: regulation by E3 ubiquitin ligases recognizing protein termini. *Mol Cell* 82: 1424 – 1438

Slabicki M, Kozicka Z, Petzold G, Li YD, Manojkumar M, Bunker RD, Donovan KA, Sievers QL, Koeppel J, Suchyta D *et al* (2020) The CDK inhibitor CR8 acts as a molecular glue degrader that depletes cyclin K. *Nature* 585: 293 – 297

Uhlen M, Fagerberg L, Hallstrom BM, Lindskog C, Oksvold P, Mardinoglu A, Sivertsson A, Kampf C, Sjostedt E, Asplund A *et al* (2015) Proteomics. Tissue-based map of the human proteome. *Science* 347: 1260419

Varadi M, Anyango S, Deshpande M, Nair S, Natassia C, Yordanova G, Yuan D, Stroe O, Wood G, Laydon A *et al* (2022) AlphaFold protein structure database: massively expanding the structural coverage of protein-sequence space with high-accuracy models. *Nucleic Acids Res* 50: D439 – D444

Wang T, Birsoy K, Hughes NW, Krupczak KM, Post Y, Wei JJ, Lander ES, Sabatini DM (2015) Identification and characterization of essential genes in the human genome. *Science* 350: 1096 – 1101

Wang RY, Song Y, Barad BA, Cheng Y, Fraser JS, DiMaio F (2016) Automated structure refinement of macromolecular assemblies from cryo-EM maps using Rosetta. *Elife* 5: e17219

Xu C, Min J (2011) Structure and function of WD40 domain proteins. *Protein Cell* 2: 202 – 214

Yam AY, Xia Y, Lin HT, Burlingame A, Gerstein M, Frydman J (2008) Defining the TRiC/CCT interactome links chaperonin function to stabilization of newly made proteins with complex topologies. *Nat Struct Mol Biol* 15: 1255 – 1262

Yan X, Wang X, Li Y, Zhou M, Li Y, Song L, Mi W, Min J, Dong C (2021) Molecular basis for ubiquitin ligase CRL2(FEM1C)-mediated recognition of C-degron. *Nat Chem Biol* 17: 263 – 271

Yang Z, Fang J, Chittuluru J, Asturias FJ, Penczek PA (2012) Iterative stable alignment and clustering of 2D transmission electron microscope images. *Structure* 20: 237 – 247

Zhang K (2016) Gctf: real-time CTF determination and correction. *J Struct Biol* 193: 1 – 12

Zhao S, Ru W, Chen X, Liao S, Zhu Z, Zhang J, Xu C (2021) Structural insights into SMCR8 C-degron recognition by FEM1B. *Biochem Biophys Res Commun* 557: 236 – 239

Zheng N, Wang P, Jeffrey PD, Pavletich NP (2000) Structure of a c-Cbl-UbcH7 complex: RING domain function in ubiquitin-protein ligases. *Cell* 102: 533 – 539

Zheng SQ, Palovcak E, Armache JP, Verba KA, Cheng Y, Agard DA (2017) MotionCor2: anisotropic correction of beam-induced motion for improved cryo-electron microscopy. *Nat Methods* 14: 331 – 332

Zivanov J, Nakane T, Forsberg BO, Kimanius D, Hagen WJ, Lindahl E, Scheres SH (2018) New tools for automated high-resolution cryo-EM structure determination in RELION-3. *Elife* 7: e42166

License: This is an open access article under the terms of the Creative Commons Attribution-NonCommercial-NoDerivs License, which permits use and distribution in any medium, provided the original work is properly cited, the use is non-commercial and no modifications or adaptations are made.

14602075, 0, Downloaded from https://www.embopress.org/doi/10.15252/embj.2022112253 by Schweizerische Akademie Der, Wiley Online Library on [08/02/2023]. See the Terms and Conditions (https://onlinelibrary.wiley.com/terms-and-conditions) on Wiley Online Library for rules of use; OA articles are governed by the applicable Creative Commons License

© 2023 Friedrich Miescher Institute for Biomedical Research

Expanded View Figures

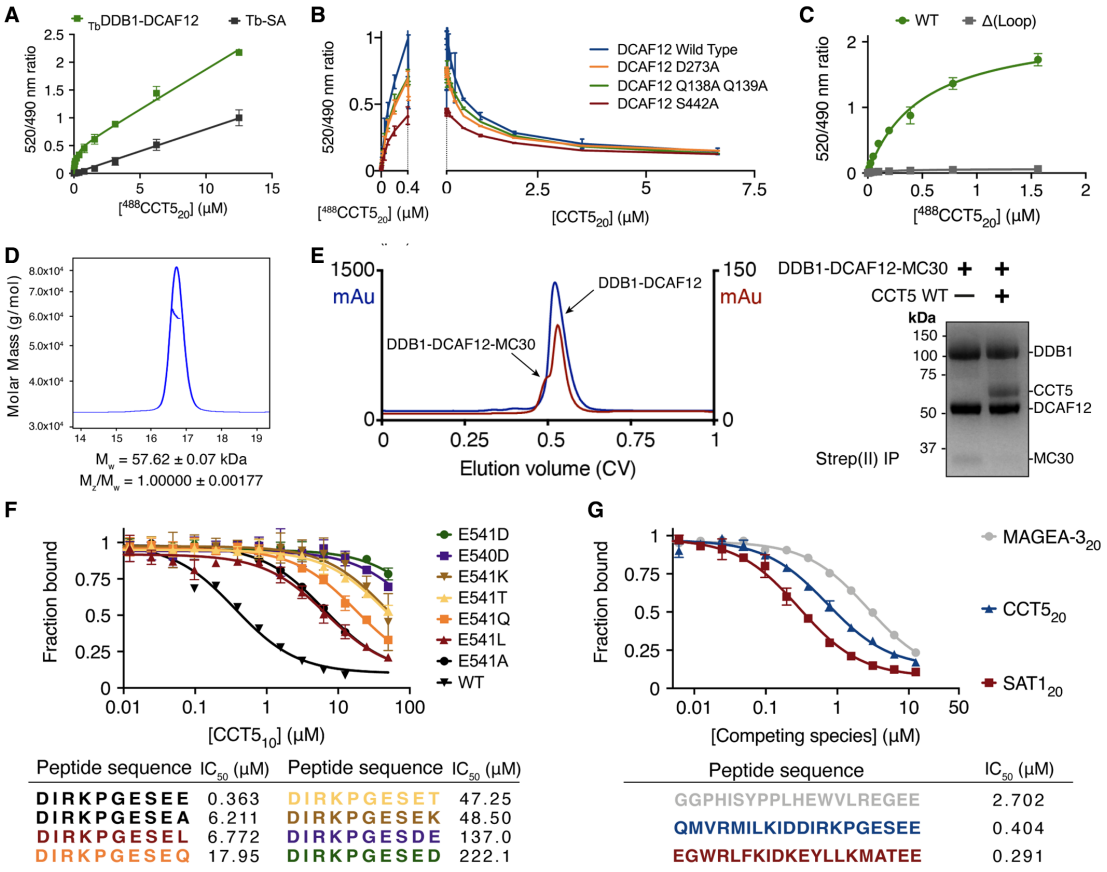

Peptide sequence	IC_{50} (μM)	Peptide sequence	IC_{50} (μM)
DIRKPGESEE	0.363	DIRKPGESET	47.25
DIRKPGESEA	6.211	DIRKPGESEK	48.50
DIRKPGESEL	6.772	DIRKPGESDE	137.0
DIRKPGESEQ	17.95	DIRKPGESED	222.1

Peptide sequence	IC_{50} (μM)
GGPHISYPPLHEWVLREGEE	2.702
QMVRMILKIDDIRKPGESEE	0.404
EGWRLFKIDKEYLLKMATEE	0.291

Figure EV1. DCAF12 binds monomeric substrates.

A Titration curves between a fluorescent $^{488}CCT5_{20}$ degron peptide and 50 nM biotinylated DDB1-DCAF12 pre-mixed with 2 nM terbium-coupled streptavidin ($_{Tb}$DDB1-DCAF12) or 2 nM terbium-coupled streptavidin (Tb-SA) ($n = 3$). Signal originating in the absence of $_{Tb}$DDB1-DCAF12 is unspecific and becomes dominant at high $^{488}CCT5_{20}$ concentrations.

B Left: titrations between 0–0.4 μM $^{488}CCT5_{20}$ and mutant $_{Tb}$DDB1-DCAF12 complexes ($n = 3$). The maximum fluorescent signal originating from the titrations was out-competed with a label-free $CCT5_{20}$ peptide (right).

C Titration curves between $^{488}CCT5_{20}$ and wild-type (WT) $_{Tb}$DDB1-DCAF12 or a mutant with DCAF12 amino acids 370–416 replaced by a flexible glycine-serine linker (Δ (Loop)) ($n = 3$).

D SEC-MALS analysis of wild-type CCT5. The chromatogram displays Rayleigh ratio curves for CCT5 together with the molar mass in Da of the main peaks. The calculated molecular weight (M_w) corresponds to a CCT5 monomer. The polydispersity of the sample (M_z/M_w) indicates a uniform species in the peak.

E Left: a representative size exclusion chromatograph (blue) for DDB1-DCAF12. A fraction of DDB1-DCAF12 is bound to a contaminant of ~ 30 kDa in size, MC30, that ends in a Glu-Thr motif. The contribution of the DDB1-DCAF12-MC30 species to the chromatograph absorbance (measured in arbitrary absorbance units, mAu) increases in low-yield purifications (red). Right: untagged CCT5 displaces MC30 from his_6-DDB1-strep(II)-DCAF12 *in vitro*.

F TR-FRET counter-titrations of label-free $CCT5_{10}$ degron peptides with mutant C-terminal amino acids ($n = 3$).

G TR-FRET counter-titrations of label-free degron peptides of different DCAF12 substrates (Koren *et al*, 2018) into $_{Tb}$DDB1-DCAF12^{488} ($n = 3$).

Data information: In (A, B, C, F, G), data are presented as mean ± 95% CI. Where indicated, "*n*" represents biological replicates.

© 2023 Friedrich Miescher Institute for Biomedical Research

14602075, 0, Downloaded from https://www.embopress.org/doi/10.15252/embj.2022112253 by Schweizerische Akademie Der, Wiley Online Library on [08/02/2023]. See the Terms and Conditions (https://onlinelibrary.wiley.com/terms-and-conditions) on Wiley Online Library for rules of use; OA articles are governed by the applicable Creative Commons License

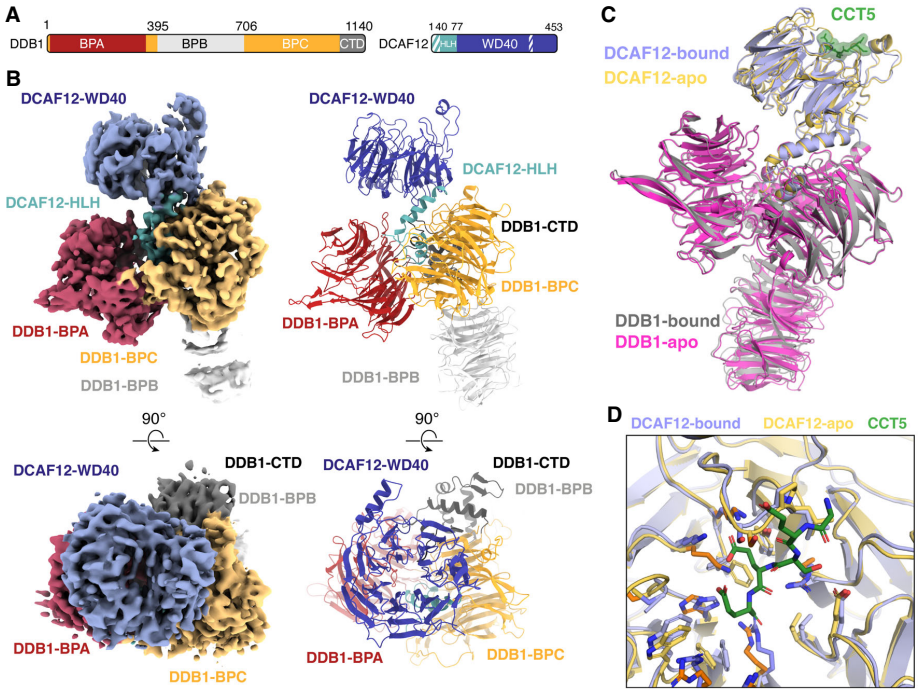

Figure EV2. Cryo-EM structure of DDB1-DCAF12 in the absence of CCT5.

A Domain organization of the proteins present in the sample. Unmodeled regions are shown as stripes.

B Different views of the DDB1-DCAF12 cryo-EM map (left) with fit structures (right). The map and models are colored as in (A).

C Superposition of the DDB1-DCAF12 (apo) and DDB1-DCAF12-CCT5 (bound) structures. Density corresponding to the CCT5 peptide (shown as green sticks with surface representation) was only observed in the DDB1-DCAF12-CCT5 structure (Fig 2). The root-mean-square deviation (RMSD) between the two structures is 1.2 Å between all atoms and 1.0 Å when excluding the flexible BPB domain of DDB1.

D Superposition of the residues forming the DCAF12 pocket between the DDB1-DCAF12 (apo) and DDB1-DCAF12-CCT5 (bound) cryo-EM structures.

© 2023 Friedrich Miescher Institute for Biomedical Research

14602075, 0, Downloaded from https://www.embopress.org/doi/10.15252/embj.2022112253 by Schweizerische Akademie Der Wiley Online Library on [08/02/2023]. See the Terms and Conditions (https://onlinelibrary.wiley.com/terms-and-conditions) on Wiley Online Library for rules of use; OA articles are governed by the applicable Creative Commons License

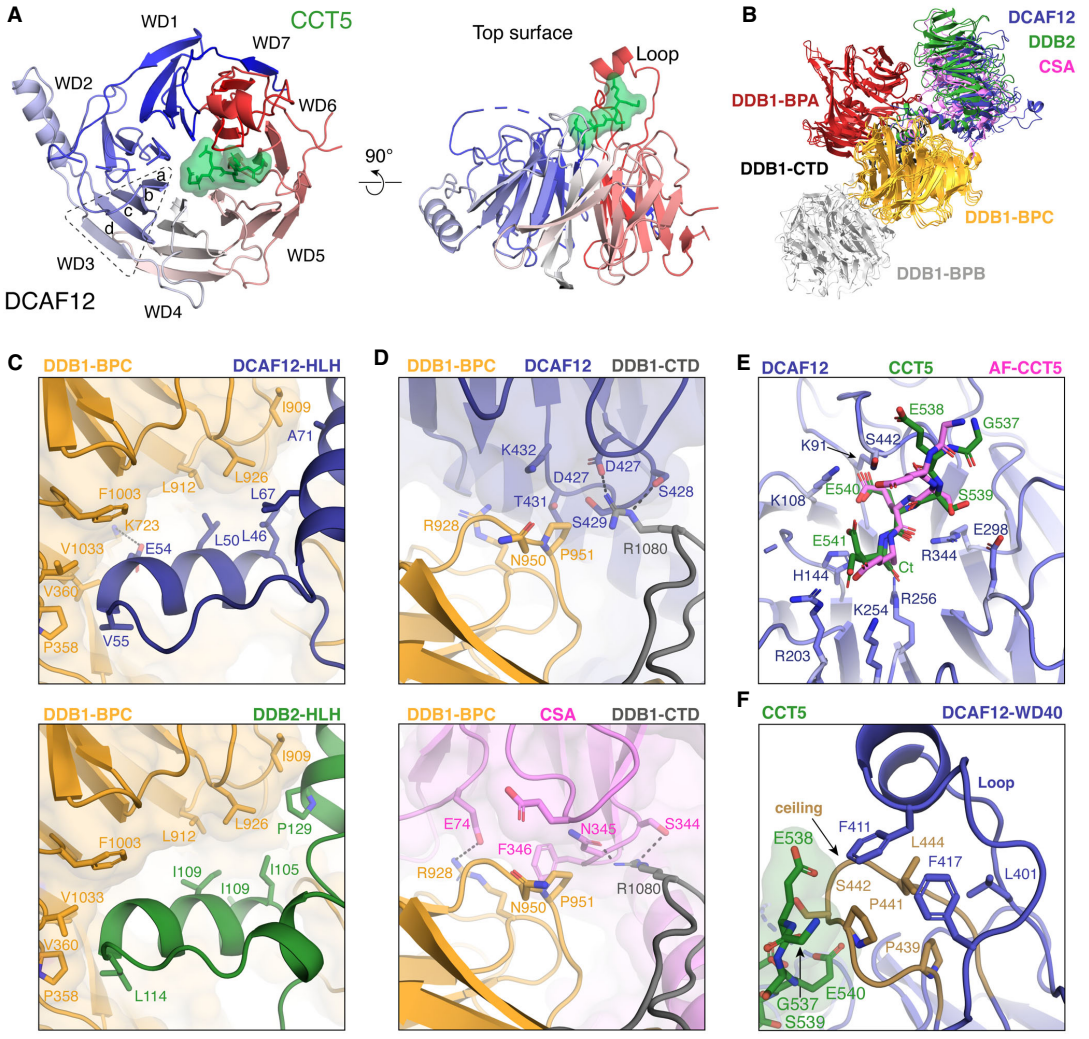

Figure EV3. DCAF12 assembles into a CRL4 ligase.

A Structural organization of the DCAF12 WD40 domain. The blades of the DCAF12 ß-propeller are labeled WD1-WD7 and colored according to their proximity to the N- or C-terminus. Each blade is composed of four ß strands labeled a-d in the outward direction. The CCT5 degron peptide is shown as green sticks and surface representation.

B Superposition between the coordinates of DDB1-DCAF12 (this study), DDB1-DDB2 (PDB ID 4A0K; Fischer *et al*, 2011) and DDB1-CSA (PDB ID 4A11; Fischer *et al*, 2011).

C, D Close-up of DDB1 residues contacted by the HLH motif (C) or ß-propeller (D) of DCAF12 (top) that are involved in binding other substrate receptors (bottom).

E Superposition of the AlphaFold2 prediction for the CCT5 peptide (AF-CCT5, violet) onto the cryo-EM coordinates of DDB1-DCAF12-CCT5 (CCT5 shown in green). The two modeled conformations of the CCT5 Glu541 side chain are depicted.

F Close-up of the hydrophobic residues mediating the interaction between the DCAF12 Loop (amino acids 370–416) and ceiling (amino acids 438–447).

© 2023 Friedrich Miescher Institute for Biomedical Research

14602075, 0, Downloaded from https://www.embopress.org/doi/10.15252/embj.2022112253 by Schweizerische Akademie Der, Wiley Online Library on [08/02/2023]. See the Terms and Conditions (https://onlinelibrary.wiley.com/terms-and-conditions) on Wiley Online Library for rules of use; OA articles are governed by the applicable Creative Commons License

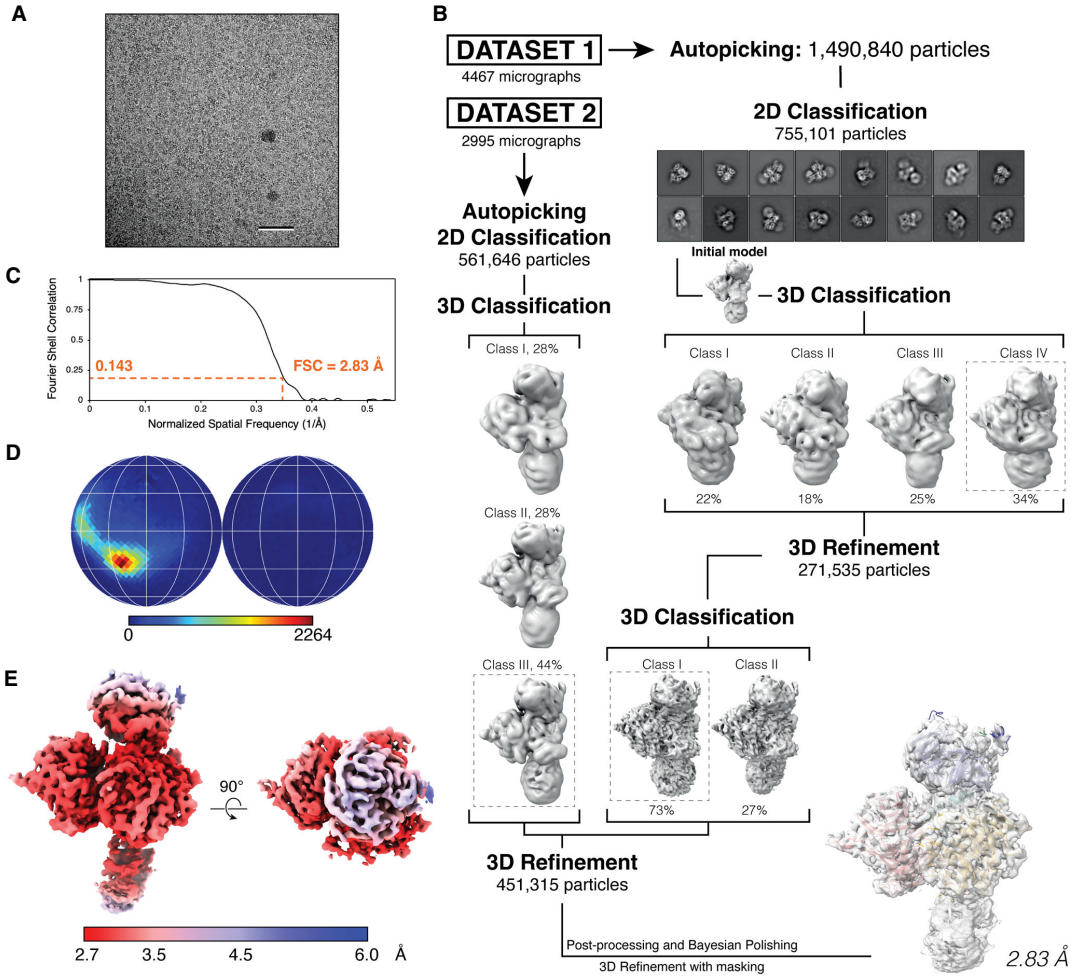

Figure EV4. DDB1-DCAF12-CCT5 cryo-EM structure determination.

A Representative micrograph from the DDB1-DCAF12-CCT5 collection. Scale bar: 50 nm.
B Workflow of cryo-EM data analysis for the DDB1-DCAF12-CCT5 cryo-EM map.
C Gold standard Fourier shell correlation (FSC) curve for the DDB1-DCAF12-CCT5 reconstruction.
D Angular distribution of DDB1-DCAF12-CCT5.
E Final cryo-EM map colored according to its local resolution, in angstroms.

© 2023 Friedrich Miescher Institute for Biomedical Research

14602075, 0, Downloaded from https://www.embopress.org/doi/10.15252/embj.2022112253 by Schweizerische Akademie Der, Wiley Online Library on [08/02/2023]. See the Terms and Conditions (https://onlinelibrary.wiley.com/terms-and-conditions) on Wiley Online Library for rules of use; OA articles are governed by the applicable Creative Commons License

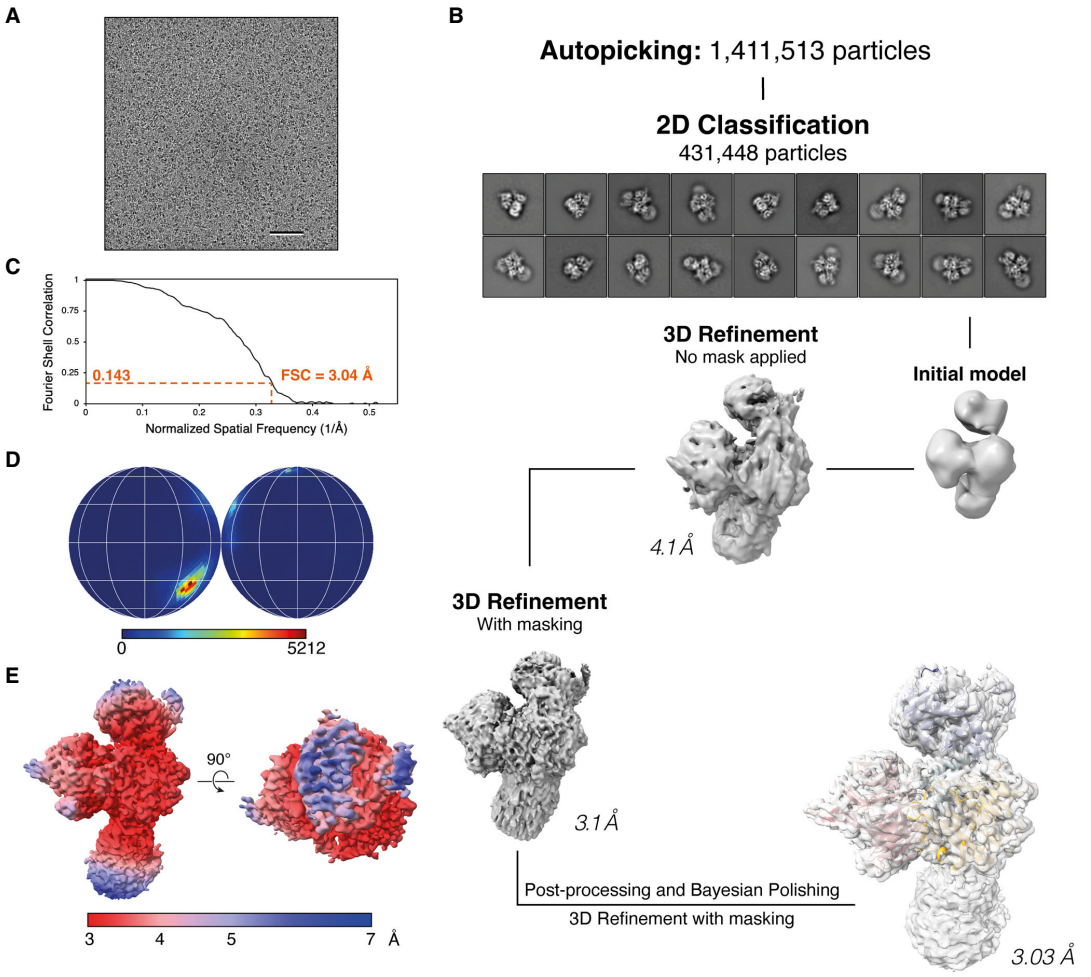

Figure EV5. DDB1-DCAF12 cryo-EM structure determination.

A Representative micrograph from the DDB1-DCAF12 collection. Scale bar: 50 nm.
B Workflow of cryo-EM data analysis for the DDB1-DCAF12 cryo-EM map. 4,568 micrographs were collected.
C Gold standard Fourier shell correlation (FSC) curve for the DDB1-DCAF12 reconstruction.
D Angular distribution of DDB1-DCAF12.
E Final cryo-EM map colored according to its local resolution, in angstroms.

© 2023 Friedrich Miescher Institute for Biomedical Research

14602075, 0, Downloaded from https://www.embopress.org/doi/10.15252/embj.2021112253 by Schweizerische Akademie Der, Wiley Online Library on [08/02/2023]. See the Terms and Conditions (https://onlinelibrary.wiley.com/terms-and-conditions) on Wiley Online Library for rules of use; OA articles are governed by the applicable Creative Commons License

APPENDIX

14602075, 0, Downloaded from https://www.embopress.org/doi/10.15252/embj.2022112253 by Schweizerische Akademie Der Wiley Online Library on [08/02/2023]. See the Terms and Conditions (https://onlinelibrary.wiley.com/terms-and-conditions) on Wiley Online Library for rules of use; OA articles are governed by the applicable Creative Commons License

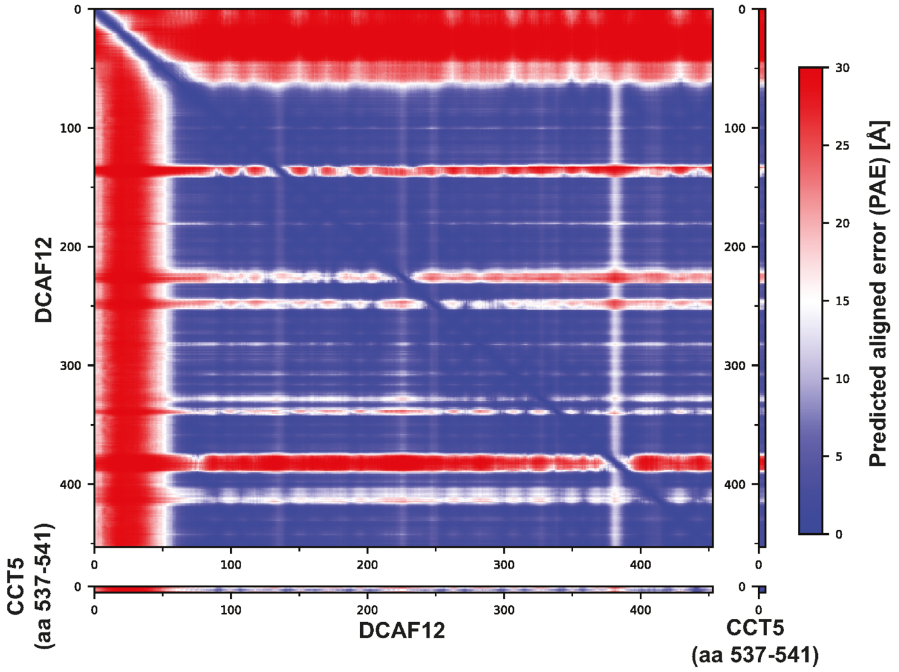

Appendix Figure S1. AlphaFold-Multimer prediction for the DDB1-DCAF12-CCT5 complex.

Predicted aligned error (PAE) from AlphaFold-Multimer for complex prediction of DCAF12 (full-length) and CCT5 degron (amino acids 537-541). For each subunit pair, the PAE values are shown in different sub-plots.

14602075, 0, Downloaded from https://www.embopress.org/doi/10.15252/embj.2022112253 by Schweizerische Akademie Der, Wiley Online Library on [08/02/2023]. See the Terms and Conditions (https://onlinelibrary.wiley.com/terms-and-conditions) on Wiley Online Library for rules of use; OA articles are governed by the applicable Creative Commons License

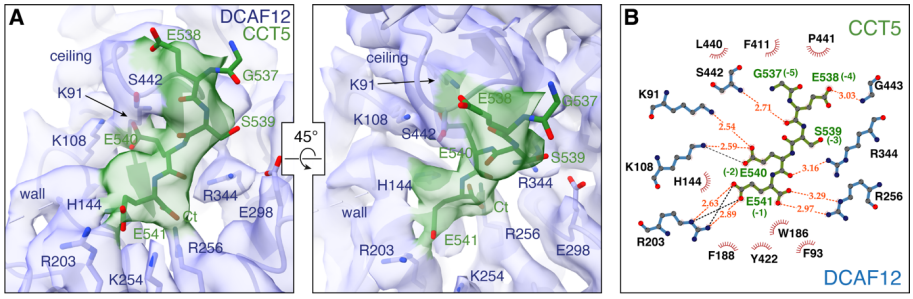

Appendix Figure S2. Alternative conformation of the CCT5 Glu541 side chain.

(A) A close-up view of the electron density around the DCAF12 pocket with an alternative conformation for the CCT5 Glu541 side chain modelled. DCAF12 is shown in light blue as cartoons, with key pocket residues shown as sticks. CCT5 residues are shown as green sticks. The electron density map is shown at a higher contour level than Fig 3A **(B)** LigPlot+ diagram of the interactions between DCAF12 and the alternative conformation of the CCT5 di-Glu degron (Laskowski & Swindells, 2011). The DCAF12 residues forming hydrogen bonds with CCT5 are shown in blue. DCAF12 residues involved in van der Waals packing are shown with eyelashes in red. CCT5 residues are shown in green with degron positions in parentheses. Hydrogen bonds and salt bridges are shown as orange and black dashed lines, respectively.

14602075, 0, Downloaded from https://www.embopress.org/doi/10.15252/embj.2022112253 by Schweizerische Akademie Der Wiley Online Library on [08/02/2023]. See the Terms and Conditions (https://onlinelibrary.wiley.com/terms-and-conditions) on Wiley Online Library for rules of use; OA articles are governed by the applicable Creative Commons License

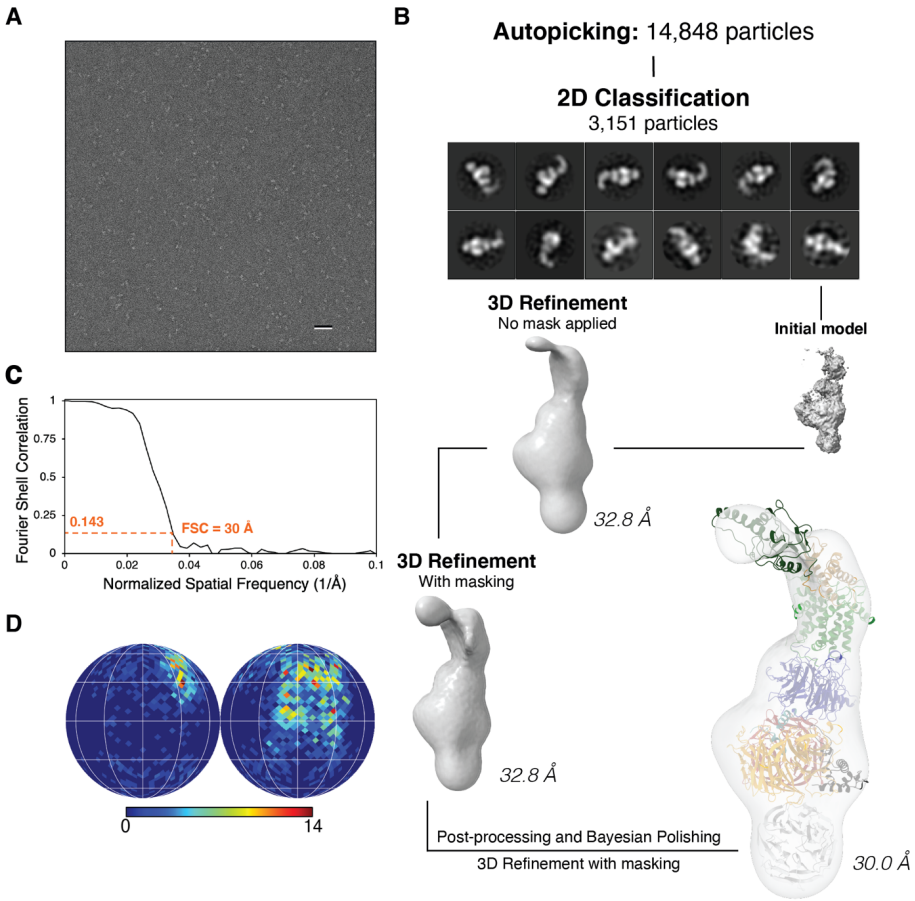

Appendix Figure S3. DDB1-DCAF12-CCT5 negative-stain EM structure determination.

(A) Representative micrograph from the DDB1-DCAF12-CCT5 negative-stain collection. Scale bar: 50 nm. **(B)** Workflow of cryo-EM data analysis for the DDB1-DCAF12-CCT5 negative-stain map. **(C)** Gold standard Fourier shell correlation (FSC) curve for the DDB1-DCAF12-CCT5 negative-stain reconstruction. **(D)** Angular distribution of DDB1-DCAF12-CCT5.

14602075, 0, Downloaded from https://www.embopress.org/doi/10.15252/embj.2022112253 by Schweizerische Akademie Der, Wiley Online Library on [08/02/2023]. See the Terms and Conditions (https://onlinelibrary.wiley.com/terms-and-conditions) on Wiley Online Library for rules of use; OA articles are governed by the applicable Creative Commons License

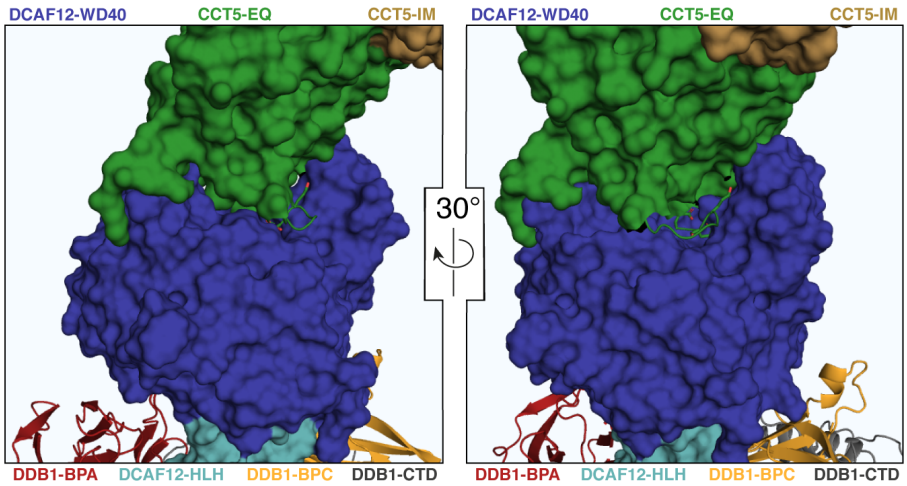

Appendix Figure S4. Binding of CCT5 to DCAF12 covers the pocket.

Different views of the interface between DCAF12 and CCT5 from the negative-stain EM map, shown in surface representation. DDB1 and the CCT5 C-terminal tail are shown as cartoons. Side chains are shown for CCT5 residues seen interacting with DCAF12 in the cryo-EM structure (Figure 3.6A).

14602075, 0, Downloaded from https://www.embopress.org/doi/10.15252/embj.2022112253 by Schweizerische Akademie Der Wiley Online Library on [08/02/2023]. See the Terms and Conditions (https://onlinelibrary.wiley.com/terms-and-conditions) on Wiley Online Library for rules of use; OA articles are governed by the applicable Creative Commons License

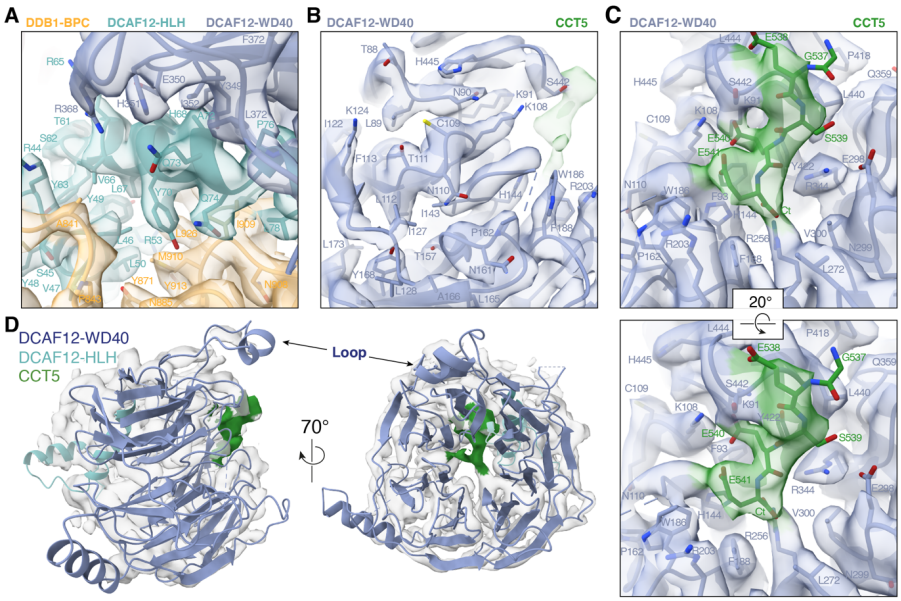

Appendix Figure S5. Model-map fitting of the CCT5-bound DDB1-DCAF12 complex.

Details of the structure of the CCT5-bound DDB1-DCAF12 complex fit into the 2.8 Å cryo-EM map are shown around the DCAF12 helix-loop-helix (HLH) motif **(A)**, and DCAF12 β-propeller blades one and two, which create the pocket wall **(B)**. DDB1 and DCAF12 are shown as cartoons, with individual residues shown as sticks. **(C)** Two close-up views of the 2.8 Å cryo-EM map around the DCAF12 pocket. DCAF12 is shown as cartoons, with individual residues shown as sticks. The CCT5 peptide is shown as sticks. **(D)** Side (left) and top (right) views of the 2.8 Å cryo-EM map around DCAF12, shown as cartoons. Density corresponding to the CCT5 peptide is colored green.

14602075, 0, Downloaded from https://www.embopress.org/doi/10.15252/embj.2022112253 by Schweizerische Akademie Der, Wiley Online Library on [08/02/2023]. See the Terms and Conditions (https://onlinelibrary.wiley.com/terms-and-conditions) on Wiley Online Library for rules of use; OA articles are governed by the applicable Creative Commons License

Appendix Table S1. IC_{50} values of degron peptides.

Peptide name	Sequence	Kd (μM)	95% CI (symmetric)	95% CI (asymmetric)
^{ATTO488}**CCT5$_{20}$**	ATTO488-QMVRMILKIDDIRKPGESEE	0.215	0.080 – 0.350	0.108 – 0.473

Peptide name	Sequence	IC50 (μM)	95% CI (symmetrical)	95% CI (asymmetrical)
CCT5$_2$	EE	383.8	13.74 – 753.90	193.30 – 6448.00
CCT5$_5$	GESEE	24.64	20.51 – 28.76	20.98 – 29.36
CCT5$_6$	PGESEE	15.59	11.95 – 19.23	12.50 – 19.86
CCT5$_7$	KPGESEE	4.955	4.137 – 5.965	4.060 – 5.850
CCT5$_8$	RKPGESEE	0.771	0.621 – 0.920	0.631 – 0.942
CCT5$_{10}$	DIRKPGESEE	0.363	0.285 – 0.441	0.291 – 0.453
CCT5$_{15}$	ILKIDDIRKPGESEE	0.614	0.564 – 0.664	0.567 – 0.666
CCT5$_{20}$	QMVRMILKIDDIRKPGESEE	0.404	0.361 – 0.457	0.363 - 0.461
CCT5$_{10}$ D532A	AIRKPGESEE	0.222	0.198 – 0.247	0.198 – 0.250
CCT5$_{10}$ I533A	DARKPGESEE	0.209	0.184 – 0.234	0.185 – 0.236
CCT5$_{10}$ R534A	DIAKPGESEE	0.395	0.327 – 0.464	0.330 – 0.474
CCT5$_{10}$ K535A	DIRAPGESEE	0.208	0.182 – 0.234	0.182 – 0.236
CCT5$_{10}$ P536A	DIRKAGESEE	0.417	0.364 – 0.470	0.366 – 0.475
CCT5$_{10}$ G537A	DIRKPAESEE	0.100	0.089 – 0.111	0.089 – 0.112
CCT5$_{10}$ E538A	DIRKPGASEE	0.571	0.468 – 0.674	0.473 – 0.688
CCT5$_{10}$ S539A	DIRKPGEAEE	0.125	0.110 – 0.139	0.110 – 0.141
CCT5$_{10}$ E540A	DIRKPGESAE	53.810	35.83 – 72.60	40.08 – 79.85
CCT5$_{10}$ E541A	DIRKPGESEA	6.211	3.182 – 9.228	3.923 – 10.490
CCT5$_{10}$ E541L	DIRKPGESEL	6.772	5.305 – 8.684	5.112 – 8.432
CCT5$_{10}$ E541Q	DIRKPGESEQ	17.95	15.06 – 21.50	14.76 – 21.15
CCT5$_{10}$ E541T	DIRKPGESET	47.25	35.44 – 64.86	33.25 – 61.25
CCT5$_{10}$ E541K	DIRKPGESEK	48.50	40.16 – 59.28	38.61 – 58.39
CCT5$_{10}$ E540D	DIRKPGESDE	137.0	88.36 – 250.3	67.49 – 206.4
CCT5$_{10}$ E541D	DIRKPGESED	222.1	102.1 – 1981	0.000 – 448.5
MAGEA3$_{20}$	GGPHISYPPLHEWVLREGEE	2.702	2.109 – 3.295	2.170 – 3.385
SAT1$_{20}$	EGWRLFKIDKEYLLKMATEE	0.291	0.253 – 0.330	0.257 – 0.332

14602075, 0, Downloaded from https://www.embopress.org/doi/10.15252/embj.2022112253 by Schweizerische Akademie Der, Wiley Online Library on [08/02/2023]. See the Terms and Conditions (https://onlinelibrary.wiley.com/terms-and-conditions) on Wiley Online Library for rules of use; OA articles are governed by the applicable Creative Commons License

THE EMBO JOURNAL

Recognition of the CCT5 di-Glu degron by CRL4DCAF12 is dependent on TRiC assembly

Carlos Pla-Prats, Simone Cavadini, Georg Kempf, and Nicolas Thomä
DOI: 10.15252/embj.2022112253

Corresponding author(s): Nicolas Thomä (Nicolas.Thoma@fmi.ch)

Review Timeline:

Submission Date:	30th Jul 22
Editorial Decision:	25th Aug 22
Revision Received:	21st Oct 22
Accepted:	14th Dec 22

Editor: Hartmut Vodermaier

Transaction Report:

(Note: With the exception of the correction of typographical or spelling errors that could be a source of ambiguity, letters and reports are not edited. Depending on transfer agreements, referee reports obtained elsewhere may or may not be included in this compilation. Referee reports are anonymous unless the Referee chooses to sign their reports.)

1st Editorial Decision **25th Aug 2022**

Thank you for submitting your study on CRL4-DCAF12 degron recognition in monomeric CCT5 to The EMBO Journal. It has now been assessed by three expert referees, whose comments are copied below for your information. I am happy to say that all reviewers appreciate the interest and timeliness of the findings and the general quality of the work, and that we would therefore be interested in pursuing the work further for publication. As you will see, the reports do still bring up a number of specific concerns and queries for clarification, which I would invite you to address in a revised version of the manuscript.

Referee #1:

The manuscript by C. Pla-Prats et al. presents structural and functional characterization on the recognition of the CCT5 C-terminal di-Glu degron by CRL4DCAF12 E3 ligase. They determine the cryo-EM structures of the DDB1-DCAF12-CCT5 complex and the DDB1- DCAF12 complex, and their structural and biochemical analyses indicate the molecular determinants of CCT5 di-Glu degron recognition. They also show that DCAF12 binds and ubiquitinates monomeric CCT5, instead of TRiC complex. Their study suggests a role for the CRL4DCAF12 E3 ligase in overseeing the assembly of the key molecular folding machinery TRiC. The overall topic is very interesting, still, the cryo-EM map and model quality need to be validated, and the structural analysis need to be better presented. Here are my comments and questions the authors need to address.

1) The authors claim their DDB1-DCAF12-CCT5 map has been resolved to 2.8 Å resolution. From the model-map fitting illustrated in Fig. S4B, it is hard to see high-resolution structural features. Please show such high-resolution features including especially the side chain model- map fitting details. Also, for Fig. 3A, it is hard to tell the fitting quality in the DCAF12-CCT5 interaction interface. Please illustrate the model-map fitting for DCAF12 and the CCT5 C- terminal 5 residues in this interface, respectively.

2) For the cryo-EM analysis of the DDB1-DCAF12-CCT5 complex, please explain why there is no indication of presence of a more complete CCT5, even in the 2D class averages. If it is due to the dynamics of the bound CCT5, the authors are suggested to perform 3D variability analysis in cryoSPARC to capture the presence of CCT5.

3) For the negative staining EM (NS-EM) map determination of the DDB1-DCAF12-CCT5 complex, please add a supplementary figure to illustrate the data processing process, especially representative reference-free 2D class averages to illustrate the presence and orientation of the associated CCT5. Also, in the NS-EM map, does the position of CCT5 allows its C-terminus to fit in the orientation obtained through the corresponding cryo-EM map?

4) Please show the detailed cryo-EM data collection, processing, and model quality in Table S1.

Minor points:

1) L.118, please define "ATTO488".

2) L. 298-299, the authors describe that "CCT5 adopts a curved shape formed by equatorial (EQ), middle (MD) and apical (AP) domains .....". In TRiC structure, the three domains are usually defined as equatorial (E), intermediate (I), and apical (A) domains.

Referee #2:

Because signal transduction relies on both transient and stable protein interactions, all organisms have evolved quality control pathways that monitor proper complex formation. While the importance of such assembly quality control has been clearly established, the underlying molecular mechanisms are still very incompletely understood and more structural and biochemical work is needed. Here, the authors present strong structural data that implicates the CRL4-DDB1-DCAF12 E3 ligase, known to function in C-end rule mediated degradation, as an assembly QC enzyme that could detect a chaperonin subunit in its free, but not complexed, state.

The authors focused their elucidation of the CRL4-DDB1-DCAF12 complex onto the candidate substrate CCT5, a subunit of the metazoan TRiC chaperonin. CCT5 contains a C-terminal di-Glu degron that they find is directly recognized by DCAF12 with decent (although maybe not high, as suggested by the authors) mid-nanomolar affinity. Having reconstituted the complex between DDB1-DCAF12 and a CCT5 C-terminal peptide, the authors proceeded to solve its cryo-EM structure, thereby revealing the mechanistic basis of C-end rule recognition. DCAF12 possesses multiple positively charged surface patches that are all essential for binding and thus read out combinatorically the carboxy-terminus and the gamma-carboxy functions of the most critical C-terminal Glu-residue in the -2 position. They noted some flexibility in recognition of the Glu side chain in the -1 position, likely explaining some variability in the C-terminal residue among DCAF12 substrates. The authors then show by a combination of negative stain EM using full-length CCT5 and published structures of assembled TRiC that both the C-terminus in CCT5 as well as the surface of CCT5 oriented towards DCAF12 are shielded from E3 ligase recognition by assembly of the TRiC complex. Using fully assembled TRiC, they accordingly found that DCAF12 can bind and ubiquitylate free CCT5, but not the CCT5 protein that is part of TRiC. This finding suggests that CUL4-DDB1-DCAF12 is a quality control E3 ligase that detects free CCT5, potentially as a consequence of aberrant or abortive TRiC assembly.

The biochemistry and structural biology reported in this paper are beautiful. The experiments have been designed and interpreted clearly and the findings are very important - they provide insight into C-end rule specificity and point towards a biological function of this pathway. I have, in fact, no criticism with respect to the data of this paper and would not ask the authors for any revision with respect to their experiments.

While the authors focus their discussion on a potential role of DCAF12 as an assembly QC enzyme, it stands to reason whether this is the key role of the E3 ligase in cells. They provide arguments that also for other targets, C-terminal complex formation might modulate recognition by DCAF12. However, it is not known whether the substrates investigated here are essential DCAF12 targets in cells. It could very well be that a crucial target that drove DCAF12 evolution uses a different mechanism (for example, unleashing a C-terminus that might be bound in cis as a response to a signaling event important for cell function or homeostasis). As distinguishing between such possibilities or identifying such a target will be a study in itself that requires very different technologies, I would not ask them to perform such experiments. However, I propose that the authors should include a discussion of potential alternative functions of DCAF12 in their paper.

Referee #3:

In the manuscript 'Recognition of the CCT5 di-Glu degron by CRL4DCAF12 is incompatible with TRiC 3 assembly', Carlos et al. detail in the recognition mechanism of di-Glu-containing substrates by DCAF12 by presenting the cryo-EM structure of the DDB1-DCAF12-CCT5 complex. They found that DCAF12 serves as a canonical WD40 DCAF substrate receptor and uses a positively charged pocket at the center of the β-propeller to bind the C-terminus of CCT5. Specifically, di-Glu motif of CCT5 displays a decisive role for the interaction. While subsequent results verified that DCAF12 only binds and ubiquitinates monomeric CCT5, and CCT5 in assembled TRiC complex is not competent for binding to DCAF12. Thus they concluded that a structurally intact TRiC complex therefore protects CCT5 from recognition by the CRL4DCAF12 E3 ligase.

Overall, most of the work is well supported by the data. This study represents an important contribution to our understanding of how CRL4DCAF12 targets di-Glu substrates. Despite these considerable strengths, there are several key areas for improvement of the manuscript.

Major comments:
1. The authors indicated that DCAF12 His144, Arg203 and Lys254 formed a positively charged patch for the stabilization of gamma carboxyl group of C-terminal Glu, this interaction seems just electrostatic attraction without forming of any direct hydrogen bond or salt bridge interactions. As the structural similarity of Asp or Gln with Glu, we are curious about whether the -1 position can be substituted by these two residues. Additionally, the authors mentioned that DCAF12 also binds Glu-Thr or Glu-Leu degron. Please titrate the mutant peptides of -1 position substituted by Asp, Gln, Thr and Leu against TbDDB1-DCAF12488, which is of importance for the analysis of specific selectivity of C-terminal Glu for DCAF12 binding.
2. In the competition experiments of different lengths of CCT5 degron peptides, the authors tested the truncation of degron peptide from 20 to 2 amino acids. They found that truncating the degron peptide to 5 residues brought a sharp decline of the binding affinity (~80-fold) comparing with the 10 residues peptide. They should narrow the gap of sequence length between 5-10 residues, such as addition of 6 or 8 residue peptide, to further confirm the minimum length of CCT5 peptide for DCAF12 binding.
3. Line 163, the authors mentioned that 'Among the residues preceding the C-terminal glutamates, the largest effects were seen for Glu538 (position -4; IC50 = 571 {plus minus} 103 nM), Pro536 (position -6; IC50 = 417 {plus minus} 53 nM) and Arg534 (position -8; IC50 = 395 {plus minus} 68 nM) (Fig 1D).'. All of these binding affinities are comparable with that of wild type CCT510 (IC50 = 390 {plus minus} 115 nM), thus this statement of 'largest effects' is not accurate and should be rewritten. However, we found that -3 or -5 substitution of CCT510 peptide by Ala showed a ~3-fold increasing of the binding, indicating some extent preference of these two positions. Please analyse this case and give a rational interpretation.
4. Line 263, the authors mentioned that 'At the base of the pocket, Arg344 further contributes to substrate binding through interactions with the CCT5 peptide backbone (Fig 3A and C). '. What kind of interactions here refer to?
5. The authors demonstrated that CRL4DCAF12 can effectively ubiquitinate monomeric CCT5, and it showed no ubiquitination activity towards TRiC. While whether this ubiquitination would lead to degradation of CCT5? Please verify this with cellular experiments, such as GPS assays or other similar experiments.
6. The authors uses time-resolved fluorescence energy transfer assay (TR-FRET) to monitor binding of a CCT5 C-terminal peptide to DDB1-DCAF12. The data indicated that the Kd for the 488CCT520 peptide was 215{plus minus}135 nM. The error value exceeds to half of the base value, and we think it is not exact enough, please redetermine this measurement.

Minor comments:
Some description is redundant and repetitive, such as '50 nM DDB1-DCAF12, 2 nM Tb-SA, 400 nM 488CCT520 (TbDDB1-DCAF12488) complex', please simplify related description or transfer the specific description into the Method section.

PLA-PRATS C, CAVADINI S, KEMPF G, THOMÄ NH
"Recognition of the CCT5 di-Glu degron by $CRL4^{DCAF12}$ is dependent on TRiC assembly"

RESPONSE TO THE REVIEWERS

REVIEWER #1: The manuscript by C. Pla-Prats et al. presents structural and functional characterization on the recognition of the CCT5 C-terminal di-Glu degron by CRL4DCAF12 E3 ligase. They determine the cryo-EM structures of the DDB1-DCAF12-CCT5 complex and the DDB1- DCAF12 complex, and their structural and biochemical analyses indicate the molecular determinants of CCT5 di-Glu degron recognition. They also show that DCAF12 binds and ubiquitinates monomeric CCT5, instead of TRiC complex. Their study suggests a role for the CRL4DCAF12 E3 ligase in overseeing the assembly of the key molecular folding machinery TRiC. The overall topic is very interesting, still, the cryo-EM map and model quality need to be validated, and the structural analysis need to be better presented. Here are my comments and questions the authors need to address.

Author comment: We thank the reviewer for their positive comments on our manuscript and helpful feedback, and have addressed their questions below.

Major comments:
1) The authors claim their DDB1-DCAF12-CCT5 map has been resolved to 2.8 Å resolution. From the model-map fitting illustrated in Fig. S4B, it is hard to see high-resolution structural features. Please show such high-resolution features including especially the side chain model- map fitting details. Also, for Fig. 3A, it is hard to tell the fitting quality in the DCAF12-CCT5 interaction interface. Please illustrate the model-map fitting for DCAF12 and the CCT5 C- terminal 5 residues in this interface, respectively.

Author response: We thank the reviewer for pointing this out. We have adapted our structural figures (Fig 2B, Fig EV2B, Fig EV4B, Fig EV5B) to better reflect the resolution of the map, and we have shown the density in Fig 3A as surface to facilitate analysis by the reader. We have also made a new figure to illustrate the DCAF12 model-map fitting and the CCT5 C-terminus interface which can be found in the Appendix (Appendix Fig S6).

2) For the cryo-EM analysis of the DDB1-DCAF12-CCT5 complex, please explain why there is no indication of presence of a more complete CCT5, even in the 2D class averages. If it is due to the dynamics of the bound CCT5, the authors are suggested to perform 3D variability analysis in cryoSPARC to capture the presence of CCT5.

Author response: We thank the reviewer for their suggestion. 3D classification were performed at several steps along the processing workflow for the 2.8 and 3.0 Å cryo-EM maps, but they did not reveal the presence of CCT5. Substantial efforts were directed at improving the completeness of the map, and over a dozen samples were analyzed by cryo-EM. The particles were homogeneous, and overpicking of particles did not reveal a subpopulation of particles with visible CCT5 regardless of whether the dataset was refined through 2D classification prior to 3D classification. We only once saw a 2D class of free DDB1 as evidence of broken particles. We believe that CCT5 is recognized almost exclusively through its C-terminus (Fig 1C; was Fig 5A at first submission) and retains significant flexibility when bound to DCAF12. We note that cross-linking the sample prior to EM analysis also did not show additional signal for CCT5. Signal for CCT5 was not observed regardless of whether 3D variability analysis was performed with RELION or cryoSPARC.

3) For the negative staining EM (NS-EM) map determination of the DDB1-DCAF12-CCT5 complex, please add a supplementary figure to illustrate the data processing process, especially representative reference-free 2D class averages to illustrate the presence and orientation of the associated CCT5. Also, in the NS-EM map, does the position of CCT5 allows its C-terminus to fit in the orientation obtained through the corresponding cryo-EM map?

Author response: A figure with the data processing workflow for the negative-stain DDB1-DCAF12-CCT5 structure has been added to the manuscript. The figure (Appendix Figure S4) is made to be comparable to Figures EV4 and EV5 that detail the cryo-EM processing workflows. Regarding the CCT5 C-terminal tail, binding of the CCT5 equatorial domain largely covers the pocket, but leaves an opening around DCAF12 β-propeller blade 6, at the entrance of the pocket. The mode of binding observed in the negative-stain structure allows the CCT5 C-terminus to fit in the pocket. Although this was briefly mentioned in the text, we have expanded our description of the binding mode and made a figure to illustrate it that can be found in the Appendix (Appendix Fig S5).

4) Please show the detailed cryo-EM data collection, processing, and model quality in Table S1.

Author response: A table is incorporated into the manuscript (Table EV1; Cryo-EM data collection, refinement and validation statistics) that shows the detailed cryo-EM data collection, processing and validation statistics for both 2.8 and 3.0 Å cryo-EM structures. Table EV2 similarly presents the equivalent parameters for the negative-stain structure.

Minor points:
1) L.118, please define "ATTO488".

Author response: We are not aware of an alternative name for the fluorescent dye ATTO488. It appears to belong to a series of fluorescent labels named after the parent company (ATTO-TEC GmbH) and wavelength in nm of the maximum fluorescent emission. We have reworded our introduction to the label to be clearer to readers (lines 120-124). It now reads: "The resulting $_{Tb}$DDB1-DCAF12 complex was mixed with a peptide corresponding to the 20 C-terminal amino acids of CCT5 (^{488}CCT5$_{20}$; CCT5 amino acids 522-541) conjugated to the fluorescent label ATTO488, which contains the di-Glu motif and acts as a fluorescence acceptor".

2) L. 298-299, the authors describe that "CCT5 adopts a curved shape formed by equatorial (EQ), middle (MD) and apical (AP) domains .....". In TRiC structure, the three domains are usually defined as equatorial (E), intermediate (I), and apical (A) domains.

Author response: We thank the reviewer for pointing this out. We have corrected the name of the domain in the manuscript (line 306) and in the related figures (Fig 2A, Fig 4A, Appendix Fig S5).

REVIEWER #2: Because signal transduction relies on both transient and stable protein interactions, all organisms have evolved quality control pathways that monitor proper complex formation. While the importance of such assembly quality control has been clearly established, the underlying molecular mechanisms are still very incompletely understood and more structural and biochemical work is needed. Here, the authors present strong structural data that implicates the CRL4-DDB1-DCAF12 E3 ligase, known to function in C-end rule mediated degradation, as an assembly QC enzyme that could detect a chaperonin subunit in its free, but not complexed, state.

The authors focused their elucidation of the CRL4-DDB1-DCAF12 complex onto the candidate substrate CCT5, a subunit of the metazoan TRiC chaperonin. CCT5 contains a C-terminal di-Glu degron that they find is directly recognized by DCAF12 with decent (although maybe not high, as suggested by the authors) mid-nanomolar affinity. Having reconstituted the complex between DDB1-DCAF12 and a CCT5 C-terminal peptide, the authors proceeded to solve its cryo-EM structure, thereby revealing the mechanistic basis of C-end rule recognition. DCAF12 possesses multiple positively charged surface patches that are all essential for binding and thus read out combinatorically the carboxy-terminus and the gamma-carboxy functions of the most critical C-terminal Glu-residue in the -2 position. They noted some flexibility in recognition of the Glu side chain in the -1 position, likely explaining some variability in the C-terminal residue among DCAF12 substrates. The authors then show by a combination of negative stain EM using full-length CCT5 and published structures of assembled TRiC that both the C-terminus in CCT5 as well as the surface of CCT5 oriented towards DCAF12 are shielded from E3 ligase recognition by assembly of the TRiC complex. Using fully assembled TRiC, they accordingly found that DCAF12 can bind and ubiquitylate free CCT5, but not the CCT5 protein that is part of TRiC. This finding suggests that CUL4-DDB1-DCAF12 is a quality control E3 ligase that detects free CCT5, potentially as a consequence of aberrant or abortive TRiC assembly.

The biochemistry and structural biology reported in this paper are beautiful. The experiments have been designed and interpreted clearly and the findings are very important - they provide insight into C-end rule specificity and point towards a biological function of this pathway. I have, in fact, no criticism with respect to the data of this paper and would not ask the authors for any revision with respect to their experiments.

While the authors focus their discussion on a potential role of DCAF12 as an assembly QC enzyme, it stands to reason whether this is the key role of the E3 ligase in cells. They provide arguments that also for other targets, C-terminal complex formation might modulate recognition by DCAF12. However, it is not known whether the substrates investigated here are essential DCAF12 targets in cells. It could very well be that a crucial target that drove DCAF12 evolution uses a different mechanism (for example, unleashing a C-terminus that might be bound in cis as a response to a signaling event important for cell function or homeostasis). As distinguishing between such possibilities or identifying such a target will be a study in itself that requires very different technologies, I would not ask them to perform such experiments. However, I propose that the authors should include a discussion of potential alternative functions of DCAF12 in their paper.

Author response: We thank the reviewer for their very positive comments on our manuscript and helpful feedback. As per their suggestion, we have added a discussion on the potential alternative functions of DCAF12 in the manuscript (Discussion; lines 434-441). It now reads: "It is conceivable, however, that the evolution of DCAF12 might have been driven by a substrate whose degradation is independent of assembly into a complex. Recognition might follow the allosteric release of a C-terminal tail in response to a post-translational modification. DCAF12 might also act on specific splicing isoforms or products of caspase cleavage, and have ubiquitin-independent functions. In drosophila, it has recently been shown that the pro-apoptotic functions of DCAF12 are partially underlain by its non-degradative inhibition of inhibitor of apoptosis proteins (IAPs), which do not contain di-Glu degrons".

REVIEWER #3: In the manuscript 'Recognition of the CCT5 di-Glu degron by CRL4DCAF12 is incompatible with TRiC assembly', Carlos et al. detail in the recognition mechanism of di-Glu-containing substrates by DCAF12 by presenting the cryo-EM structure of the DDB1-DCAF12-CCT5 complex. They found that DCAF12 serves as a canonical WD40 DCAF substrate receptor and uses a positively charged pocket at the center of the β-propeller to bind the C-terminus of CCT5. Specifically, di-Glu motif of CCT5 displays a decisive role for the interaction. While subsequent results verified that DCAF12 only binds and ubiquitinates monomeric CCT5, and CCT5 in assembled TRiC complex is not competent for binding to DCAF12. Thus they concluded that a structurally intact TRiC complex therefore protects CCT5 from recognition by the CRL4DCAF12 E3 ligase.

Overall, most of the work is well supported by the data. This study represents an important contribution to our understanding of how CRL4DCAF12 targets di-Glu substrates. Despite these considerable strengths, there are several key areas for improvement of the manuscript.

Author response: We thank the reviewer for their positive comments on our manuscript and helpful feedback. Regarding their additional suggestions:

Major comments:
1. The authors indicated that DCAF12 His144, Arg203 and Lys254 formed a positively charged patch for the stabilization of gamma carboxyl group of C-terminal Glu, this interaction seems just electrostatic attraction without forming of any direct hydrogen bond or salt bridge interactions. As the structural similarity of Asp or Gln with Glu, we are curious about whether the -1 position can be substituted by these two residues. Additionally, the authors mentioned that DCAF12 also binds Glu-Thr or Glu-Leu degron. Please titrate the mutant peptides of -1 position substituted by Asp, Gln, Thr and Leu against TbDDB1-DCAF12488, which is of importance for the analysis of specific selectivity of C-terminal Glu for DCAF12 binding.

Author response: We have performed the suggested experiment and incorporated the results into a new figure panel (Figure EV1F; described in lines 164-166). We found that the affinity between Glu541Leu and Glu541Ala mutants was similar, and higher than the affinity of the polar mutants (Glu541Gln, Glu541Thr). We also found that a Glu541Asp mutant had the lowest affinity of all the peptides, below that of polar and hydrophobic substitutions and additional Glu540Asp and Glu541Lys mutant peptides that we designed. This suggests a more complex recognition code than previously anticipated.

2. In the competition experiments of different lengths of CCT5 degron peptides, the authors tested the truncation of degron peptide from 20 to 2 amino acids. They found that truncating the degron peptide to 5 residues brought a sharp decline of the binding affinity (~80-fold) comparing with the 10 residues peptide. They should narrow the gap of sequence length between 5-10 residues, such as addition of 6 or 8 residue peptide, to further confirm the minimum length of CCT5 peptide for DCAF12 binding.

Author response: We have performed the suggested experiment and incorporated the results into the manuscript (Figure 1D; described in lines 144-151). We found the affinities of the $CCT5_6$ and $CCT5_8$ peptides were very close to that of the $CCT5_5$ and $CCT5_{10}$ peptides respectively, indicating that a big increase in binding affinity occurs between 7 and 8 residues. This is now described in the text as follows: "We observed maximal binding when the C-terminal CCT5 peptides were eight residues or longer (Fig 1D). Truncating the degron peptide to six residues or less impaired binding, such that the $^{488}CCT5_{20}$ probe was not fully outcompeted at a concentration of 12.5 μM. Only traces of binding were observed for a CCT5 di-peptide at 12.5 μM, our highest tested experimental concentration (Fig 1D). The sequence features of di-Glu degrons were initially identified in peptides of at least ten residues in length. Our measurements thus show that a sequence context of seven to eight residues is sufficient for di-Glu degron binding".

3. Line 163, the authors mentioned that 'Among the residues preceding the C-terminal glutamates, the largest effects were seen for Glu538 (position -4; IC50 = 571 {plus minus} 103 nM), Pro536 (position -6; IC50 = 417 {plus minus} 53 nM) and Arg534 (position -8; IC50 = 395 {plus minus} 68 nM) (Fig 1D).'. All of these binding affinities are comparable with that of wild type CCT510 (IC50 = 390 {plus minus} 115 nM), thus this statement of 'largest effects' is not accurate and should be rewritten. However, we found that -3 or -5 substitution of CCT510 peptide by Ala showed a ~3-fold increasing of the binding, indicating some extent preference of these two positions. Please analyse this case and give a rational interpretation.

Author response: We thank the reviewer for pointing this out. While we see a clear and reproducible trend in the rank-order of these peptides, it is absolutely correct that the differences are small and that the errors are overlapping. We have therefore acknowledged the magnitude of these differences and the increase in binding affinity after alanine mutations in the -3 and -5 positions particularly, re-writing the paragraph as follows (lines 166-180): "Mutations in the amino acids preceding the C-terminal glutamates did not exhibit equally pronounced effects {{referring to mutations in the C-terminal glutamates}} when mutated to alanine, and displayed different behaviors (Fig 1E). Peptides mutated in degron positions -4 (Glu538Ala; IC_{50} = 571 ± 103 nM), -6 (Pro536Ala; IC_{50} = 417 ± 53 nM) and -8 (Arg534Ala; IC_{50} = 395 ± 68 nM) displayed similar affinities than the wild type sequence (WT; IC_{50} = 363 ± 78 nM), while mutations in positions -3 (Ser539Ala; IC_{50} = 125 ± 15 nM), -5 (Gly537Ala; IC_{50} = 100 ± 11 nM), -7 (Lys535Ala; IC_{50} = 208 ± 26 nM), -9 (Ile539Ala; IC_{50} = 209 ± 25 nM) and -10 (Glu532Ala; IC_{50} = 222 ± 25 nM) gave rise to slightly better binding when mutated to alanine (Fig 1E). Taken together, our measurements confirm that degron binding is driven by the C-terminal glutamates and highlight the importance of the -2 degron position for binding. We find that DCAF12 shows only moderate preference for individual degron residues preceding the C-terminal glutamates, in line with degradation reporters in cells that show little effect for mutations N-terminal of the di-Glu motif. However, the increased binding of alanine mutants of degron positions -3, -5, -7, -9 and -10 suggest that the CCT5 C-terminus is not the optimal di-Glu degron sequence bound by $CRL4^{DCAF12}$ ". In our structure, the -3 and -5 positions are close to the ceiling, which is formed by hydrophobic residues that drive interactions with the DCAF12 Loop (Fig EV3F). Assuming that the peptide chain trajectory remains unchanged, we speculate that alanine residues in the -3 and -5 positions interact favorably with ceiling amino acids Leu440, Pro441 and Phe411.

4. Line 263, the authors mentioned that 'At the base of the pocket, Arg344 further contributes to substrate binding through interactions with the CCT5 peptide backbone (Fig 3A and C). '. What kind of interactions here refer to?

Author response: We thank the reviewer for pointing out the lack of clarity in our writing. DCAF12 Arg344 interacts through electrostatic interactions with the backbone carbonyl between CCT5 Glu540 and Glu541. This interaction persists during the (minimal) rotation of the CCT5 peptide backbone that accompanies the flexibility of the Glu541 side chain, and is therefore expected to persist with amino acid substitutions of the -1 degron position.

5. The authors demonstrated that CRL4DCAF12 can effectively ubiquitinate monomeric CCT5, and it showed no ubiquitination activity towards TRiC. While whether this ubiquitination would lead to degradation of CCT5? Please verify this with cellular experiments, such as GPS assays or other similar experiments.

Author response: We thank the reviewer for their suggestion, which is well taken. The study by Koren I. *et al*. that is referenced throughout our manuscript identified degrons recognized by DCAF12 by carrying out GPS reporter assays in cells. They first identified proteasomally degraded proteins *in vivo*, and then used targeted E3 ligase disruption to assign degradation activity for each reporter construct to a specific E3 ligase, reaching the conclusion that DCAF12 downregulated protein constructs that ended in a di-Glu motif. They showed DCAF12-mediated degradation for reporters containing a CCT5 C-terminal peptide and the full length

CCT5 protein. The *in vivo* ubiquitin-dependent degradation of CCT5 by DCAF12 has therefore already been demonstrated. Building on that study, we now provide a molecular rationale for the CRL4^{DCAF12} ubiquitination activity, and propose a biological role for the CRL4^{DCAF12} ligase in AQC. A study by Elliot K.L. *et al.* (https://doi.org/10.1091/mbc.E15-01-0048) indicates that recombinantly fusing GFP to the N-terminus of CCT5 prevents TRiC assembly and renders CCT5 monomeric *in vivo*. We believe, in fact, that the degradation of the overexpressed GFP-CCT5 reporter constructs reported by Koren I. *et al* reflects the degradation of monomeric CCT5. Engineering a GFP-CCT5 construct that maintains TRiC assembly and CRL4^{DCAF12} binding and ubiquitination is non-trivial. We believe that, additionally, the difficulty of establishing the right controls would yield GPS reporter experiments inconclusive. We thus consider this experiment outside the scope of this work.

6. The authors uses time-resolved fluorescence energy transfer assay (TR-FRET) to monitor binding of a CCT5 C-terminal peptide to DDB1-DCAF12. The data indicated that the Kd for the 488CCT520 peptide was 215{plus minus}135 nM. The error value exceeds to half of the base value, and we think it is not exact enough, please redetermine this measurement.

Author response: We thank the reviewer for their observation. We have repeated the measurements, obtaining a value for the affinity of 245 {plus minus} 52 nM. The new data has been incorporated into the results section (line 129 and Fig 1B, as well as the associated K_i value in the main text (line 134)).

Minor comments:
Some description is redundant and repetitive, such as '50 nM DDB1-DCAF12, 2 nM Tb-SA, 400 nM 488CCT520 (TbDDB1-DCAF12488) complex', please simplify related description or transfer the specific description into the Method section.

Author response: We thank the reviewer for their suggestions to improve the clarity of our manuscript. We have kept the qualitative descriptions of the $_{Tb}$DDB1-DCAF12 and $_{Tb}$DDB1-DCAF12^{ATTO488} complexes in the main text, which we believe help understand the described experiments, but have restricted the detailed concentration information to the methods section (lines 526-541).

1st Revision - Editorial Decision **14th Dec 2022**

Thank you for submitting your final revised manuscript for our consideration. I am pleased to inform you that in light of the positive re-reviews copied below, we have now accepted it for publication in The EMBO Journal.

Referee #1:

The authors have addressed my comments and questions in a satisfactory way. I would suggest publication of the manuscript.

Referee #3:

The authors largely addressed our comments on their manuscript. I agree with the publication of the revised manuscript on EMBO Journal.

Chapter 8

Materials and Methods

8.1 Biochemical Methods

8.1.1 Cloning, protein expression and purification

DDB1-DCAF12-CCT5 complexes

DNA sequences encoding *H. sapiens* DDB1 (UniProt ID: Q16531), DCAF12 (Q5T6F0) and CCT5 (P48643) were codon-optimized for expression in insect cells. Unless stated otherwise, recombinant proteins were cloned into pAC-derived expression vectors and expressed as N-terminal fusions of his_6, strep(II) or strep(II)-avi affinity tags in *T. ni* High Five insect cells using the baculovirus expression system (Invitrogen) [440]. For structure determination, cells expressing strep(II)-DCAF12 and his_6-DDB1 were harvested 36h after infection and lysed by sonication in lysis buffer (50 mM Tris pH 8, 200 mM NaCl, 0.5 mM TCEP and 1x protease inhibitor cocktail (Sigma-Aldrich)). The lysate was centrifuged at 40,000 rcf for 40 min and the resulting supernatant applied to a gravity column with Strep-Tactin (IBA life sciences) affinity resin. The resin was washed extensively in lysis buffer and eluted in a buffer containing 50 mM Tris pH 8, 100 mM NaCl, 0.5 mM TCEP and 5 mM D-Desthiobiotin (IBA life sciences). The eluate was loaded onto a

Poros 50 HQ column (Life Technologies) and eluted with a 100mM - 1M NaCl gradient. Early peak fractions were subjected to size exclusion chromatography (Superdex200, Cytiva) in a buffer containing 50 mM 4-(2-hydroxyethyl)-1-piperazineethanesulfonic acid (HEPES) pH 7.4, 200 mM NaCl and 0.5 mM TCEP. Fractions were selected with care to not include impurities. Pure fractions were individually flash-frozen in liquid nitrogen without concentrating and stored at -80 °C. A persistent contaminant in the DDB1-DCAF12 purifications, which we named MC30, was identified mass-spectrometrically as originating from the baculoviral expression system and ends in a Glu-Leu motif (UniProt ID P41473). The purification scheme devised allowed separating DDB1-DCAF12 from the DDB1-DCAF12-MC30 complex. For the structural characterization of the CCT5-bound DDB1-DCAF12, the same purification protocol was applied to cells infected with an additional virus encoding his_6-CCT5. MC30 impurities were not observed in DDB1-DCAF12-CCT5 purifications. For TR-FRET and in vitro ubiquitination analysis, wild type or mutant DDB1-DCAF12 complexes were expressed as strep(II)-avi-DDB1-strep(II)-DCAF12 and purified as above.

Monomeric CCT5

Cells expressing wild type or (1-529) strep(II)-CCT5 were lysed by sonication in a buffer containing 50 mM Tris pH 8, 200 mM NaCl, 0.5 mM TCEP and 1x protease inhibitor cocktail (Sigma-Aldrich). The lysate was cleared by centrifugation at 40,000 rcf for 40 min and the resulting supernatant applied to a gravity column loaded with Strep-Tactin Sepharose affinity resin (IBA life sciences). The sample was washed in lysis buffer and eluted in a buffer containing 50 mM Tris pH 8, 50 mM NaCl, 0.5 mM TCEP and 5 mM D-Desthiobiotin (IBA Life Sciences). The eluate was further

purified via ion exchange chromatography on a Poros 50 HQ column (Life Technologies) and subjected to size exclusion chromatography (Superdex200, Cytiva) in a buffer containing 50 mM HEPES pH 7.4, 200 mM NaCl and 0.5 mM TCEP. Pure fractions were pooled, flash-frozen in liquid nitrogen and stored at -80 °C. The purified CCT5 was monomeric and monodisperse **(Figure 2.2B)**.

TRiC

An internal his_6 tag was recombinantly inserted into a surface-exposed loop of TRiC subunit CCT7, resulting in a GGSHHHHHHGS insertion after Gln470 [361]. The resulting his_6-CCT7-expressing baculovirus was used to co-infect High Five insect cells with baculoviruses expressing untagged wild type CCT1-6A and CCT8. Cells were harvested 36h after infection and lysed by sonication in a buffer containing 150 mM HEPES pH 7.4, 50 mM NaCl, 5 mM $MgCl_2$, 15 mM imidazole, 0.5 mM TCEP, 10% v/v glycerol, 1x protease inhibitor cocktail (Sigma-Aldrich) and 5 U/ml Benzonase (Sigma-Aldrich). The lysate was cleared by centrifugation at 40,000 rcf for 40 min, and the resulting supernatant applied to a gravity column loaded with cOmplete His-tag purification resin (Roche). The resin was washed with buffer A (50 mM HEPES pH 7.4, 5mM $MgCl_2$, 0.5 mM TCEP, 10% v/v glycerol) + 50 mM NaCl + 20 mM imidazole. Two more washing steps with buffer A + 500 mM NaCl + 20 mM imidazole and then with buffer A + 20 mM imidazole + 1 mM ATP were performed before eluting with buffer A + 400 mM imidazole. The eluate was further purified by ion exchange chromatography on a Poros 50 HE column (ThermoFisher scientific) and then on a MonoQ column (Cytiva) using 100 mM – 1M NaCl gradients. Fractions containing TRiC were concentrated using 100,000 Mw cut-off Amicon

concentrators (Merck), supplemented with 1 mM ATP and run on a Superose6 size exclusion chromatography column (Cytiva) in buffer A + 50 mM NaCl. Samples containing TRiC were individually flash-frozen in liquid nitrogen without concentration and stored at -80 °C.

8.1.2 Expression tests

10 ml of *T. ni* High Five insect cells were infected via direct addition of 100 µL of baculoviruses expressing his6-tagged human DDB1 and strep(II)-tagged DCAF12 constructs. Cells were harvested 36h after infection and lysed by sonication in lysis buffer (50 mM Tris pH 8, 200 mM NaCl, 0.5 mM tris(2-carboxyethyl) phosphine (TCEP), 0.05% TWEEN-20 and 1x protease inhibitor cocktail (Sigma-Aldrich)). The lysate was centrifuged at 17,100 rcf for 10 min in a table-top centrifuge and the resulting supernatant incubated with 20 µL of Strep-Tactin (IBA life sciences) affinity resin. The resin was washed extensively in lysis buffer. Bound proteins were eluted directly with SDS protein dye and samples analyzed by SDS-PAGE.

8.1.3 Biotinylation of DDB1-DCAF12 complexes

Biotinylation reactions were set in vitro by mixing purified wild type or mutant strep(II)-avi-DDB1-strep(II)-DCAF12 complexes at variable concentrations of 25–50 µM with 2.5 µM BirA enzyme and 0.2 mM D-Biotin in a reaction buffer containing 50 mM HEPES pH 7.4, 200 mM NaCl, 10 mM $MgCl_2$, 0.25 mM TCEP and 20 mM ATP. The reaction was incubated for 30 min at room temperature and then 14-16 h at 4 °C. Biotinylated DDB1-DCAF12 complexes were purified by size exclusion chromatography (Superdex200, Cytiva), flash-frozen in liquid nitrogen and stored at −80 °C.

8.1.4 Time-resolved fluorescence energy transfer (TR-FRET)

Increasing concentrations of an ATTO488-labeled peptide corresponding to the 20 C-terminal amino acids of CCT5 ($^{ATTO488}CCT5_{20}$, Biosyntan GmbH) were added to biotinylated DDB1-DCAF12 complexes at 50 nM pre-mixed with 2 nM terbium-coupled streptavidin (Tb-SA, Invitrogen) (final concentrations) in 384-well microplates (Greiner Bio-One, 784075) in a buffer containing 50 mM HEPES pH 7.4, 200 mM NaCl, 0.5 mM TCEP, 0.1% Pluronic acid and 2.5% dimethyl sulfoxide (DMSO). The reactions were incubated for 15 min at room temperature and then measured using a PHERAstar FS microplate reader (BMG Labtech). Three biological replicates were carried out per experiment, and 60 technical replicates of each data point were measured at intervals of 1 min. After excitation of terbium fluorescence with a 337 nm wavelength, emission at 490 nm (Tb) and at 520 nm (Alexa 488) was recorded with a 70 μs delay to reduce background fluorescence. The TR-FRET signal of each data point was obtained by calculating the 520/490 nm fluorescence ratio. The signal contribution of unspecific interactions between terbium and $^{ATTO488}CCT5_{20}$, as measured by the signal in the absence of DDB1-DCAF12, was measured and subtracted for every experiment. Data was analyzed with GraphPad Prism 6 assuming equimolar binding of the probe ($^{ATTO488}CCT5_{20}$) to the receptor ($_{Tb}$DDB1-DCAF12).

Competition assays were carried out by mixing increasing concentrations of unlabeled competing ligands with a pre-mixed complex of biotinylated DDB1-DCAF12 at 50 nM, Tb-SA at 2 nM and $^{ATTO488}CCT5_{20}$ at 400 nM ($_{Tb}$DDB1-DCAF12^{ATTO488}, final concentrations) in 384-well microplates (Greiner Bio-One, 784075) in a buffer containing 50 mM HEPES

pH 7.4, 200 mM NaCl, 0.5 mM TCEP, 0.1% Pluronic acid, 2.5% DMSO and 10% glycerol. The reactions were incubated for 15 min at room temperature and then measured using a PHERAstar FS microplate reader (BMG Labtech). Three biological replicates were carried out per experiment. The TR-FRET signal was plotted to calculate the half maximal inhibitory concentrations (IC_{50}) assuming a single binding site using GraphPad Prism 6.

8.1.5 In vitro ubiquitination

In vitro ubiquitination reactions were set by mixing 70 nM wild type or mutant biotinylated DDB1-DCAF12 with 70 nM CUL4B-RBX1 purified as previously described [388] in the presence or absence of 500 nM CCT5 or 250 nM TRiC (which contains two copies of CCT5) in a reaction mixture containing a 50 nM E1 enzyme (UBA1, Boston Biochem), a 1 μM E2 enzyme (UBCH5α, Boston Biochem) and 20 mM ubiquitin. Reactions were carried out in 50 mM Tris pH 7.5, 200 mM NaCl, 5 mM $MgCl_2$, 0.2 mM CaCl2, 0.5 mM TCEP, 1 mM ATP, 0.1% Triton X-100, 0.1 mg/ml BSA and 10% v/v glycerol and incubated for 0-30 min at 30°C. Reactions were then analyzed by Western blot on 0.2 μm nitrocellulose membranes using a mouse anti-CCT5 primary antibody (Santa Cruz Biotechnology, sc-376188, 1:5000) and an Alexa Fluor 790-labeled anti-mouse secondary antibody (Invitrogen, #A11375, 1:10,000) using an Odyssey DLx (LiCor Biosciences).

8.2 Structural methods

8.2.1 Negative-stain specimen preparation and data collection

3.5 µL of a DDB1-DCAF12-CCT5 sample at ~0.01 mg/ml were applied to a PureCarbon grid (#01840, Ted Pella) glow discharged with a Pelco EasyGlow (15 mA current, 45 s) (Ted Pella) and stained three times with 5 µL of a 2% w/v uranyl acetate solution. Data for the DDB1-DCAF12-CCT5 complex was acquired with a Tecnai Spirit (FEI) transmission electron microscope in low-dose mode operated at 120 keV. 167 images were recorded with an Eagle camera (FEI) at a nominal magnification of 49,000x resulting in a pixel size of 2.125 Å. Images were recorded by varying the defocus between -1 and -3 µm.

8.2.2 Negative-stain EM data processing

14,848 particles were selected from 167 micrograph images using cisTEM [441] and imported into SPHIRE [442] for further processing. CTF parameters for each micrograph were estimated using CTER [443]. Unbinned particle images were extracted from the micrographs using a box size of 128 x 128 pixels. The dataset was subjected to reference-free 2D classification using ISAC [444]. Selected particles were then imported into RELION [445] and 3D classified using an initial model obtained from VIPER [442]. 2923 particles were then refined and polished, yielding a map at 30 Å resolution.

8.2.3 Cryo-EM specimen preparation and data collection

DDB1-DCAF12: 3.5 µL of a his_6-DDB1-Strep(II)-DCAF12 sample at 3.0 µM were applied to a Quantifoil R 1.2/1.3 Cu 200 mesh carbon grid

(Quantifoil Micro Tools GmbH) glow discharged with a Pelco EasyGlow (15 mA current, 45 s). After a 4 s incubation time inside a chamber at 85% humidity, the grid was blotted for 3 s in Whatman #1 filter paper with a blot force of 20 and immediately vitrified by plunging into liquid nitrogen-cooled liquid ethane with a Vitrobot (ThermoFisher Scientific). Cryo-EM data was collected on a Cs-corrected FEI Titan Krios TEM (ThermoFisher Scientific) operated at 300 kV acceleration voltage using a Falcon 4 direct electron detector. 4568 EER movies were recorded with the microscope set at 75,000× nominal magnification, resulting in a calibrated pixel size of 0.845 Å, using a total dose of 50 electrons per $Å^2$. The EER files were converted to standard MRC file and fractionated into 50 frames for further processing. The defocus range was -0.5 to -2.5 µm.

DDB1-DCAF12-CCT5: 3.5 µL of a his_6-DDB1-Strep(II)-DCAF12-his_6-CCT5 sample at 2.7 µM were applied to a Quantifoil R 1.2/1.3 Cu 200 mesh carbon grid glow discharged with a Pelco EasyGlow (15 mA current, 45 s) (Ted Pella). After a 5 s incubation time inside a chamber at 85% humidity, the grid was blotted for 3 s in Whatman #1 filter paper with a blot force of 25 and immediately vitrified by plunging into liquid nitrogen-cooled liquid ethane with a Vitrobot (ThermoFisher Scientific). Cryo-EM data was collected on a Cs-corrected FEI Titan Krios TEM (ThermoFisher Scientific) operated at 300 kV acceleration voltage using a K2 direct electron detector. 4467 micrographs were recorded with the microscope set at 130,000× nominal magnification, resulting in a calibrated pixel size of 0.86 Å, using a total dose of 51.8 electrons per $Å^2$ fractionated into 50 frames and a defocus range of -0.5 to -2.5 µm.

8.2.4 Cryo-EM data processing

Unless specified otherwise, all processing steps were done within the RELION3 (v.3.1.3) package [445]. For DDB1-DCAF12-CCT5 **(Figure 3.3)**, electron micrograph movies were drift-corrected and dose-weighed using MOTIONCOR2 [446] and CTF parameters estimated using Gctf [447]. 1.5m particles were selected using the Laplacian-of-Gaussian algorithm implemented in RELION3, extracted and rescaled to 1.72 Å per pixel. The dataset was refined through sequential 2D and 3D classification, and 272k selected particles were re-extracted with a pixel size of 0.86 Å and 3D refined. After a round of 3D classification 199k particles were selected and polished, and a final round of 3D refinement masking out the DDB1 BPB domain was carried out in RELION, yielding a map at 2.83 Å resolution **(Figure 3.1)**. 3D classification along the processing flowchart did not reveal CCT5 peptide-free 3D classes.

For DDB1-DCAF12 **(Figure 3.4)**, electron micrograph movies were drift-corrected and dose-weighed using MOTIONCOR2 [446] and CTF parameters estimated using GCTF [447]. 1.4m particles were selected using the Laplacian-of-Gaussian algorithm implemented in RELION3, extracted and rescaled to 2.535 Å per pixel. The dataset was refined through several rounds of 2D classification, and 431k selected particles were re-extracted with a pixel size of 0.845 Å. Particles were 3D refined and the resulting map used to make a mask for a further refinement. Particles were polished and used for a final round of 3D refinement, yielding a map at 3.03 Å resolution **(Figure 3.2)**. 3D classification along the processing flowchart did not reveal significant variability in the model.

8.2.5 Model building and refinement

To interpret the DDB1-DCAF12-CCT5 cryo-EM map, the atomic structure of DDB1 (PDB ID: 3EI3) [386] and a prediction model for DCAF12 from trRosetta [448] were docked into the 2.8 Å cryo-EM map with Coot [449]. DCAF12 features were evident from the map, but the predicted ß-propeller did not readily fit as a rigid body. Thus, the individual ß-propeller blades were fit into the density with Coot, and the model was manually rebuilt with Coot and ChimeraX/Isolde [450]. During the course of this work, AlphaFold v.2 was released [392, 393], allowing us to cross-validate the model and build the DCAF12 Loop (amino acids 370-416). The structure was then refined using the Rosetta density-guided FastRelax protocol in combination with density scoring [451]. No overfitting was observed when refining against half-maps and the full map was used in final refinements steps. B factors were fit at a final stage using Rosetta. An in-house pipeline was used to run the Rosetta protocols (https://github.com/fmi-basel/RosEM). Phenix real-space refinement in combination with tight reference coordinate restraints was used to further reduce geometry outliers [452]. For modeling of the CCT5 degron peptide, different conformations were sampled using the Rosetta local rebuilding protocol (described in Wang et al, 2016) and predicted the DCAF12-degron complex with AlphaFold-multimer [453]. Guided by these results, the peptide was manually modeled, assigning an alternative conformation for the CCT5 Glu541 side chain due to more favorable density. The presented structural data suggest a conformational equilibrium for the gamma carboxyl group of Glu541, shifting between the Arg203/Lys254 patch and a histidine residue (His144) on the base of the pocket. Occupancies for the two envisioned Glu541 side chain conformations were assigned 70/30 %

on the basis of observed density, amino acid conservation and functional effect of the DCAF12 alanine mutations **(Figure 3.6E)**.

To interpret the DDB1-DCAF12 cryo-EM map, the DDB1-DCAF12 coordinates from the DDB1-DCAF12-CCT5 structure were docked into the map and found that they easily matched the cryo-EM map. Further refinement with Coot/Isolde/Rosetta/Phenix (as described above) showed only minor differences (RMSD=1.029 Å). Validation for both models was performed using Phenix [454], EMRinger [455] and MolProbity [456] **(Table 3.1)**. Side chains without sufficient density were marked by zero occupancy values.

For the DDB1-DCAF12-CCT5 negative-stain map, the coordinates for DDB1-DCAF12-CCT5 and full-length CCT5 (PDD ID: 6NR8) [361] could be confidently fit into the map despite the low resolution according to the distinct shape of the complex. The different structures could be rigid-body fit almost without clashes. CCT5 amino acids 530-536 that connect to the degron (amino acids 537-541) in the DDB1-DCAF12-CCT5 cryo-EM structure are likely flexible in solution and were removed. The structure was minimized using Rosetta FastRelax in torsional space in combination with a low-density weight of 20. This was followed by coordinate restrained minimization with Phenix real-space refinement **(Table 3.1)**. Side chains were removed from the final model.

Structural figures were generated using PyMol (Schrödinger, Inc) and ChimeraX [457]. Interface areas were calculated using the PDBe PISA server [458].

Chapter 9

Bibliography

1 Simpson, M.V. (1953) The release of labeled amino acids from the proteins of rat liver slices. *J Biol Chem* 201, 143-154

2 De Duve, C.*, et al.* (1955) Tissue fractionation studies. 6. Intracellular distribution patterns of enzymes in rat-liver tissue. *Biochem J* 60, 604-617

3 Mego, J.L.*, et al.* (1972) An adenosine triphosphate-dependent stabilization of proteolytic activity in heterolysosomes. Evidence for a proton pump. *Biochem J* 128, 763-769

4 Segal, H.L.*, et al.* (1976) A correlation between turnover rates and lipophilic affinities of soluble rat liver proteins. *Biochem Biophys Res Commun* 73, 79-84

5 Etlinger, J.D. and Goldberg, A.L. (1977) A soluble ATP-dependent proteolytic system responsible for the degradation of abnormal proteins in reticulocytes. *Proc Natl Acad Sci U S A* 74, 54-58

6 Bigelow, S.*, et al.* (1981) The selective degradation of injected proteins occurs principally in the cytosol rather than in lysosomes. *Cell* 25, 83-93

7 Ciehanover, A.*, et al.* (1978) A heat-stable polypeptide component of an ATP-dependent proteolytic system from reticulocytes. *Biochem Biophys Res Commun* 81, 1100-1105

8 Hershko, A.*, et al.* (1979) Resolution of the ATP-dependent proteolytic system from reticulocytes: a component that interacts with ATP. *Proc Natl Acad Sci U S A* 76, 3107-3110

9 Ciechanover, A.*, et al.* (1980) ATP-dependent conjugation of reticulocyte proteins with the polypeptide required for protein degradation. *Proc Natl Acad Sci U S A* 77, 1365-1368

10 Hershko, A.*, et al.* (1980) Proposed role of ATP in protein breakdown: conjugation of protein with multiple chains of the polypeptide of ATP-dependent proteolysis. *Proc Natl Acad Sci U S A* 77, 1783-1786

11 Ciechanover, A.*, et al.* (1984) Ubiquitin dependence of selective protein degradation demonstrated in the mammalian cell cycle mutant ts85. *Cell* 37, 57-66

12 Finley, D.*, et al.* (1984) Thermolability of ubiquitin-activating enzyme from the mammalian cell cycle mutant ts85. *Cell* 37, 43-55

13 Bachmair, A.*, et al.* (1986) In vivo half-life of a protein is a function of its amino-terminal residue. *Science* 234, 179-186

14 Hershko, A.*, et al.* (1982) Immunochemical analysis of the turnover of ubiquitin-protein conjugates in intact cells. Relationship to the breakdown of abnormal proteins. *J Biol Chem* 257, 13964-13970

15 Goldstein, G.*, et al.* (1975) Isolation of a polypeptide that has lymphocyte-differentiating properties and is probably represented universally in living cells. *Proc Natl Acad Sci U S A* 72, 11-15

16 Wilkinson, K.D.*, et al.* (1980) Ubiquitin is the ATP-dependent proteolysis factor I of rabbit reticulocytes. *J Biol Chem* 255, 7529-7532

17 Goldknopf, I.L. and Busch, H. (1977) Isopeptide linkage between nonhistone and histone 2A polypeptides of chromosomal conjugate-protein A24. *Proc Natl Acad Sci U S A* 74, 864-868

18 Levinger, L. and Varshavsky, A. (1982) Selective arrangement of ubiquitinated and D1 protein-containing nucleosomes within the Drosophila genome. *Cell* 28, 375-385

19 Hershko, A.*, et al.* (1981) Identification of the active amino acid residue of the polypeptide of ATP-dependent protein breakdown. *J Biol Chem* 256, 1525-1528

20 Edmunds, T. and Pennington, R.J. (1982) A high molecular weight peptide hydrolase in erythrocytes. *Int J Biochem* 14, 701-703

21 Hough, R.*, et al.* (1986) Ubiquitin-lysozyme conjugates. Identification and characterization of an ATP-dependent protease from rabbit reticulocyte lysates. *J Biol Chem* 261, 2400-2408

22 Eytan, E.*, et al.* (1989) ATP-dependent incorporation of 20S protease into the 26S complex that degrades proteins conjugated to ubiquitin. *Proc Natl Acad Sci U S A* 86, 7751-7755

23 Driscoll, J. and Goldberg, A.L. (1990) The proteasome (multicatalytic protease) is a component of the 1500-kDa proteolytic complex which degrades ubiquitin-conjugated proteins. *J Biol Chem* 265, 4789-4792

24 Ciechanover, A.*, et al.* (1981) Activation of the heat-stable polypeptide of the ATP-dependent proteolytic system. *Proc Natl Acad Sci U S A* 78, 761-765

25 Haas, A.L. and Rose, I.A. (1982) The mechanism of ubiquitin activating enzyme. A kinetic and equilibrium analysis. *J Biol Chem* 257, 10329-10337

26 Pickart, C.M. and Rose, I.A. (1985) Functional heterogeneity of ubiquitin carrier proteins. *J Biol Chem* 260, 1573-1581

27 Hershko, A.*, et al.* (1983) Components of ubiquitin-protein ligase system. Resolution, affinity purification, and role in protein breakdown. *J Biol Chem* 258, 8206-8214

28 Hershko, A.*, et al.* (1986) The protein substrate binding site of the ubiquitin-protein ligase system. *J Biol Chem* 261, 11992-11999

29 Matsui, S.*, et al.* (1982) Isopeptidase: a novel eukaryotic enzyme that cleaves isopeptide bonds. *Proc Natl Acad Sci U S A* 79, 1535-1539

30 Pickart, C.M. and Rose, I.A. (1985) Ubiquitin carboxyl-terminal hydrolase acts on ubiquitin carboxyl-terminal amides. *J Biol Chem* 260, 7903-7910

31 Wilkinson, K.D.*, et al.* (1989) The neuron-specific protein PGP 9.5 is a ubiquitin carboxyl-terminal hydrolase. *Science* 246, 670-673

32 Baker, R.T.*, et al.* (1992) Ubiquitin-specific proteases of Saccharomyces cerevisiae. Cloning of UBP2 and UBP3, and functional analysis of the UBP gene family. *J Biol Chem* 267, 23364-23375

33 Bachmair, A. and Varshavsky, A. (1989) The degradation signal in a short-lived protein. *Cell* 56, 1019-1032

34 Ball, E.*, et al.* (1987) Arthrin, a myofibrillar protein of insect flight muscle, is an actin-ubiquitin conjugate. *Cell* 51, 221-228

35 Chau, V.*, et al.* (1989) A multiubiquitin chain is confined to specific lysine in a targeted short-lived protein. *Science* 243, 1576-1583

36 Finley, D. (2009) Recognition and processing of ubiquitin-protein conjugates by the proteasome. *Annu Rev Biochem* 78, 477-513

37 Arnason, T. and Ellison, M.J. (1994) Stress resistance in Saccharomyces cerevisiae is strongly correlated with assembly of a novel type of multiubiquitin chain. *Mol Cell Biol* 14, 7876-7883

38 Spence, J.*, et al.* (1995) A ubiquitin mutant with specific defects in DNA repair and multiubiquitination. *Mol Cell Biol* 15, 1265-1273

39 Xu, P.*, et al.* (2009) Quantitative proteomics reveals the function of unconventional ubiquitin chains in proteasomal degradation. *Cell* 137, 133-145

40 Ozkaynak, E.*, et al.* (1984) The yeast ubiquitin gene: head-to-tail repeats encoding a polyubiquitin precursor protein. *Nature* 312, 663-666

41 Wiborg, O.*, et al.* (1985) The human ubiquitin multigene family: some genes contain multiple directly repeated ubiquitin coding sequences. *Embo j* 4, 755-759

42 Baker, R.T. and Board, P.G. (1987) The human ubiquitin gene family: structure of a gene and pseudogenes from the Ub B subfamily. *Nucleic Acids Res* 15, 443-463

43 Baker, R.T. and Board, P.G. (1991) The human ubiquitin-52 amino acid fusion protein gene shares several structural features with mammalian ribosomal protein genes. *Nucleic Acids Res* 19, 1035-1040

44 Finley, D.*, et al.* (1989) The tails of ubiquitin precursors are ribosomal proteins whose fusion to ubiquitin facilitates ribosome biogenesis. *Nature* 338, 394-401

45 Vijay-Kumar, S.*, et al.* (1985) Three-dimensional structure of ubiquitin at 2.8 A resolution. *Proc Natl Acad Sci U S A* 82, 3582-3585

46 Ramage, R.*, et al.* (1994) Synthetic, structural and biological studies of the ubiquitin system: the total chemical synthesis of ubiquitin. *Biochem J* 299 (Pt 1), 151-158

47 Komander, D. and Rape, M. (2012) The ubiquitin code. *Annu Rev Biochem* 81, 203-229

48 Pierce, N.W.*, et al.* (2009) Detection of sequential polyubiquitylation on a millisecond timescale. *Nature* 462, 615-619

49 Chen, Z. and Pickart, C.M. (1990) A 25-kilodalton ubiquitin carrier protein (E2) catalyzes multi-ubiquitin chain synthesis via lysine 48 of ubiquitin. *J Biol Chem* 265, 21835-21842

50 Baboshina, O.V. and Haas, A.L. (1996) Novel multiubiquitin chain linkages catalyzed by the conjugating enzymes E2EPF and RAD6 are recognized by 26 S proteasome subunit 5. *J Biol Chem* 271, 2823-2831

51 Kirisako, T.*, et al.* (2006) A ubiquitin ligase complex assembles linear polyubiquitin chains. *Embo j* 25, 4877-4887

52 Hershko, A.*, et al.* (1984) Role of the alpha-amino group of protein in ubiquitin-mediated protein breakdown. *Proc Natl Acad Sci U S A* 81, 7021-7025

53 Yau, R.G.*, et al.* (2017) Assembly and Function of Heterotypic Ubiquitin Chains in Cell-Cycle and Protein Quality Control. *Cell* 171, 918-933.e920

54 Chen, Z.J. and Sun, L.J. (2009) Nonproteolytic functions of ubiquitin in cell signaling. *Mol Cell* 33, 275-286

55 Schulman, B.A. and Harper, J.W. (2009) Ubiquitin-like protein activation by E1 enzymes: the apex for downstream signalling pathways. *Nat Rev Mol Cell Biol* 10, 319-331

56 Hochstrasser, M. (2009) Origin and function of ubiquitin-like proteins. *Nature* 458, 422-429

57 Cappadocia, L. and Lima, C.D. (2018) Ubiquitin-like Protein Conjugation: Structures, Chemistry, and Mechanism. *Chem Rev* 118, 889-918

58 Ayusawa, D.*, et al.* (1992) Complementation by a cloned human ubiquitin-activating enzyme E1 of the S-phase-arrested mouse FM3A cell mutant with thermolabile E1. *Cell Struct Funct* 17, 113-122

59 Zhu, H.*, et al.* (2004) Identification and characteristics of a novel E1 like gene nUBE1L in human testis. *Acta Biochim Biophys Sin (Shanghai)* 36, 227-234

60 Walden, H.*, et al.* (2003) The structure of the APPBP1-UBA3-NEDD8-ATP complex reveals the basis for selective ubiquitin-like protein activation by an E1. *Mol Cell* 12, 1427-1437

61 Jin, J.*, et al.* (2007) Dual E1 activation systems for ubiquitin differentially regulate E2 enzyme charging. *Nature* 447, 1135-1138

62 Hoege, C.*, et al.* (2002) RAD6-dependent DNA repair is linked to modification of PCNA by ubiquitin and SUMO. *Nature* 419, 135-141

63 Olsen, S.K.*, et al.* (2010) Active site remodelling accompanies thioester bond formation in the SUMO E1. *Nature* 463, 906-912

64 Lee, I. and Schindelin, H. (2008) Structural insights into E1-catalyzed ubiquitin activation and transfer to conjugating enzymes. *Cell* 134, 268-278

65 Olsen, S.K. and Lima, C.D. (2013) Structure of a ubiquitin E1-E2 complex: insights to E1-E2 thioester transfer. *Mol Cell* 49, 884-896

66 Haas, A.L.*, et al.* (1988) Functional diversity among putative E2 isozymes in the mechanism of ubiquitin-histone ligation. *J Biol Chem* 263, 13268-13275

67 Huang, D.T.*, et al.* (2007) Basis for a ubiquitin-like protein thioester switch toggling E1-E2 affinity. *Nature* 445, 394-398

68 Ye, Y. and Rape, M. (2009) Building ubiquitin chains: E2 enzymes at work. *Nat Rev Mol Cell Biol* 10, 755-764

69 Rodrigo-Brenni, M.C. and Morgan, D.O. (2007) Sequential E2s drive polyubiquitin chain assembly on APC targets. *Cell* 130, 127-139

70 Hofmann, R.M. and Pickart, C.M. (1999) Noncanonical MMS2-encoded ubiquitin-conjugating enzyme functions in assembly of novel polyubiquitin chains for DNA repair. *Cell* 96, 645-653

71 Petroski, M.D. and Deshaies, R.J. (2005) Mechanism of lysine 48-linked ubiquitin-chain synthesis by the cullin-RING ubiquitin-ligase complex SCF-Cdc34. *Cell* 123, 1107-1120

72 Kirkpatrick, D.S.*, et al.* (2006) Quantitative analysis of in vitro ubiquitinated cyclin B1 reveals complex chain topology. *Nat Cell Biol* 8, 700-710

73 Alpi, A.F.*, et al.* (2008) Mechanistic insight into site-restricted monoubiquitination of FANCD2 by Ube2t, FANCL, and FANCI. *Mol Cell* 32, 767-777

74 Petroski, M.D.*, et al.* (2007) Substrate modification with lysine 63-linked ubiquitin chains through the UBC13-UEV1A ubiquitin-conjugating enzyme. *J Biol Chem* 282, 29936-29945

75 Williamson, A.*, et al.* (2009) Identification of a physiological E2 module for the human anaphase-promoting complex. *Proc Natl Acad Sci U S A* 106, 18213-18218

76 Verma, R.*, et al.* (1997) SIC1 is ubiquitinated in vitro by a pathway that requires CDC4, CDC34, and cyclin/CDK activities. *Mol Biol Cell* 8, 1427-1437

77 Rape, M.*, et al.* (2006) The processivity of multiubiquitination by the APC determines the order of substrate degradation. *Cell* 124, 89-103

78 Eddins, M.J.*, et al.* (2006) Mms2-Ubc13 covalently bound to ubiquitin reveals the structural basis of linkage-specific polyubiquitin chain formation. *Nat Struct Mol Biol* 13, 915-920

79 Eletr, Z.M.*, et al.* (2005) E2 conjugating enzymes must disengage from their E1 enzymes before E3-dependent ubiquitin and ubiquitin-like transfer. *Nat Struct Mol Biol* 12, 933-934

80 Huang, D.T.*, et al.* (2005) Structural basis for recruitment of Ubc12 by an E2 binding domain in NEDD8's E1. *Mol Cell* 17, 341-350

81 Bencsath, K.P.*, et al.* (2002) Identification of a multifunctional binding site on Ubc9p required for Smt3p conjugation. *J Biol Chem* 277, 47938-47945

82 Brzovic, P.S.*, et al.* (2006) A UbcH5/ubiquitin noncovalent complex is required for processive BRCA1-directed ubiquitination. *Mol Cell* 21, 873-880

83 Zheng, N.*, et al.* (2000) Structure of a c-Cbl-UbcH7 complex: RING domain function in ubiquitin-protein ligases. *Cell* 102, 533-539

84 Christensen, D.E.*, et al.* (2007) E2-BRCA1 RING interactions dictate synthesis of mono- or specific polyubiquitin chain linkages. *Nat Struct Mol Biol* 14, 941-948

85 Wu, Y.*, et al.* (2014) Phosphorylation of p53 by TAF1 inactivates p53-dependent transcription in the DNA damage response. *Mol Cell* 53, 63-74

86 Jin, L.*, et al.* (2008) Mechanism of ubiquitin-chain formation by the human anaphase-promoting complex. *Cell* 133, 653-665

87 Sievers, Q.L.*, et al.* (2018) Genome-wide screen identifies cullin-RING ligase machinery required for lenalidomide-dependent CRL4(CRBN) activity. *Blood* 132, 1293-1303

88 Ravid, T. and Hochstrasser, M. (2007) Autoregulation of an E2 enzyme by ubiquitin-chain assembly on its catalytic residue. *Nat Cell Biol* 9, 422-427

89 Li, W.*, et al.* (2007) A ubiquitin ligase transfers preformed polyubiquitin chains from a conjugating enzyme to a substrate. *Nature* 446, 333-337

90 Petroski, M.D. and Deshaies, R.J. (2003) Context of multiubiquitin chain attachment influences the rate of Sic1 degradation. *Mol Cell* 11, 1435-1444

91 Das, R.*, et al.* (2009) Allosteric activation of E2-RING finger-mediated ubiquitylation by a structurally defined specific E2-binding region of gp78. *Mol Cell* 34, 674-685

92 Buetow, L.*, et al.* (2015) Activation of a primed RING E3-E2-ubiquitin complex by non-covalent ubiquitin. *Mol Cell* 58, 297-310

93 Baek, K.*, et al.* (2020) NEDD8 nucleates a multivalent cullin-RING-UBE2D ubiquitin ligation assembly. *Nature* 578, 461-466

94 Thrower, J.S.*, et al.* (2000) Recognition of the polyubiquitin proteolytic signal. *Embo j* 19, 94-102

95 Zheng, N.*, et al.* (2002) Structure of the Cul1-Rbx1-Skp1-F boxSkp2 SCF ubiquitin ligase complex. *Nature* 416, 703-709

96 Deshaies, R.J. and Joazeiro, C.A. (2009) RING domain E3 ubiquitin ligases. *Annu Rev Biochem* 78, 399-434

97 Li, W.*, et al.* (2008) Genome-wide and functional annotation of human E3 ubiquitin ligases identifies MULAN, a mitochondrial E3 that regulates the organelle's dynamics and signaling. *PLoS One* 3, e1487

98 Hashizume, R.*, et al.* (2001) The RING heterodimer BRCA1-BARD1 is a ubiquitin ligase inactivated by a breast cancer-derived mutation. *J Biol Chem* 276, 14537-14540

99 Wang, H.*, et al.* (2004) Role of histone H2A ubiquitination in Polycomb silencing. *Nature* 431, 873-878

100 Linares, L.K.*, et al.* (2003) HdmX stimulates Hdm2-mediated ubiquitination and degradation of p53. *Proc Natl Acad Sci U S A* 100, 12009-12014

101 Horn-Ghetko, D. and Schulman, B.A. (2022) New classes of E3 ligases illuminated by chemical probes. *Curr Opin Struct Biol* 73, 102341

102 Hopf, L.V.M.*, et al.* (2022) Structure of CRL7(FBXW8) reveals coupling with CUL1-RBX1/ROC1 for multi-cullin-RING E3-catalyzed ubiquitin ligation. *Nat Struct Mol Biol* 29, 854-862

103 Scheffner, M.*, et al.* (1995) Protein ubiquitination involving an E1-E2-E3 enzyme ubiquitin thioester cascade. *Nature* 373, 81-83

104 Zheng, N. and Shabek, N. (2017) Ubiquitin Ligases: Structure, Function, and Regulation. *Annu Rev Biochem* 86, 129-157

105 Freemont, P.S.*, et al.* (1991) A novel cysteine-rich sequence motif. *Cell* 64, 483-484

106 Hanson, I.M.*, et al.* (1991) New genes in the class II region of the human major histocompatibility complex. *Genomics* 10, 417-424

107 Joazeiro, C.A.*, et al.* (1999) The tyrosine kinase negative regulator c-Cbl as a RING-type, E2-dependent ubiquitin-protein ligase. *Science* 286, 309-312

108 Lorick, K.L.*, et al.* (1999) RING fingers mediate ubiquitin-conjugating enzyme (E2)-dependent ubiquitination. *Proc Natl Acad Sci U S A* 96, 11364-11369

109 Spratt, D.E.*, et al.* (2014) RBR E3 ubiquitin ligases: new structures, new insights, new questions. *Biochem J* 458, 421-437

110 Zheng, Q.*, et al.* (2016) Dysregulation of Ubiquitin-Proteasome System in Neurodegenerative Diseases. *Front Aging Neurosci* 8, 303

111 Reverter, D. and Lima, C.D. (2005) Insights into E3 ligase activity revealed by a SUMO-RanGAP1-Ubc9-Nup358 complex. *Nature* 435, 687-692

112 Scott, D.C.*, et al.* (2014) Structure of a RING E3 trapped in action reveals ligation mechanism for the ubiquitin-like protein NEDD8. *Cell* 157, 1671-1684

113 Plechanovová, A.*, et al.* (2012) Structure of a RING E3 ligase and ubiquitin-loaded E2 primed for catalysis. *Nature* 489, 115-120

114 Dou, H.*, et al.* (2012) BIRC7-E2 ubiquitin conjugate structure reveals the mechanism of ubiquitin transfer by a RING dimer. *Nat Struct Mol Biol* 19, 876-883

115 Wright, J.D.*, et al.* (2016) Secondary ubiquitin-RING docking enhances Arkadia and Ark2C E3 ligase activity. *Nat Struct Mol Biol* 23, 45-52

116 Pickart, C.M. (2001) Mechanisms underlying ubiquitination. *Annu Rev Biochem* 70, 503-533

117 Huang, L.*, et al.* (1999) Structure of an E6AP-UbcH7 complex: insights into ubiquitination by the E2-E3 enzyme cascade. *Science* 286, 1321-1326

118 Verdecia, M.A.*, et al.* (2003) Conformational flexibility underlies ubiquitin ligation mediated by the WWP1 HECT domain E3 ligase. *Mol Cell* 11, 249-259

119 Kamadurai, H.B.*, et al.* (2013) Mechanism of ubiquitin ligation and lysine prioritization by a HECT E3. *Elife* 2, e00828

120 Maspero, E.*, et al.* (2013) Structure of a ubiquitin-loaded HECT ligase reveals the molecular basis for catalytic priming. *Nat Struct Mol Biol* 20, 696-701

121 Wenzel, D.M.*, et al.* (2011) UBCH7 reactivity profile reveals parkin and HHARI to be RING/HECT hybrids. *Nature* 474, 105-108

122 Shimura, H.*, et al.* (2000) Familial Parkinson disease gene product, parkin, is a ubiquitin-protein ligase. *Nat Genet* 25, 302-305

123 Ravid, T. and Hochstrasser, M. (2008) Diversity of degradation signals in the ubiquitin-proteasome system. *Nat Rev Mol Cell Biol* 9, 679-690

124 Meszaros, B.*, et al.* (2017) Degrons in cancer. *Sci Signal* 10

125 Varshavsky, A. (2011) The N-end rule pathway and regulation by proteolysis. *Protein Sci* 20, 1298-1345

126 Koren, I.*, et al.* (2018) The Eukaryotic Proteome Is Shaped by E3 Ubiquitin Ligases Targeting C-Terminal Degrons. *Cell* 173, 1622-1635 e1614

127 Kanelis, V.*, et al.* (2001) Solution structure of a Nedd4 WW domain-ENaC peptide complex. *Nat Struct Biol* 8, 407-412

128 Muñoz-Escobar, J.*, et al.* (2015) The MLLE domain of the ubiquitin ligase UBR5 binds to its catalytic domain to regulate substrate binding. *J Biol Chem* 290, 22841-22850

129 Rosenbaum, J.C.*, et al.* (2011) Disorder targets misorder in nuclear quality control degradation: a disordered ubiquitin ligase directly recognizes its misfolded substrates. *Mol Cell* 41, 93-106

130 Wang, F., *et al.* (2013) A cotranslational ubiquitination pathway for quality control of misfolded proteins. *Mol Cell* 50, 368-378

131 Foresti, O., *et al.* (2014) Quality control of inner nuclear membrane proteins by the Asi complex. *Science* 346, 751-755

132 Sung, M.K., *et al.* (2016) A conserved quality-control pathway that mediates degradation of unassembled ribosomal proteins. *Elife* 5

133 Jaakkola, P., *et al.* (2001) Targeting of HIF-alpha to the von Hippel-Lindau ubiquitylation complex by O2-regulated prolyl hydroxylation. *Science* 292, 468-472

134 Ivan, M., *et al.* (2001) HIFalpha targeted for VHL-mediated destruction by proline hydroxylation: implications for O2 sensing. *Science* 292, 464-468

135 Hon, W.C., *et al.* (2002) Structural basis for the recognition of hydroxyproline in HIF-1 alpha by pVHL. *Nature* 417, 975-978

136 Min, J.H., *et al.* (2002) Structure of an HIF-1alpha -pVHL complex: hydroxyproline recognition in signaling. *Science* 296, 1886-1889

137 Winston, J.T., *et al.* (1999) The SCFbeta-TRCP-ubiquitin ligase complex associates specifically with phosphorylated destruction motifs in IkappaBalpha and beta-catenin and stimulates IkappaBalpha ubiquitination in vitro. *Genes Dev* 13, 270-283

138 Wu, G., *et al.* (2003) Structure of a beta-TrCP1-Skp1-beta-catenin complex: destruction motif binding and lysine specificity of the SCF(beta-TrCP1) ubiquitin ligase. *Mol Cell* 11, 1445-1456

139 Hao, B., *et al.* (2005) Structural basis of the Cks1-dependent recognition of p27(Kip1) by the SCF(Skp2) ubiquitin ligase. *Mol Cell* 20, 9-19

140 Sheaff, R.J., *et al.* (1997) Cyclin E-CDK2 is a regulator of p27Kip1. *Genes Dev* 11, 1464-1478

141 Tang, X., *et al.* (2007) Suprafacial orientation of the SCFCdc4 dimer accommodates multiple geometries for substrate ubiquitination. *Cell* 129, 1165-1176

142 Hao, B., *et al.* (2007) Structure of a Fbw7-Skp1-cyclin E complex: multisite-phosphorylated substrate recognition by SCF ubiquitin ligases. *Mol Cell* 26, 131-143

143 Orlicky, S.*, et al.* (2003) Structural basis for phosphodependent substrate selection and orientation by the SCFCdc4 ubiquitin ligase. *Cell* 112, 243-256

144 Manford, A.G.*, et al.* (2021) Structural basis and regulation of the reductive stress response. *Cell* 184, 5375-5390.e5316

145 Hwang, C.S.*, et al.* (2010) N-terminal acetylation of cellular proteins creates specific degradation signals. *Science* 327, 973-977

146 Timms, R.T.*, et al.* (2019) A glycine-specific N-degron pathway mediates the quality control of protein N-myristoylation. *Science* 365

147 Tan, X.*, et al.* (2007) Mechanism of auxin perception by the TIR1 ubiquitin ligase. *Nature* 446, 640-645

148 Sheard, L.B.*, et al.* (2010) Jasmonate perception by inositol-phosphate-potentiated COI1-JAZ co-receptor. *Nature* 468, 400-405

149 Murase, K.*, et al.* (2008) Gibberellin-induced DELLA recognition by the gibberellin receptor GID1. *Nature* 456, 459-463

150 Shimada, A.*, et al.* (2008) Structural basis for gibberellin recognition by its receptor GID1. *Nature* 456, 520-523

151 Alvarez, S.E.*, et al.* (2010) Sphingosine-1-phosphate is a missing cofactor for the E3 ubiquitin ligase TRAF2. *Nature* 465, 1084-1088

152 Dueber, E.C.*, et al.* (2011) Antagonists induce a conformational change in cIAP1 that promotes autoubiquitination. *Science* 334, 376-380

153 Turner, G.C.*, et al.* (2000) Peptides accelerate their uptake by activating a ubiquitin-dependent proteolytic pathway. *Nature* 405, 579-583

154 Fischer, E.S.*, et al.* (2014) Structure of the DDB1-CRBN E3 ubiquitin ligase in complex with thalidomide. *Nature* 512, 49-53

155 Kronke, J.*, et al.* (2014) Lenalidomide causes selective degradation of IKZF1 and IKZF3 in multiple myeloma cells. *Science* 343, 301-305

156 Lu, G.*, et al.* (2014) The myeloma drug lenalidomide promotes the cereblon-dependent destruction of Ikaros proteins. *Science* 343, 305-309

157 Kronke, J.*, et al.* (2015) Lenalidomide induces ubiquitination and degradation of CK1alpha in del(5q) MDS. *Nature* 523, 183-188

158 Petzold, G.*, et al.* (2016) Structural basis of lenalidomide-induced CK1alpha degradation by the CRL4(CRBN) ubiquitin ligase. *Nature* 532, 127-130

159 An, J.*, et al.* (2017) pSILAC mass spectrometry reveals ZFP91 as IMiD-dependent substrate of the CRL4(CRBN) ubiquitin ligase. *Nat Commun* 8, 15398

160 Han, T.*, et al.* (2017) Anticancer sulfonamides target splicing by inducing RBM39 degradation via recruitment to DCAF15. *Science* 356

161 Słabicki, M.*, et al.* (2020) The CDK inhibitor CR8 acts as a molecular glue degrader that depletes cyclin K. *Nature* 585, 293-297

162 Monte, I.*, et al.* (2014) Rational design of a ligand-based antagonist of jasmonate perception. *Nat Chem Biol* 10, 671-676

163 Aghajan, M.*, et al.* (2010) Chemical genetics screen for enhancers of rapamycin identifies a specific inhibitor of an SCF family E3 ubiquitin ligase. *Nat Biotechnol* 28, 738-742

164 Orlicky, S.*, et al.* (2010) An allosteric inhibitor of substrate recognition by the SCF(Cdc4) ubiquitin ligase. *Nat Biotechnol* 28, 733-737

165 Chan, C.H.*, et al.* (2013) Pharmacological inactivation of Skp2 SCF ubiquitin ligase restricts cancer stem cell traits and cancer progression. *Cell* 154, 556-568

166 Wu, L.*, et al.* (2012) Specific small molecule inhibitors of Skp2-mediated p27 degradation. *Chem Biol* 19, 1515-1524

167 Lu, J.*, et al.* (2015) Hijacking the E3 Ubiquitin Ligase Cereblon to Efficiently Target BRD4. *Chem Biol* 22, 755-763

168 Matyskiela, M.E.*, et al.* (2016) A novel cereblon modulator recruits GSPT1 to the CRL4(CRBN) ubiquitin ligase. *Nature* 535, 252-257

169 Winter, G.E.*, et al.* (2015) Phthalimide conjugation as a strategy for in vivo target protein degradation. *Science* 348, 1376-1381

170 Diehl, C.J. and Ciulli, A. (2022) Discovery of small molecule ligands for the von Hippel-Lindau (VHL) E3 ligase and their use as inhibitors and PROTAC degraders. *Chem Soc Rev*

171 Yen, H.C. and Elledge, S.J. (2008) Identification of SCF ubiquitin ligase substrates by global protein stability profiling. *Science* 322, 923-929

172 Emanuele, M.J.*, et al.* (2011) Global identification of modular cullin-RING ligase substrates. *Cell* 147, 459-474

173 Lin, H.C.*, et al.* (2015) SELENOPROTEINS. CRL2 aids elimination of truncated selenoproteins produced by failed UGA/Sec decoding. *Science* 349, 91-95

174 Scott, D.C.*, et al.* (2016) Two Distinct Types of E3 Ligases Work in Unison to Regulate Substrate Ubiquitylation. *Cell* 166, 1198-1214.e1124

175 Horn-Ghetko, D.*, et al.* (2021) Ubiquitin ligation to F-box protein targets by SCF-RBR E3-E3 super-assembly. *Nature* 590, 671-676

176 Mohamed, W.I.*, et al.* (2021) The CRL4(DCAF1) cullin-RING ubiquitin ligase is activated following a switch in oligomerization state. *Embo j* 40, e108008

177 DaRosa, P.A.*, et al.* (2015) Allosteric activation of the RNF146 ubiquitin ligase by a poly(ADP-ribosyl)ation signal. *Nature* 517, 223-226

178 Zhang, Y.*, et al.* (2011) RNF146 is a poly(ADP-ribose)-directed E3 ligase that regulates axin degradation and Wnt signalling. *Nat Cell Biol* 13, 623-629

179 Wang, H.*, et al.* (2020) FBXL5 Regulates IRP2 Stability in Iron Homeostasis via an Oxygen-Responsive [2Fe2S] Cluster. *Mol Cell* 78, 31-41.e35

180 Williamson, A.*, et al.* (2011) Regulation of ubiquitin chain initiation to control the timing of substrate degradation. *Mol Cell* 42, 744-757

181 Wauer, T.*, et al.* (2015) Mechanism of phospho-ubiquitin-induced PARKIN activation. *Nature* 524, 370-374

182 Dou, H.*, et al.* (2012) Structural basis for autoinhibition and phosphorylation-dependent activation of c-Cbl. *Nat Struct Mol Biol* 19, 184-192

183 Debonneville, C.*, et al.* (2001) Phosphorylation of Nedd4-2 by Sgk1 regulates epithelial Na(+) channel cell surface expression. *Embo j* 20, 7052-7059

184 Khosravi, R., *et al.* (1999) Rapid ATM-dependent phosphorylation of MDM2 precedes p53 accumulation in response to DNA damage. *Proc Natl Acad Sci U S A* 96, 14973-14977

185 Fujimitsu, K., *et al.* (2016) Cyclin-dependent kinase 1-dependent activation of APC/C ubiquitin ligase. *Science* 352, 1121-1124

186 Zhang, S., *et al.* (2016) Molecular mechanism of APC/C activation by mitotic phosphorylation. *Nature* 533, 260-264

187 Lamothe, B., *et al.* (2007) Site-specific Lys-63-linked tumor necrosis factor receptor-associated factor 6 auto-ubiquitination is a critical determinant of I kappa B kinase activation. *J Biol Chem* 282, 4102-4112

188 Ben-Saadon, R., *et al.* (2006) The polycomb protein Ring1B generates self atypical mixed ubiquitin chains required for its in vitro histone H2A ligase activity. *Mol Cell* 24, 701-711

189 Mallery, D.L., *et al.* (2002) Activation of the E3 ligase function of the BRCA1/BARD1 complex by polyubiquitin chains. *Embo j* 21, 6755-6762

190 Fang, S., *et al.* (2000) Mdm2 is a RING finger-dependent ubiquitin protein ligase for itself and p53. *J Biol Chem* 275, 8945-8951

191 de Bie, P. and Ciechanover, A. (2011) Ubiquitination of E3 ligases: self-regulation of the ubiquitin system via proteolytic and non-proteolytic mechanisms. *Cell Death Differ* 18, 1393-1402

192 Li, Y., *et al.* (2004) Stability of homologue of Slimb F-box protein is regulated by availability of its substrate. *J Biol Chem* 279, 11074-11080

193 Zhou, P. and Howley, P.M. (1998) Ubiquitination and degradation of the substrate recognition subunits of SCF ubiquitin-protein ligases. *Mol Cell* 2, 571-580

194 Bashir, T., *et al.* (2004) Control of the SCF(Skp2-Cks1) ubiquitin ligase by the APC/C(Cdh1) ubiquitin ligase. *Nature* 428, 190-193

195 Wei, W., *et al.* (2004) Degradation of the SCF component Skp2 in cell-cycle phase G1 by the anaphase-promoting complex. *Nature* 428, 194-198

196 Hori, T., *et al.* (1999) Covalent modification of all members of human cullin family proteins by NEDD8. *Oncogene* 18, 6829-6834

197 Soucy, T.A., *et al.* (2009) An inhibitor of NEDD8-activating enzyme as a new approach to treat cancer. *Nature* 458, 732-736

198 Petroski, M.D. and Deshaies, R.J. (2005) Function and regulation of cullin-RING ubiquitin ligases. *Nat Rev Mol Cell Biol* 6, 9-20

199 Feldman, R.M., *et al.* (1997) A complex of Cdc4p, Skp1p, and Cdc53p/cullin catalyzes ubiquitination of the phosphorylated CDK inhibitor Sic1p. *Cell* 91, 221-230

200 Skowyra, D., *et al.* (1997) F-box proteins are receptors that recruit phosphorylated substrates to the SCF ubiquitin-ligase complex. *Cell* 91, 209-219

201 Angers, S., *et al.* (2006) Molecular architecture and assembly of the DDB1-CUL4A ubiquitin ligase machinery. *Nature* 443, 590-593

202 Fischer, E.S., *et al.* (2011) The molecular basis of CRL4DDB2/CSA ubiquitin ligase architecture, targeting, and activation. *Cell* 147, 1024-1039

203 Lonergan, K.M., *et al.* (1998) Regulation of hypoxia-inducible mRNAs by the von Hippel-Lindau tumor suppressor protein requires binding to complexes containing elongins B/C and Cul2. *Mol Cell Biol* 18, 732-741

204 Kipreos, E.T., *et al.* (1996) cul-1 is required for cell cycle exit in C. elegans and identifies a novel gene family. *Cell* 85, 829-839

205 Nikolaev, A.Y., *et al.* (2003) Parc: a cytoplasmic anchor for p53. *Cell* 112, 29-40

206 Arai, T., *et al.* (2003) Targeted disruption of p185/Cul7 gene results in abnormal vascular morphogenesis. *Proc Natl Acad Sci U S A* 100, 9855-9860

207 Zachariae, W., *et al.* (1998) Mass spectrometric analysis of the anaphase-promoting complex from yeast: identification of a subunit related to cullins. *Science* 279, 1216-1219

208 Yu, H., *et al.* (1998) Identification of a cullin homology region in a subunit of the anaphase-promoting complex. *Science* 279, 1219-1222

209 Kamura, T., *et al.* (1999) Rbx1, a component of the VHL tumor suppressor complex and SCF ubiquitin ligase. *Science* 284, 657-661

210 Ohta, T.*, et al.* (1999) ROC1, a homolog of APC11, represents a family of cullin partners with an associated ubiquitin ligase activity. *Mol Cell* 3, 535-541

211 Tan, P.*, et al.* (1999) Recruitment of a ROC1-CUL1 ubiquitin ligase by Skp1 and HOS to catalyze the ubiquitination of I kappa B alpha. *Mol Cell* 3, 527-533

212 Seol, J.H.*, et al.* (1999) Cdc53/cullin and the essential Hrt1 RING-H2 subunit of SCF define a ubiquitin ligase module that activates the E2 enzyme Cdc34. *Genes Dev* 13, 1614-1626

213 Skowyra, D.*, et al.* (1999) Reconstitution of G1 cyclin ubiquitination with complexes containing SCFGrr1 and Rbx1. *Science* 284, 662-665

214 Swaroop, M.*, et al.* (1999) Expression, purification, and biochemical characterization of SAG, a ring finger redox-sensitive protein. *Free Radic Biol Med* 27, 193-202

215 Duan, H.*, et al.* (1999) SAG, a novel zinc RING finger protein that protects cells from apoptosis induced by redox agents. *Mol Cell Biol* 19, 3145-3155

216 Bai, C.*, et al.* (1996) SKP1 connects cell cycle regulators to the ubiquitin proteolysis machinery through a novel motif, the F-box. *Cell* 86, 263-274

217 Xu, L.*, et al.* (2003) BTB proteins are substrate-specific adaptors in an SCF-like modular ubiquitin ligase containing CUL-3. *Nature* 425, 316-321

218 Furukawa, M.*, et al.* (2003) Targeting of protein ubiquitination by BTB-Cullin 3-Roc1 ubiquitin ligases. *Nat Cell Biol* 5, 1001-1007

219 Kleiger, G.*, et al.* (2009) Rapid E2-E3 assembly and disassembly enable processive ubiquitylation of cullin-RING ubiquitin ligase substrates. *Cell* 139, 957-968

220 Ohh, M.*, et al.* (2002) An intact NEDD8 pathway is required for Cullin-dependent ubiquitylation in mammalian cells. *EMBO Rep* 3, 177-182

221 Saha, A. and Deshaies, R.J. (2008) Multimodal activation of the ubiquitin ligase SCF by Nedd8 conjugation. *Mol Cell* 32, 21-31

222 Yamoah, K.*, et al.* (2008) Autoinhibitory regulation of SCF-mediated ubiquitination by human cullin 1's C-terminal tail. *Proc Natl Acad Sci U S A* 105, 12230-12235

223 Liu, J.*, et al.* (2002) NEDD8 modification of CUL1 dissociates p120(CAND1), an inhibitor of CUL1-SKP1 binding and SCF ligases. *Mol Cell* 10, 1511-1518

224 Zheng, J.*, et al.* (2002) CAND1 binds to unneddylated CUL1 and regulates the formation of SCF ubiquitin E3 ligase complex. *Mol Cell* 10, 1519-1526

225 Goldenberg, S.J.*, et al.* (2004) Structure of the Cand1-Cul1-Roc1 complex reveals regulatory mechanisms for the assembly of the multisubunit cullin-dependent ubiquitin ligases. *Cell* 119, 517-528

226 Pierce, N.W.*, et al.* (2013) Cand1 promotes assembly of new SCF complexes through dynamic exchange of F box proteins. *Cell* 153, 206-215

227 Lyapina, S.*, et al.* (2001) Promotion of NEDD-CUL1 conjugate cleavage by COP9 signalosome. *Science* 292, 1382-1385

228 Schwechheimer, C.*, et al.* (2001) Interactions of the COP9 signalosome with the E3 ubiquitin ligase SCFTIRI in mediating auxin response. *Science* 292, 1379-1382

229 Cavadini, S.*, et al.* (2016) Cullin-RING ubiquitin E3 ligase regulation by the COP9 signalosome. *Nature* 531, 598-603

230 Lingaraju, G.M.*, et al.* (2014) Crystal structure of the human COP9 signalosome. *Nature* 512, 161-165

231 Emberley, E.D.*, et al.* (2012) Deconjugation of Nedd8 from Cul1 is directly regulated by Skp1-F-box and substrate, and the COP9 signalosome inhibits deneddylated SCF by a noncatalytic mechanism. *J Biol Chem* 287, 29679-29689

232 Groisman, R.*, et al.* (2003) The ubiquitin ligase activity in the DDB2 and CSA complexes is differentially regulated by the COP9 signalosome in response to DNA damage. *Cell* 113, 357-367

233 Chew, E.H. and Hagen, T. (2007) Substrate-mediated regulation of cullin neddylation. *J Biol Chem* 282, 17032-17040

234 Schulman, B.A.*, et al.* (2000) Insights into SCF ubiquitin ligases from the structure of the Skp1-Skp2 complex. *Nature* 408, 381-386

235 Cardote, T.A.F.*, et al.* (2017) Crystal Structure of the Cul2-Rbx1-EloBC-VHL Ubiquitin Ligase Complex. *Structure* 25, 901-911.e903

236 Stebbins, C.E., *et al.* (1999) Structure of the VHL-ElonginC-ElonginB complex: implications for VHL tumor suppressor function. *Science* 284, 455-461

237 Mukhopadhyay, D. and Riezman, H. (2007) Proteasome-independent functions of ubiquitin in endocytosis and signaling. *Science* 315, 201-205

238 Kim, I., *et al.* (2004) Multiple interactions of rad23 suggest a mechanism for ubiquitylated substrate delivery important in proteolysis. *Mol Biol Cell* 15, 3357-3365

239 Verma, R., *et al.* (2004) Multiubiquitin chain receptors define a layer of substrate selectivity in the ubiquitin-proteasome system. *Cell* 118, 99-110

240 Richly, H., *et al.* (2005) A series of ubiquitin binding factors connects CDC48/p97 to substrate multiubiquitylation and proteasomal targeting. *Cell* 120, 73-84

241 Livneh, I., *et al.* (2016) The life cycle of the 26S proteasome: from birth, through regulation and function, and onto its death. *Cell Res* 26, 869-885

242 Cromm, P.M. and Crews, C.M. (2017) The Proteasome in Modern Drug Discovery: Second Life of a Highly Valuable Drug Target. *ACS Cent Sci* 3, 830-838

243 Dou, Q.P. and Goldfarb, R.H. (2002) Bortezomib (millennium pharmaceuticals). *IDrugs* 5, 828-834

244 Roelofs, J., *et al.* (2009) Chaperone-mediated pathway of proteasome regulatory particle assembly. *Nature* 459, 861-865

245 Funakoshi, M., *et al.* (2009) Multiple assembly chaperones govern biogenesis of the proteasome regulatory particle base. *Cell* 137, 887-899

246 Kaneko, T., *et al.* (2009) Assembly pathway of the Mammalian proteasome base subcomplex is mediated by multiple specific chaperones. *Cell* 137, 914-925

247 Saeki, Y., *et al.* (2009) Multiple proteasome-interacting proteins assist the assembly of the yeast 19S regulatory particle. *Cell* 137, 900-913

248 Jung, T. and Grune, T. (2013) The proteasome and the degradation of oxidized proteins: Part I-structure of proteasomes. *Redox Biol* 1, 178-182

249 Husnjak, K.*, et al.* (2008) Proteasome subunit Rpn13 is a novel ubiquitin receptor. *Nature* 453, 481-488

250 Shi, Y.*, et al.* (2016) Rpn1 provides adjacent receptor sites for substrate binding and deubiquitination by the proteasome. *Science* 351

251 Fu, H.*, et al.* (1998) Multiubiquitin chain binding and protein degradation are mediated by distinct domains within the 26 S proteasome subunit Mcb1. *J Biol Chem* 273, 1970-1981

252 Verma, R.*, et al.* (2002) Role of Rpn11 metalloprotease in deubiquitination and degradation by the 26S proteasome. *Science* 298, 611-615

253 Yao, T. and Cohen, R.E. (2002) A cryptic protease couples deubiquitination and degradation by the proteasome. *Nature* 419, 403-407

254 Sahu, I.*, et al.* (2021) The 20S as a stand-alone proteasome in cells can degrade the ubiquitin tag. *Nat Commun* 12, 6173

255 Saric, T.*, et al.* (2004) Pathway for degradation of peptides generated by proteasomes: a key role for thimet oligopeptidase and other metallopeptidases. *J Biol Chem* 279, 46723-46732

256 Hadari, T.*, et al.* (1992) A ubiquitin C-terminal isopeptidase that acts on polyubiquitin chains. Role in protein degradation. *J Biol Chem* 267, 719-727

257 Amerik, A.*, et al.* (1997) In vivo disassembly of free polyubiquitin chains by yeast Ubp14 modulates rates of protein degradation by the proteasome. *Embo j* 16, 4826-4838

258 Huttlin, E.L.*, et al.* (2017) Architecture of the human interactome defines protein communities and disease networks. *Nature* 545, 505-509

259 Sydow, J.F. and Cramer, P. (2009) RNA polymerase fidelity and transcriptional proofreading. *Curr Opin Struct Biol* 19, 732-739

260 Nicholson, P. and Muhlemann, O. (2010) Cutting the nonsense: the degradation of PTC-containing mRNAs. *Biochem Soc Trans* 38, 1615-1620

261 van Hoof, A.*, et al.* (2002) Exosome-mediated recognition and degradation of mRNAs lacking a termination codon. *Science* 295, 2262-2264

262 Frischmeyer, P.A.*, et al.* (2002) An mRNA surveillance mechanism that eliminates transcripts lacking termination codons. *Science* 295, 2258-2261

263 Harigaya, Y. and Parker, R. (2010) No-go decay: a quality control mechanism for RNA in translation. *Wiley Interdiscip Rev RNA* 1, 132-141

264 Meaux, S. and Van Hoof, A. (2006) Yeast transcripts cleaved by an internal ribozyme provide new insight into the role of the cap and poly(A) tail in translation and mRNA decay. *RNA* 12, 1323-1337

265 Prabhakar, A.*, et al.* (2017) Dynamic basis of fidelity and speed in translation: Coordinated multistep mechanisms of elongation and termination. *Protein Sci* 26, 1352-1362

266 Brandman, O.*, et al.* (2012) A ribosome-bound quality control complex triggers degradation of nascent peptides and signals translation stress. *Cell* 151, 1042-1054

267 Wang, F.*, et al.* (2015) Ubiquitination of newly synthesized proteins at the ribosome. *Biochimie* 114, 127-133

268 Bengtson, M.H. and Joazeiro, C.A. (2010) Role of a ribosome-associated E3 ubiquitin ligase in protein quality control. *Nature* 467, 470-473

269 Shao, S.*, et al.* (2013) Listerin-dependent nascent protein ubiquitination relies on ribosome subunit dissociation. *Mol Cell* 50, 637-648

270 Arribere, J.A.*, et al.* (2016) Translation readthrough mitigation. *Nature* 534, 719-723

271 Inada, T. and Aiba, H. (2005) Translation of aberrant mRNAs lacking a termination codon or with a shortened 3'-UTR is repressed after initiation in yeast. *EMBO J* 24, 1584-1595

272 Dimitrova, L.N.*, et al.* (2009) Nascent peptide-dependent translation arrest leads to Not4p-mediated protein degradation by the proteasome. *J Biol Chem* 284, 10343-10352

273 Ito-Harashima, S.*, et al.* (2007) Translation of the poly(A) tail plays crucial roles in nonstop mRNA surveillance via translation repression and protein destabilization by proteasome in yeast. *Genes Dev* 21, 519-524

274 Sundaramoorthy, E.*, et al.* (2017) ZNF598 and RACK1 Regulate Mammalian Ribosome-Associated Quality Control Function by Mediating Regulatory 40S Ribosomal Ubiquitylation. *Mol Cell* 65, 751-760 e754

275 Garzia, A.*, et al.* (2017) The E3 ubiquitin ligase and RNA-binding protein ZNF598 orchestrates ribosome quality control of premature polyadenylated mRNAs. *Nat Commun* 8, 16056

276 Juszkiewicz, S.*, et al.* (2020) The ASC-1 Complex Disassembles Collided Ribosomes. *Mol Cell* 79, 603-614 e608

277 Verma, R.*, et al.* (2013) Cdc48/p97 promotes degradation of aberrant nascent polypeptides bound to the ribosome. *Elife* 2, e00308

278 Kuroha, K.*, et al.* (2009) Upf1 stimulates degradation of the product derived from aberrant messenger RNA containing a specific nonsense mutation by the proteasome. *EMBO Rep* 10, 1265-1271

279 Heck, J.W.*, et al.* (2010) Cytoplasmic protein quality control degradation mediated by parallel actions of the E3 ubiquitin ligases Ubr1 and San1. *Proc Natl Acad Sci U S A* 107, 1106-1111

280 Duttler, S.*, et al.* (2013) Principles of cotranslational ubiquitination and quality control at the ribosome. *Mol Cell* 50, 379-393

281 Balchin, D.*, et al.* (2016) In vivo aspects of protein folding and quality control. *Science* 353, aac4354

282 Ellis, R.J. (2007) Protein misassembly: macromolecular crowding and molecular chaperones. *Adv Exp Med Biol* 594, 1-13

283 Hipp, M.S.*, et al.* (2014) Proteostasis impairment in protein-misfolding and -aggregation diseases. *Trends Cell Biol* 24, 506-514

284 Nillegoda, N.B.*, et al.* (2010) Ubr1 and Ubr2 function in a quality control pathway for degradation of unfolded cytosolic proteins. *Mol Biol Cell* 21, 2102-2116

285 Klinge, S. and Woolford, J.L., Jr. (2019) Ribosome assembly coming into focus. *Nat Rev Mol Cell Biol* 20, 116-131

286 Li, G.W.*, et al.* (2014) Quantifying absolute protein synthesis rates reveals principles underlying allocation of cellular resources. *Cell* 157, 624-635

287 Burkhardt, D.H.*, et al.* (2017) Operon mRNAs are organized into ORF-centric structures that predict translation efficiency. *Elife* 6

288 Chen, J.*, et al.* (2020) Pervasive functional translation of noncanonical human open reading frames. *Science* 367, 1140-1146

289 Zhang, X. and Smith, T.F. (1998) Yeast "operons". *Microb Comp Genomics* 3, 133-140

290 Pizzinga, M.*, et al.* (2019) Translation factor mRNA granules direct protein synthetic capacity to regions of polarized growth. *J Cell Biol* 218, 1564-1581

291 Nair, R.R.*, et al.* (2021) Multiplexed mRNA assembly into ribonucleoprotein particles plays an operon-like role in the control of yeast cell physiology. *Elife* 10

292 Shiber, A.*, et al.* (2018) Cotranslational assembly of protein complexes in eukaryotes revealed by ribosome profiling. *Nature* 561, 268-272

293 Bertolini, M.*, et al.* (2021) Interactions between nascent proteins translated by adjacent ribosomes drive homomer assembly. *Science* 371, 57-64

294 Shieh, Y.W.*, et al.* (2015) Operon structure and cotranslational subunit association direct protein assembly in bacteria. *Science* 350, 678-680

295 Hauser, T.*, et al.* (2015) Role of auxiliary proteins in Rubisco biogenesis and function. *Nat Plants* 1, 15065

296 Chari, A. and Fischer, U. (2010) Cellular strategies for the assembly of molecular machines. *Trends Biochem Sci* 35, 676-683

297 McShane, E.*, et al.* (2016) Kinetic Analysis of Protein Stability Reveals Age-Dependent Degradation. *Cell* 167, 803-815 e821

298 Mena, E.L.*, et al.* (2018) Dimerization quality control ensures neuronal development and survival. *Science* 362

299 Harper, J.W. and Bennett, E.J. (2016) Proteome complexity and the forces that drive proteome imbalance. *Nature* 537, 328-338

300 Ori, A.*, et al.* (2016) Spatiotemporal variation of mammalian protein complex stoichiometries. *Genome Biol* 17, 47

301 Warner, J.R. (1977) In the absence of ribosomal RNA synthesis, the ribosomal proteins of HeLa cells are synthesized normally and degraded rapidly. *J Mol Biol* 115, 315-333

302 Blikstad, I.*, et al.* (1983) Synthesis and assembly of spectrin during avian erythropoiesis: stoichiometric assembly but unequal synthesis of alpha and beta spectrin. *Cell* 32, 1081-1091

303 Steinberg, R.A. and Agard, D.A. (1981) Turnover of regulatory subunit of cyclic AMP-dependent protein kinase in S49 mouse lymphoma cells. Regulation by catalytic subunit and analogs of cyclic AMP. *J Biol Chem* 256, 10731-10734

304 Warner, J.R.*, et al.* (1985) Saccharomyces cerevisiae coordinates accumulation of yeast ribosomal proteins by modulating mRNA splicing, translational initiation, and protein turnover. *Mol Cell Biol* 5, 1512-1521

305 Jones, C. and Holland, I.B. (1985) Role of the SulB (FtsZ) protein in division inhibition during the SOS response in Escherichia coli: FtsZ stabilizes the inhibitor SulA in maxicells. *Proc Natl Acad Sci U S A* 82, 6045-6049

306 Flückiger, J. and Christen, P. (1988) Degradation of the precursor of mitochondrial aspartate aminotransferase in chicken embryo fibroblasts. *J Biol Chem* 263, 4131-4138

307 Maicas, E.*, et al.* (1988) The accumulation of three yeast ribosomal proteins under conditions of excess mRNA is determined primarily by fast protein decay. *Mol Cell Biol* 8, 169-175

308 Tsay, Y.F.*, et al.* (1988) Ribosomal protein synthesis is not regulated at the translational level in Saccharomyces cerevisiae: balanced accumulation of ribosomal proteins L16 and rp59 is mediated by turnover of excess protein. *Genes Dev* 2, 664-676

309 Schwanhausser, B.*, et al.* (2011) Global quantification of mammalian gene expression control. *Nature* 473, 337-342

310 Schubert, U.*, et al.* (2000) Rapid degradation of a large fraction of newly synthesized proteins by proteasomes. *Nature* 404, 770-774

311 Vabulas, R.M. and Hartl, F.U. (2005) Protein synthesis upon acute nutrient restriction relies on proteasome function. *Science* 310, 1960-1963

312 Kim, W.*, et al.* (2011) Systematic and quantitative assessment of the ubiquitin-modified proteome. *Mol Cell* 44, 325-340

313 Pla-Prats, C. and Thoma, N.H. (2022) Quality control of protein complex assembly by the ubiquitin-proteasome system. *Trends Cell Biol*

314 Padovani, C.*, et al.* (2022) Quality control of protein complex composition. *Mol Cell* 82, 1439-1450

315 Yanagitani, K., *et al.* (2017) UBE2O is a quality control factor for orphans of multiprotein complexes. *Science* 357, 472-475

316 Nguyen, A.T., *et al.* (2017) UBE2O remodels the proteome during terminal erythroid differentiation. *Science* 357

317 Shemorry, A., *et al.* (2013) Control of protein quality and stoichiometries by N-terminal acetylation and the N-end rule pathway. *Mol Cell* 50, 540-551

318 Zeng, Z., *et al.* (2010) Structural basis of selective ubiquitination of TRF1 by SCFFbx4. *Dev Cell* 18, 214-225

319 Zavodszky, E., *et al.* (2021) Identification of a quality-control factor that monitors failures during proteasome assembly. *Science* 373, 998-1004

320 Mena, E.L., *et al.* (2020) Structural basis for dimerization quality control. *Nature* 586, 452-456

321 Natarajan, N., *et al.* (2020) Quality Control of Protein Complex Assembly by a Transmembrane Recognition Factor. *Mol Cell* 77, 108-119 e109

322 Li, S., *et al.* (2008) Novel centrosome protein, TCC52, is a cancer-testis antigen. *Cancer Sci* 99, 2274-2279

323 Jin, J., *et al.* (2006) A family of diverse Cul4-Ddb1-interacting proteins includes Cdt2, which is required for S phase destruction of the replication factor Cdt1. *Mol Cell* 23, 709-721

324 Fukumoto, Y., *et al.* (2008) Schizosaccharomyces pombe Ddb1 recruits substrate-specific adaptor proteins through a novel protein motif, the DDB-box. *Mol Cell Biol* 28, 6746-6756

325 Higa, L.A., *et al.* (2006) CUL4-DDB1 ubiquitin ligase interacts with multiple WD40-repeat proteins and regulates histone methylation. *Nat Cell Biol* 8, 1277-1283

326 He, Y.J., *et al.* (2006) DDB1 functions as a linker to recruit receptor WD40 proteins to CUL4-ROC1 ubiquitin ligases. *Genes Dev* 20, 2949-2954

327 Uhlen, M., *et al.* (2015) Proteomics. Tissue-based map of the human proteome. *Science* 347, 1260419

328 Patron, L.A., *et al.* (2019) Cul4 ubiquitin ligase cofactor DCAF12 promotes neurotransmitter release and homeostatic plasticity. *J Cell Biol* 218, 993-1010

329 Hwangbo, D.S.*, et al.* (2016) Control of apoptosis by Drosophila DCAF12. *Dev Biol* 413, 50-59

330 Jiao, D.*, et al.* (2022) DCAF12 promotes apoptosis and inhibits NF-kappaB activation by acting as an endogenous antagonist of IAPs. *Oncogene* 41, 3000-3010

331 Cho, Y.S.*, et al.* (2020) CDK7 regulates organ size and tumor growth by safeguarding the Hippo pathway effector Yki/Yap/Taz in the nucleus. *Genes Dev* 34, 53-71

332 Lidak, T.*, et al.* (2021) CRL4-DCAF12 Ubiquitin Ligase Controls MOV10 RNA Helicase during Spermatogenesis and T Cell Activation. *Int J Mol Sci* 22

333 Ravichandran, R.*, et al.* (2019) Regulation of MAGE-A3/6 by the CRL4-DCAF12 ubiquitin ligase and nutrient availability. *EMBO Rep* 20, e47352

334 Sherpa, D.*, et al.* (2022) How the ends signal the end: Regulation by E3 ubiquitin ligases recognizing protein termini. *Mol Cell* 82, 1424-1438

335 Yan, X.*, et al.* (2021) Molecular basis for ubiquitin ligase CRL2(FEM1C)-mediated recognition of C-degron. *Nat Chem Biol* 17, 263-271

336 Chen, X.*, et al.* (2021) Molecular basis for arginine C-terminal degron recognition by Cul2(FEM1) E3 ligase. *Nat Chem Biol* 17, 254-262

337 Rusnac, D.V.*, et al.* (2018) Recognition of the Diglycine C-End Degron by CRL2(KLHDC2) Ubiquitin Ligase. *Mol Cell* 72, 813-822 e814

338 Zhao, S.*, et al.* (2021) Structural insights into SMCR8 C-degron recognition by FEM1B. *Biochem Biophys Res Commun* 557, 236-239

339 Lin, H.C.*, et al.* (2018) C-Terminal End-Directed Protein Elimination by CRL2 Ubiquitin Ligases. *Mol Cell* 70, 602-613 e603

340 Cheng, M.Y.*, et al.* (1989) Mitochondrial heat-shock protein hsp60 is essential for assembly of proteins imported into yeast mitochondria. *Nature* 337, 620-625

341 Hemmingsen, S.M.*, et al.* (1988) Homologous plant and bacterial proteins chaperone oligomeric protein assembly. *Nature* 333, 330-334

342 Skjaerven, L.*, et al.* (2015) Dynamics, flexibility, and allostery in molecular chaperonins. *FEBS Lett* 589, 2522-2532

343 Hayer-Hartl, M., *et al.* (2016) The GroEL-GroES Chaperonin Machine: A Nano-Cage for Protein Folding. *Trends Biochem Sci* 41, 62-76

344 Clare, D.K., *et al.* (2012) ATP-triggered conformational changes delineate substrate-binding and -folding mechanics of the GroEL chaperonin. *Cell* 149, 113-123

345 Kusmierczyk, A.R. and Martin, J. (2003) Nucleotide-dependent protein folding in the type II chaperonin from the mesophilic archaeon Methanococcus maripaludis. *Biochem J* 371, 669-673

346 Lopez, T., *et al.* (2015) The Mechanism and Function of Group II Chaperonins. *J Mol Biol* 427, 2919-2930

347 Douglas, N.R., *et al.* (2011) Dual action of ATP hydrolysis couples lid closure to substrate release into the group II chaperonin chamber. *Cell* 144, 240-252

348 Rivenzon-Segal, D., *et al.* (2005) Sequential ATP-induced allosteric transitions of the cytoplasmic chaperonin containing TCP-1 revealed by EM analysis. *Nat Struct Mol Biol* 12, 233-237

349 Gestaut, D., *et al.* (2022) Structural visualization of the tubulin folding pathway directed by human chaperonin TRiC/CCT. *Cell* 185, 4770-4787 e4720

350 Leitner, A., *et al.* (2012) The molecular architecture of the eukaryotic chaperonin TRiC/CCT. *Structure* 20, 814-825

351 Pereira, J.H., *et al.* (2010) Crystal structures of a group II chaperonin reveal the open and closed states associated with the protein folding cycle. *J Biol Chem* 285, 27958-27966

352 Jin, M., *et al.* (2019) TRiC/CCT Chaperonin: Structure and Function. *Subcell Biochem* 93, 625-654

353 Geissler, S., *et al.* (1998) A novel protein complex promoting formation of functional alpha- and gamma-tubulin. *EMBO J* 17, 952-966

354 Vainberg, I.E., *et al.* (1998) Prefoldin, a chaperone that delivers unfolded proteins to cytosolic chaperonin. *Cell* 93, 863-873

355 Cuellar, J., *et al.* (2008) The structure of CCT-Hsc70 NBD suggests a mechanism for Hsp70 delivery of substrates to the chaperonin. *Nat Struct Mol Biol* 15, 858-864

356 Yam, A.Y., *et al.* (2008) Defining the TRiC/CCT interactome links chaperonin function to stabilization of newly made proteins with complex topologies. *Nat Struct Mol Biol* 15, 1255-1262

357 Plimpton, R.L., *et al.* (2015) Structures of the Gbeta-CCT and PhLP1-Gbeta-CCT complexes reveal a mechanism for G-protein beta-subunit folding and Gbetagamma dimer assembly. *Proc Natl Acad Sci U S A* 112, 2413-2418

358 Frydman, J., *et al.* (1994) Folding of nascent polypeptide chains in a high molecular mass assembly with molecular chaperones. *Nature* 370, 111-117

359 Joachimiak, L.A., *et al.* (2014) The structural basis of substrate recognition by the eukaryotic chaperonin TRiC/CCT. *Cell* 159, 1042-1055

360 Reissmann, S., *et al.* (2012) A gradient of ATP affinities generates an asymmetric power stroke driving the chaperonin TRIC/CCT folding cycle. *Cell Rep* 2, 866-877

361 Gestaut, D., *et al.* (2019) The Chaperonin TRiC/CCT Associates with Prefoldin through a Conserved Electrostatic Interface Essential for Cellular Proteostasis. *Cell* 177, 751-765 e715

362 Kalisman, N., *et al.* (2013) The crystal structures of the eukaryotic chaperonin CCT reveal its functional partitioning. *Structure* 21, 540-549

363 Cong, Y., *et al.* (2010) 4.0-A resolution cryo-EM structure of the mammalian chaperonin TRiC/CCT reveals its unique subunit arrangement. *Proc Natl Acad Sci U S A* 107, 4967-4972

364 Martin-Benito, J., *et al.* (2007) The inter-ring arrangement of the cytosolic chaperonin CCT. *EMBO Rep* 8, 252-257

365 Dekker, C., *et al.* (2011) The crystal structure of yeast CCT reveals intrinsic asymmetry of eukaryotic cytosolic chaperonins. *EMBO J* 30, 3078-3090

366 Liou, A.K. and Willison, K.R. (1997) Elucidation of the subunit orientation in CCT (chaperonin containing TCP1) from the subunit composition of CCT micro-complexes. *EMBO J* 16, 4311-4316

367 Llorca, O., *et al.* (2000) Eukaryotic chaperonin CCT stabilizes actin and tubulin folding intermediates in open quasi-native conformations. *EMBO J* 19, 5971-5979

368 Llorca, O., *et al.* (1999) Eukaryotic type II chaperonin CCT interacts with actin through specific subunits. *Nature* 402, 693-696

369 Kalisman, N.*, et al.* (2012) Subunit order of eukaryotic TRiC/CCT chaperonin by cross-linking, mass spectrometry, and combinatorial homology modeling. *Proc Natl Acad Sci U S A* 109, 2884-2889

370 Cuellar, J.*, et al.* (2019) Structural and functional analysis of the role of the chaperonin CCT in mTOR complex assembly. *Nat Commun* 10, 2865

371 Wang, T.*, et al.* (2015) Identification and characterization of essential genes in the human genome. *Science* 350, 1096-1101

372 Blomen, V.A.*, et al.* (2015) Gene essentiality and synthetic lethality in haploid human cells. *Science* 350, 1092-1096

373 Balchin, D.*, et al.* (2018) Pathway of Actin Folding Directed by the Eukaryotic Chaperonin TRiC. *Cell* 174, 1507-1521 e1516

374 Munoz, I.G.*, et al.* (2011) Crystal structure of the open conformation of the mammalian chaperonin CCT in complex with tubulin. *Nat Struct Mol Biol* 18, 14-19

375 Pavel, M.*, et al.* (2016) CCT complex restricts neuropathogenic protein aggregation via autophagy. *Nat Commun* 7, 13821

376 Grantham, J. (2020) The Molecular Chaperone CCT/TRiC: An Essential Component of Proteostasis and a Potential Modulator of Protein Aggregation. *Front Genet* 11, 172

377 Roh, S.H.*, et al.* (2015) Contribution of the Type II Chaperonin, TRiC/CCT, to Oncogenesis. *Int J Mol Sci* 16, 26706-26720

378 Vytautas Iesmantavicius. https://orcid.org/0000-0002-2512-9957

379 Daniel Hess. https://orcid.org/0000-0002-1642-5404

380 Simone Cavadini. https://orcid.org/0000-0003-2777-7584

381 Wang, G.*, et al.* (2017) Validation of whole-blood transcriptome signature during microdose recombinant human erythropoietin (rHuEpo) administration. *BMC Genomics* 18, 817

382 Zhu, J.*, et al.* (2015) Application of human haploid cell genetic screening model in identifying the genes required for resistance to environmental toxicants: Chlorpyrifos as a case study. *J Pharmacol Toxicol Methods* 76, 76-82

383 The UniProt, C. (2017) UniProt: the universal protein knowledgebase. *Nucleic Acids Res* 45, D158-D169

384 Zimmermann, L.*, et al.* (2018) A Completely Reimplemented MPI Bioinformatics Toolkit with a New HHpred Server at its Core. *J Mol Biol* 430, 2237-2243

385 Gabler, F.*, et al.* (2020) Protein Sequence Analysis Using the MPI Bioinformatics Toolkit. *Curr Protoc Bioinformatics* 72, e108

386 Scrima, A.*, et al.* (2008) Structural basis of UV DNA-damage recognition by the DDB1-DDB2 complex. *Cell* 135, 1213-1223

387 Georg Kempf. https://orcid.org/0000-0002-0228-6730

388 Slabicki, M.*, et al.* (2020) The CDK inhibitor CR8 acts as a molecular glue degrader that depletes cyclin K. *Nature* 585, 293-297

389 Bussiere, D.E.*, et al.* (2020) Structural basis of indisulam-mediated RBM39 recruitment to DCAF15 E3 ligase complex. *Nat Chem Biol* 16, 15-23

390 Xu, C. and Min, J. (2011) Structure and function of WD40 domain proteins. *Protein Cell* 2, 202-214

391 Schapira, M.*, et al.* (2017) WD40 repeat domain proteins: a novel target class? *Nat Rev Drug Discov* 16, 773-786

392 Jumper, J.*, et al.* (2021) Highly accurate protein structure prediction with AlphaFold. *Nature* 596, 583-589

393 Varadi, M.*, et al.* (2022) AlphaFold Protein Structure Database: massively expanding the structural coverage of protein-sequence space with high-accuracy models. *Nucleic Acids Res* 50, D439-D444

394 Laskowski, R.A. and Swindells, M.B. (2011) LigPlot+: multiple ligand-protein interaction diagrams for drug discovery. *J Chem Inf Model* 51, 2778-2786

395 Russo, C.J. and Passmore, L.A. (2014) Robust evaluation of 3D electron cryomicroscopy data using tilt-pairs. *J Struct Biol* 187, 112-118

396 Boland, A.*, et al.* (2017) Cryo-EM structure of a metazoan separase-securin complex at near-atomic resolution. *Nat Struct Mol Biol* 24, 414-418

397 da Fonseca, P.C. and Morris, E.P. (2015) Cryo-EM reveals the conformation of a substrate analogue in the human 20S proteasome core. *Nat Commun* 6, 7573

398 Pantelic, R.S.*, et al.* (2010) Graphene oxide: a substrate for optimizing preparations of frozen-hydrated samples. *J Struct Biol* 170, 152-156

399 Dubochet, J.*, et al.* (1971) A new preparation method for dark-field electron microscopy of biomacromolecules. *J Ultrastruct Res* 35, 147-167

400 Russo, C.J. and Passmore, L.A. (2014) Electron microscopy: Ultrastable gold substrates for electron cryomicroscopy. *Science* 346, 1377-1380

401 Passmore, L.A. and Russo, C.J. (2016) Specimen Preparation for High-Resolution Cryo-EM. *Methods Enzymol* 579, 51-86

402 Glaeser, R.M. and Han, B.G. (2017) Opinion: hazards faced by macromolecules when confined to thin aqueous films. *Biophys Rep* 3, 1-7

403 Baker, M.R.*, et al.* (2015) Single-Particle Cryo-EM of the Ryanodine Receptor Channel in an Aqueous Environment. *Eur J Transl Myol* 25, 4803

404 Vagenende, V.*, et al.* (2009) Mechanisms of protein stabilization and prevention of protein aggregation by glycerol. *Biochemistry* 48, 11084-11096

405 Basanta, B.*, et al.* (2022) A case for glycerol as an acceptable additive for single-particle cryoEM samples. *Acta Crystallogr D Struct Biol* 78, 124-135

406 Shabek, N.*, et al.* (2018) Structural insights into DDA1 function as a core component of the CRL4-DDB1 ubiquitin ligase. *Cell Discov* 4, 67

407 Olma, M.H.*, et al.* (2009) An interaction network of the mammalian COP9 signalosome identifies Dda1 as a core subunit of multiple Cul4-based E3 ligases. *J Cell Sci* 122, 1035-1044

408 Stark, H. (2010) GraFix: stabilization of fragile macromolecular complexes for single particle cryo-EM. *Methods Enzymol* 481, 109-126

409 Smyth, M.S. and Martin, J.H. (2000) x ray crystallography. *Mol Pathol* 53, 8-14

410 Pereira, J.H.*, et al.* (2017) Structure of the human TRiC/CCT Subunit 5 associated with hereditary sensory neuropathy. *Sci Rep* 7, 3673

411 Gallagher, J.R., *et al.* (2019) Negative-Stain Transmission Electron Microscopy of Molecular Complexes for Image Analysis by 2D Class Averaging. *Curr Protoc Microbiol* 54, e90

412 Scarff, C.A., *et al.* (2018) Variations on Negative Stain Electron Microscopy Methods: Tools for Tackling Challenging Systems. *J Vis Exp*

413 Baek, K., *et al.* (2020) NEDD8 nucleates a multivalent cullin-RING-UBE2D ubiquitin ligation assembly. *Nature* 578, 461-466

414 Baek, K., *et al.* (2021) NEDD8 and ubiquitin ligation by cullin-RING E3 ligases. *Curr Opin Struct Biol* 67, 101-109

415 Ferreyra, R.G. and Frydman, J. (2000) Purification of the cytosolic chaperonin TRiC from bovine testis. *Methods Mol Biol* 140, 153-160

416 Cong, Y., *et al.* (2012) Symmetry-free cryo-EM structures of the chaperonin TRiC along its ATPase-driven conformational cycle. *EMBO J* 31, 720-730

417 Zang, Y., *et al.* (2016) Staggered ATP binding mechanism of eukaryotic chaperonin TRiC (CCT) revealed through high-resolution cryo-EM. *Nat Struct Mol Biol* 23, 1083-1091

418 Pappenberger, G., *et al.* (2006) Quantitative actin folding reactions using yeast CCT purified via an internal tag in the CCT3/gamma subunit. *J Mol Biol* 360, 484-496

419 Knee, K.M., *et al.* (2013) Human TRiC complex purified from HeLa cells contains all eight CCT subunits and is active in vitro. *Cell Stress Chaperones* 18, 137-144

420 Machida, K., *et al.* (2012) Reconstitution of the human chaperonin CCT by co-expression of the eight distinct subunits in mammalian cells. *Protein Expr Purif* 82, 61-69

421 Luckow, V.A., *et al.* (1993) Efficient generation of infectious recombinant baculoviruses by site-specific transposon-mediated insertion of foreign genes into a baculovirus genome propagated in Escherichia coli. *J Virol* 67, 4566-4579

422 Gibson, D.G., *et al.* (2009) Enzymatic assembly of DNA molecules up to several hundred kilobases. *Nat Methods* 6, 343-345

423 Selleck, W.*, et al.* (2001) A histone fold TAF octamer within the yeast TFIID transcriptional coactivator. *Nat Struct Biol* 8, 695-700

424 Chang, L.*, et al.* (2015) Atomic structure of the APC/C and its mechanism of protein ubiquitination. *Nature* 522, 450-454

425 Weissmann, F.*, et al.* (2016) biGBac enables rapid gene assembly for the expression of large multisubunit protein complexes. *Proc Natl Acad Sci U S A* 113, E2564-2569

426 Brackley, K.I. and Grantham, J. (2010) Subunits of the chaperonin CCT interact with F-actin and influence cell shape and cytoskeletal assembly. *Exp Cell Res* 316, 543-553

427 Grantham, J.*, et al.* (2006) Substantial CCT activity is required for cell cycle progression and cytoskeletal organization in mammalian cells. *Exp Cell Res* 312, 2309-2324

428 Elliott, K.L.*, et al.* (2015) A novel function of the monomeric CCTepsilon subunit connects the serum response factor pathway to chaperone-mediated actin folding. *Mol Biol Cell* 26, 2801-2809

429 Chen, D.H.*, et al.* (2013) Visualizing GroEL/ES in the act of encapsulating a folding protein. *Cell* 153, 1354-1365

430 Sergeeva, O.A.*, et al.* (2019) Co-expression of CCT subunits hints at TRiC assembly. *Cell Stress Chaperones* 24, 1055-1065

431 Kulak, N.A.*, et al.* (2014) Minimal, encapsulated proteomic-sample processing applied to copy-number estimation in eukaryotic cells. *Nat Methods* 11, 319-324

432 Matalon, O.*, et al.* (2014) Different subunits belonging to the same protein complex often exhibit discordant expression levels and evolutionary properties. *Curr Opin Struct Biol* 26, 113-120

433 Mathieson, T.*, et al.* (2018) Systematic analysis of protein turnover in primary cells. *Nat Commun* 9, 689

434 Zou, X.D.*, et al.* (2016) Genome-wide Analysis of WD40 Protein Family in Human. *Sci Rep* 6, 39262

435 Szczesniak, M.W.*, et al.* (2011) Primate and rodent specific intron gains and the origin of retrogenes with splice variants. *Mol Biol Evol* 28, 33-37

436 Lobanov, M.Y., *et al.* (2010) Library of disordered patterns in 3D protein structures. *PLoS Comput Biol* 6, e1000958

437 Pegg, A.E. (2008) Spermidine/spermine-N(1)-acetyltransferase: a key metabolic regulator. *Am J Physiol Endocrinol Metab* 294, E995-1010

438 Marsh, J.A., *et al.* (2013) Protein complexes are under evolutionary selection to assemble via ordered pathways. *Cell* 153, 461-470

439 Pla-Prats, C., *et al.* (2023) Recognition of the CCT5 di-Glu degron by CRL4(DCAF12) is dependent on TRiC assembly. *EMBO J*, e112253

440 Abdulrahman, W., *et al.* (2009) A set of baculovirus transfer vectors for screening of affinity tags and parallel expression strategies. *Anal Biochem* 385, 383-385

441 Grant, T., *et al.* (2018) cisTEM, user-friendly software for single-particle image processing. *Elife* 7

442 Moriya, T., *et al.* (2017) High-resolution Single Particle Analysis from Electron Cryo-microscopy Images Using SPHIRE. *J Vis Exp*

443 Penczek, P.A., *et al.* (2014) CTER-rapid estimation of CTF parameters with error assessment. *Ultramicroscopy* 140, 9-19

444 Yang, Z., *et al.* (2012) Iterative stable alignment and clustering of 2D transmission electron microscope images. *Structure* 20, 237-247

445 Zivanov, J., *et al.* (2018) New tools for automated high-resolution cryo-EM structure determination in RELION-3. *Elife* 7

446 Zheng, S.Q., *et al.* (2017) MotionCor2: anisotropic correction of beam-induced motion for improved cryo-electron microscopy. *Nat Methods* 14, 331-332

447 Zhang, K. (2016) Gctf: Real-time CTF determination and correction. *J Struct Biol* 193, 1-12

448 Du, Z., *et al.* (2021) The trRosetta server for fast and accurate protein structure prediction. *Nat Protoc* 16, 5634-5651

449 Emsley, P., *et al.* (2010) Features and development of Coot. *Acta Crystallogr D Biol Crystallogr* 66, 486-501

450 Croll, T.I. (2018) ISOLDE: a physically realistic environment for model building into low-resolution electron-density maps. *Acta Crystallogr D Struct Biol* 74, 519-530

451 Wang, R.Y.*, et al.* (2016) Automated structure refinement of macromolecular assemblies from cryo-EM maps using Rosetta. *Elife* 5

452 Afonine, P.V.*, et al.* (2018) Real-space refinement in PHENIX for cryo-EM and crystallography. *Acta Crystallogr D Struct Biol* 74, 531-544

453 Bryant, P.*, et al.* (2022) Improved prediction of protein-protein interactions using AlphaFold2. *Nat Commun* 13, 1265

454 Liebschner, D.*, et al.* (2019) Macromolecular structure determination using X-rays, neutrons and electrons: recent developments in Phenix. *Acta Crystallogr D Struct Biol* 75, 861-877

455 Barad, B.A.*, et al.* (2015) EMRinger: side chain-directed model and map validation for 3D cryo-electron microscopy. *Nat Methods* 12, 943-946

456 Chen, V.B.*, et al.* (2010) MolProbity: all-atom structure validation for macromolecular crystallography. *Acta Crystallogr D Biol Crystallogr* 66, 12-21

457 Pettersen, E.F.*, et al.* (2021) UCSF ChimeraX: Structure visualization for researchers, educators, and developers. *Protein Sci* 30, 70-82

458 Krissinel, E. and Henrick, K. (2007) Inference of macromolecular assemblies from crystalline state. *J Mol Biol* 372, 774-797

This Thesis would not have been possible without the professional and personal support of a series of people to whom I will forever be grateful.

First and foremost, I owe a debt of gratitude to Nico Thomä, for accepting me in his group and then guiding my research along a productive path. Our two manuscripts together are a testament to the quality of his guidance. Doing a PhD in his lab has helped me grow professionally and personally, and has allowed me to entertain the scientific curiosity that first drove me to research. I have learnt a lot from Nico, and I recall specific personal and lab-wide discussions as some of the most stimulating experiences of my PhD. I am privileged to have carried out my PhD in this lab, city and country.

A lot of people at FMI have helped me throughout these years, and I want to thank all members of our technical platforms. In particular, I want to thank Simone Cavadini and Georg Kempf, for being incredibly helpful and always available. I am also grateful to Marc Bühler and Brenda Schulman for their guidance and encouragement as part of my thesis committee, and to all members of the lab, both present and past, for their invaluable discussions, help, inspiration, and kindness. It has been great to carry out my PhD in the company of people whom I consider friends.

I am thankful for my friends in and out of the FMI, who knowingly or unknowingly have provided crucial encouragement and motivation and have made these years a truly enjoyable experience. And I am especially thankful for Vittoria, in whose acknowledgments I hope to be soon.

Lastly, I want to thank my parents for instilling in me a life-lasting curiosity and drive to learn, for their continuous help and support, and for always believing in me. I would not have become a doctor without them.